THE UNIVERSITY
of EDINBURGH

The interaction of alphaviruses chikungunya and Semliki Forest with cells of the mononuclear phagocyte system.

Adrian Krzysztof Zagrajek

Submitted for the degree of Doctor of Philosophy

The University of Edinburgh

2016

Table of contents

Disclaimer

I (Adrian Krzysztof Zagrajek) declare that this thesis has been composed by myself and all the work included in this thesis is my own except where otherwise stated. No part of this work has been, or will be submitted for any other degree or professional qualification.

Adrian Krzysztof Zagrajek

30th July 2016

The Roslin Institute
The University of Edinburgh
Easter Bush
EH25 9RG
Scotland

Abstract

Introduction

Chikungunya virus (CHIKV) is an alphavirus in the family *Togaviridae*. Since 2005 the virus has caused a major epidemic of disease in humans, ranging from Central Africa, South-East Asia, Caribbean and more recently the Americas. The virus is spread by mosquitoes, most notably *Aedes aegypti* and *Ae. albopictus*. CHIKV causes an acute disease in humans, which is characterised by a rapid onset of high fever, rash, myalgia and arthralgia. The symptoms typically resolve within a week. Remarkably, up to a third of patients who recover from acute chikungunya develop chronic arthritis/arthralgia, which may last for months or years and has a large negative impact on the quality of life. The mechanism by which this occurs is not yet fully understood. CHIKV can infect human monocytes, and macrophages positive for CHIKV antigen have been observed in joint tissue from patients recovered from acute CHIKV infection but with chronic arthritis. Furthermore, it has been demonstrated that macrophages can be infected with CHIKV *in vitro* by a mechanism involving apoptotic debris from CHIKV-infected cells.

Hypothesis and aims

Infection of monocytes and macrophages with CHIKV contributes to clinical disease and virus persistence *in vivo*. The aim of this project was to investigate the mechanism by which alphaviruses infect macrophages *in vitro*, and to generate a CHIKV which is unable to replicate in monocytes and macrophages *in vitro*, and to study its pathogenicity *in vivo*.

Materials and methods

HeLa cells were infected with Semliki Forest virus (SFV), an alphavirus closely related to CHIKV, or SFV replicon particles (SFV VRP). Following cell death, whole cell supernatant or clarified cell supernatant from SFV- and SFV VRP-infected cells was passaged onto human monocyte-derived macrophages (MDMs). These cells were observed microscopically for expression of the fluorescent marker encoded by the SFV. Virus and VRP-infected apoptotic debris were inspected for the

presence of alphavirus replication complexes by electron microscopy. Subsequently, a recognition element (RE) for a haematopoietic-specific miRNA (miR-142-3P) was incorporated into the genome of SFV (proof-of-concept) and CHIKV to investigate if blocking virus replication in cells of the mononuclear phagocyte system altered virus kinetics *in vitro*. The replication of the modified viruses was investigated in macrophage/monocyte cell lines Thp-1 and IC-21, and in HEK 293 cells modified to express miR-142-3P under the control of an inducible tetracycline promoter. Modified viruses were tested in animal models of disease (mouse for SFV and non-human primate for CHIKV) to investigate the pathogenicity of these viruses *in vivo*.

Results

The presence of apoptotic debris from SFV-infected cells was required to infect MDMs with SFV. The presence or absence of infectious virus particles in the apoptotic debris did not affect the infection rate. Intact alphavirus replication complexes were found within the apoptotic debris. MiR-142-3P RE was successfully incorporated into the genome of both SFV and CHIKV. RE-virus replication in all cells expressing miR-142-3P was reduced by 90-99% when compared to control viruses. RE-virus replication was not affected in cells which did not express miR-142-3P. In interferon-α/β receptor knockout mice, RE-SFV generated viraemia comparable to the control virus, but could not infect efficiently the population of macrophages resident in the marginal zone of the spleen. RE-CHIKV was found to be genetically stable *in vitro* following multiple passages on BHK-21 cells in the absence of a selective pressure from miR-142-3P. RE-CHIKV was inoculated into two cynomolgus macaques. The data from this experiment are not yet available.

Conclusion

SFV was shown to infect MDM via apoptotic debris containing intact alphavirus replication complexes, which were the most likely infectious agent. SFV and CHIKV unable to replicate in haematopoietic cells *in vitro* were successfully engineered. The pathogenicity of modified SFV and CHIKV was investigated *in vivo*.

Lay summary

Chikungunya virus (CHIKV) causes a serious disease in people that is characterised by high fever, rash, muscle pain and joint pain. It typically lasts for up to a week but in some patients the muscle and joint pain may last for months or years. We do not fully understand the process responsible for this long-term disease. CHIKV infects mostly cells of the connective tissue (fibroblasts) and muscle cells (myoblasts). However, white blood cells monocytes and macrophages infected with CHIKV have been observed in patients suffering from the CHIKV disease. Human CHIKV infection has been successfully simulated in cynomolgus macaques, creating an accurate animal model of human CHIKV disease. The aim of this project was to investigate how CHIKV infects human macrophages, and to create a modified CHIKV that cannot replicate in monocytes and macrophages, and to study its ability to cause a CHIKV disease in cynomolgus macaques.

Semliki Forest virus (SFV), a virus closely related to CHIKV, was used in initial proof-of-concept experiments. Human epithelial and fibroblast cells were infected with SFV. The virus infection killed those cells, creating cell debris. Human macrophages were fed with the resulting cell debris and then observed under a microscope for evidence of SFV infection. Cell debris was also inspected by electron microscopy. SFV and CHIKV were genetically modified to block their ability to replicate in monocytes and macrophages without affecting their ability to replicate in other cells, including fibroblasts and myoblasts. The replication of modified viruses was investigated in macrophages and monocytes. Modified viruses were tested in animal models of disease (mouse for SFV and cynomolgus macaque for CHIKV).

The presence of debris from cells infected with SFV was required to infect human macrophages with SFV. The presence or absence of infectious virus particles in the cell debris did not change the ability of the cell debris to infect macrophages. Undamaged sites of SFV replication called virus replication complexes were found inside the cell debris by electron microscopy. Replication of modified SFV and CHIKV in monocytes and macrophages was reduced by 90-99% when compared to

control viruses. In a mouse model of SFV disease, the modified SFV could not infect the population of macrophages present in the spleen. Modified CHIKV was found to be genetically stable. The virus was used to infect two cynomolgus macaques. The data from this experiment are not yet available.

In conclusion, SFV was shown to infect human macrophages using cell debris containing intact virus replication complexes even when no infectious virus particles were present. SFV and CHIKV unable to replicate in monocytes and macrophages were successfully created. The ability of modified CHIKV to cause a disease was investigated in cynomolgus macaques.

Acknowledgments

I would like to thank my supervisors **John Fazakerley** and **Finn Grey** for their support, guidance and never-ending patience throughout my PhD. John provided an unlimited source of knowledge and has inspired me in many ways as a scientist and as a person. Finn helped me to shape my project and took me under his wings when John moved out of Edinburgh.

Many thanks belong to **Rennos Fragkoudis** who offered his expertise, help and friendship throughout my project. Even when busy, Rennos always made himself available to discuss my work, to challenge my understanding of it, and to explore new avenues of research.

I would also like to thank all members of the lab, past and present: **Alain Kohl**, **Lesley Bell-Sakyi**, **Gerald Barry**, **Mhairi Ferguson**, **Claire Donald**, **Joana Ferrolho**, **Julio Rodriguez**, **Sabine Weisheit**, **Claudia Rückert**, **Stacey Human**, **Karen Sherwood**, **Esther Schnettler**, **Ricky Sui** and **Sue Jacobs**. Your friendship and support during the project was invaluable to me and made my time in the group an amazing experience that I will never forget.

Special thanks belong to **Andres Merits**, **Aleksei Lulla**, **Pierre Roques**, **Tero Ahola**, **Philippe Gasque, Peter Liljeström** and **David Hume**. Your expertise, advice and help had a great impact on many aspects of my project.

Finally, I would like to thank my parents **Tadeusz** and **Maria**, and my brother **Paweł**. Your never-ending love, support and motivation have been fundamental to everything I have done. Without you none of this would have been possible.

Last but not least, I would like to thank **Gosia Borkowska** for always being there for me, for putting up with me, for challenging me, and for inspiring me. You are a wonderful person and I cannot imagine not having you in my life.

Abbreviations

2SGP – duplicated subgenomic promoter
4B – 4-nucleotide spacer
A – adenine
ACD – anticoagulant citrate dextrose
ACDP – Advisory Committee on Dangerous Pathogens
ADE – antibody-dependent enhancement
Apaf-1 – protease-activating factor-1
ATP – adenosine triphosphate
BHK – Baby Hamster Kidney
bp – base pairs
BRF – Biological Research Resources
BSA – bovine serum albumin
C – capsid
CC – cell culture
cDNA – complementary DNA
CHIKV – chikungunya virus
CHO – Chinese hamster ovary
CL – containment level
CMC – carboxymethylcellulose sodium salt
CMV – cytomegalovirus
CO_2 – carbon dioxide
CPE – cytopathic effect
CPV-1 – type I cytoplasmic vacuoles
Cq – quantification cycle
CSE – conserved sequence element
CTP – cytidine triphosphate
DAPI – 4',6-Diamidino-2-Phenylindole
DC – dendritic cells
DENV – dengue virus
DISC – death-inducing signalling complex

DMEM – Dulbecco's Modified Eagle's Medium
DMSO – dimethyl sulfoxide
DNA – deoxyribonucleic acid
dNTP – deoxyrybonucleotide
DOX – doxycycline
ds – double-stranded
E – envelope
EDTA – ethylene diamine tetraacetic acid
EEEV – Eastern equine encephalitis virus
eGFP – enhanced green fluorescent protein
ER – endoplasmic reticulum
FADD – Fas-associated death domain
Fas – First apoptosis signal
FBS – foetal bovine serum
FLuc – Firefly luciferase
FMDV – foot and mouth disease virus
For – forward
G – guanine
GFP – green fluorescent protein
GLuc – Gaussia luciferase
GMEM – Glasgow's Minimum Essential Medium
GOI – gene of interest
GP – genomic promoter
GTP – guanosine triphosphate
H_2O – water
HCl – hydrochloric acid
HEPES – 4-(2-Hydroxyethyl)piperazine-1-ethanesulfonic acid
HG – hazard group
HIV – human immunodeficiency virus
HS – Heparan sulphate
icDNA – DNA infectious clone
ICRES – Integrated Chikungunya Research

IFN – interferon
IFNAR – IFN-α/ß receptor knockout mice of A129/SvEv background
IL – Interleukin
IP – intraperitoneal
IU – infectious units
IV – intravenous
J – junction region
LN2 – liquid nitrogen
LOD – level of detection
MAYV – Mayaro virus
MBSC – microbiological safety cabinet
MCP – macrophage chemoatractant protein
MCS – multiple cloning site
MDM – monocyte-derived macrophages
MIP – macrophage inflammatory protein
miRNA – micro RNA
MOI – multiplicity of infection
mRNA – messenger RNA
NaCl – sodium chloride
NaOH – sodium hydroxide
NBCS – newborn calf serum
NC – nucleocapsid
NHDF – normal human dermal fibroblast
NK – Natural Killer cells
nsP – non-structural protein
NTR – non-translated
OCT – optimum cutting temperature
ONNV – O'nyong-nyong virus
ORF – open reading frame
P/S – penicillin/streptomycin
PBMCs – peripheral blood mononuclear cells
PBS – phosphate buffered saline

PBSA – PBS with 0.75 % w / v bovine serum albumin

PCR – polymerase chain reaction

PERK – protein kinase RNA-like endoplasmic reticulum kinase

PFU – plaque forming units

PI3K – phosphatidylinositol 3-kinase

PM – plasma membrane

PMA – phorbol 12-myristate 13-acetate

pre-miRNA – pre-micro RNA

pri-miRNA – pri-microRNA

qPCR – quantitative (real-time) polymerase chain reaction

RANTES – regulated on activation, normal T cell expressed and secreted

RBCs – red blood cells

RCF – relative centrifugal force

RE – recognition element

Rev – reverse

rhCSF-1 – recombinant human Colony Stimulating Factor-1

RISC – RNA-induced silencing complex

RLU – relative luminescence units

RLuc – Renilla luciferase

RNA – ribonucleic acid

RPM – revolutions per minute

RPMI – Roswell Park Memorial Institute

RPV – replication-proficient virus

RRV – Ross River virus

RSE – repeated sequence element

RT – room temperature

SAPO – Specified Animal Pathogen Order

SC – sub-cutaneous

SD – standard deviation

SFV – Semliki Forest virus

SGP – subgenomic promoter

SINV – Sindbis virus

SIV – simian immunodeficiency virus
SRV-1 – simian type D retrovirus
SRV-2 – simian retrovirus serotype 2
STLV – simian T lymphotropic virus
T – thymine
TAE – Tris Acetate-EDTA buffer
TC – tissue culture
TEM – transmission electron microscope
TetO2 – Tet operator 2
TetR – Tet repressor
T_m – melting temperature
TNE – TrisHCl/NaCl/EDTA buffer
TNF – tumour necrosis factor
TPB – tryptose phosphate broth
TRIS – Tris(hydroxymethyl)aminomethane
TS – target sequence
TSAP – thermosensitive alkaline phosphatase
U – uracil
UTP – uridine triphosphate
UTR – untranslatable region
UV – ultra violet
VDAC – voltage-dependent anion channel
VEEV – Venezuelan equine encephalitis virus
VLPs – virus-like particles
VRP – virus replicon particles
WEEV – Western equine encephalitis virus

Chapter 1:

General introduction

Contents:

1.1 Chikungunya virus (CHIKV)

Chikungunya virus (CHIKV) is an alphavirus in the family *Togaviridae* (Westaway et al. 1985). It belongs to the Semliki Forest virus (SFV) antigenic complex together with SFV, Mayaro virus (MAYV), Ross River virus (RRV), Getah virus and O'nyong-nyong virus (ONNV) (Powers et al. 2001). Other notable alphaviruses include Sindbis virus (SINV), and Venezuelan, Eastern and Western equine encephalitis viruses (VEEV, EEEV and WEEV). Until recently, the knowledge of the molecular virology and cellular pathogenesis of CHIKV was largely based on what we knew of related alphaviruses, such as SFV and SINV. However, in recent years there has been an increase in fundamental research on CHIKV infection, replication and pathogenesis.

1.2 CHIKV structure

CHIKV is a small, spherical virus of 70 nm in diameter (Higashi et al. 1967, Strauss et al. 1994). The alphavirus nucleocapsid (NC) is 40 nm in diameter and is composed of 240 copies of capsid protein (C) arranged as hexamers and pentamers in a T=4 icosahedral symmetry and complexed with viral genome (Simizu et al. 1984, Strauss et al. 1994, Cheng et al. 1995, Mancini et al. 2000, Perera et al. 2001, Mukhopadhyay et al. 2006). Similarly to SFV, CHIKV NC is surrounded by a cell membrane-derived lipid bilayer containing 240 copies of viral glycoproteins E1 and E2, which are arranged as trimers of heterodimers to form the 80 glycoprotein spikes of the virion (Simizu et al. 1984, Strauss et al. 1994, Mancini et al. 2000, Voss et al. 2010). The envelope glycoproteins are, like the capsid, arranged in a T=4 icosahedral symmetry (Akahata et al. 2010, Voss et al. 2010). The alphavirus genome is a non-segmented, single-stranded positive sense RNA with 5'-terminal 7-methylguanylate cap and 3' poly(A) tail (Kääriäinen et al. 1978, Strauss et al. 1994). Consequently, viral RNA resembles cellular mRNA and is infectious in the absence of viral proteins. CHIKV genome is 11,811 nucleotides long (LR2006 OPY1 strain), excluding 5'-cap nucleotide and poly(A) tail (GenBank accession no. DQ443544) (Parola et al. 2006). CHIKV contains two open reading frames (ORFs). The non-structural ORF of 7,425 nucleotides and the structural ORF of 4,245 nucleotides are located in the 5' two thirds and 3' one third of the genome, respectively (Strauss et

al. 1994). The non-structural ORF encodes 4 non-structural proteins (nsP1-4) while the structural ORF encodes 5 structural proteins (C, E3, E2, 6K, E1). The two ORFs are separated by a non-coding Junction (J) region of 68 nucleotides. The first 76 and the last 501 nucleotides of the genome are the 5' and 3' untranslatable regions (UTRs), respectively. Khan et al. (2002) identified an internal polyadenylation (I-poly(A)) site located within the 3' UTR of the S27 strain, which had been highly passaged. However, this does not seem to be a typical CHIKV feature. Similar to other alphaviruses, in CHIKV three repeated sequence elements (RSE) of 21-35 nucleotides exist in the 3' UTR (Pfeffer et al. 1998, Khan et al. 2002, Zhang et al. 2013). In addition, a 19-nucleotide highly conserved sequence element (CSE) found in all alphaviruses is located directly adjacent to the poly(A) tail (Khan et al. 2002, Parola et al. 2006). The schematic organisation of CHIKV LR2006 OPY1 genome is presented in Figure 1.1.

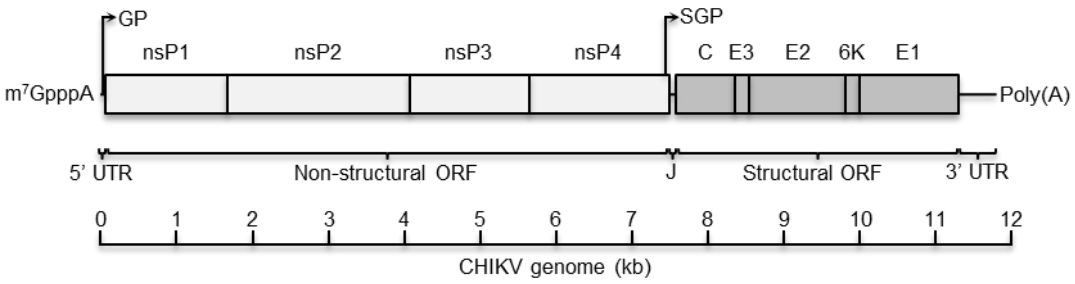

Figure 1.1 Genomic organisation of CHIKV strain LR2006 OPY1. CHIKV has a non-segmented, single-stranded positive sense RNA genome of 11,811 nucleotides with a 5'-terminal cap and 3' poly(A) tail. Two open reading frames (ORFs) encode 4 non-structural proteins (nsP1-4) and 5 structural proteins (C, E3, E2, 6K, E1). An internal subgenomic promoter (SGP) located at the boundary between nsP4 and J region drives the transcription of alphavirus subgenomic RNA. Untranslatable regions (UTRs) of 76 and 501 nucleotides long are located at the 5' and 3' ends of virus genome, respectively.

1.3 CHIKV life cycle

The life cycle of CHIKV and other alphaviruses such as SFV and SINV is summarized in Figure 1.2 and described in detail below.

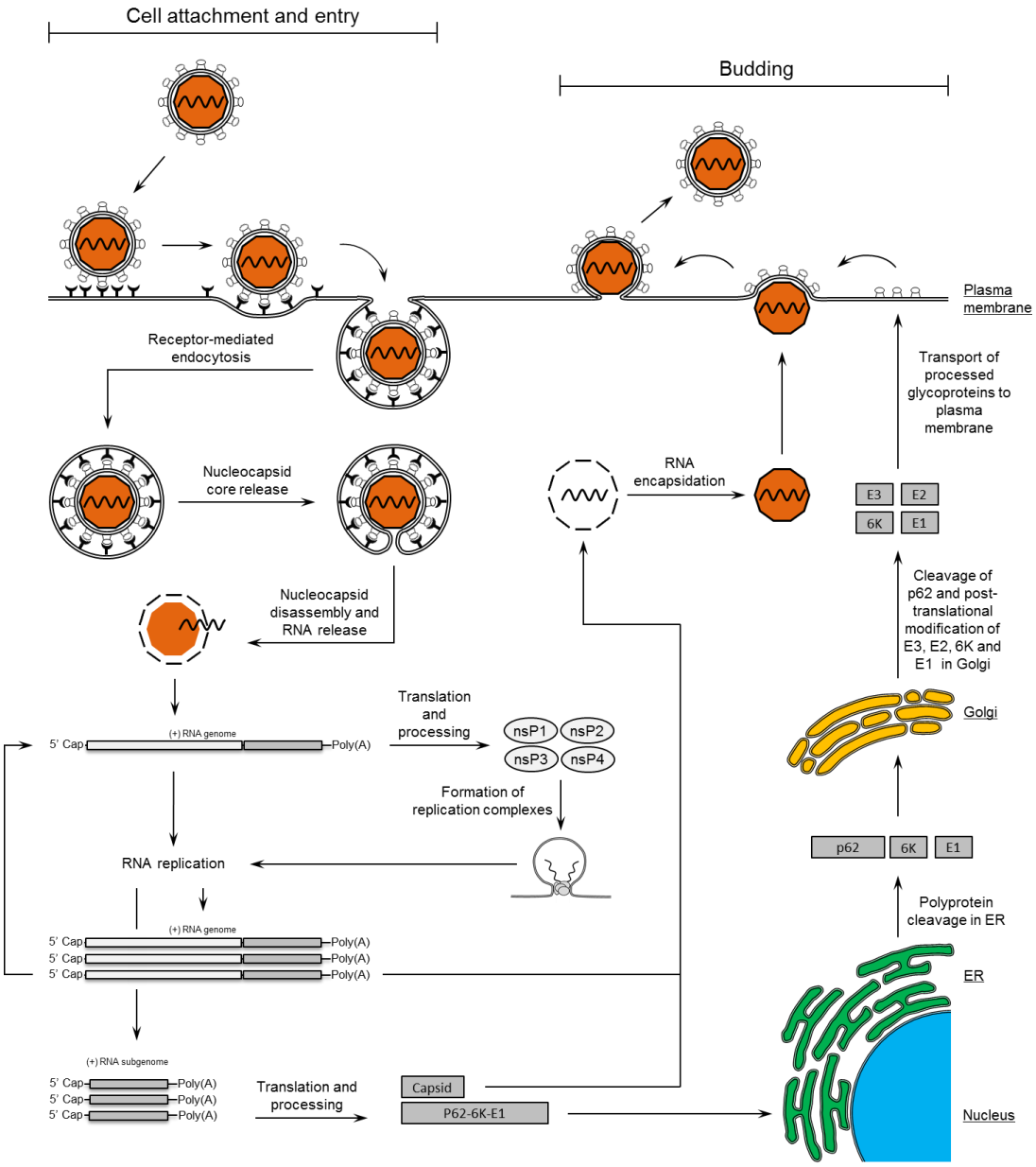

Figure 1.2 Life cycle of an alphavirus. CHIKV enters cells by receptor-mediated endocytosis. E1 mediates virus–host cell membrane fusion. Nucleocapsid is disassembled in the cytoplasm. The non-structural polyprotein is translated from the virus genomic RNA by cellular machinery and processed into its individual components by the nsP2. Non-structural proteins interact with virus genomic RNA leading to formation and maturation of virus replication complexes. Replication of virus RNA yields full length genomic RNAs and subgenomic RNAs. Structural polyproteins are translated from subgenomic RNAs. Capsid is cleavage autoproteolyticly from p62-6K-E1 polyprotein. It is released into the cytoplasm where it interacts with virus genomic RNA to form a nucleocapsid. The p62-6K-E1 polyprotein is processed in the endoplasmic reticulum (ER) and in the Golgi apparatus. Mature glycoproteins are exported to the plasma membrane. Interaction of E2 with a nucleocapsid drives budding and release of a new virus particle.

1.3.1 CHIKV cell entry

CHIKV can infect a wide range of human, mouse, macaque and *Aedes* spp. cells *in vitro* and *in vivo* (Tsetsarkin et al. 2006, Ozden et al. 2007, Sourisseau et al. 2007, Couderc et al. 2008, 2009, Her et al. 2009, Labadie et al. 2010, Krejbich-Trotot et al. 2011, Thon-Hon et al. 2012, Lim et al. 2014). Endocytosis of an alphavirus particle is initiated by binding of E2, a type I transmembrane glycoprotein, to a cellular receptor (Strauss et al. 1994, Roussel et al. 2006, Voss et al. 2010). Consequently, E2 largely defines the cellular tropism of CHIKV. Uptake of virus particle into both mosquito and mammalian cells is driven by receptor-mediated endocytosis and access to an early endosome is a requisite for productive infection of mammalian cells (Sourisseau et al. 2007, Salvador et al. 2009, Bernard et al. 2010, Tsetsarkin et al. 2011, Gay et al. 2012). In general, alphaviruses enter cells in clathrin coated vesicles (Sánchez-San Martín et al. 2009, Kielian et al. 2010, Singh et al. 2011). Knock-down of dynamin-2, a key player in the formation of clathrin-coated vesicles, is associated with a 20-fold reduction in the infectivity of cells with CHIKV (Sourisseau et al. 2007). In contrast, Bernard et al. (2010) demonstrated that CHIKV enters cells by a clathrin-independent Eps15-dependent mechanism. It is possible that CHIKV uses a range of pathways to enter specific cell types. Following endocytosis, the increase in endosome acidity leads to a conformational change in the virus spike glycoproteins leading to exposure of E1, a class II viral fusion protein (Kielian et al. 2010, Voss et al. 2010, Leung et al. 2011, Tang 2012). E1 mediates fusion of the virus envelope with the vesicle membrane and release of nucleocapsid into the cytoplasm where it is disassembled leading to release of the RNA genome (Kielian et al. 2010, Voss et al. 2010, Leung et al. 2011, Tang 2012). Cholesterol present in cell membrane lipid rafts plays an important role in the successful fusion of alphavirus and cell membranes (Phalen et al. 1991, Lu et al. 1999, Sourisseau et al. 2007, Tsetsarkin et al. 2007, Solignat et al. 2009, Bernard et al. 2010, Gay et al. 2012). It appears to be required for the interaction between E1 and the target membrane (Phalen et al. 1991). Alphavirus dependence on cholesterol can be modulated by amino acid in position 226 in E1 (Vashishtha et al. 1998, Lu et al. 1999). Adaptation of CHIKV to *Ae. albopictus* (E1-A226V) coincided with increased dependence of CHIKV on cholesterol (Tsetsarkin et al. 2007, Kuo et al. 2012, Gay et al. 2012).

Putative receptors for several alphaviruses have been identified. DC-SIGN, L-SIGN, high-affinity laminin receptor and NRAMP have been described as attachment receptors for SINV (Wang et al. 1992, Klimstra et al. 2003, Rose et al. 2011). Prohibitin 1 (PHB1), expressed on the surface of human microglial cell line CHME-5, is the first cellular receptor identified for CHIKV (Wintachai et al. 2012). Heparan sulphate (HS), a ubiquitously expressed negatively charged cell surface glycosaminoglycan, has been demonstrated to facilitate cell entry for VEEV, SINV, RRV, SFV and CHIKV (Byrnes et al. 1998, Klimstra et al. 1998, Bernard et al. 2000, Heil et al. 2001, Smit et al. 2002, Gardner et al. 2014, Silva et al. 2014, Ferguson et al. 2015). The affinity of alphaviruses for HS is typically acquired following serial passage in cell culture and results from the selection of viruses with positively-charged amino acids in virus glycoprotein E2 (Klimstra et al. 1998, Ferguson et al. 2015). However, natural isolates of EEEV have also been shown to bind HS (Gardner et al. 2011, 2013). SINV incorporating the uncleaved precursor envelope protein p62 into its virion was demonstrated to efficiently bind HS (Klimstra et al. 1999, Ryman et al. 2004). The interaction is mediated via the presence of an intact furin cleavage site, which acts as a HS-binding domain. Virus adaptation to HS by *in vitro* passage can reduce efficient spread of virus *in vivo* and lead to attenuation at least in animal models of alphavirus disease (Bernard et al. 2000, Ryman et al. 2004, Gardner et al. 2014). However, adaptation of SFV, SINV and EEEV to HS has been demonstrated to contribute to the neurovirulence of these viruses by enhancing their ability to cross the blood-brain barrier and to replicate in brain tissue (Ryman et al. 2007, Gardner et al. 2011, Ferguson et al. 2015). Krejbich-Trotot et al. (2011) proposed a new, receptor-independent, mechanism by which CHIKV spread between neighbouring cells in culture via apoptotic blebs from virus-infected cells (discussed in more detail in 1.11).

1.3.2 CHIKV replication

Alphavirus replication (Figure 1.3) takes place in the host cell cytoplasm. Following the disassembly of a nucleocapsid, virus genomic RNA is translated to produce the non-structural polyprotein nsP1234, which is the replicase (Glanville et al. 1976, Strauss et al. 1994, Parola et al. 2006). An opal stop codon (UGA) near the terminus

of nsP3 is present in the majority of alphaviruses, (Strauss et al. 1983, 1988, Lanciotti et al. 1998, Weaver et al. 1999, Lavergne et al. 2006). In the presence of an opal stop codon, the differential expression of nsP123 and nsP1234 is controlled by the read-through translation (Strauss et al. 1983, Strauss et al. 1994). Full-length nsP1234 is produced approximately 5-20% of the time (de Groot et al. 1990, Shirako et al. 1994). Most CHIKV strains have a sense codon in place of the opal stop codon (Khan et al. 2002, Parola et al. 2006). However, Schuffenecker et al. (2006) reported that some Indian Ocean isolates do contained an opal stop codon between nsP3 and nsP4. Similar strain-specific variations were observed in ONNV (Lanciotti et al. 1998) and SINV (Simpson et al. 1996). In ONNV, the presence of an opal stop codon between nsP3 and nsP4 was shown to provide a fitness advantage in mosquitoes (Myles et al. 2006) while passaging on Vero cells lead to the replacement of the opal stop codon with a sense codon (Lanciotti et al. 1998). Altogether these data suggest that in ONNV the presence of an opal stop codon in virus quasispecies may be driven by alternative replication in both vertebrate and invertebrate hosts (Atkins 2013). Interestingly, EEEV was also demonstrated to replace the opal stop codon with a sense codon following a serial passage *in vitro* (Weaver et al. 1999). Contrary to ONNV, this process is driven by the adaptation of EEEV to mosquito and not mammalian cells and therefore is likely to be subject to a different selective pressure. The role of the opal codon in CHIKV is yet to be investigated in detail.

Similarly to other alphaviruses, CHIKV polyprotein nsP1234 is processed into its individual components in a highly regulated sequential process driven by the nsP2, which encodes a papain-like cysteine protease domain in its C-terminal (Ding et al. 1989, Hardy et al. 1989, de Groot et al. 1990, Strauss et al. 1992, Lemm et al. 1994, Merits et al. 2001, Vasiljeva et al. 2003, Pastorino et al. 2008, Lulla et al. 2013). First, the non-structural polyprotein nsP1234 is cleaved *in cis* into nsP123 and nsP4, the RNA-dependent RNA polymerase containing GDD amino acid polymerase motif within its C-terminal region (Keränen et al. 1979, Kamer et al. 1984, Hahn et al. 1989, Tomar et al. 2006, Rubach et al. 2009). This process is essential for alphavirus replication (Shirako et al. 1994). It has been suggested that nsP4 has a limited protease activity that contributes to cleavage between nsP3 and nsP4 (Kamer et al.

1984, Takkinen et al. 1990, Takkinen et al. 1991). Cleaved wild-type nsP4 invariably contains an aromatic amino acid tyrosine in the N-terminus causing its rapid degradation by the N-end rule pathway and likely contributing to the temporal control of the viral RNA replication (Wellink et al. 1988, de Groott et al. 1991). However, in SINV the nsP4 N-terminal tyrosine was successfully substituted with phenylalanine, tryptophan (both aromatic amino acids) or histidine without the loss of wild-type nsP4 polymerase activity *in vitro* (Shirako et al. 1998). Any other amino acid at that position rendered the virus nonviable emphasising the biological role of this amino acid in virus fitness. NsP4 of SINV has terminal adenyl-transferase activity involved in the maintenance of the virus poly(A) tail (Tomar et al. 2006).

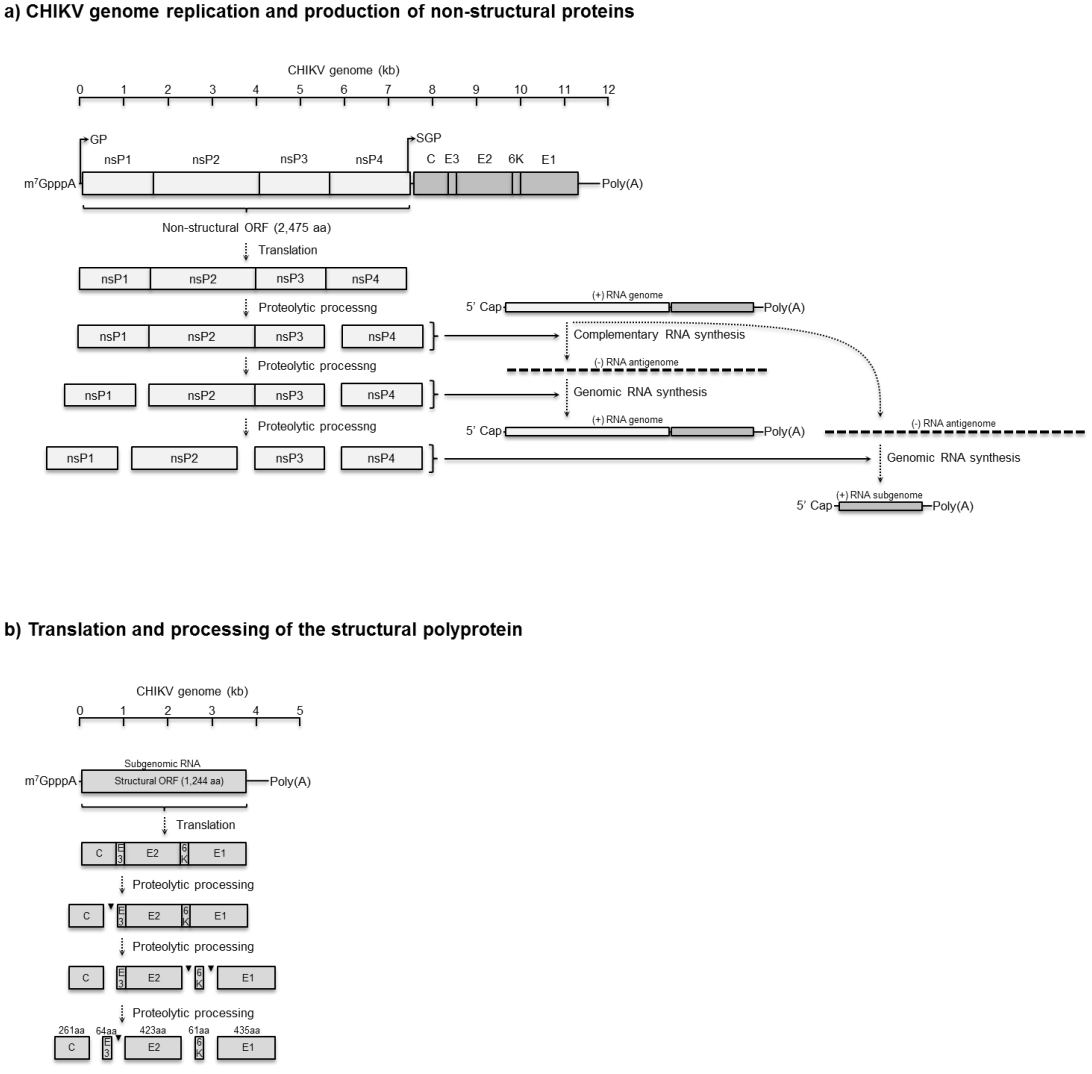

Figure 1.3. Diagrammatic representation of alphavirus replication. The replication cycle is shown as a series of tightly regulated steps (a) Translation and processing of the non-structural polyprotein, synthesis of the complementary RNA (antigenome), synthesis of progeny genomes and synthesis of subgenomic RNAs. (b) Translation and processing of the structural polyprotein. Autoproteolytic cleavage of capsid from p62-6K-E1 polyprotein, capsid is released into cytoplasm, the translation of p62-6K-E1 is directed to the endoplasmic reticulum (ER), the polyprotein is cleaved to p62, 6K and E1 in the ER by signalase and p62 is cleaved to E3 and E2 by furin in the Golgi apparatus, finally E3, E2, 6K and E1 are modified post-translationally in the Golgi apparatus.

The release of nsP4 leads to the synthesis of a negative strand RNA (antigenome) replication intermediate (Shirako et al. 1994, Vasiljeva et al. 2003). The synthesis of this negative strand is initiated by nsP1 interacting with a region in the 3' UTR of viral genome (Sawicki et al. 1981, Hahn et al. 1989, Wang et al. 1991, Shirako et al. 2000). NsP1 may directly interact with nsP4 to initiate the negative-strand synthesis (Shirako et al. 2000). Das et al. (2014) demonstrated that the nsP2 of CHIKV acts as a directional RNA helicase and a RNA-strand annealing protein. It is involved in unwinding virus genome during its replication process.

NsP123 is further processed to produce nsP23 and nsP1, which allows synthesis of both negative- and positive-strand RNAs (Kim et al. 2004). An internal subgenomic promoter (SGP), which drives the transcription of alphavirus subgenomic RNA, is located at the boundary between nsP4 and the J region (Ou et al. 1982, Grakoui et al. 1989, Strauss et al. 1994). In SINV, the minimum size of the SGP sufficient to transcribe detectable levels of subgenomic RNA is 24 nucleotides (Ou et al. 1982, Levis et al. 1990). This sequence is highly conserved across alphaviruses. At this stage of replication, the genomic positive-strand RNA is generated in preference to the subgenomic RNA. All positive-strand RNAs are capped by nsP1, which encodes methyl and guanylyl transferase domains in its N-terminal (Ahola et al. 1997). NsP2 is also involved in this process through the activity of its trisphosphatase domains (Rikkonen et al. 1994, Gomez de Cedrón et al. 1999, Vasiljeva et al. 2000).

The next stage of polyprotein processing is the cleavage of nsP23 to produce nsP2 and nsP3 (Lulla et al. 2012). The fully cleaved replicase preferentially produces subgenomic positive-strand RNA. Subgenomic RNA is transcribed in 5-20-fold molar excess over genomic RNA (Shirako et al. 1994, Strauss et al. 1994, Kim et al. 2004). In mammalian cells this switch to preferential production of the positive-strand RNA occurs approximately 3 hours post-infection (Shirako et al. 1994).

Replication of alphaviruses is associated with cellular membranes (Salonen et al. 2005). The formation and maturation of membrane-bound alphavirus replication complexes is a dynamic process (Spuul et al. 2010). It is summarised in Figure 1.4.

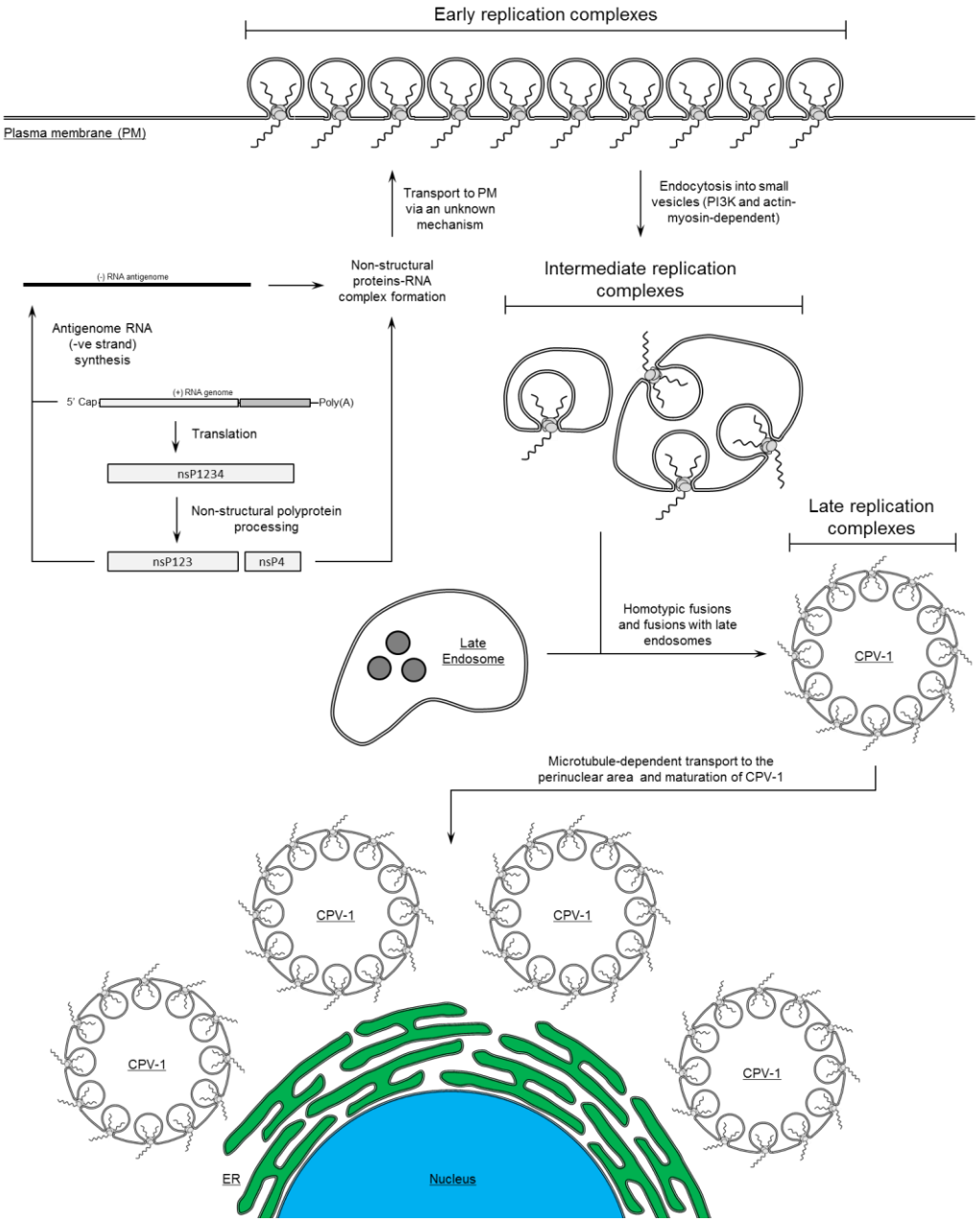

Figure 1.4. Formation of alphavirus replication complexes. Virus replicase polyprotein nsP1234 is translated from virus genomic RNA and then cleaved into nsP123 and nsP4 by nsP2. This leads to synthesis of a negative strand RNA that forms a macromolecular complex with nsP123 and nsP4. The complex is transported to the plasma membrane (PM). NsP1 anchors the complex to the PM, which drives invagination of the PM and formation of spherules (early replication complexes). Spherules are transferred by endocytosis from the PM to small cytoplasmic vesicles leading to formation of intermediate replication complexes. Homotypic fusions and fusions with lysosomes and/or late endosomes lead to formation of type I cytopathic vacuoles (CPV-1) that contain hundreds of individual spherules on their surface (late replication complexes). CPV-1 are transported to the perinuclear area where their maturation is completed. Based on a model proposed by Spuul et al. (2010).

The initial cleavage of nsP4 from the non-structural polyprotein leads to synthesis of a negative strand RNA that forms a macromolecular complex with nsP123 and nsP4. The complex is transported to the plasma membrane (PM) by an unknown mechanism (Grimley et al. 1968, Froshauer et al. 1988, Spuul et al. 2010, Frolova et al. 2010). NsP1 anchors viral replicase proteins to the PM via an amphipathic helix and palmitoylation residues (Froshauer et al. 1988, Laakkonen et al. 1996, 1998, Kujala et al. 2001a, Spuul et al. 2007, 2010). This drives invagination of the PM and formation of spherules (Figure 1.5), which are approximately 50 nm in diameter and remain open to the cytoplasm via a narrow neck of 5-10 nm in diameter (Froshauer et al. 1988, Peränen et al. 1991). These early replication complexes can be detected microscopically at the PM as early as 45 minutes post infection reaching a maximum local density of up to 100/μm^2 (Spuul et al. 2010).

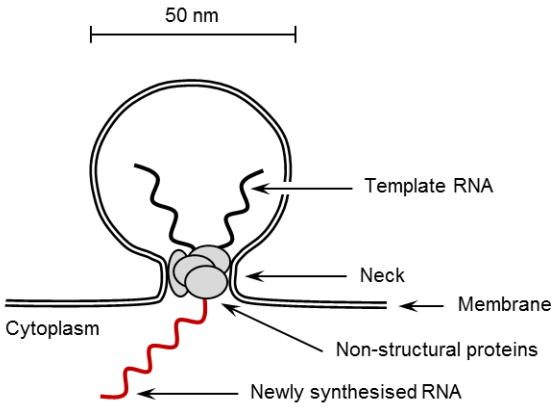

Figure 1.5. Alphavirus spherule. Spherule membrane is continuous with the plasma/vesicle membrane its inside remains open to the cytoplasm via a narrow neck of 5-10 nm in diameter. Virus RNA is replicated inside the spherules and the newly synthesised RNA is released into the cytoplasm. Virus replicase proteins (nsP1-4) are located within the neck controlling the transport of cellular and virus components between the inside of a spherule and the cytoplasm. Spherules can be detected at the plasma membrane as early as 45 minutes post infection.

Virus RNA is replicated inside the spherules and the newly synthesised RNA is released into the cytoplasm. Virus non-structural proteins are located primarily within the neck of a spherule controlling transport of cellular and virus material between the inside of a spherule and the cytoplasm (Spuul et al. 2010, Frolova et al. 2010). RNA template and viral replicase proteins are required for the formation of spherules and the size of the RNA template directly governs the size of spherules (Kujala et al. 2001, Kallio et al. 2013). Kallio et al. (2013) demonstrated that SFV spherules located on the PM were present only in cells actively replicating viral genome and that all spherules were active in viral RNA replication.

The maturation of alphavirus replication complexes is associated with sequential processing of nsP123 to its individual components. As discussed previously, this highly controlled process driven by nsP2 changes the preference of the replicase from synthesis of negative strand RNAs to synthesis of positive strand genomic and subgenomic RNAs (Figure 1.3).

Between 2 and 4 hours post-infection spherules are transferred from the PM to small cytoplasmic vesicels by endocytosis in phosphatidylinositol 3-kinase (PI3K)- and actin-myosine-dependent manner (Spuul et al. 2010). NsP3 may play a role in the initiation of this process, however, the mechanism is not well understood (Salonen et al. 2003, Spuul et al. 2010). The inside of spherules remains continuously open to the cytoplasm. Each individual cytoplasmic vesicle carries several spherules and is often termed an intermediate replication complex (Spuul et al. 2010). These vesicles are localised primarily at the periphery of the cytoplasm and demonstrate short distance and multidirectional movement (Spuul et al. 2010).

Homotypic fusions of intermediate replication complexes and fusions with pre-existing acidic organelles, such as late endosomes, lead to formation of late replication complexes (Figure 1.6), also named type I cytopathic vacuoles (CPV-1) (Grimley et al. 1968, Froshauer et al. 1988, Spuul et al. 2010). Late replication complexes are quickly transported in a microtubule-dependant manner to the perinuclear area where their maturation is completed (Spuul et al. 2010). The

formation of CPV-1 can be observed from 2.5 hours post-infection (Spuul et al. 2010). They become the predominant type of a replication complex present by 4 hours post-infection. Mature replication complexes are larger than unmodified endosomes (0.5-2 μm) and contain hundreds of individual spherules on their surface (Spuul et al. 2010). They are very stable, protecting the negative strand RNA template from degradation and ensuring a steady rate of positive sense RNA synthesis for several hours (Kääriäinen et al. 2002, Spuul et al. 2010).

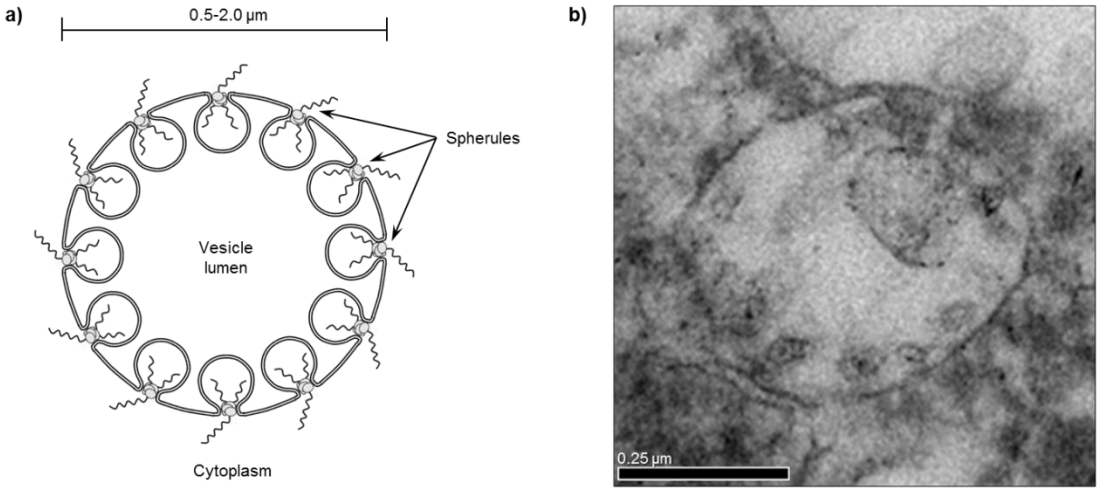

Figure 1.6. Alphavirus late replication complex (CPV-1) structure. a) Schematic structure of a mature CPV-1. Each vacuole may contain hundreds of individual spherules on its surface. The membrane of each spherule is continuous with the vesicle membrane and the inside of each spherule remains continuously open to the cytoplasm. b) Transmission electron microscopy showing a mature CPV-1 (approximately 0.6 μm in diameter) in SFV4-steGFP-infected HeLa cells. Image taken using Phillips CM120 transmission electron microscope and a Gatan Orius CCD camera at the Electron Microscope facility of the School of Biological Sciences, the University of Edinburgh. Spherules connected with the cytoplasm via a neck are visible in the lower part of the replication complex.

The subgenomic RNA is translated into a structural polyprotein C-p62-6K-E1, which is processed co-translationally and post-translationally into structural proteins. The capsid protein (C) has an autoproteolytic function, which drives its rapid cleavage and release into the cytoplasm (Aliperti et al. 1978). This process exposes a signal sequence in the N-terminal of p62 (precursor to E3 and E2), which directs the translation of p62-6K-E1 to the endoplasmic reticulum (ER) (Bonatti et al. 1984, Melancon et al. 1986, Garoff et al. 1990). The polyprotein is cleaved to p62, 6K and E1 in the ER by signalase and p62 is cleaved to E3 and E2 by furin in the Golgi apparatus (Zhang et al. 2003). E3, E2, 6K and E1 are modified post-translationally in the Golgi apparatus. Finally, the glycoproteins migrate to the cell membrane.

The RNA poly(A) tail plays an important role in alphavirus replication. As mentioned previously, in SINV it is involved in the initiation of negative-strand synthesis. However, it is not well understood if the length of the poly(A) tail is a determinant of RNA replication efficiency.

1.3.3 CHIKV maturation

In the cytoplasm, 240 capsid proteins interact with each other to form 12 pentamers and 30 hexamers, which bind to virus positive-strand genomic RNA via a packaging signal located in the nsP2 gene, to form the nucleocapsid (Weiss et al. 1989, Frolova et al. 1997). In SINV, residues 97 through 106 of the capsid protein were suggested to dictate the specificity of viral RNA encapsidation (Owen et al. 1996, Kim et al. 2011). A mutant in which these residues were deleted was shown to encapsidate both genomic and subgenomic viral RNAs.

At the plasma membrane, E1 and E2 form trimers of heterodimers (Voss et al. 2010). Then, E2 interacts with the nucleocapsid via its cytoplasmic tail. This process drives budding and release of new virus particles (Pathak et al. 1976, Suomalainen et al. 1992, Lopez et al. 1994). Budding can be observed from as early as 3 hours post-infection (Johnson et al. 1981). In SFV, the 6K protein, although not a structural component of the virus, is essential for the assembly of the virus glycoprotein spikes (Liljeström et al. 1991, McInerney et al. 2004).

1.4 CHIKV and apoptosis

Apoptosis is a process of programmed cell death (Kerr et al. 1972, Elmore 2007). It is a natural process that is essential in development, differentiation and maintenance of cell populations within tissues (Vaux et al. 1999, Elmore 2007). Apoptosis is also a first line of defence against viral infections and consequently a crucial component of the innate immune host responses (Everett et al. 1999, Allsopp et al. 2000, Elmore 2007, Barry et al. 2010, Krejbich-Trotot et al. 2011). In this context, apoptosis of virus-infected cells can be viewed as an altruistic auto-elimination that limits virus release and therefore the infection of surrounding cells (Allsopp et al. 2000, Elmore 2007). It can be highly effective when it occurs prior to completion of virus replication and virion assembly. As a consequence, most large DNA viruses that are characterised by a long replication have evolved strategies to block or postpone the induction of apoptosis (Teodoro et al. 1997, Everett et al. 1999, Chen et al. 2006, White 2006, Kepp et al. 2009). On the other hand, small RNA viruses such as alphaviruses can replicate to high titres before infected cells can undergo apoptosis without the need to suppress it (Barry et al. 2010). Interestingly, some viruses have evolved to exploit the apoptosis in order to maximise their replication and overall fitness (Krakauer et al. 1997).

Apoptosis is a highly regulated, complex and energy-dependent process (Elmore 2007). It requires activation of highly conserved cysteine proteases called caspsases (Thornberry et al. 1998, Danial et al. 2004, Kurokawa et al. 2009). Once caspases are activated, the cell is irreversibly committed towards its death. Various cell types may react in different ways in response to a single stimulus, some inducing apoptosis and some not. There are two main molecular pathways involved in apoptosis. Both have been implicated in cell death induced by viruses (Urban et al. 2008).

The intrinsic pathway is initiated in response to a cell stress. It is controlled by members of the Bcl-2 protein family that are classified into two groups, pro-survival and pro-apoptotic (Adams et al. 1998, Narita et al. 1998, Shimizu et al. 1999, Willis et al. 2005). Activated pro-apoptotic Bcl-2 protein family members such as Bad, Bax and Bak form a pore complex with voltage-dependent anion channels (VDACs) on

the outer membrane of mitochondria. This leads to an increase of mitochondrial membrane permeability, loss of mitochondrial transmembrane potential and release of cytochrome *c* and other apoptogenic factors into the cytosol (Narita et al. 1998, Shimizu et al. 1999, Kroemer et al. 2007, Elmore 2007). Cytosolic cytochrome *c* interacts with protease-activating factor-1 (Apaf-1) and the initiatory caspase-9 to promote self-cleavage of caspase-9 and the formation of an apoptosome complex (Cecconi et al. 1998, Srinivasula et al. 1998, Yoshida et al. 1998, Zou et al. 1999). Conversely, binding of pro-survival Bcl-2 protein family members such as Bcl-2 and Bcl-xL to VDACs on the outer membrane of mitochondria blocks the channels and prevents the release of the cytochrome *c* into the cytosol (Shimizu et al. 1999). The extrinsic pathway of apoptosis involves stimulation of death receptors that are members of the tumour necrosis factor (TNF) receptor gene superfamily by an external ligand such as TNF-α or First apoptosis signal (Fas) ligand (Thorburn 2004, Elmore 2007, Wilson et al. 2009). Binding of the ligand to the receptor leads to formation of the death-inducing signalling complex (DISC) that consists of Fas-associated death domain (FADD) and the initiatory caspase-8 or caspase-10 (Sprick et al. 2002, Thorburn 2004). Both intrinsic and extrinsic pathways lead to cleavage and activation of executioner caspases-3, -6 and-7 (Elmore 2007, Kurokawa et al. 2009). These caspases activate cytoplasmic endonucleases that degrade chromosomal DNA, proteases that degrade nuclear and cytoskeletal proteins, and tissue transglutaminases that cross-link cellular proteins.

As a direct consequence of the action of effector endonucleases, proteases and transglutaminases, a cell dying of apoptosis undergoes various morphological and biochemical changes (Kerr et al. 1972, Elmore 2007, Kurokawa et al. 2009). During early stages of apoptosis cells shrink and the DNA chromatin is condensed. As a result of a smaller cell size, the organelles are more closely packed within a condensed cytoplasm. Extensive formation of cytoplasmic blebs and fragmentation of the nucleus is observed next. This is followed by formation of apoptotic bodies and consequently by cell fragmentation. Apoptotic bodies are characterised by an intact plasma membrane, dense cytoplasm and tightly packed organelles that typically maintain their integrity. Nucleic acids may be present within apoptotic

bodies. In addition, the outer layer of an apoptotic body plasma membrane express unique cell surface markers that include phosphatidylserine, Annexin I and calreticulin (Elmore 2007). Finally, apoptotic bodies and smaller blebs are phagocytosed by macrophages and subsequently degraded within phagolysosomes (Elmore 2007). The recognition of apoptotic debris by macrophages is facilitated by the presence of the unique apoptotic markers on their plasma membrane, in particular phosphatidylserine. The phagocytosis of apoptotic debris by macrophages is a rapid and non-inflammatory process.

Virus infection can induce apoptosis by inhibiting cellular protein transcription and/or translation, affecting cellular stress pathways, perturbing protein-chaperone systems or by activating a range of cellular sensors such as protein kinase R, protein kinase RNA-like endoplasmic reticulum kinase (PERK), and ceramide-activate kinases (Everett et al. 1999, Allsopp et al. 2000, Gorchakov et al. 2005). This can take place at any stage of virus infection, from virus-receptor binding to egress from an infected cell.

Alphavirus infection of mammalian cells triggers apoptosis both *in vitro* and *in vivo*. This has been clearly demonstrated for SFV, SINV, VEEV, RRV and CHIKV (Levine et al. 1993, Lewis et al. 1996, Lundstrom et al. 1997, Scallan, Allsopp, et al. 1997, Glasgow et al. 1997, 1998, Griffin et al. 1997, Jackson et al. 1997, Antalis et al. 1998, Nava et al. 1998, Jan et al. 1999, Allsopp et al. 2000, Moriishi et al. 2002, Sourisseau et al. 2007, Barry et al. 2010, Krejbich-Trotot et al. 2011). The mechanism, by which alphaviruses trigger apoptosis, has been investigated in some detail using SFV and SINV. UV-inactivated SINV was shown to induce apoptosis in Chinese hamster ovary (CHO) cells in both presence and absence of protein biosynthesis inhibitor cycloheximide (Jan et al. 1999). SINV induced cell deaths by sphingomyelin degradation and release of ceramide. The apoptotic cascade was triggered at the time of virus fusion with the cell membrane, and in absence of virus replication. In contrast, SFV requires intact RNA to trigger apoptosis as UV-inactivated SFV does not kill cells (Urban et al. 2008). This discrepancy may, however, be explained by significantly different experimental designs (Urban et al.

2008). The nsP2 of SINV and SFV drives shutdown of host cell transcription and translation (Gorchakov et al. 2005, Garmashova et al. 2007a, Tamm et al. 2008). It was shown to be cytotoxic in absence of any other virus proteins and mutations in its C terminus are often responsible for prolonged survival of infected cells or persistent infection (Dryga et al. 1997, Glasgow et al. 1998, Frolov et al. 1999, 2009, Perri et al. 2000, Gorchakov et al. 2005, Garmashova et al. 2006, Garmashova et al. 2007a, Tamm et al. 2008). In contrast, the New World alphaviruses VEEV and EEEV use the capsid protein for induction of transcriptional shutoff (Garmashova et al. 2007a, Garmashova et al. 2007b). The transmembrane domain of SINV envelope glycoproteins was also shown to induce apoptosis (Joe et al. 1998). SFV envelope glycoproteins were shown to accelerate the apoptotic cell death by induction of the ER stress response (Barry et al. 2010).

In neurons, the SINV- and SFV-induced apoptosis is dependent on the virus strain and the maturation and differentiation status of neurons (Fazakerley et al. 1993, Levine et al. 1993, Ubol et al. 1994, Lewis et al. 1996, Oliver et al. 1998, Allsopp et al. 2000). Immature neurons readily undergo apoptosis following an infection while mature neurons can remain functional and survive for long periods of time (Lewis et al. 1996, Allsopp et al. 2000). The ability of SFV and SINV to trigger apoptosis in neurons correlates with neurovirulence and fatal encephalitis observed *in vivo* (Levine et al. 1993, Lewis et al. 1996, Allsopp et al. 2000).

SFV and SINV use primarily the intrinsic pathway for induction of apoptosis (Moriishi et al. 2002, Urban et al. 2008). The process is dependent primarily on pro-apoptotic Bad (SINV) and Bak (SFV) (Moriishi et al. 2002, Urban et al. 2008). Fibroblast cells deficient in Apaf-1 were shown to be resistant to SINV-induced apoptosis (Balachandran et al. 2000). The overexpression of pro-survival Bcl-2 or Bcl-xL can delay induction of apoptosis and lead to persistent infection (Levine et al. 1993, Cheng et al. 1996, Lundstrom et al. 1997, Scallan & Allsopp 1997, Murphy et al. 2001, Moriishi et al. 2002, Urban et al. 2008). However, some studies failed to detect a protective effect of Bcl-2 against SFV- and SINV-induced apoptosis (Grandgirard et al. 1998, Murphy et al. 2001, Kiiver et al. 2008). In addition, Nava et

al. (1998) suggested that SINV-induced apoptosis has some characteristics of an extrinsic pathway. These findings suggest that multiple and independent pathways may be involved in the induction of apoptosis in SFV- and SINV-infected cells.

In recent years CHIKV-induced apoptosis has been investigated in some detail (Sourisseau et al. 2007, Krejbich-Trotot et al. 2011, Dhanwani et al. 2012, Joubert et al. 2012, Judith et al. 2013). In vertebrate cells, CHIKV infection leads to extensive cell death and a large amount of cell debris within 24 hours post-infection (Sourisseau et al. 2007). Similar to SINV and SFV, CHIKV uses primarily the intrinsic pathway for induction of apoptosis (Krejbich-Trotot et al. 2011). The process is dependent on pro-apoptotic Bax. The translocation of Bax to mitochondria and the release of cytochrome *c* into the cytosol are visible in HeLa cells from 16 hours post-infection. Interestingly, Krejbich-Trotot et al. (2011) observed activation of caspase-8 in HeLa cells infected at MOI=0.01 from 24 hours post-infection suggesting a late involvement of an extrinsic apoptosis pathway. Furthermore, bystander caspase-8-dependent induction of apoptosis was observed in CHIKV-negative cells from 24 hours post-infection. Unfortunately, the signal that initiated the extrinsic pathway in these cells was not identified. Similar to SFV and contrary to SINV, the capacity of CHIKV to trigger apoptosis is dependent on the presence of intact virus RNA and its replication (Krejbich-Trotot et al. 2011). Inhibition of CHIKV-induced apoptosis by chemical inhibitors limited the spread of CHIKV in HeLa cells culture suggesting that CHIKV exploits apoptosis in order to maximise its replication (Krejbich-Trotot et al. 2011). Interestingly, CHIKV-induced autophagy was shown to inhibit caspase-dependent apoptosis in mouse cells *in vitro* and *in vivo* (Joubert et al. 2012, Judith et al. 2013). Yet, in human cells CHIKV-triggered autophagy promotes viral replication (Judith et al. 2013).

1.5 Global distribution and epidemics

CHIKV was first isolated in 1952 in the Newala district of Tanzania (Ross 1956). After the initial outbreak the virus spread across sub-Saharan Africa, where it has become endemic (Powers et al. 2007). Subsequently, the virus spread east. The first outbreak in Asia was observed in 1958 in Bangkok (Sudeep et al. 2008). There was a series of significant urban outbreaks in India from 1963 through 1970 (Ligon 2006, Staples et al. 2009). No major epidemics occurred for the next 30 years. The virus rose to prominence in 2005 when a large explosive epidemic started on the French island of La Réunion (Powers et al. 2007, Her et al. 2009). Between February 2005 and June 2006 there were 266,000 estimated cases and 237 resultant deaths (Townson et al. 2008, Schwartz et al. 2010). Strikingly, a third of La Réunion population (~785,000) was affected. Since then, CHIKV has spread across South-East Asia and caused large epidemics in India (2006-2007), Malaysia (2009) and Thailand (2009) with 1.4-6.4 million, 3,000 and 42,000 estimated cases, respectively (Schwartz et al. 2010). First CHIKV outbreak in Europe was observed in 2007, when 292 human cases of local transmission were reported in north-eastern Italy (Rezza et al. 2007, Townson et al. 2008). The source of the outbreak was traced to a traveller returning from India (Cavrini et al. 2009, Ng et al. 2010). In September 2010, the first autochthonous CHIKV transmission was observed in Europe, in southern France (Grandadam et al. 2011). Between 2009 and 2014, CHIKV outbreaks were confirmed in China, Bhutan, Yemen, Saudi Arabia, New Caledonia, Papua New Guinea, Tonga, French Polynesia and the Lao People's Democratic Republic (Sam et al. 2015). In December 2013, an autochthonous outbreak was reported for the first time in the Americas, on the island of Saint Martin in the Caribbean region (Hamer et al. 2014, Sam et al. 2015). Since then, CHIKV has spread to over 50 countries and territories in the area, including the United States and Brazil, causing over 1.5 million suspected cases (Powers 2015, Sam et al. 2015). So far CHIKV has been observed in over 60 countries and there is a real potential for the emergence and spread of the virus in Europe.

1.6 CHIKV transmission

CHIKV is an arthropod-borne virus (arbovirus). It is spread by mosquitoes, most notably *Aedes aegypti* and *Ae. Albopictus* (Pialoux et al. 2007). Monkeys, birds and rodents are the primary non-human reservoir of CHIKV (Her et al. 2009). There are two distinct transmission cycles (Figure 1.7): sylvatic and urban (Sudeep et al. 2008, Thiboutot et al. 2010). Prior to 2005, *Ae. aegypti* was the primary vector of CHIKV. However, A226V mutation in E1 glycoprotein of CHIKV was observed in 90% of CHIKV isolates after September 2005 (Schuffenecker et al. 2006). The mutation increased the transmissibility of the virus by *Ae. albopictus* 100-fold, which had a significant impact on the global epidemiology of CHIKV (Tsetsarkin et al. 2007, Ng et al. 2010). *Ae. albopictus* is a competent vector. It survives in both rural and urban environments, it is long lived (4-8 weeks), has a long flight radius, is aggressive, silent, diurnal and its eggs are resistant to environmental factors (Schwartz et al. 2010). Furthermore, its global distribution is expanding. Currently it is present in Indian Ocean region, South-East Asia, 25% of the United States and at least 12 European countries. However, according to European CDC (2009) the mosquito will be present in >90% of European territory by 2030. Introduction of CHIKV bearing the A226V mutation into an area where *Ae. albopictus* is present may contribute to an explosive epidemic similar to that seen in La Réunion.

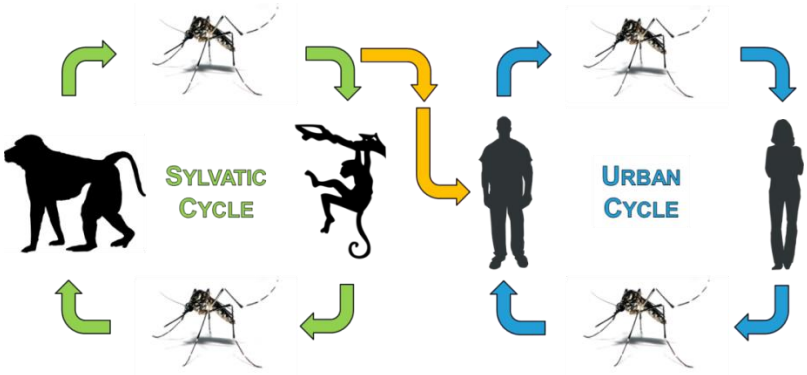

Figure 1.7. Life cycle of chikungunya virus. Sylvatic cycle is observed primarily in Africa, CHIKV is maintained between forest-dwelling *Aedes* mosquitoes and wild non-human primates, human outbreaks are usually small and confined. Urban transmission cycle is observed primarily in Asia, Indian Ocean and Caribbean region, CHIKV circulates between humans and mosquitoes.

1.7 Chikungunya disease

Deaths directly or indirectly caused by CHIKV are rare (approximately 1 in 1000) (Staples et al. 2009). Risk factors include underlying medical conditions (hypertension, diabetes mellitus, respiratory conditions), co-infection (particularly by Dengue virus) and age > 85 years (Das et al. 2010). Approximately 95% of individuals infected with CHIKV is symptomatic (Thiboutot et al. 2010, Das et al. 2010). The incubation period is 2-7 days. Infection is characterised by a transient high-titre viraemia (10^5-10^9 plaque forming units per ml of blood) that peaks around day 1-2 post-infection and lasts for up to a week (Hoarau et al. 2010). The symptoms start abruptly with high fever, myalgia, rash and severe polyarthralgia, which is the defining characteristic of CHIKV (Staikowsky et al. 2009, Staples et al. 2009, Thiboutot et al. 2010, Simon et al. 2011). Additional symptoms may include headache, fatigue, nausea, vomiting and conjunctivitis. The pain affects primarily limbs and is symmetric (Staples et al. 2009, de Andrade et al. 2010). It occurs mostly in ankles, wrists, fingers, knees, shoulders and elbows (Table 1.1). The joint and muscle pain is incapacitating and it causes a characteristic stooped posture in affected individuals. Thus the name 'chikungunya', which means "that which bends up" in the Makonde language (Cavrini et al. 2009). The acute symptoms of CHIKV infection typically resolve within 2 weeks, except for polyarthralgia.

Table 1.1. **Joint pain manifestation in patients suffering from CHIKV infection.** (de Andrade et al. 2010)

Location of joint pain	**Percentage of patients (%)**
Shoulder	54
Elbow	48
Hand / wrist	77
Hip	9
Knee	72
Ankle / foot	81

A study by de Andrade et al. (2010) showed that over 50% of convalescent patients suffered from chronic pain for a mean duration of 90 days. Females were more likely to suffer from chronic pain than males, which was also observed in Singapore (Win et al. 2010). Similarly, Sissoko et al. (2009) reported that at 15 months following the disease onset 57% of patients reported rheumatic symptoms, 36% reported permanent suffering and 22% reported recurring symptoms. Risk factors included age ≥45 years, severe initial joint pain, and presence of osteoarthritis. Bouquillard et al. (2009) reported condition similar to rheumatoid arthritis in 10-20% of patients 4 to 36 months post the onset of acute infection. Joint manifestations are not usually observed in neonates and infants (Suhrbier et al. 2009).

Atypical symptoms associated with CHIKV infection have been reviewed by Rajapakse et al. (2010). Most notably, they include neurological manifestations. Conditions such as, seizures, acute flaccid paralysis meningitis, encephalitis, meningoencephalitis, encephalomyeloradiculitis, altered level of consciousness and Guillain-Barré syndrome have been reported, most notably in neonates but also in young children and adults (Arpino et al. 2009, Staples et al. 2009, Das et al. 2010). The onset of neurological symptoms is usually within 24 hours from the onset of fever. CHIKV infection has a significant impact on the quality of life, with working, mood and sleep affected the most (Soumahoro et al. 2009, de Andrade et al. 2010).

Robust host immune response is observed during the acute phase of infection. It includes dendritic cells (DC), Natural Killer cells (NK), and CD4- and CD8-positive T lymphocytes (Hoarau et al. 2010). The acute phase is universally characterised by an early IFN-α response (Hoarau et al. 2010, Chow et al. 2011, Wauquier et al. 2011, Kelvin et al. 2011, Dupuis-Maguiraga et al. 2012). Overall, the expression of Th1 and Th2 cytokines (including tumour necrosis factor-α) is low. However, high levels of interferon (IFN)-γ and interleukin (IL)-12 were reported in some acute patients (Hoarau et al. 2010, Wauquier et al. 2011). There is a correlation between the viral load and concentrations of IFN-α, IL-1-RA, IL-6, macrophage chemoattractant protein (MCP)-1, IL-12, interferon-inducible protein (IP)-10, IL-18 and IL-18BP (Chaaithanya et al. 2011, Chow et al. 2011).

The chronic phase of infection is associated with increased levels of IL-6, IL-12, and granulocyte-macrophage colony stimulating factor (GM-CSF) (Hoarau et al. 2010, Chow et al. 2011). However, the upregulation of all the above factors has never been observed at once. Anti-CHIKV IgM can persist for up to 24 months after the onset of the disease (Malvy et al. 2009, Hoarau et al. 2010). The role of the adaptive immune response in the CHIKV chronic disease is not currently known.

1.8 Treatment and vaccination

Presently, there is no effective treatment against CHIKV infection. The therapy is usually supportive and aims to alleviate symptoms. However, studies continue to investigate effective treatments (Pohjala et al. 2011, Kaur et al. 2013, Parashar et al. 2014, Lani et al. 2015). Interestingly, human immune plasma was shown to be effective in a mouse model when administrated up to 8 hours post-infection (Couderc et al. 2009). Similar treatment had been proven effective in humans against West Nile virus (Shimoni et al. 2001). There is no commercially available vaccine for CHIKV infection. However, multiple candidates are currently being investigated (Plante et al. 2011, García-Arriaza et al. 2014, Roy et al. 2014, Weger-Lucarelli et al. 2014, Chang et al. 2014, Hallengärd et al. 2014). Preliminary data from most studies are encouraging. A vaccine based on virus-like particles (VLPs) successfully completed a phase 1 clinical trial in humans (Chang et al. 2014).

1.9 Mononuclear phagocyte system and alphavirus arthritis

Mononuclear phagocyte system has been defined as a haematopoietic cell lineage derived from progenitor cells in the bone marrow, which differentiates to form monocytes circulating in the blood that can enter tissue to become resident tissue macrophages (Hume et al. 2002). Colony-stimulating factor-1 (CSF-1) has been identified as the key macrophage growth factor (Hume 2006). The importance of macrophages in the development of rheumatoid arthritis has been well established (Kinne et al. 2000, Suhrbier et al. 2009). However, the involvement of macrophages in the pathogenesis of viral arthritis is generally not well understood (Perl 1999, Assunção-Miranda et al. 2013).

RRV is an alphavirus closely related to CHIKV. Human infection can cause arthralgia and arthritis similar to that of CHIKV (Rulli et al. 2005). In a mouse model of RRV disease, infiltration of mononuclear cells into skeletal muscles and joints is observed (Rulli et al. 2005, Morrison et al. 2006). Infection of macrophages with RRV *in vitro* leads to an increased expression of proinflammatory factors TNF-α, macrophage inflammatory protein (MIP)-1α, MCP-1, IL-1β, IL-8 and IFN-γ, which contributes to RRV-induced inflammatory disease (Mateo et al. 2000, Lidbury et al. 2008). Mice depleted of macrophages and infected with RRV showed reduced levels of proinflammatory factors detected and did not develop inflammation of joints and skeletal muscles (Lidbury et al. 2008). The adaptive immune response was demonstrated not to play a role in RRV-induced arthralgia/arthritis (Morrison et al. 2006). RRV was found to persist in human macrophages for up to 170 days post-infection (Rulli et al. 2005). It has been proposed that a spontaneous or stress-induced increase in RRV replication in persistently infected macrophages may be associated with the periodical relapses of symptoms observed in RRV disease (Way et al. 2002). RRV infection of monocytes and macrophages can be promoted by antibody-dependent enhancement (Linn et al. 1996, Takada et al. 2003).

SINV is another alphavirus that causes arthritis in humans. Its replication in human macrophages was demonstrated by Assunção-Miranda et al. (2010). The infection promotes macrophage activation and leads to expression of proinflammatory cytokines TNF-α, IL-1β and IL-6, which is followed by expression of matrix metalloproteinases (MMPs) 1 and 3.

1.10 Chikungunya infection of human monocytes and macrophages

Infection of human monocytes and macrophages with CHIKV has been studied in some detail *in vitro* and *in vivo*. However, there is still debate as to the sensitivity of these cells to CHIKV (Schwartz et al. 2010). Her et al. (2010) observed CHIKV antigens in blood monocytes from acutely infected patients (n=14). He also noted a correlation between the number of monocytes positive for CHIKV antigen and the viral load. This was not supported by Sourisseau et al. (2007) who reported no detectable levels of viral RNA in blood cells from acutely infected patients with high

viral load in blood plasma (n=3). Unfortunately, the number of samples tested in both studies was low and patient-specific factors or differences in virus strains may have contributed to the observed discrepancy. Sourisseau et al. also reported that peripheral blood mononuclear cells (PBMCs) from healthy donors were not susceptible to infection with CHIKV *in vitro* at MOI of 10. By contrast, Her et al. (2010) and Teng et al. (2012) demonstrated that monocytes, and to very small extent B-cells, from whole blood were susceptible to infection with CHIKV *in vitro* at MOI of 10. Human monocyte-derived-macrophages were shown to be productively infected with CHIKV *in vitro* (Sourisseau et al. 2007, Labadie et al. 2010).

The lack of consistency between the *in vitro* studies described above has been a matter of debate for some time. It has been suggested, that the differences observed may have been be due to the quality of the virus inoculum used. One of the theories proposed that presence of apoptotic debris in cell-culture-derived CHIKV inoculum that was not suitably purified (e.g. by ultracentrifugation via a sucrose gradient) could promote infection of macrophages with CHIKV by a novel mechanism. This was investigated by Krejbich-Trotot et al. (2011) who demonstrated that CHIKV may infect mouse and human macrophages via engulfment of apoptotic blebs from virus-infected neighbouring cells. In brief, primary cultures of mouse macrophages and macrophages derived from PMA-differentiated cell lines MM6 and Thp-1 were infected with supernatant from CHIKV-infected HeLa cells that was either depleted for apoptotic debris (filtered through 0.2 μm) or used crude (unfiltered). The viral load in both inoculums was comparable. The presence of apoptotic debris significantly contributed to CHIKV infection of macrophages even though they were refractory to infection with CHIKV alone. The direct interaction between the apoptotic blebs positive for CHIKV antigen and macrophages was confirmed microscopically. The infection of differentiated Thp-1 cells via apoptotic debris was inhibited when Thp-1 cells were pre-treated with engulfment inhibitors Annexin V and Cytochlasin B. CHIKV replication in macrophages infected via apoptotic debris did not induce a proinflammatory response. This novel mechanism may allow CHIKV to escape host cell defences and induce a robust adaptive immune response against self-antigens contained within the blebs leading to an autoimmune response

(Rosen et al. 1995, Krejbich-Trotot, et al. 2011). If true for CHIKV, this could contribute to the long-term persistence of the virus in joints of some patients, and the joint disease itself. Interestingly, in 1995 Rosen et al. reported presence of nucleocapsids in apoptotic blebs budding from HeLa cells infected with a different alphavirus, SINV. Unfortunately Krejbich-Trotot et al. did not investigate the role of apoptotic debris in the infection of human primary macrophages and fibroblasts, the nature of the infectious material present within the apoptotic blebs (e.g. intact virus or genomic RNA), or the detailed mechanism by which it can infect macrophages following the engulfment of the apoptotic blebs.

The antibody-dependent enhancement (ADE) may also play a role in the establishment of persistent CHIKV infection in macrophages *in vivo*. The ADE of virus infection is a process in which non-neutralising virus-specific antibodies enhance virus infection of Fc receptor-positive cells such as monocytes, macrophages and granulocytes (Tirado et al. 2003, Flipse et al. 2013). As a consequence, it can result in an overall increase of virus replication, a higher viral load and a more severe disease. The ADE is initiated when antibodies bind to virus particles. The resulting virus-antibody complexes bind to Fc receptors on the surface of cells leading to increased infectivity in these cells. There are several possible mechanisms to explain this process. Most likely the ADE involves bringing virus particles into close proximity to virus-specific cell surface receptors, or a promotion of virus uptake into target cells via Fc receptor-mediated phagocytosis. Invariably, the ADE can bypass the normal mode of virus cell entry resulting in an infection of cells that the virus does not normally infect. Among viruses that cause arthritis, the ADE has been well documented for RRV (as mentioned previously) and dengue virus (DENV) (Tirado et al. 2003, Chareonsirisuthigul et al. 2007, Flipse et al. 2013). Interestingly, RRV can induce immunosuppressive L-10 and suppress proinflammatory TNF-α and inducible nitric oxide synthase production in macrophages infected via ADE (Takada et al. 2003, Rulli et al. 2005). Similarly, ADE of DENV infection upregulates the production of anti-inflammatory cytokines (Chareonsirisuthigul et al. 2007). The role of ADE in CHIKV infection of monocytes and macrophages is not yet known.

Finally, RNA and CHIKV antigens were found in perivascular synovial macrophages of a chronic patient 18 months post-infection (Hoarau et al. 2010). Levels of MCP-1, IL-6 and IL-8 observed in synovial fluid were high in comparison to serum of the same patient. Secretion profiles from monocytes infected with CHIKV *in vitro* showed high levels of IFN-α, IL-12, IL-1Ra and IP10, and decreased levels of RANTES, IL-8 and MIP-1β (Her et al. 2010, Ng et al. 2010).

1.11 Animal models of CHIKV infection

CHIKV does not readily infect adult wild-type mice and hence generating a mouse model that accurately mimics the disease observed in humans is challenging (Teo et al. 2012). Initial models relied on animals that were immunocompromised, either IFN-α/ß receptor knockout mice (IFNAR) or neonatal mice. As a result they could not accurately reproduce CHIKV pathogenesis observed in humans. In 2010, Gardner et al. proposed a model that reproduced some aspects of CHIKV-induced arthralgia/arthritis in adult wild-type mice of C57BL/6 background. Mice are inoculated with 10^4 $CCID_{50}$ of virus in 40 µl of RPMI medium subcutaneously into the ventral side of each hind foot, toward the ankle. Infection leads to the development of a transient peripheral blood viraemia and foot swelling. Virus is detected in muscle tissue. Symptoms of arthritis in the foot are associated with a prolific infiltration of monocytes and macrophages into and around of the synovial membrane and the underlying connective tissue. The infiltrates are observed in the peritendinous tissue for up to 21 days. The infection is associated with increased levels of TNF-α, MCP-1, IFN-γ, IL-6 and IFN-α (Gardner et al. 2010, Rulli et al. 2011). Depletion of macrophages ameliorates but not eliminates the rheumatic disease. Primary mouse macrophages are productively infected *in vitro*. However, there is no evidence that they are infected with CHIKV *in vivo*. Treatment with Bindarit (MCP inhibitor) reduces the number of muscle and joint tissue-infiltrating mononuclear cells and ameliorates CHIKV disease in mice (Rulli et al. 2011).

Nonhuman primates have the physiology and the immune system very similar to that of humans (Walsh et al. 1996). They have been shown to be relevant for studies of alphavirus pathogenesis and arthritic diseases (Reed et al. 2005, Vierboom et al.

2007). Labadie et al. (2010) established a nonhuman model of CHIKV infection in cynomolgus macaques (*Macaca fascicularis*). A clear relationship between the inoculation dose and the severity of the disease was observed. Typically, animals inoculated with a high dose of CHIKV (>10^7 PFU) demonstrate swelling of joints, clinical symptoms of meningoencephalitis and/or mortality. On the other hand, animals inoculated with a low dose (10^1 PFU) do not develop a clinical disease. The pathophysiological basis of CHIKV disease were analysed in 3-5 year old males intravenously infected with an intermediate dose of 10^3 PFU. The model mimics viral, clinical and pathological features of human acute disease, however, the chronic arthritis/arthralgia are not well reproduced.

The acute phase of infection lasts for up to a week. It is characterised by a high viraemia lasting 4-7 days (10^8-10^9 genome copies/ml), high fever (up to 39.6 ºC), skin rash, lymphopenia, monocytopenia, granulocytosis, mononuclear cell infiltration of synovial tissue, sharp rise and then fall of IFN-α/ß and IL-6 concentrations, and gradual rise and then decline of MCP-1 and IFN-γ concentrations. The level of TNF-α is significantly increased. Cytokine profiles are similar to the mouse model described above and are consistent with monocyte recruitment and macrophage activation. CHIKV RNA is detected at high levels in spleen, lymph nodes, liver, and at moderate levels in joints, skin, muscle, and central nervous system.

The chronic phase of the infection is characterised by the return of leukocyte levels to normal, presence of CHIKV RNA in lymphoid organs and liver for up to 2 months, persistence of activated macrophages, and persistence of CHIKV RNA and antigen in lymphoid organs and liver for up to 90 days post-infection. Monocytes and macrophages are infected with CHIKV *in vivo*. $CD68^+$ cells positive for viral antigen were present in spleens of all animals 90 days post infection with CHIKV. Viral RNA was detected in these cells for up 19 days post-infection. Interestingly, two days post-infection the majority of $CD68^+$ cells in spleen were CHIKV antigen-positive. CD68 is a type I transmembrane proteins that is expressed in the endosomal compartment of all cells of the mononuclear phagocyte lineage, including monocytes and macrophages (Gough et al. 2001). It is conserved across mammals, including

humans and macaques. CD68 expression is believed to be driven by a macrophage-specific promoter (Gough et al. 2001). As a consequence, it is often used as a selective marker for monocytes and macrophages. However, there is evidence to suggest that CD68 is expressed in a range of haematopoietic and non-haematopoietic cells and is merely enriched in macrophages (Gottfried et al. 2008). Labadie et al. (2010) postulated that persistently infected macrophages acted as a reservoir for CHIKV during the late stages of infection in macaques.

In 2013, Messaoudi et al. demonstrated that reduced immune response (both innate and adaptive) in aged Rhesus macaques (*Macaca mulatta*) (>17 years old) promoted a long-term virus persistence in spleen relative to adult macaques (6-13 years old).

1.12 Semliki Forest virus as a model alphavirus

SFV is an alphavirus most closely related to CHIKV (Fazakerley 2002). It was first isolated in Uganda in 1942 from *Ae. abnormalis* mosquitoes (Smithburn et al. 1944). SFV is naturally found in sub-Saharan Africa where it is transmitted predominantly by *Ae. africanus* and *Ae. aegypti* mosquitoes. The natural vertebrate host of SFV is unknown but infections of monkeys, humans and horses have been reported (Robin et al. 1974, Willems et al. 1979, Mathiot et al. 1990, Fazakerley 2002).

In humans, SFV infections are typically asymptomatic or very mild (Mathiot et al. 1990). When present, symptoms include fever, headaches, myalgia and arthralgia. The acute phase lasts usually 2-4 days. The only recorded casualty attributed to SFV infection was a person who had a history of compromised immune system (Willems et al. 1979). In addition to the typical symptoms described above, the patient suffered from loss of speech, convulsion, coma, and cardiovascular and respiratory failure. The post-mortem examination revealed a typical viral meningoencephalomyelitis and SFV was isolated from both the cerebrospinal fluid and the brain.

Several wild-type strains of SFV have been demonstrated to infect mice, guinea pigs, rabbits and rats (Seamer et al. 1967, Bradish et al. 1971). Mouse models of SFV infection have been proven particularly valuable in studying virus pathogenesis

(Fazakerley 2004, Fragkoudis et al. 2007, Barry et al. 2010). SFV strains can be divided into two groups based on their virulence in adult mice (Bradish et al. 1971, Fazakerley 2002). Virulent strains of SFV include the L10, V13, Osterrieth and prototype (Bradish et al. 1971, Glasgow et al. 1991). The A7, A7(74), A8, V42 and MRS MP192/7 strains are avirulent (Henderson et al. 1970, Bradish et al. 1971, Deuber et al. 2007). In adult mice inoculated intraperitoneally (IP), all strains of SFV initially replicate in smooth muscles and in lymph nodes (Grimley et al. 1970, Murphy et al. 1970, Pusztai et al. 1971, Amor et al. 1996). A high titre plasma viraemia is observed within the first 24 hours post-infection (Pusztai et al. 1971, Fazakerley 2002). It peaks between 1 and 2 days post-infection and then falls rapidly. SFV is rarely detected in the blood after 4 days post-infection (Pusztai et al. 1971, Fazakerley et al. 1993). SFV is neuroinvasive (Fazakerley 2002). It enters the brain via cerebrovascular endothelial cells (Pathak et al. 1974). The virus replicates in oligodendrocytes and neurons (Pathak et al. 1978, Balluz et al. 1993, Fazakerley et al. 1993, Amor et al. 1996). SFV virulent strain L10 rapidly disseminates throughout the brain causing a fatal panencephalitis 3-4 days post-infection (Fazakerley et al. 1993). Post-mortem examination of infected brains shows widespread neuronal cell death (Fazakerley et al. 1993). The replication of SFV avirulent strain A7(74) is restricted in neurons of adult mice (>14 days of age) resulting in minimal cell death and survival of the infected animals (Fazakerley et al. 1993). Interestingly, mice infected with the A7(74) strain at the age of 12 days or less die of panencephalitis similar to that caused by the L10 strain (Fleming 1977, Fazakerley et al. 1993). The age-dependent virulence of the A7(74) strain is believed to be determined by the maturation status of the central nervous system (Fleming 1977, Fazakerley et al. 1993, Oliver et al. 1997, 1998).

SFV prototype strain was isolated from the same mosquito pool as the L10 strain (Bradish et al. 1971). It was one of the first viruses to be sequenced (Garoff et al. 1980, Takkinen 1986). SFV4 is the molecular clone of the prototype strain (Liljeström & Garoff 1991, Liljeström et al. 1991). *In vitro*, both SFV4 and SFV L10 demonstrate similar replication kinetics. However, in adult mice inoculated IP, SFV4 is only virulent when administered at a high dose (Fazakerley 2002). High-

throughput sequencing of the SFV L10 stock revealed 12 nucleotide differences between the two strains, six of which were nonsynonymous (Ferguson et al. 2015). A single amino acid changes in virus glycoprotein E2 was shown to increase the affinity of SFV4 to heparan sulphate resulting in a lower plasma virus load. A molecular clone of SFV L10 was generated in 2015 (Ferguson et al. 2015).

In the UK, SFV is classified as a hazard group (HG) 2 agent by Advisory Committee on Dangerous Pathogens (ACDP). It is not rated under the Specified Animal Pathogen Order (SAPO). In addition, many established cell lines are permissive to SFV infection *in vitro* (Deuber et al. 2007). Hence, SFV can often be used as a safer alternative to closely related but more pathogenic alphaviruses such as CHIKV (ACDP HG3) in proof-of-concept studies.

1.13 Alphavirus as a research tool

Alphavirus genome can be easily manipulated at the cDNA level. First, the infectious cDNA (icDNA) clone is generated by inserting virus cDNA into an expression vector, under control of the SP6, T7 or CMV immediate early promoter. Such icDNAs have been generated for many alphaviruses, including SFV and CHIKV (Rice et al. 1987, Davis et al. 1989, Liljeström & Garoff 1991).

Foreign sequences can be inserted into the genome of an alphavirus within its non-structural ORF, structural ORF, 3’ UTR and J region (Figure 1.8) (Pugachev et al. 1995, Higgs et al. 1999, Thomas et al. 2003, Bick et al. 2003, Vanlandingham et al. 2005, Frolova et al. 2006, Tsetsarkin et al. 2006, Tamberg et al. 2007, Atasheva et al. 2007, Fragkoudis et al. 2007, Sun et al. 2014). A large array of inserts has been tested and used with alphaviruses and multiple inserts can be cloned into one virus genome. The maximum size of all inserts is limited to approximately 5,000 nucleotides per genome and is determined by the packaging capacity of an alphavirus capsid (Andres Merits, the University of Tartu, personal communication).

The length and the nature of an insert are important determinants of genetic stability demonstrated by the virus. Typically, the larger the insert, the less stable the virus is (Hahn et al. 1989, Chen et al. 1995, Pugachev et al. 1995, Caley et al. 1999, Higgs et al. 1999, Sun et al. 2014). Genetic stability is also affected by the location of an insert. Typically, transgenes cloned into either the non-structural or the structural ORFs are more stable than transgenes cloned into either the J region or the 3' UTR (Pugachev et al. 1995, Caley et al. 1999, Vanlandingham et al. 2005, Tsetsarkin et al. 2006, Fragkoudis et al. 2007). In addition, constructs inserted into the J region are typically more stable than constructs inserted into the 3' UTR (Pugachev et al. 1995, Brault et al. 2004, Vanlandingham et al. 2005, Tsetsarkin et al. 2006).

The expression of foreign genes cloned into the non-structural ORF is not as strong and prolonged as the expression of genes under control of the subgenomic promoter, or a duplicated subgenomic promoter (Pugachev et al. 1995, Caley et al. 1999, Vanlandingham et al. 2005, Tsetsarkin et al. 2006, Garmashova et al. 2006).

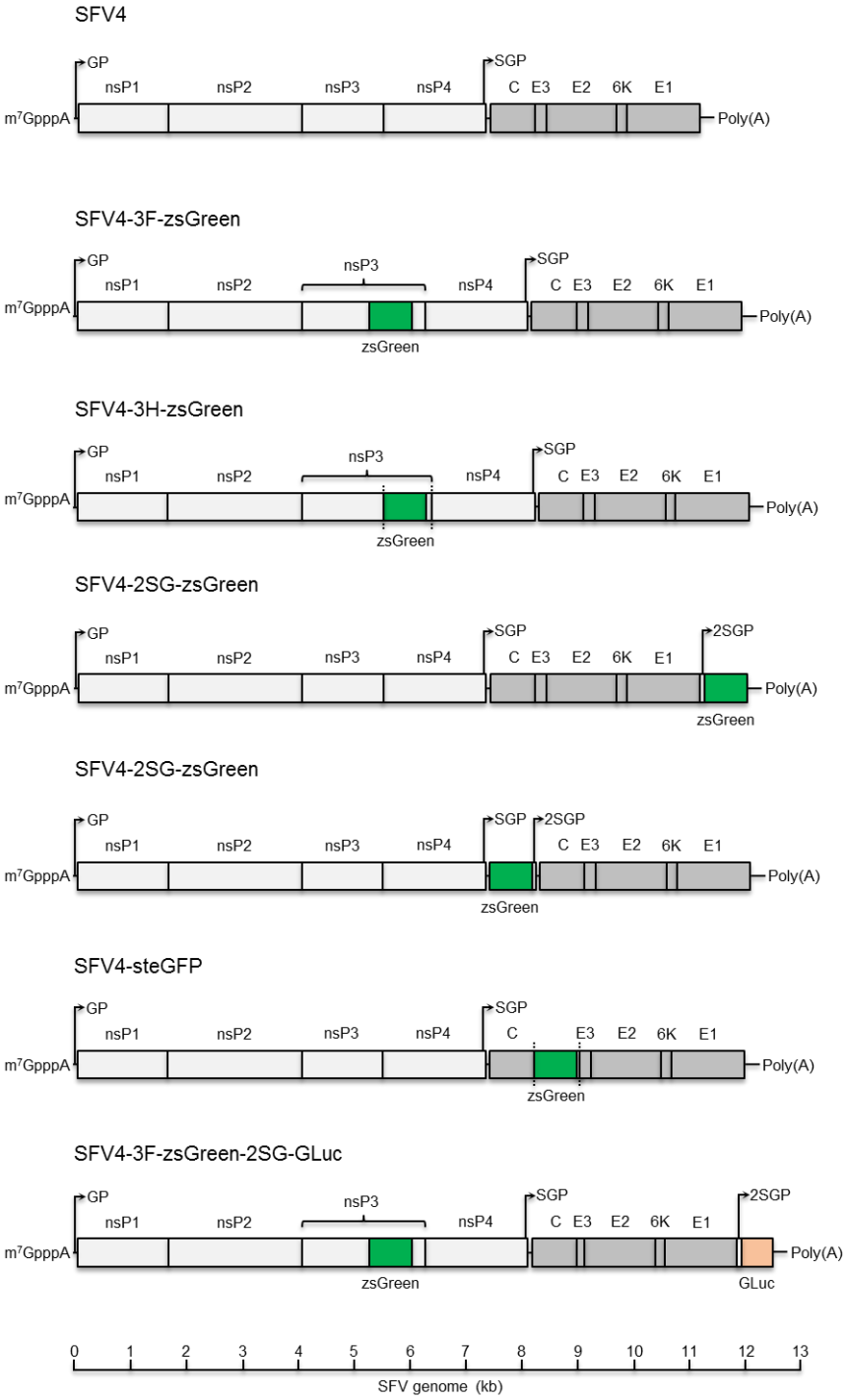

Figure 1.8. Schematic representation of potential SFV4 clones encoding marker genes in different genomic locations. nsP-non-structural protein; GP – genomic promoter; SGP – subgenomic promoter; 2SGP – duplicated subgenomic promoter; C – capsid; E1-E3 – envelope glycoproteins; GLuc – *Gaussia* luciferase; vertical dashed line – protein cleavage sites; Poly(A) – Poly(A) tail; m^7GpppA – 5' CAP; 3F – fused to nsP3; 3H – cleaved from nsP3.

Virus replicons do not encode the structural ORF in their genome (Figure 1.9). They are replication-deficient and cannot establish a productive infection. To generate virus replicon particles (VRPs) structural genes have to be provided *in trans* as a separate RNA that lacks the packaging signal, or in a packaging cell line (Figure 1.10) (Polo et al. 1999, Karlsson et al. 2003).

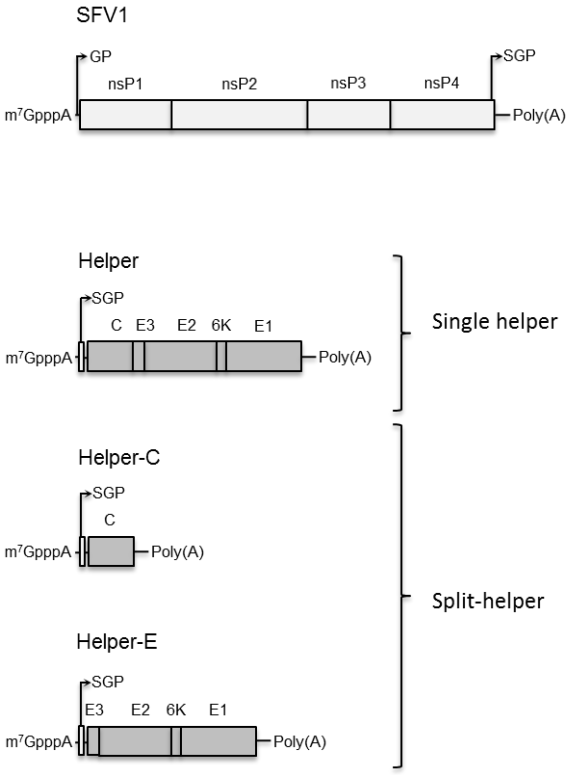

Figure 1.9. Schematic representation of SFV replicon, single-helper construct, and split-helper constructs. SFV1 – Semliki Forest virus replicon based on SFV4; nsP-non-structural protein; GP – genomic promoter; SGP – subgenomic promoter; C – capsid; E1-E3 – envelope glycoproteins; Poly(A) – Poly(A) tail; m^7GpppA – 5' CAP.

To generate VRPs, structural genes may be provided *in trans* using either a single helper system or a split-helper system (Figure 1.9). In a single helper system, all structural genes are provided on a single RNA message. However, recombinations between replicon and helper plasmids can lead to production of an infectious virus (Berglund et al. 1993, Pushko et al. 1997). This problem is circumvented in the split-helper system where glycoproteins and capsid are provided as two separate RNA messages (Smerdou et al. 1999).

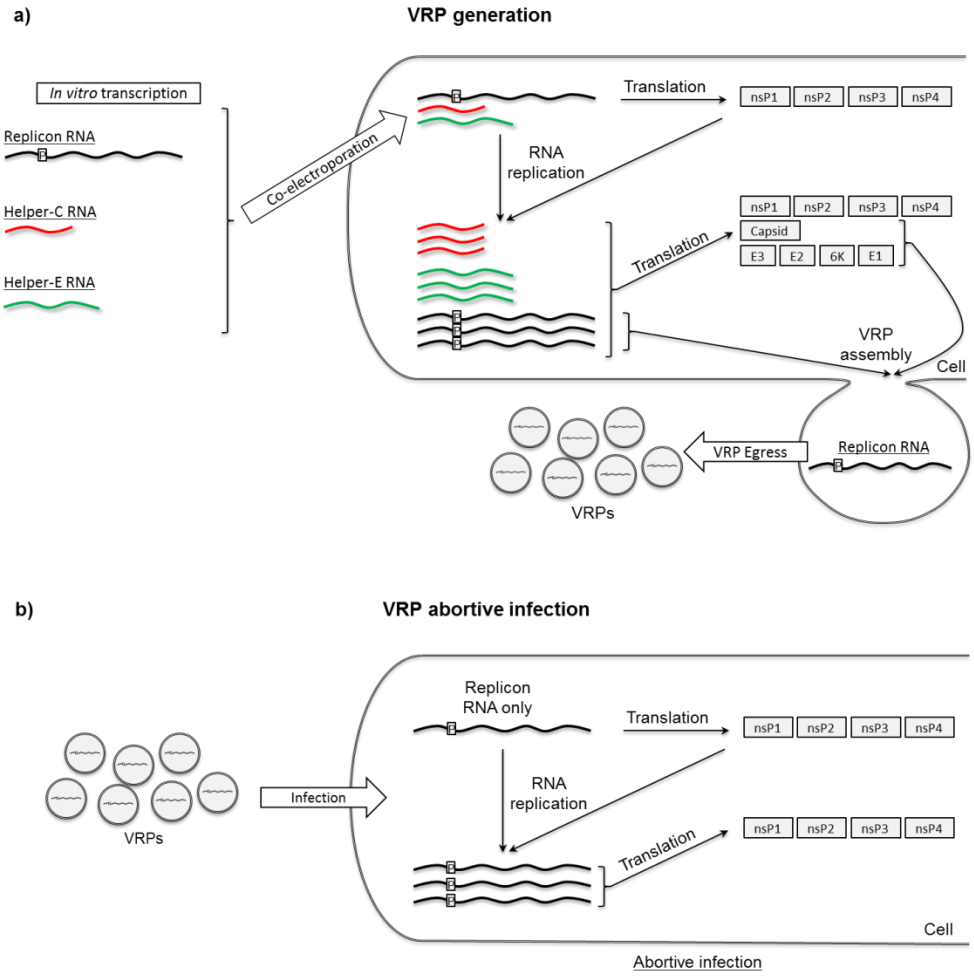

Figure 1.10. Schematic representations of VRP production and VRP infection. (a) Virus replicon RNA, Helper-C RNA and Helper-E RNA are electroporated/ transfected into cells to generate VRPs. Only replicon RNA encodes the packaging signal [P] located within the gene of nsP2. (b) Upon infection of a cell, replicon genome is replicated. However, in absence of the structural ORF no virus particles are being produced.

Similarly to full-length virus, replicons may be modified to encode marker genes in multiple genomic locations (Figure 1.11). Since replicons lack the structural region, their coding capacity is increased in comparison to a replication-competent virus.

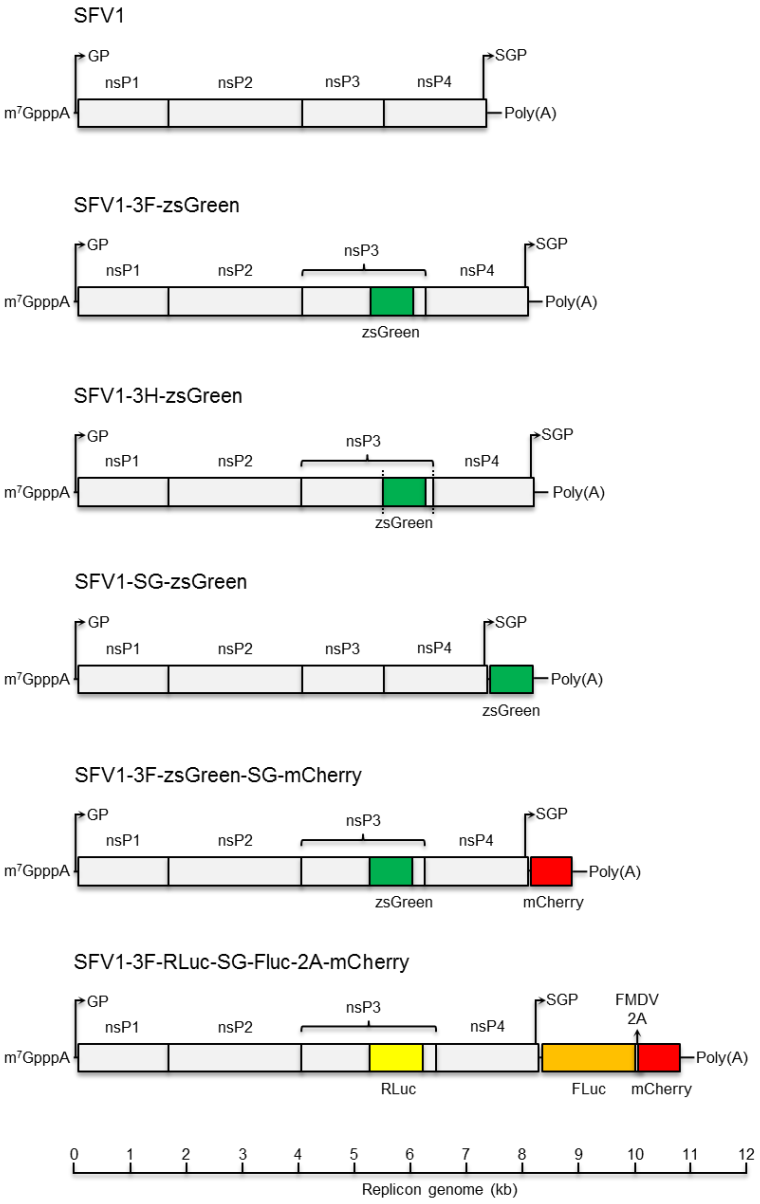

Figure 1.11. Schematic representation of SFV1 clones encoding marker genes in different genomic locations. SFV1 – Semliki Forest virus replicon based on SFV4; nsP-non-structural protein; GP – genomic promoter; SGP – subgenomic promoter; C – capsid; E1-E3 – envelope glycoproteins; GLuc – *Gaussia* luciferase; Poly(A) – Poly(A) tail; m^7GpppA – 5' CAP; 3F – fused to nsP3; 3H – cleaved from nsP3.

SFV has been successfully used as a vector for vaccines and transgene expression (Frolov et al. 1996, Colmenero et al. 2001, Lundstrom et al. 2001). This has been possible because of its unique features:

1. Safe to use.
2. Large coding capacity.
3. High level of transient heterologous protein expression.
4. Ability to induce humoral and cellular immunity.
5. Wide host and cell tropism.
6. Lack of pre-existing immunity.

1.14 Harnessing endogenous cellular miRNAs to control viral tissue tropism

MicroRNAs (miRNAs) are 18-22 nucleotide long endogenous RNAs that function as post-transcriptional regulators of gene expression (He et al. 2004, Bushati et al. 2007). MiRNAs do so by binding to complementary sequences present primarily in the 3' non-translated (NTR) region of host messenger RNAs (mRNAs) (Bartel 2004, Lim et al. 2005, Guo et al. 2010). The extent of complementarity between a miRNA and its target mRNA leads to either translational repression of the mRNA or its degradation (Lagos-Quintana et al. 2001, Bartel 2004, Doench 2004, Bushati et al. 2007, Guo et al. 2010, Djuranovic et al. 2012).

MiRNAs are encoded in mammalian genome within introns of protein-coding pre-mRNAs or as independent transcription entities (Lagos-Quintana et al. 2001, Lau et al. 2001, Swaminathan et al. 2013). The primary miRNA transcript (pri-miRNA) is generated by RNA polymerase II and it contains a stem-loop-like structure (Lee et al. 2004). Pri-miRNAs are processed by the nuclear microprocessor complex, which is composed of the RNase III protein Drosha and a double-stranded RNA (dsRNA)-binding protein DGCR8 (the DiGeorge syndrome critical region 8) to produce a 60-70 nucleotide hairpin termed pre-miRNA (Bartel 2004). The pre-mRNA hairpin contains a 3' overhang of 2 nucleotides that is necessary for transport of the pre-miRNA into the cytoplasm via Exportin 5 (Yi et al. 2003, Lund et al. 2004). In the cytoplasm, pre-miRNAs are recognised and processed by RNase III protein Dicer to produce an RNA duplex of 10-25 nucleotides (Koscianska et al. 2011). One of the

two strands, known as the guide strand (the miRNA), is recruited into the multiprotein RNA-induced silencing complex (RISC). A miRNA-loaded RISC binds the target mRNA in a sequence-dependent manner via the seed region of the miRNA (bases 2-8 of the miRNA) (Lai 2002, Lewis et al. 2005, tenOever 2013, Swaminathan et al. 2013). The base pairing must occur with full complementarity in the miRNA seed region but occurs only with partial complementarity outside of. This leads to a translational repression of the mRNA but not its degradation. However, miRNA-loaded RISC will cleave a fully complementary target, including viral RNA (Figure 1.12) (tenOever 2013). In such case, the miRNA acts effectively like a small interfering RNA (siRNA) (tenOever 2013).

MiRNAs are involved in cell development and they control many aspects of cellular physiology (Chen et al. 2007). As a result, miRNA expression patterns are tissue specific and tissues are defined by expression of specific miRNAs (Lagos-Quintana et al. 2002, Chen et al. 2004, Barnes et al. 2008). The abundance of an individual miRNA may vary greatly between different cell lineages and tissues (Lagos-Quintana et al. 2002, Lu et al. 2005, Kelly et al. 2008).

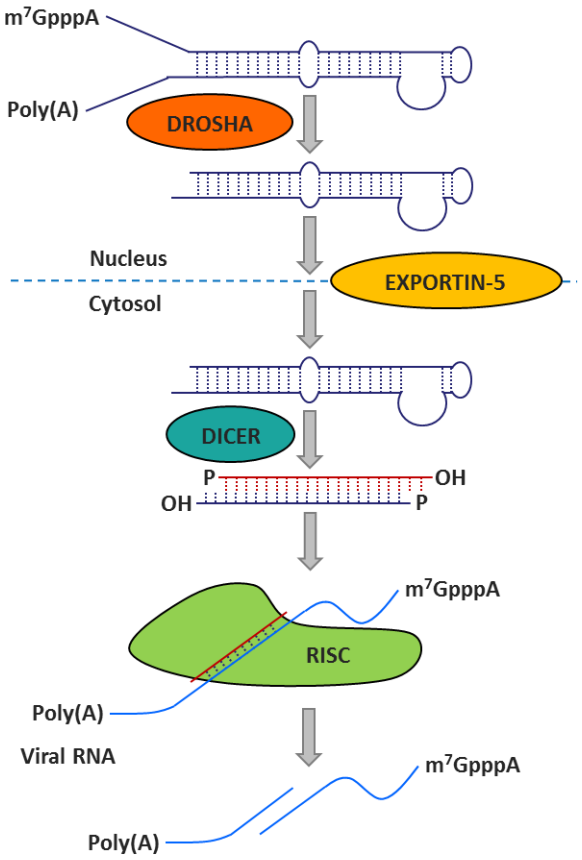

Figure 1.12. Using cellular RNA silencing pathway to target alphavirus genome for degradation. The primary miRNA transcript (pri-miRNA) is generated by RNA polymerase II. The pri-miRNAs are processed by Drosha to produce a pre-miRNA, which is transported into the cytoplasm via Exportin 5. In cytoplasm, pre-miRNAs are processed Dicer to produce an RNA duplex of 10-25 nucleotides. MiRNA is recruited into the RISC complex. The miRNA-loaded RISC mediates cleavage of the target viral RNA encoding a fully complementary miRNA target sequence.

In recent years, host miRNAs have been employed to control tissue tropism of dengue virus, SFV, influenza A virus, vesicular stomatitis virus, poliovirus, lentivirus, Japanese encephalitis virus and measles virus (Brown et al. 2006, Gottwein et al. 2006, Barnes et al. 2008, Edge et al. 2008, Papapetrou et al. 2009, Colin et al. 2009, Perez et al. 2009, Kelly et al. 2010, Lee et al. 2010, Kamrud et al. 2010, Heiss et al. 2011, 2012, Leber et al. 2011, Yen et al. 2011, Pham et al. 2012, Langlois et al. 2012, Ratnik et al. 2013, Ylösmäki et al. 2013, Shen et al. 2015,

Tsetsarkin et al. 2015, Feng et al. 2015). The tropism of each virus was restricted by a miRNA recognition element (RE) inserted into the virus genome, most often in its 3' UTR but also in the coding region. Each miRNA RE was designed to incorporate one to six copies of a target sequence fully complementary to an endogenous miRNA that was cell-, tissue- or species-specific. Replication of the resulting viruses was significantly inhibited in the presence of their cognate miRNAs but not otherwise. This typically led to an attenuated phenotype and a strong protective immunity observed *in vivo*. Neuronal-specific miR-124, haematopoietic-specific miR-124-3P and ubiquitously expressed miRNA let-7 were exploited to inhibit virus replication most frequently.

Ratnik et al. (2013) demonstrated that a miRNA RE inserted into the coding region of a virus was not as effective at attenuating virus replication as an identical RE inserted into the 3' UTR. Heiss et al. (2012) demonstrated that a single copy of a target sequence to miR-124 inserted into the 3' UTR of a chimeric tick borne encephalitis virus/dengue virus was sufficient to prevent virus neurovirulence in the mature mouse central nervous system. However, the virus was shown to revert to its neurovirulent phenotype by accumulating single point mutations within the target sequence. Incorporation of multiple targets (up to 4) increased the stability of the virus and the RE with four targets yielded the most attenuated phenotype *in vivo*. Pham et al. (2012) reported that a highly attenuated dengue virus encoding a RE with 4 copies of target sequence to miR-142-3P was reverting to its virulent phenotype by complete excision of the RE from the virus genome *in vivo*.

As discussed above, miR-142-3P is commonly used to control viral tissue tropism in haematopoietic cells. It is highly conserved in all vertebrates and it is expressed to high levels in haematopoietic cells (Region, Lagos-Quintana et al. 2002, Baskerville et al. 2005, Ramkissoon et al. 2006, Jin et al. 2008, Yuan et al. 2008, Reddy et al. 2009, Sun et al. 2010, Bissels et al. 2011, Wang et al. 2012, Hamer et al. 2014). In fact, it is one of the most highly expressed cellular miRNAs in haematopoietic cells (Nimmo et al. 2013, Sun et al. 2015), it is constitutively expressed (Sun et al. 2013) and its activity is robust (Brown et al. 2006). MiR-142-3P has been implicated in

regulation of cell maturation and differentiation (Yuan et al. 2008, Liao et al. 2008, Sun et al. 2011, 2013, Wang et al. 2012, Nishiyama et al. 2012, Lagrange et al. 2013, Nimmo et al. 2013, Lu et al. 2013). Abnormal expression of miR-142-3P has been observed in some cancers (Yuan et al. 2008, Wu et al. 2011, Lv et al. 2012, Kwanhian et al. 2012).

Remarkably, Trobaugh et al. (2014) reported presence of four functional miR-142-3P target sites in the 3'UTR of wild-type North American EEEV. Three of them were conserved in 17 out of 23 sequenced isolates of North American EEEV strains. The authors postulated that the restriction of EEEV replication in myeloid cells limited the induction of innate immune response in these cells and consequently promoted the neurological disease. The region encompassing the target sites was required for an efficient infection of mosquito vectors with EEEV. This may explain why the target sites were maintained in EEEV despite its rapid RNA mutation rate.

1.15 Hypothesis and aims

1.15.1 Hypothesis:

1) Human primary macrophages can be infected with CHIKV/SFV by a mechanism involving apoptotic debris from virus-infected fibroblasts.

   The hypothesis is based on previously discussed findings by Krejbich-Trotot et al. (2011) who demonstrated that primary cultures of mouse macrophages and macrophage cell lines (MM6 and Thp-1) were infected with CHIKV by engulfment of apoptotic debris from virus-infected epithelial HeLa cells even though they were refractory to infection with CHIKV alone.

2) Infection of monocytes and macrophages with CHIKV contributes to clinical disease and virus persistence.

   The hypothesis is based on several previously discussed findings. Human monocyte-derived macrophages are productively infected with CHIKV (Sourisseau et al. 2007, Labadie et al. 2010). RNA and CHIKV antigens were found in perivascular synovial macrophages of a chronic CHIKV patient 18 months post-infection (Hoarau et al. 2010). In spleens from CHIKV infected macaques, $CD68^+$ macrophages positive for viral antigen are present 90 days post infection (Labadie et al. 2010). Viral RNA is detected in these cells for up 19 days post-infection. Persistently infected macrophages may act as a reservoir for CHIKV during the late stage of infection in macaques (Labadie et al. 2010). Persistent infection of mouse macrophages with CHIKV *in vitro* has been reported (Kumar et al. 2012). Her et al. (2010) observed CHIKV antigens in blood monocytes from acutely infected patients. These cells may act as vehicles for virus dissemination during the early phase of CHIKV infection. Her et al. (2010) and Teng et al. (2012) demonstrated that monocytes from whole blood were susceptible to infection with CHIKV *in vitro*.

1.15.2 Aims:

1) To determine the mechanism of human MDM infection with SFV (Chapter 3).

   SFV was used as a surrogate for CHIKV. The capacity of purified virus to infect human MDMs *in vitro* was investigated. The capacity of cell debris from SFV-infected human cell lines to increase the rate at which SFV infects human MDMs was tested. The nature of the infectious material present within cell debris from SFV-infected cells was investigated.

2) To design and generate a miRNA recognition element (RE) that will inhibit alphavirus replication in haematopoietic cells (Chapter 4).

   A miRNA RE with target sequences fully complementary to haematopoietic-specific miR-142-3P (miR-142-3P RE) was designed and generated.

3) To investigate the effect of miR-142-3P RE on alphavirus replication in cells that express miR-142-3P using SFV in proof-of-concept studies (Chapter 4).

   SFV was modified to encode miR-142-3P RE in the 3' UTR of the genome. Replication of the modified virus was investigated *in vitro* in haematopoietic cells, *in vitro* in non-haematopoietic cells induced to express miR-142-3P, and *in vivo* in IFN-α/ß receptor knockout mice. The stability of the virus (*in vitro* and *in vivo*) was tested.

4) To generate CHIKV that is unable to replicate in haematopoietic cells (Chapter 5).

   CHIKV was modified to encode miR-142-3P RE in the J region of the genome. Replication of the modified virus was investigated *in vitro* in haematopoietic cells and in non-haematopoietic cells induced to express miR-142-3P. The *in vitro* stability of the virus was tested.

5) To investigating the role of monocyte and macrophage infection with CHIKV in the nonhuman primate model of chikungunya disease.

The pathogenesis of CHIKV encoding miR-142-3P RE was investigated in the cynomolgus macaque model of CHIKV disease. At the time of writing this thesis the study was not yet completed.

Chapter 2:

Materials and methods

Contents:

2.1 Details of reagents, consumables, buffers and equipment

The full details of all reagents, consumables, buffers and equipment used in this project are located in Annex 1-11. The details were accurate on 1st June 2015.

2.2 Cells

2.2.1 Primary cells

Primary cells and cell lines used in this project are listed and described in Table 2.1.

Table 2.1. Primary cells used in this project.

Name	Type	Species	Further details	Source
NHDF	Fibroblast	Human	Normal human dermal fibroblast (NHDF), from foreskin. Non-haematopoietic. Adherent. Cells at passage 10-20 were used. Cells were supplied upon request. All cells used originated from a single master stock deposited in liquid nitrogen (LN_2).	Dr Finn Grey, The Roslin Institute
PBMCs	Peripheral blood cells	Human	Peripheral blood mononuclear cells (PBMCs). Haematopoietic. Suspension. PBMCs freshly isolated from whole blood of voluntary donors were used to culture monocyte-derived macrophages (MDM) as described in 2.1.7. Surplus PBMCs was deposited in LN_2 according to the protocol described in 2.1.9.	Voluntary donors, The Roslin Institute

2.2.2 Continuous cell lines

Continuous cell lines used in this project are listed and briefly described in Table 2.2.

Upon receipt of a new cell line a master stock was prepared and deposited in liquid nitrogen (LN_2) as described in 2.2.9. All experiments using a particular cell line were performed using cells originating from a single master stock.

Table 2.2. Continuous cell lines used in this project.

Name	Type	Species	Further details	Source
BHK-21 (C-13)	Epithelial	Hamster	Baby hamster kidney cells. Non-haematopoietic. Adherent.	Prof Peter Liljeström, Karolinska Institutet
2fTGH	Fibroblast	Human	Human fibrosarcoma cells, IFN competent. Non-haematopoietic. Adherent.	Dr Mhairi Ferguson, The Pirbright Institute
U4C	Fibroblast	Human	2fTGH mutant, truncated JAK1 messenger RNA causing lack of functional JAK1 protein and defective IFN response. Non-haematopoietic. Adherent.	Dr Mhairi Ferguson, The Pirbright Institute
NIH 3T3	Fibroblast	Mouse	Mouse embryo fibroblast. Non-haematopoietic. Adherent.	Dr Gerald Barry, University College Dublin
Hek 293T	Epithelial	Human	Human epithelial kidney cells constitutively expressing SV40 Large T antigen. Non-haematopoietic. Adherent.	Dr Helen Wise, The Roslin Institute.
HeLa	Epithelial	Human	Human cervix carcinoma epithelial cells, marginal interferon (IFN) production. Non-haematopoietic. Adherent.	Dr Gerald Barry, University College Dublin
Thp-1	Monocyte	Human	Monocyte cell line from acute monocytic leukaemia. Haematopoietic. Suspension.	Dr Finn Grey, The Roslin Institute
IC-21	Macrophage	Mouse	Peritoneal macrophage cell line; SV40 transformed. Haematopoietic. Adherent.	Dr Finn Grey, The Roslin Institute
Hek 293 Flp-In T-Rex	Epithelial	Human	Human embryonic kidney cells for the FLP-In™ TRex™ system, Invitrogen™, R750-07. Non-haematopoietic. Adherent.	Dr Finn Grey, The Roslin Institute
Hek 293 miR-142	Epithelial	Human	Hek 293 Flp-In™ TRex™ cells transformed using a modified pcDNA™5/FRT/TO vector to express miR-142-3P under control of a tetracycline-inducible promoter.	Adrian Zagrajek, The Roslin Institute (see Chapter 4)
Hek 293 Control	Epithelial	Human	Hek 293 Flp-In TRex cells transformed using an unmodified pcDNA™5/FRT/TO vector to express nothing under control of a tetracycline-inducible promoter.	Adrian Zagrajek, The Roslin Institute (see Chapter 4)

2.2.3 Maintenance and incubation conditions

Unless stated otherwise, all cells were maintained and/or incubated at 37 ºC and 5% CO_2 in a humidified incubator (Panasonic, Annex 10). Sterile, tissue culture (TC)-treated cell culture (CC) flasks and multi-well plates supplied by Thermo Scientific™ Nunc™ (Annex 1) were used. BHK-21, NIH 3T3, Hek 293T, Hek 293 Flp-In TRex, Hek 293 miR-142, Hek 293 Control, 2fTGH, U4C, NHDF and IC-21 cells were cultured in T-175 TC flasks. Thp-1 cells were cultured in T-80 TC flasks. Monocyte-derived macrophages (MDM) were maintained in 100 mm petri dishes.

2.2.4 Counting cells

Cells were counted using a Neubauer Improved Haemocytometer (0.1 mm depth). First, cells were re-suspended as described in 2.2.6. Next, cell suspension was diluted 1 in 10 in Mg^{2+} and Ca^{2+}-free Phosphate Buffered Saline (PBS) (Sigma-Aldrich®, Annex 4), applied to the haemocytometer and then cells were counted in four 1 mm^2 squares. The concentration of cells in suspension was calculated according to the following formula:

$$Cells/ml = Average\ number\ of\ cells\ per\ 1\ mm^2\ x\ 10\ x\ 10^4$$

Where:
10 – PBS dilution factor
10^4 – Volume adjustment to 1 ml

2.2.5 Heat inactivation and storage of serum

Foetal Bovine Serum (FBS) and Newborn Calf Serum (NBCS) were stored at or below -20 ºC upon receipt. When needed, serum was thawed at 37 ºC, mixed gently to prevent formation of bubbles, and incubated at 42 ºC for 30 minutes in a water bath (heat-inactivation). Subsequently, serum was aliquoted and stored at 4 ºC for up to one month or at -20 º C for up to six months.

2.2.6 Harvesting and sub-culturing of cells

All cells with the exception of PBMCs were sub-cultured. Composition of complete media used is detailed in Table 2.3. Details of all reagents are located in Annex 4.

Table 2.3. Composition of complete cell culture media used.

Name	Cells	Composition
Complete DMEM	NIH 3T3, NHDF, 2fTGH, U4C, Hek 293T, Hek 293 Flp-In T-Rex, Hek 293 miR-142, Hek 293 Control	• Dulbecco's modified Eagle's medium with 4 mM L-glutamine and 4.5 g / L glucose (DMEM) • 10 % v/v FBS, heat-inactivated • 50 U/ml penicillin and 50 µg/ml of streptomycin (P/S)
Complete GMEM	BHK-21	• Glasgow's minimum essential medium with 2 mM L-glutamine (GMEM) • 10 % v/v NBCS, heat inactivated • 10% v/v tryptose phosphate broth (TPB) • P/S
Complete RPMI	IC-21, Thp-1, MDM	• Roswell Park Memorial Institute 1640 (RPMI 1640) without Phenol red • 10 % v/v FBS, heat-inactivated • 25 mM 4-(2-Hydroxyethyl)piperazine-1-ethanesulfonic acid (HEPES) • GlutaMAX™ • P/S

2.2.6.1 Non-haematopoietic cells

Cells were harvested by trypsinisation. Cell monolayer at 80-90% confluence was washed once with 10 ml of Mg^{2+}- and Ca^{2+}-free sterile PBS, covered with 5 ml of 0.05% Trypsin-ethylene diamine tetraacetic acid (Trypsin-EDTA) and incubated at room temperature (RT) until cells detached. Next, complete cell culture medium (volume equal to Trypsin-EDTA used) was added to inactivate trypsin. Cell suspension was pipetted up and down several times to disrupt any cell clumps and then centrifuged for 5 minutes at 200 x g and RT. Subsequently, the cell supernatant was removed and the cell pellet was re-suspended in 5-10 ml of complete cell culture medium. Cells were counted, if required. Desired number of cells was seeded into new cell culture flasks with complete cell culture medium (final volume of 30 ml). The doubling time for all no-haematopoietic cells used was approximately 24 hours. Cells were sub-cultured every 2-3 days. Typically, cells were passaged 20-40 times, depending on the cell type (e.g. NHDF could be sub-cultured up to passage 20 only while BHK-21 cells were typically be sub-cultured up to passage 40).

2.2.6.2 IC-21 cells

First, cells were washed twice with 10 ml of Mg^{2+}- and Ca^{2+}-free PBS, covered with 10 ml of Mg^{2+}- and Ca^{2+}-free sterile PBS and incubated for approximately 1 hour at RT. Subsequently, flasks were tapped vigorously on their side with the palm of a hand to detach the cells from the flask. Cell suspension was centrifuged for 10 minutes at 200 x g and RT. Subsequently, the cell supernatant was removed and the cell pellet was re-suspended in 10 ml of complete cell culture medium (complete RPMI). Cells were counted, if required. Desired number of cells was seeded into new cell culture flasks with complete cell culture medium (final volume of 35 ml). The doubling time for IC-21 cells was approximately 36 hours. Cells were sub-cultured every 3-4 days. Cell culture medium was replaced every 2 days as acidic pH negatively affected the cell viability of IC-21 cells. Typically, IC-21 cells were passaged 20-30 times. Cell culture media without Phenol red was used as prolonged metabolism of Phenol red could increase auto-fluorescence of haematopoietic cells (Prof David Hume, The Roslin Institute, personal communication).

2.2.6.3 Thp-1 cells

A required amount of cells was removed from a flask and centrifuged for 10 minutes at 200 x g and RT. Subsequently, the cell supernatant was removed and the cell pellet was re-suspended in 10 ml of complete cell culture medium (complete RPMI). Cells were counted, if required. Desired number of cells was seeded into new cell culture flasks cells with complete RPMI (final volume of 40 ml). The doubling time for Thp-1 cells was 36-48 hours. Cells were sub-cultured every 3-4 days. Thp-1 cells were passaged 20-40 times.

2.2.7 Differentiation of Thp-1 cells into macrophage-like cells

Thp-1 cells were differentiated into macrophage-like cells by treatment with Phorbol 12-myristate 13-acetate (PMA, Sigma-Aldrich®, Annex 4) at 20 ng/ml for 48 hours. The chosen concentration of PMA was identified as the lowest required to ensured complete change of Thp-1 cell morphology and strong adherence (microscopy, cell viability, data not shown). At this concentration stable differentiation of Thp-1 cells should be induced without upregulation of undesirable genes (Park et al. 2007).

2.2.8 Monocyte-derived macrophages (MDMs)

Human blood was obtained from healthy volunteers by a certified phlebotomist in a designated room at the Roslin Institute. Consent form was obtained. 50-120 mls of blood was withdrawn from an antecubital fossa vein into 60 ml syringes (Terumo Medical Products, Annex 2) that were pre-filled with 4 ml of anticoagulant citrate dextrose (ACD) (Sigma-Aldrich®, Annex 5). Syringes were transported in a closed container into a cell culture lab.

Blood was centrifuged for 15 min at 1200 x g and RT, no brake. Plasma supernatant was discarded up to 1 cm above the buffy coat, which was subsequently collected. Buffy coat was diluted 1:3 in complete RPMI. Next, PBMCs were isolated by ficoll gradient separation. In brief, 15 ml of Histopaque-1077 (Sigma-Aldrich®, Annex 4) was added to 50 ml centrifuge tubes (Greiner Bio-One, Annex 2), gently overlaid with 25 ml of diluted buffy coat and centrifuged for 45 min at 200 x g and RT, no brake. Subsequently, 5 defined layers were visible. From the bottom of the tube these were: red blood cells (RBCs) pellet, thin white layer of neutrophils directly on top of RBCs, ficoll layer, fluffy white layer of PBMCs and diluted plasma with platelets. The top layer was discarded and PBMCs were collected without disturbing RBCs. PBMCs were washed once with complete cell culture medium and two times with Ca^{2+}- and Mg^{2+}-free sterile PBS by centrifugation for 10 min at 300 x g and 10 ºC. Cells were re-suspended in Ca^{2+}- and Mg^{2+}-free sterile PBS and counted.

At this stage, positive selection of monocytes was performed using MACS® anti-human CD14 microbeads (Miltenyi Biotec, Annex 9). Manufacturer's protocol was followed. In brief, cells were pelleted by centrifugation at 300 x g for 10 min. The cell supernatant was aspirated completely and cells were re-suspended in 80 µl of MACS buffer (Annex 11) per 1 x 10^7 cells. Next, 20 µl of microbeads was added per 1 x 10^7 cells, mixed well and incubated at 4 ºC for 15 min. Cells were washed by adding 2 ml of MACS buffer per 1 x 10^7 cells and centrifugation at 300 x g for 10 min. Cells were re-suspended in 500 µl of MACS buffer per up to 1 x 10^8 cells. Subsequently, MS column (Miltenyi Biotec, Annex 9) was placed in a magnetic field of a MACS separator (Miltenyi Biotec, Annex 10) and rinsed with 500 µl of MACS

buffer. Next, cell suspension was applied to the column and allowed to pass through by gravity flow. Subsequently, three washing steps were performed by applying 500µl of MACS buffer to the column and allowing it to pass through by gravity flow. Finally, the column was removed from the magnetic field, 1 ml of MACS buffer was added to the column and the cells were flushed into a clean tube by firmly applying a plunger into the column.

Purified CD14+ monocytes were centrifuged for 10 min at 400 x g and 10 ºC and re-suspended at 1 x 10^6 monocytes per ml in complete RPMI containing 1 x 10^4 U/ml of recombinant human colony stimulating factor-1 (rhCSF-1) (Annex 4). Cells were added into a 100 mm sterile square petri dish and incubated for 5 days. Monocytes adhered to the surface of the dish within 2 hours. Monocytes started differentiation into MDMs due to presence of hrCSF-1.

Next, cell culture medium was removed, monocytes/MDMs were washed twice with sterile Mg^{2+}- and Ca^{2+}-free PBS and covered with complete RPMI supplemented with 1 x 10^4 U/ml rhCSF-1. Cells were incubated for another two days to complete differentiation. MDMs were detached from the dish by repeated pipetting or by incubation with collagenase type I (Sigma-Aldrich®, Annex 4), 4mg/ml, in RPMI (no FBS, no P/S). Detached MDMs were washed in Mg^{2+}- and Ca^{2+}-free PBS as described before, counted, re-suspended in complete RPMI with 1 x 10^4 U/ml rhCSF-1 and plated. MDMs were cultured for further 48 hours before infection.

2.2.9 Freezing cells for storage in liquid nitrogen

Cells in the middle of their growth phase were used to prepare aliquots for storage in LN_2 (vapour phase). The optimal balance between the growth phase and yield was achieved when cells were passaged 20-24 hours earlier and the confluence of the monolayer was 70-80%. Cells were harvested, counted and pelleted as described in 2.2.6. The pellet was re-suspended in FBS supplemented with 10% v/v dimethyl sulfoxide (DMSO, Annex 4) at a concentration of 5 x 10^6 cells/ml. Cell aliquots were prepared by adding 1 ml of cell suspension into 1.8 ml CryoTube™ (Thermo Scientific™ Nunc™, Annex 2). Cells were moved into a -80 ºC freezer inside a Mr.

Frosty™ (Thermo Scientific™, Annex 2) container filled with propan-2-ol (Sigma-Aldrich®, Annex 5) that ensured a constant freezing rate of -1 ºC per minute. Cells were moved to LN_2 (vapour phase) 24 hours later.

2.2.10 Resurrecting cells from liquid nitrogen

An aliquot of cells was removed from LN_2, kept on dry ice and then rapidly warmed up in a water bath at 37 ºC. Cells were diluted in 10 ml of complete cell culture medium and centrifuged for 5 min at 200 x g and RT to remove the cryoprotectant (DMSO). Next, the supernatant was carefully removed and the pellet was re-suspended in 10 ml of complete cell culture medium, transferred to a T-80 flask and subsequently subcultured.

2.2.11 Generating stable Flp-In™ T-Rex™ 293 expression cell lines

Stable expression cell lines were generated using Flp-In™ T-Rex™ System and Flp-In™ T-Rex™ 293 cells. Following resurrection from LN_2, Flp-In™ T-Rex™ 293 cells were sub-cultured for one week. Cells were split every 1-2 days to prevent monolayer confluence of more than 75%. Next, cells were seeded into 6-well plates at 5 x 10^5 cells/well in 2 ml complete DMEM with no P/S. After 24 hours, cells were co-transfected with 9.0 μg pOG44 and 1.0 μg of a pcDNA5/FRT/TO using Lipofectamin 2000® Transfection Reagent (Invitrogen™ Life Technologies, Annex 6), following the protocol in 2.10.2. Cells transfected with pOG44 alone, pcDNA5/FRT/TO alone and transfection reagent alone were used as controls. After 24 hours, cell culture supernatant was removed, cells were washed gently with Mg^{2+} and Ca^{2+}-free PBS, and fresh 2 ml of complete DMEM with P/S was added to each well. After further 24 hours, cells in each well were harvested, split 1:2 and re-seeded into two 100 mm cell culture dishes (Corning, Annex 1) in 10 ml of complete DMEM supplemented with 100 μg/ml hygromycin B (Calbiochem, Annex 4). After 24 hours, cell culture supernatant was removed and fresh complete DMEM supplemented with 200 μg/ml hygromycin B was added. Cells were incubated for further 4 days. Subsequently, cell culture supernatant was removed and cells were washed gently with Mg^{2+} and Ca^{2+}-free PBS. Next, silicon-greased cloning cylinders prepared as described in 2.2.12 were placed over 6 hygromycin-resistant cell foci

(approximately 32 cells in size) for each cell line. Cells isolated by each cylinder were immediately harvested (50 µl of trypsin per cylinder) and sub-cultured into 96-well plates in presence of hygromycin B at 200 µg/ml. Over the period of two weeks, cells were sub-cultured into plates with progressively larger wells (24-, 12- and 6-well plates), in presence of hygromycin B at 200 µg/ml. Next, the expression of the gene of interest (GOI) in all cells was assayed by qPCR following the protocol described in 2.13. Selected cell lines were sub-cultured into progressively larger flasks (T-80 and T-175) without hygromycin B and then frozen at LN_2. The LN_2 masterstock was assigned Passage number 0.

2.2.12 Preparation of cloning cylinders for cell colony picking

First, surface a sterile petri dish (Thermo Scientific™ Sterilin™, Annex 2) was coated with a thin layer of silicon grease (Beckman Coulter, Annex 5) inside a class II microbiological safety cabinet (MBSC). The closed petri dish was microwaved at full power for 1 min (Panasonic, Annex 10). Subsequently, the petri dish was moved back to the MBSC and cloning cylinders (Sigma-Aldrich®, Annex 2) were pressed gently against the silicon grease to ensure complete coating of their edge.

2.3 Viruses

2.3.1 Semliki Forest virus (SFV)

SFV clones used in this project were of SFV4 backbone and were available as DNA infectious clones (icDNA). To generate virus stock, SFV was rescued from icDNAs following the protocol outlined in 2.3.3.

Five clones of SFV were available at the beginning of this project. They are summarised in Figure 2.1 and Table 2.4. During this project, 10 further clones were generated. They are summarised in Table 2.5. Their full design, cloning and testing is described in detail in Chapter 4.

Sequence of the unmodified SFV4 is provided in Annex 13. Sequences of all SFV icDNAs used in this project are provided in Supplementary Data, Appendix 1.

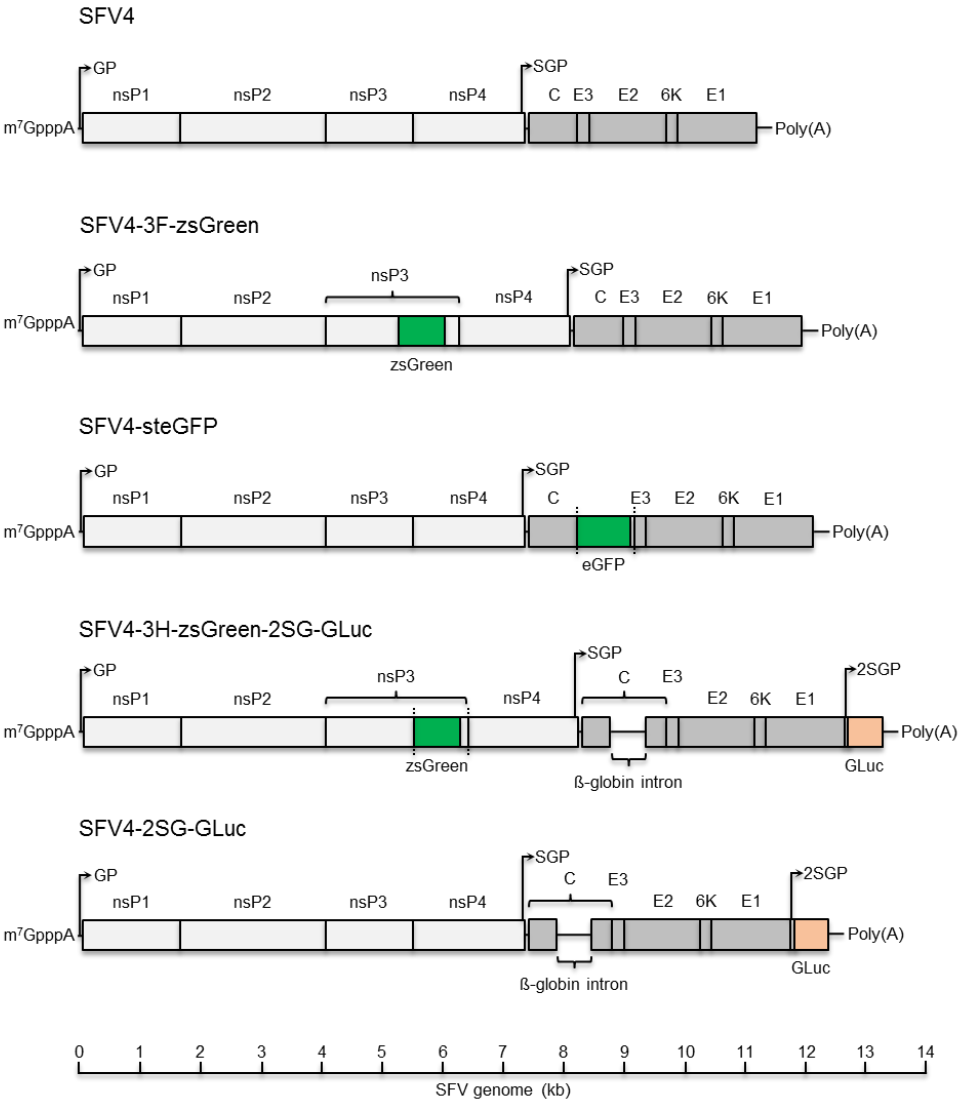

Figure 2.1. Schematic representation of SFV4 clones available at the beginning of this project. nsP-non-structural protein; GP – genomic promoter; SGP – subgenomic promoter; 2SGP – duplicated subgenomic promoter; C – capsid; E1-E3 – envelope glycoproteins; GLuc – *Gaussia* luciferase; vertical dashed line – protein cleavage sites; Poly(A) – Poly(A) tail; m^7GpppA – 5' CAP.

Table 2.4. SFV4 clones available at the beginning of this project.

Construct name	Construct type	Construct details	Source
SFV4	Infectious clone, SP6 promoter	Unmodified SFV4.	Dr Mhairi Ferguson, The Pirbright Institute (originally from Prof Andres Merits, University of Tartu)
SFV4-steGFP	Infectious clone, SP6 promoter	eGFP inserted into the structural open reading frame, downstream of capsid protein, followed by FMDV 2A autoprotease sequence. eGFP is released into the cytoplasm of infected cells.	Dr Rennos Fragkoudis, The Pirbright Institute
SFV4-3F-zsGreen	Infectious clone, SP6 promoter	zsGreen fused to C-terminus of nsP3 protein. zsGreen is localised to replication complexes in the cytoplasm.	Dr Rennos Fragkoudis, The Pirbright Institute (originally from Prof Andres Merits, University of Tartu)
SFV4-2SG-GLuc	Infectious clone, CMV promoter	*Gaussia luciferase* (GLuc) inserted downstream of the structural polyprotein stop codon, under control of a duplicated subgenomic promoter. GLuc is secreted into cell culture supernatant. ß-globin intron is inserted in the capsid region to disrupt a cryptic *E.coli* promoter.	Prof Andres Merits, University of Tartu
SFV4-3H-zsGreen-2SG-GLuc	Infectious clone, CMV promoter	zsGreen inserted in the C-terminus of nsP3, it is cleaved from nsP3 during non-structural polyprotein processing. zsGreen is released into the cytoplasm of infected cells. Second marker GLuc is inserted in the 3'UTR as per SFV4-2SG-GLuc described above. ß-globin intron is inserted in the capsid region to disrupt a cryptic *E.coli* promoter.	Prof Andres Merits, University of Tartu

Table 2.5. SFV4 clones generated during this project.

Construct name	Construct type	Construct details	Source
SFV4-3F-zsGreen-2SG-GLuc	Infectious clone, CMV promoter	zsGreen fused to C-terminus of nsP3 protein. GLuc inserted downstream of the structural polyprotein stop codon, under control of a duplicated subgenomic promoter. GLuc is secreted into cell culture supernatant.	Adrian Zagrajek, The Roslin Institute (see Chapter 4)
SFV4-3F-zsGreen-miR-142-3P RE	Infectious clone, CMV promoter	zsGreen fused to C-terminus of nsP3 protein. Recognition element (RE) for miR-142-3P inserted in the 3'UTR.	Adrian Zagrajek, The Roslin Institute (see Chapter 4)
SFV4-3F-zsGreen-miR-142-3P Antisense RE	Infectious clone, CMV promoter	zsGreen fused to C-terminus of nsP3 protein. Antisense RE for miR-142-3P inserted in the 3'UTR.	Adrian Zagrajek, The Roslin Institute (see Chapter 4)
SFV4-3F-zsGreen-miRNA RE Control	Infectious clone, CMV promoter	zsGreen fused to C-terminus of nsP3 protein. Control miRNA RE inserted in the 3'UTR.	Adrian Zagrajek, The Roslin Institute (see Chapter 4)
SFV4-3H-zsGreen-miR-142-3P RE	Infectious clone, CMV promoter	As for SFV4-3F-zsGreen-miR-142-3P RE, but zsGreen is cleaved from nsP3 as per SFV4-3H-zsGreen-2SG-GLuc.	Adrian Zagrajek, The Roslin Institute (see Chapter 4)
SFV4-3H-zsGreen-miR-142-3P Antisense RE	Infectious clone, CMV promoter	As for SFV4-3F-zsGreen-miR-142-3P Antisense RE, but zsGreen is cleaved from nsP3 as per SFV4-3H-zsGreen-2SG-GLuc.	Adrian Zagrajek, The Roslin Institute (see Chapter 4)
SFV4-3H-zsGreen-miRNA RE Control	Infectious clone, CMV promoter	As for SFV4-3F-zsGreen-miRNA RE Control, but zsGreen is cleaved from nsP3 as per SFV4-3H-zsGreen-2SG-GLuc.	Adrian Zagrajek, The Roslin Institute (see Chapter 4)
SFV4-3F-zsGreen-2SG-GLuc-miR-142-3P RE	Infectious clone, CMV promoter	As for SFV4-3F-zsGreen-miR-142-3P RE, but GLuc under control of a duplicated subgenomic promoter is inserted between the structural polyprotein stop codon and the RE.	Adrian Zagrajek, The Roslin Institute (see Chapter 4)
SFV4-3F-zsGreen-2SG-GLuc-miR-142-3P Antisense RE	Infectious clone, CMV promoter	As for SFV4-3F-zsGreen-miR-142-3P Antisense RE, but GLuc under control of a duplicated subgenomic promoter is inserted between the structural polyprotein stop codon and the RE.	Adrian Zagrajek, The Roslin Institute (see Chapter 4)
SFV4-3F-zsGreen-2SG-GLuc-miRNA RE Control	Infectious clone, CMV promoter	As for SFV4-3F-zsGreen-miRNA RE Control, but GLuc under control of a duplicated subgenomic promoter is inserted between the structural polyprotein stop codon and the RE	Adrian Zagrajek, The Roslin Institute (see Chapter 4)

2.3.2 Chikungunya virus (CHIKV)

CHIKV clones used in this project were of ICRES1 (LR2006 OPY1) backbone and were available as icDNAs. To generate virus stock, CHIKV was rescued from icDNAs following the protocol outlined in 2.3.3.

Five clones of CHIKV were available at the beginning of this project. They are summarised in Figure 2.2 and Table 2.6. During this project, 4 further clones were generated. They are summarised in Table 2.7. Their full design, cloning and testing is described in detail in Chapter 5.

Sequence of the unmodified ICRES1 is provided in Annex 14. Sequences of CHIKV icDNAs used in this project are provided in Supplementary Data, Appendix 2.

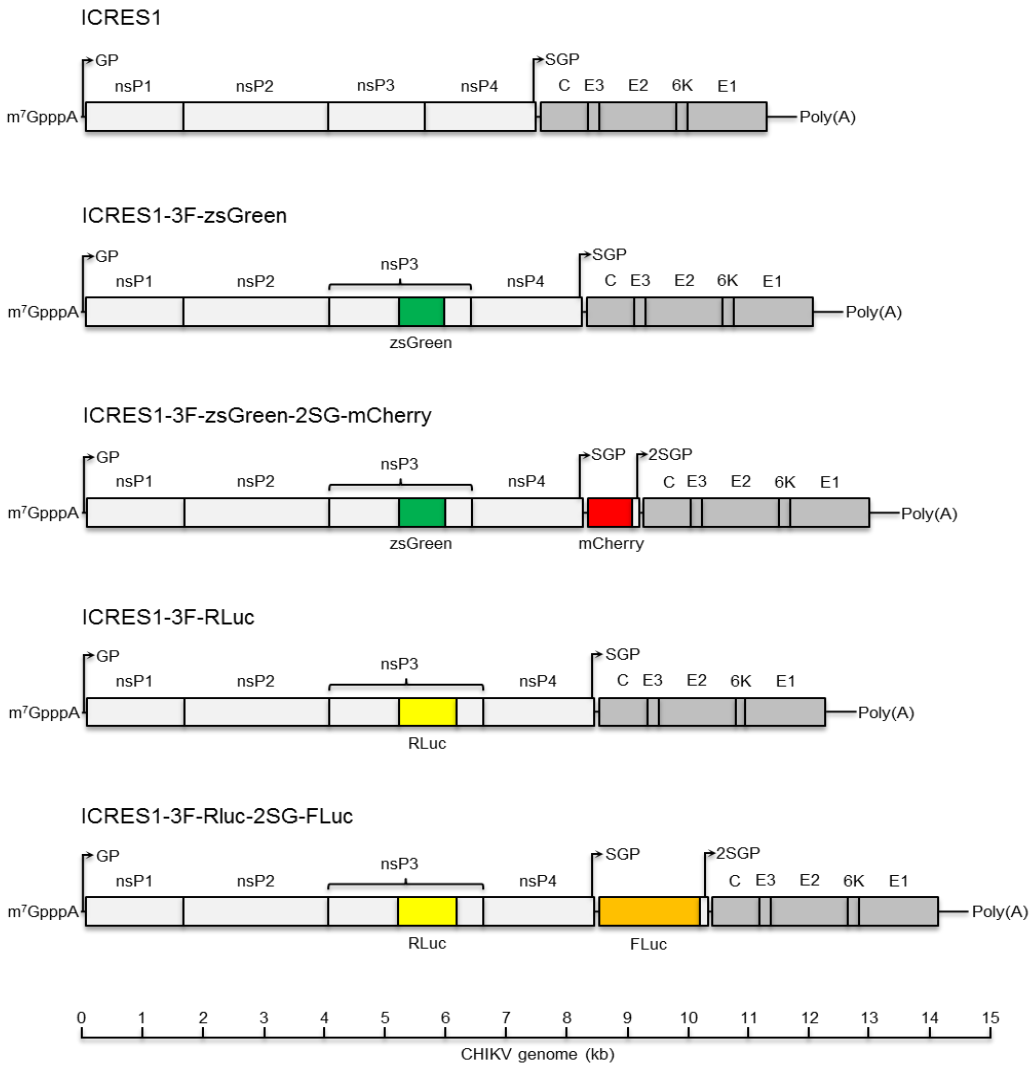

Figure 2.2. Schematic representation of CHIKV clones available at the beginning of this project. ICRES1 – CHIKV strain LR2006 OPY1; nsP-non-structural protein; GP – genomic promoter; SGP – subgenomic promoter; 2SGP – duplicated subgenomic promoter; C – capsid; E1-E3 – envelope glycoproteins; RLuc – *Renilla* luciferase; FLuc – *Firefly* luciferase; Poly(A) – Poly(A) tail; m^7GpppA – 5' CAP.

Table 2.6. CHIKV clones available at the beginning of this project.

Construct name	Construct type	Construct details	Source
ICRES1	Infectious clone, SP6 promoter	Unmodified infectious clone of CHIKV strain LR2006 OPY1.	Dr Aleksei Lulla and Prof Andres Merits, University of Tartu
ICRES1-3F-zsGreen	Infectious clone, SP6 promoter	zsGreen fused to C-terminus of nsP3 protein. zsGreen is localised to replication complexes in the cytoplasm.	Dr Aleksei Lulla and Prof Andres Merits, University of Tartu
ICRES1-3F-zsGreen-2SG-mCherry	Infectious clone, SP6 promoter	zsGreen fused to C-terminus of nsP3 protein as in ICRES1-3F-zsGreen. mCherry followed by a duplicated subgenomic promoter inserted between non-structural and structural ORFs.	Dr Aleksei Lulla and Prof Andres Merits, University of Tartu
ICRES1-3F-RLuc	Infectious clone, SP6 promoter	Marker gene *Renilla* luciferase (RLuc) fused to C-terminus of nsP3 protein. RLuc is localised to replication complexes in the cytoplasm. Fusion of RLuc to nsP3 does not inhibit RLuc activity.	Dr Aleksei Lulla and Prof Andres Merits, University of Tartu
ICRES1-3F-RLuc-2SG-FLuc	Infectious clone, SP6 promoter	Marker gene RLuc fused to nsP3 as in ICRES1-3F-RLuc. *Firefly* luciferase (FLuc) followed by a duplicated subgenomic promoter inserted between non-structural and structural ORFs.	Dr Aleksei Lulla and Prof Andres Merits, University of Tartu

Table 2.7. CHIKV clones generated during this project.

Construct name	Construct type	Characteristic	Source
ICRES1-3F-zsGreen-miR-142-3P RE	Infectious clone, SP6 promoter	zsGreen fused to C-terminus of nsP3 protein as per ICRES1-3F-zsGreen. RE for miR-142-3P inserted between the non-structural and structural ORFs.	Adrian Zagrajek, The Roslin Institute (see Chapter 4)
ICRES1-3F-zsGreen-miRNA RE Control	Infectious clone, SP6 promoter	zsGreen fused to C-terminus of nsP3 protein as per ICRES1-3F-zsGreen. Control miRNA RE inserted between the non-structural and structural ORFs.	Adrian Zagrajek, The Roslin Institute (see Chapter 4)
ICRES1-3F-RLuc-miR-142-3P RE	Infectious clone, SP6 promoter	RLuc fused to C-terminus of nsP3 protein as per ICRES1-3F-RLuc. RE for miR-142-3P inserted between the non-structural and structural ORFs.	Adrian Zagrajek, The Roslin Institute (see Chapter 4)
ICRES1-3F-RLuc-miRNA RE Control	Infectious clone, SP6 promoter	RLuc fused to C-terminus of nsP3 protein as per ICRES1-3F-RLuc. Control miRNA RE inserted between the non-structural and structural ORFs.	Adrian Zagrajek, The Roslin Institute (see Chapter 4)

2.3.3 Virus rescue

To generate virus stock, both SFV and CHIKV were rescued from icDNAs, as described below. A range of DNA expression vectors was used as the backbone for icDNAs (e.g. modified pMA vector from GeneArt® was used for all ICRES1 constructs). In all cases, virus was cloned under control of either the SP6 polymerase promoter or the CMV immediate early enhancer/promoter. The type of promoter present in the icDNA determined how a particular virus clone was rescued.

2.3.3.1 Virus cloned under control of the SP6 polymerase promoter

First, 10 µg of an icDNA was linearized by restriction digest as described in 2.16. SFV4 icDNAs were cut with SpeI (New England Biolabs, Annex 6) while ICRES1 were cut with NotI (Roche, Annex 6). Next, linearized DNA was purified using NucleoSpin® Gel and PCR Clean-up (Macherey-Nagel, Annex 8) following the protocol outlined in 2.15.7. The purified DNA was inspected on an agarose gel as outlined in 2.14 to confirm the presence of a single band of the expected size. DNA concentration and purity was measured using NanoDrop™ spectrophotometer (Thermo Scientific™, Annex 10). For subsequent steps, samples with concentration of >200 ng/µl and A260/280 of >1.9 were used.

Viral genomic RNA was prepared by *in vitro* transcription of 1 µg of the purified linear icDNA using MEGAscript® SP6 kit (Life Technologies Ambion™, Annex 6). Manufacturer's protocol was followed (September 2010 version; Supplementary Data, Appendix 14). Cap analogue $M^7G(S')ppp(S')G$ (Life Technologies Ambion™, Annex 6) was added to the reaction mixture at the same final concentration as ribonucleotides ATP, CTP and UTP. To facilitate Cap analogue incorporation the molar amount of GTP was diluted 1 in 5. Recombinant RNasin® Plus Ribonuclease Inhibitor (Promega, Annex 6) was added at 40 U per reaction. The *in vitro* transcription was carried over a period of 1.5-2 hours. Synthesised viral genomic RNA was subsequently stored on ice until required, but not longer than 2-4 hours, or frozen at -80 ºC. In the latter case, the RNA was first aliquoted and subsequently allowed to thaw only once to preserve its integrity.

Viral genomic RNA from the *in vitro* transcription (total reaction volume) was electroporated into BHK-21 cells to rescue the virus. In brief, 70-80% confluent BHK-21 cells sub-cultured 20-24 hours earlier were harvested, washed twice with Ca^{2+}- and Mg^{2+}-free sterile PBS by centrifugation for 5 min at 200 x g and RT, and counted. Subsequently, cells were pelleted by centrifugation for 5 min at 200 x g and RT, and re-suspended in Opti-MEM® (Invitrogen™ Life Sciences Gibco®, Annex 4) at 2 x 10^7 cells per 800 µl. Viral genomic RNA was mixed gently with 800 µl of the cell suspension and incubated on ice for 10 minutes. Next, the cells/RNA mixture was transferred into a 0.4 cm cuvette (Bio-Rad, Annex 2) and electroporated using the Gene Pulser Xcell™ Electroporation System (Bio-Rad, Annex 10). The following square wave protocol was used:

- Voltage – 850 V
- Pulse length – 4.0 msec
- Number of pulses – 2
- Pulse interval – 5.0 sec

Electroporated cells were seeded into a T-175 flask in 20 ml of complete GMEM and incubated for 48 hours. Cell culture supernatant was collected 24 and 48 hours post-electroporation and stored at 4 ºC for up to one week. At 24-hour point it was replaced with fresh complete GMEM. Next, the collected supernatant was clarified by centrifugation for 45 minutes at 4500 x g and 4 ºC. The clarified supernatant was aliquoted and frozen at -80 ºC unless further concentration was required (see below).

Viruses were concentrated by ultracentrifugation through a 20% w/v sucrose cushion, when required. In brief, 8 ml of 20% w/v sucrose in TNE buffer (Annex 11) was added into an Ultra-Clear™ ultracentrifugation tube (Beckman, Annex 2) and overlaid with 30 ml of the clarified cell culture supernatant containing the virus. Tubes were then ultracentrifuged for 90 min at 86,400 x g and 4 ºC using either L8-70M Ultracentrifuge and SW28.1 rotor (Beckman Coulter, Annex 10) or Optima™ L-100K Ultracentrifuge and SW32 Ti rotor (Beckamn Coulter, Annex 10). Finally, all liquid was gently discarded, and the virus pellet was re-suspended in TNE buffer (100-500 µl per tube) for 2 hours on ice, aliquoted and frozen at -80 ºC.

2.3.3.2 Virus cloned under control of the CMV promoter

The icDNA was electroporated directly into BHK-21 cells without any processing of the plasmid. Only icDNAs with concentration of >500 ng/µl and A260/280 of >1.9 were used. The protocol outlined in 2.3.3.1 was followed, with one modification. Instead of RNA from *in vitro* transcription, 10 µg of icDNA in Opti-MEM® in total volume of 20 µl was mixed with cells prior to electroporation.

2.3.4 Virus stability

SFV and CHIKV were passaged on BHK-21 cells at a 'high' MOI (estimated at 1-5) or at a 'low' MOI (estimated at 0.01-0.05), in quadruplicates. Depending on the virus used and the MOI required, 3 to10 passages were completed.

For a 'high' MOI passage, BHK-21 cells were first harvested, counted and seeded into T25 flasks at 1 x 10^6 cells/flask in 5 ml of complete GMEM. After 24 hours, cell supernatant was removed and 1 ml of virus inoculum at MOI of 0.1 in PBS with Mg^{2+}, Ca^{2+} and 0.75% w/v Bovine Serum Albumin (PBSA) (Annex 11) was added to cells. Flasks were incubated for 1 hour at RT, after which 4 ml of complete GMEM was added. Flasks were incubated for 48 hours. Subsequently, 1 ml of the cell culture supernatant was collected and frozen at -80 ºC (Passage 1). For each subsequent passage 1 µl of the cell culture supernatant from previous passage was added to 999 µl of fresh PBSA and used to infect new BHK-21 cells, as described above.

For a 'low' MOI passage, the procedure described for a 'high' MOI was followed, however, initial infection was done at MOI=0.001 and for each subsequent passage 1 µl of 1:100 diluted cell culture supernatant was used.

2.3.5 Virus titration

SFV and CHIKV were titrated by plaque assay on BHK-21 cells. First, cells were harvested, counted and seeded into either 6-well plates at 3 x 10^5 cells per well in 2 ml of complete GMEM or into 24-well plates at 6 x 10^4 cells per well in 0.5 ml of complete GMEM. There was no significant difference between virus titres obtained using 6- and 24-well plates (data not shown).

Plates were incubated overnight. The desired cell monolayer confluence on the day of infection was 80%. Next, 10-fold serial dilutions of virus were performed in PBSA. Cell culture medium was aspirated from plates and 400 µl or 125 µl of each dilution was added in duplicates to wells in 6- or 24-well plates, respectively. Plates were rocked gently for 1-1.5 hour at RT. Plaque assay overlay was prepared by mixing GMEM complemented with 2% v/v NBCS, TPB and P/S with melted 4% w/v agar (Annex 11) at ration of 3:1 or with 2% w/v carboxymethyl cellulose (CMC) (Annex 11) at ratio of 3:2. There was no significant difference between virus titres obtained using 4% w/v agar or 2% w/v CMC (data not shown). Next, 3 ml or 1 ml of the overlay was added to each well of 6- or 24-well plates, respectively. Finally, plates were incubated for 48-72 hours, fixed with 10% v/v neutral buffered formalin (Leica Biosystems, Annex 5) for at least 1 hour (SFV) or 4 hours (CHIKV), stained with 0.1% toluidine blue (Sigma-Aldrich, Annex 7) for 30 min, washed with tap water and inspected for plaques. The titre expressed in Plaque Forming Units (PFU) per ml (PFU/ml) was calculated using the following formula:

$$\mathrm{PFU/ml} = \frac{\text{average number of plaques from duplicate wells}}{\text{volume of inoculum in ml} \times \text{dilution factor}}$$

In general, virus stocks were titrated using 6-well plates and experimental samples were titrated using 24-well plates. The overlay containing CMC was used in most cases. Importantly, all samples within one experiment and samples from all experiments to be directly compared with each other used the same format of the plaque assay (the type of plates and the type of overlay).

2.3.6 Assessing stability of SFV and CHIKV encoding miR-142-3P RE

The development and optimisation of this assay is described in detail in 4.15. First, Hek 293 miR-142 and Hek 293 Control cells were harvested, counted and seeded into 6-well plates at 2.5 x 10^6 cells/well in 2 ml of complete DMEM with doxycycline at 100 ng/ml (Sigma-Aldrich®, Annex 4). Plates were incubated for 24-26 hours. Next, 10-fold serial dilutions of virus samples were performed in PBSA. In addition, 10-fold serial dilutions of a reference virus not affected by the presence of

miR-142-3P (e.g. SFV4-3F-zsGreen, ICRES1-3F-zsGreen) were performed in PBSA, in quadruplicates. The assay overlay was prepared by mixing 3 parts of DMEM supplemented with 5% v/v FBS and P/S with 2 parts of 2% CMC. Doxycycline was added to the overlay at 100 ng/ml final concentration. Next, cell culture medium was aspirated from plates and 650 µl of each dilution was added gently to wells in both Hek 293 miR-142 and Hek 293 Control plates, in duplicates. Plates were rocked gently by hand and then placed on a flat surface for 1-1.5 hours. The volume of inoculum was sufficient to stop the monolayers from drying out without constant rocking. However, cells were rocked very gently by hand every 15-20 minutes to ensure equal distribution of virus inoculum. As cells were not strongly adherent, any excessive handling would detach them from the surface of wells. Next, virus inoculum was gently pipetted off and discarded, and 3 ml of the overlay was added gently to each well. Plates were incubated for 48 hours. Finally, plates were fixed overnight with 10% v/v neutral buffered formalin, washed gently with tap water, and overlaid with 1 ml of PBS with Mg^{2+} and Ca^{2+} per well. Plates were inspected microscopically for the presence of virus plaques as indicated by localised expression of zsGreen encoded by all tested viruses (see 2.7.1). Any foci of infection bigger than 8 cells were treated as a plaque (see Chapter 4 for details). The formula described in 2.3.5 was used to calculate the titre of each sample on both Hek 293 miR-142 and Hek 293 Control cells. Next, the fraction of virus able to replicate in the presence of miR-142-3P (in %) was calculated by normalising the titre obtained on Hek 293 miR-142 cells to the titre obtained on Hek 293 Control cells. The above data were further normalised to the average titres obtained for the control virus (e.g. SFV4-3F-zsGreen, ICRES1-3F-zsGreen) to compensate for any differences in the infectivity of Hek 293 miR-142 and Hek 293 Control cells. Virus stability was expressed as the fraction of virus (in %) unable to form plaques in presence of miR-142-3P.

2.3.7 One-step growth curves

BHK-21 cells were harvested, counted and seeded into 24-well plates at 6 x 10^4 cells/well, in 0.5 ml of complete GMEM, and incubated overnight. Next, cell supernatant was removed and cells were infected with 0.2 ml of each virus in PBSA

at MOI of 10, in quadruplicates. Plates were rocked for 1 hour at RT. Next, virus inoculum was removed, and 0.6 ml of complete GMEM was added to all wells. Plates were rocked gently for 1 minute and 0.1 ml was collected from each well (0 h sample), living the final volume of 0.5 ml in all wells. Plates were incubated for 2 hours. Next, 0.1 ml was removed from each well (2 h samples) and replaced with 0.1 ml of fresh complete GMEM. Plates were returned to the incubator. The sampling was repeated 4, 6, 8, 10, 12, 16, 20 and 24 hours post-infection. Samples were stored at 4 ºC until all collections were completed. Then, all samples were frozen at -80 ºC. Virus replication was tested by plaque assay (all samples), and luciferase assay if available (SFV4 clones expressing GLuc).

2.4 Virus replicon particles (VRPs)

2.4.1 Semliki Forest VRPs

One clone of SFV replicon was used in this project, SFV1-3F-zsGreen. The replicon was of SFV1 backbone, which was based on SFV4. To generate VRP stock, SFV1-3F-zsGreen was rescued following the protocol outlined in 2.4.3. Split-helper system was used. The SFV1-3F-zsGreen and the split-helper constructs used are summarised in Figure 2.3 and Table 2.8. Their plasmid sequences are provided in Supplementary Data, Appendix 3.

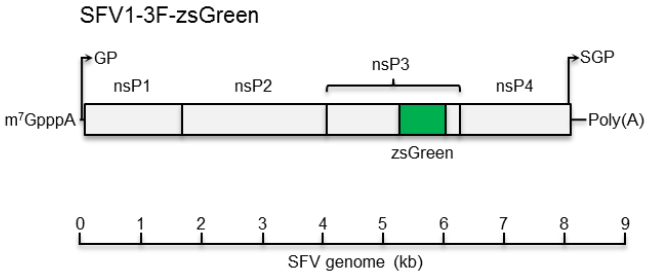

Figure 2.3. Schematic representation of SFV1-3F-zsGreen replicon. nsP-non-structural protein; GP – genomic promoter; SGP – subgenomic promoter; Poly(A) – Poly(A) tail; m^7GpppA – 5' CAP**.**

Table 2.8. SF replicons and helper constructs used in this project.

Construct name	Construct type	Characteristic	Source
SFV1(3F)-zsGreen	Replicon, SP6 promoter	zsGreen fused to C-terminus of nsP3 protein. zsGreen is localised to replication complexes in the cytoplasm. Replicon equivalent of SFV4-3F-zsGreen.	Dr Rennos Fragkoudis, The Pirbright Institute (originally from Prof Andres Merits, University of Tartu)
SFV-Helper-S2	Helper, SP6 promoter	Encodes envelope glycoproteins only under control of the subgenomic promoter.	Dr Rennos Fragkoudis, The Pirbright Institute (originally from Prof Andres Merits, University of Tartu)
SFV-Helper-C	Helper, SP6 promoter	Encodes capsid protein only under control of the subgenomic promoter.	Dr Rennos Fragkoudis, The Pirbright Institute (originally from Prof Andres Merits, University of Tartu)

2.4.2 Chikungunya VRPs

Chikungunya replicons used in this project were of ChikRepl backbone, which was based on ICRES1. To generate VRP stock, chikungunya replicons were rescued as described in 2.4.3. Split-helper system was used. Five clones of chikungunya replicons were available at the beginning of this project. They are summarised in Figure 2.4 and Table 2.9. During this project, 4 further clones were generated. They are summarised in Table 2.10. Their full design and cloning is described in detail in Chapter 5. Sequences of all chikungunya replicons and helper plasmids used in this project are provided in Supplementary Data, Appendix 4.

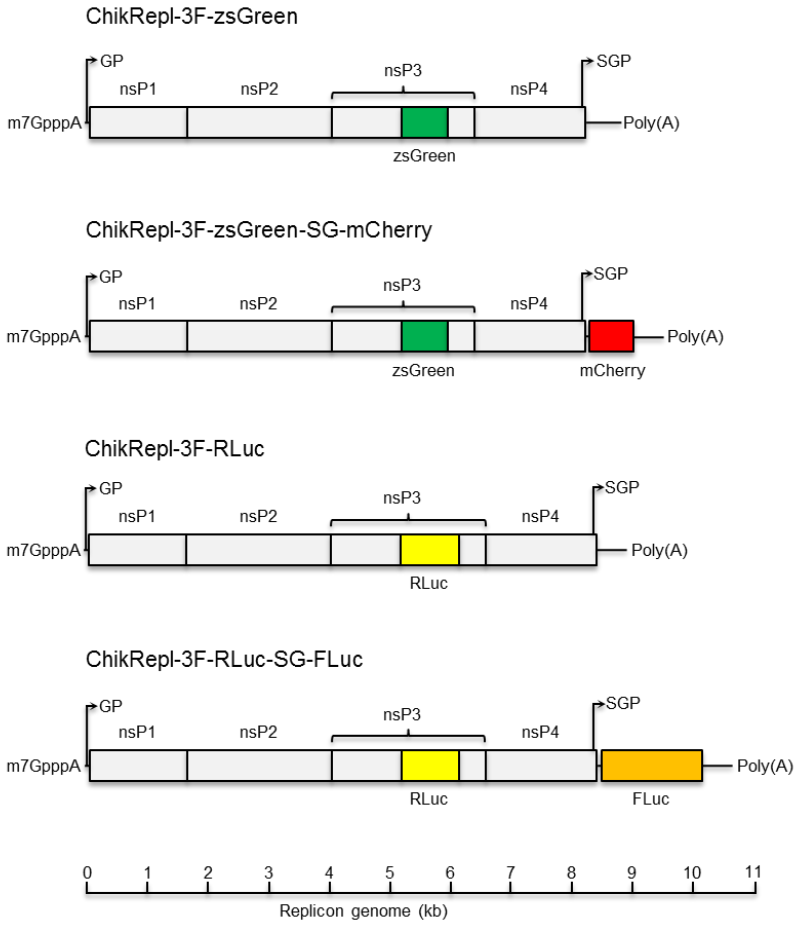

Figure 2.4. Schematic representation of chikungunya replicons available at the beginning of the project. nsP-non-structural protein; GP – genomic promoter; SGP – subgenomic promoter; RLuc – *Renilla* luciferase; FLuc – *Firefly* luciferase; m^7GpppA – 5' CAP.

Table 2.9. Chikungunya replicons and helper constructs available at the beginning of this project.

Construct name	Construct type	Characteristic	
ChikRepl-3F-zsGreen	Replicon, SP6 promoter	zsGreen fused to C-terminus of nsP3 protein. zsGreen is localised to replication complexes in the cytoplasm. Replicon equivalent of ICRES1-3F-zsGreen.	Prof Andres Merits and Dr Aleksei Lulla, University of Tartu
ChikRepl -3F-zsGreen-2SG-mCherry	Replicon, SP6 promoter	zsGreen fused to nsP3 as in ChikRepl-3F-zsGreen. mCherry inserted downstream of the non-structural ORF. mCherry can be used to indirectly monitor the activity of the subgenomic promoter in the absence of the structural ORF. Replicon equivalent of ICRES1-3F-zsGreen-2SG-mCherry.	Prof Andres Merits and Dr Aleksei Lulla, University of Tartu
ChikRepl -3F-RLuc	Replicon, SP6 promoter	RLuc fused to C-terminus of nsP3 protein. RLuc is localised to replication complexes in the cytoplasm. Fusion of RLuc to nsP3 does not inhibit RLuc activity. Replicon equivalent of ICRES1-3F-RLuc.	Prof Andres Merits and Dr Aleksei Lulla, University of Tartu
ChikRepl -3F-RLuc-2SG-FLuc	Replicon, SP6 promoter	RLuc fused to nsP3 as in ChikRepl-3F-RLuc. FLuc inserted downstream of the non-structural ORF. FLuc can be used to indirectly monitor the activity of the subgenomic promoter in the absence of the structural ORF. Replicon equivalent of ICRES1-3F-RLuc-2SG-FLuc.	Prof Andres Merits and Dr Aleksei Lulla, University of Tartu
Chik-Helper-S	Helper	Encodes envelope glycoproteins under control of the subgenomic promoter.	Prof Andres Merits and Dr Aleksei Lulla, University of Tartu
Chik-Helper-C	Helper	Encodes capsid protein under control of the subgenomic promoter.	Prof Andres Merits and Dr Aleksei Lulla, University of Tartu

Table 2.10. Chikungunya replicons generated during this project.

Construct name	Construct type	Characteristic	Source
ChikRepl-3F-zsGreen-miR-142-3P RE	Replicon, SP6 promoter	zsGreen fused to C-terminus of nsP3 protein. zsGreen is localised to replication complexes in the cytoplasm. RE for miR-142-3P inserted downstream of the non-structural ORF. Replicon equivalent of ICRES1-3F-zsGreen-miR-142-3P RE.	Adrian Zagrajek, The Roslin Institute (see Chapter 5)
ChikRepl -3F-zsGreen-miRNA RE Control	Replicon, SP6 promoter	zsGreen fused to C-terminus of nsP3 protein. zsGreen is localised to replication complexes in the cytoplasm. Control miRNA RE inserted downstream of the non-structural ORF. Replicon equivalent of ICRES1-3F-zsGreen-miRNA RE Control.	Adrian Zagrajek, The Roslin Institute (see Chapter 5)
ChikRepl -3F-RLuc-miR-142-3P-RE	Replicon, SP6 promoter	RLuc fused to C-terminus of nsP3 protein. RLuc is localised to replication complexes in the cytoplasm. Fusion of RLuc to nsP3 does not inhibit RLuc activity. RE for miR-142-3P inserted downstream of the non-structural ORF. Replicon equivalent of ICRES1-3F-RLuc-miR-142-3P RE.	Adrian Zagrajek, The Roslin Institute (see Chapter 5)
ChikRepl -3F-RLuc-miRNA RE Control	Replicon, SP6 promoter	RLuc fused to C-terminus of nsP3 protein. RLuc is localised to replication complexes in the cytoplasm. Fusion of RLuc to nsP3 does not inhibit RLuc activity. Control miRNA RE inserted downstream of the non-structural ORF. Replicon equivalent of ICRES1-3F-RLuc-miRNA RE Control.	Adrian Zagrajek, The Roslin Institute (see Chapter 5)

2.4.3 VRP rescue

To generate VRP stock, both Semliki Forest and chikungunya replicons were rescued as described for infectious virus (see 2.3.3), with minor modifications (see below). All Semliki Forest and chikungunya replicons and helper constructs were cloned under control of the SP6 polymerase promoter. Only helper constructs from the split-helper system were used to provide virus structural genes *in trans* during VRP generation.

Linearized chikungunya replicon and Helper-C constructs were always tested by Polymerase Chain Reaction (PCR) for the presence of CHIKV E1 prior to *in vitro* transcription according to the protocol outlined in 2.11.1. The primers and cycling conditions (Annex 12, protocol 1) were adopted from Hoarau et al. (2010).

Replicons and split helper constructs were transcribed *in vitro* at the same time. The RNA from all 3 reaction was mixed and electroporated into BHK-21 cells. VRPs were collected 16-20 and then 40-44 hours post-electroporation. VRP stock was always concentrated by ultracentrifugation through a 20% w/v sucrose cushion.

2.4.4 VRP titration

VRP were titrated as described for infectious virus plaque assay, in the 6-well plate format (see 2.3.5), with minor changes. BHK-21 cells were fixed 14-18 hours post-infection with 10% v/v neutral buffered formalin for at least 1 hour (SFV1) or 4 hours (ChikRepl). Subsequently, plates were washed with tap water, covered with PBS containing Mg^{2+} and Ca^{2+} (2 ml per well) and observed microscopically for cells expressing the fluorescent marker (see 2.7.1). If VRPs did not encode a fluorescent marker, the cell monolayer was first immunostained for viral nsP3 (see 2.6). VRP titre expressed in Infectious Units per ml (IU/ml) was calculated according to the formula used to calculate a virus titre (see 2.3.5).

2.4.5 Confirmation of absence of propagating virus in VRP stock

Virus isolation was performed to confirm that a VRP stock was free of replication-competent virus. In brief, 50% confluent BHK-21 cells in a T-175 flask were washed

once with Mg^{2+} and Ca^{2+}-free PBS, covered with 10 ml of PBSA containing 50 µl of a purified VRP stock and incubated at RT for 1 hour. Next, 20 ml of complete GMEM was added to the flask. Cells were incubated for 3 days. Next, 10 ml of the cell culture supernatant was transferred to a fresh T-175 flask with 50% confluent BHK-21 cells in 20 ml of complete GMEM. The second flask was incubated for 4 days and observed daily for presence of cytopathic effect (CPE). If no CPE was observed at the end of day 4, VRP stock was free of replication-competent virus.

However, in case of chikungunya VRPs, all virus-isolation negative VRP stock and the cell culture supernatant at the end of virus isolation were further tested by PCR for presence of structural genes. The additional layer of control was required as presence of any replication-competent virus in the VRP stock would result in ACDP HG 3 material being handled in a CL 2 laboratory. In brief, RNA was extracted from 50 µl of the VRP stock and the cell culture supernatant at the end of virus isolation using QIAamp Viral RNA Mini Kit (Qiagen, Annex 8), as described in 2.15.5. Next, cDNA was generated from 100 ng of purified RNA as described in 2.12. Finally, the cDNA was tested by PCR for CHIKV E1 (Annex 12, protocol 1), CHIKV nsP4-E1 (Annex 12, protocol 2) and CHIKV nsP4-E3 (Annex 12, protocol 3). The latter two assays were developed specifically to test VRPs for recombination between the replicon RNA and helper RNAs. Chikungunya VRPs were used only when virus isolation and both PCRs were negative.

2.4.6 Preparation of chikungunya replicon RNA for transfection

First, chikungunya replicon was transcribed *in vitro* following the protocol outlined in 2.4.3. No plasmids encoding CHIKV structural genes were handled at the same time. Next, replicon RNA was purified from the reaction mixture using RNeasy® Mini Kit as described in 2.15.5. The quality of purified RNA was inspected on a non-denaturing agarose gel as outlined in 2.14. RNA concentration and purity was measured using NanoDrop™ spectrophotometer. Finally, the RNA was aliquoted, snap-frozen on dry ice, and moved to -80 ºC freezer. RNA aliquots were thawed only once to preserve the RNA integrity.

2.5 *In vitro* infections

2.5.1 Infecting cells (other than MDM) with virus or VRPs

First, cells were harvested, counted and seeded according to Table 2.11. If required, 13 mm sterile cover glasses (VWR, Annex 9) were first added to wells of 24-well plates. On the day of infection, virus/VRP inoculum was prepared in PBSA at the required MOI (the amount of virus was calculated assuming that the cell number doubled every 24 hours with the exception of Thp-1 cells, which would not divide following the induction with PMA). Cell supernatant was removed and 200 µl and 33 µl of virus/VRP inoculum was added per well into 24- and 96-well plates, respectively. Plates were rocked gently for 1 hour at RT. Special care was paid to Hek 293T, Hek 293 miR-142 and Hek 293 miRNA RE Control cells. These cells would detach from the surface of wells/cover glass if not handled carefully. Next, virus inoculum was removed. NHDF, 2fTGH and U4C cells were washed once with Mg^{2+}- and Ca^{2+}-free PBS. IC-21 and Thp-1 cells were washed three times with Mg^{2+}- and Ca^{2+}-free PBS. Hek 293T, Hek 293 miR-142, Hek 293 miRNA RE Control, NIH 3T3 and BHK-21 cells were not washed. Finally, 0.6 ml and 0.1 ml of complete medium per well was added to 24- and 96-well plates, respectively. Plates were incubated for 20 hours, unless otherwise stated.

Table 2.11. Seeding cells for virus infections.

Cells	Cell density (cells/well)		Time prior to infection	Comments
	24-well plate (0.5 ml/well)	96-well plate (0.1 ml/well)		
IC-21; NIH-3T3	8×10^4	1.3×10^4	24 hours	-
Thp-1	1.6×10^5	2.7×10^4	48 hours	Complete medium supplemented with 20 ng/ml PMA.
BHK-21; NHDF	6×10^4	1×10^4	24 hours	-
Hek 293T	1.5×10^5	2.5×10^4	24 hours	-
Hek 293 miR-142-3P; Hek 293 miRNA RE Control	2.5×10^5	4.2×10^4	24 hours	Complete medium supplemented with 100 ng/ml doxycycline, if required (details in Chapter 4).

2.5.2 Collecting and analysing samples post *in vitro* infection

At the end of an *in vitro* experiment all required samples were collected, processed and/or stored as described below, unless indicated otherwise. For a plaque assay, cell culture supernatant (at least 100 µl) was collected and frozen at -80 ºC as soon as feasible. Samples were analysed as described in 2.3.5. For a GLuc assay, cell culture supernatant (at least 100 µl) was collected and stored at 4ºC for a short-term storage (up to 1 week) or frozen at -80 ºC for a long-term storage. Samples were analysed as described in 2.9.3. For RLuc assay (CHIKV), samples were analysed immediately as described in 2.9.1. For RLuc assay (ChikRepl), samples were analysed immediately as described in 2.9.2. For microscopy, cells were immediately fixed in 10% v/v neutral buffered formalin for at least 1 hour (SFV) or 4 hours (CHIKV), processed as described in 2.6 and analysed as described in 2.7.1 and 2.7.4.

2.5.3 Generating cell debris from virus-infected cells

HeLa, 2fTGH or U4C cells were harvested, counted and seeded into T-25 flasks at 1 x 10^6 cells/flask in 5 ml of complete DMEM. Flasks were incubated overnight. Next, cells were washed with Mg^{2+}- and Ca^{2+}-free PBS and covered with 1 ml of virus/VRP diluted in PBSA to give MOI of 5. Flasks were rocked for 1 hour at RT, after which they were topped up with 8 ml of complete DMEM and incubated for 72 hours. Next, cell culture supernatant (approximately 8 ml) was collected and pre-clarified by centrifugation at 3000 x g and 4 ºC for 10 min. Approximately 75% of the supernatant was removed, and passed through 0.2 µm, 0.45 µm or 0.8 µm filter (clarified supernatant). The debris pellet was re-suspended in the remaining 25% of the supernatant (unclarified supernatant).

2.5.4 Infection of MDMs with cell debris

MDMs were harvested, counted and seeded into 24-well plates at 1.6 x 10^5 cells/well in 0.5 ml of complete RPMI. After 48 hours, cell supernatant was removed and cells were washed once with Mg^{2+}- and Ca^{2+}-free PBS. Next, clarified or unclarified supernatant (see 2.5.3) diluted in complete RPMI with 40 U/ml rhCSF1 was added to cells, as described below.

Initial experiments used supernatants diluted 1 in 10 in the final volume of 1 ml per well. Plates were incubated for 2-3 days, during which the inoculum was not removed. Live cells were inspected microscopically for the expression of the fluorescent marker encoded by the virus/VRP every 24 hours using Zeiss Axio Observer.D1 inverted microscope (Zeiss, Annex 10) (see 2.7.1).

Later experiments used cell supernatants diluted 1 in 2 in the final volume of 0.5 ml. In addition, MDMs were seeded onto sterile cover glasses placed at the bottom of all plate wells. Following addition of complete RPMI with cell debris, plates were incubated for 6 hours. Next, the cell supernatant was removed and MDMs were washed 3 times with Mg^{2+} and Ca^{2}+-free PBS. Finally, 1 ml of fresh complete RPMI with 1 x rhCSF1 was added to each well. Plates were incubated for 2 days. After 24 hours, live cells were inspected microscopically using Zeiss Axio Observer.D1 inverted microscope (see 2.7.1). After 48 hours, cells were fixed in 10% v/v neutral buffered formalin for 1 hour and washed three times with Mg^{2+} and Ca^{2}+-free PBS. Next, cover glasses were removed from plates and mounted using VECTASHIELD mounting medium with DAPI (Vector Laboratories, Annex 9). Cells were inspected microscopically for the expression of the fluorescent marker encoded by the virus/VRP using Zeiss Axioskop 2 upright microscope (Zeiss, Annex 10) (see 2.7.1).

2.5.5 Infection of MDMs with purified virus

MDMs were harvested, counted and seeded into 96-well plates as described in 2.5.4. After 48 hours, cell culture supernatant was removed and cells were washed with Mg^{2+}- and Ca^{2+}-free PBS. Next, 270 µl of complete RPMI with 40 U/ml rhCSF1 was added to each well. Finally, 30 µl of SFV4-steGFP diluted in PBSA to give the desired MOI (1, 50,100,500 and 1000) was added directly into the cell supernatant. Plates were incubated for 48 hours. Live cells were inspected microscopically for the expression of virus-encoded eGFP every 24 hours using Zeiss Axio Observer.D1 inverted microscope (see 2.7.1).

2.5.6 Infection of MDMs with purified virus mixed with cell debris from uninfected HeLa cells

First, cell debris from non-infected cells was generated. In brief, HeLa cells were harvested, counted and seeded as described in 2.5.3. Next, cells were washed twice with Mg^{2+}- and Ca^{2+}-free PBS and then covered with 8 ml of Mg^{2+}- and Ca^{2+}-free PBS. Flasks were incubated for 72 hours. Clarified and unclarified cell culture supernatant was prepared as described in 2.5.3 and then diluted 1 in 2 in complete RPMI with 40 U/ml rhCSF.

MDMs were harvested, counted, seeded into 24-well plates and incubated for 48 hours as described in 2.5.4 (no cover glasses used). Next, MDM supernatant was removed and cells were washed once with Mg^{2+}- and Ca^{2+}-free PBS. Clarified and unclarified supernatants diluted 1:2 in complete RPMI were added to MDMs at 0.5 ml per well with 40 U/ml rhCSF. Finally, 100 µl of SFV4-steGFP diluted in PBSA to give MOI of 50 was added to all wells. Plates were incubated for 48 hours. Live cells were inspected microscopically for the expression of eGFP every 24 hours using Zeiss Axio Observer.D1 inverted microscope (see 2.7.1).

2.6 Immunostaining (SFV nsP3)

First, virus-infected cells were fixed for 1-4 hours with 10% v/v neutral buffered formalin. Next, cells were washed with PBS containing Mg^{2+} and Ca^{2+} for 5 minutes, three times. Cells were covered in 0.3% v/v Triton™ X-100 in PBS (Annex 9) for 20 minutes. Cells were washed with PBS as above and incubated for 30 minutes with CAS-BLOCK™ (ZYMED Laboratories, Annex 9). Next, rabbit polyclonal anti-SFV nsP3 antibody (from Dr Tero Ahola, Annex 9) was diluted 1:800 in CAS-BLOCK™. Subsequently, CAS-BLOCK™ was removed from cells and the primary antibody was applied. Cells were incubated at RT for 90 minutes in a humid chamber and subsequently washed in PBS for 10 minutes, three times. Donkey anti-Rabbit Secondary Antibody conjugated to Alexa Fluor® 488 (Life Technologies, Annex 9) was diluted 1:1000 in CAS-BLOCK™ and applied to cells. Next, cells were incubated at RT for 45 minutes in a humid chamber and subsequently washed in PBS for 10 minutes, three times.

Optionally, cells were incubated with DAPI (Sigma-Aldrich®, Annex 9) in H_2O at 0.1 mg/ml for 15 minutes at RT. If this step was followed, cells were subsequently washed with PBS for 10 minutes, three times.

Cells on a cover glass or a glass slide were mounted with VECTASHIELD mounting medium with or without DAPI (Vector Laboratories, Annex 9). If cells were on a surface of a multi-well dish, 0.5 ml of PBS with Mg^{2+} and Ca^{2+} was added to all wells. Samples were stored in dark at 4 ºC until observed microscopically (see 2.7.1).

2.7 Microscopy

2.7.1 Epifluorescent microscopy

Zeiss Axioskop 2 upright microscope and Zeiss Axio Observer.D1 inverted microscope were used. Both microscopes were fitted with filters suitable for visualisation of DAPI, eGFP, zsGreen, Alexa Fluor® 488, mCherry and Alexa Fluor® 594. Zeiss AxioVision 4.8 digital image processing software was used. All images taken were saved as uncompressed zvi files.

2.7.2 Confocal microscopy

The confocal microscopy was done by Dr Pippa Hawes at the Pirbright Institute using Leica TCS SP5 confocal microscope.

2.7.3 Transmission electron microscopy (TEM) of cell debris

First, cell debris from virus/VRP infected cells was prepared as described in 2.5.3, with one alteration. Following centrifugation of cell culture supernatant at 3000 x g and 4 ºC for 10 min, all supernatant was removed. Next, the debris pellet was re-suspended in 1 ml of 3% v/v glutaraldehyde in cacodylate buffer (received from Steven Mitchell, the University of Edinburgh) and placed on ice. Within 3 hours, samples were moved to the Electron Microscope facility of the School of Biological Sciences, the University of Edinburgh.

Next, samples were processed by Steven Mitchell, the University of Edinburgh. In brief, samples were post-fixed in 1% osmium tetroxide in cacodylate buffer, dehydrated in acetone, embedded in Araldite resin, sectioned on a Reichert OMU4 ultramicrotome (Leica) and stained in uranyl acetate and lead citrate.

Finally, samples were viewed and imaged using a Phillips CM120 transmission electron microscope and a Gatan Orius CCD camera.

2.7.4 Calculating the proportion of virus-infected cells

For live cells, 5-10 random areas per each well were screened for adherent cells expressing virus-encoded fluorescent marker using fluorescence microscopy at 10 x magnification. For each well, the proportion of fluorescent marker-positive cells in each individual area was estimated (in %), and then averaged.

For cells fixed in 10% v/v neutral buffered formalin, cell nuclei were first stained with DAPI (see 2.6). Next, 5 random areas per each well were visualised using fluorescence microscopy at 10 x magnification and photographed. Cells expressing virus-encoded fluorescent marker and total cells (as indicated by DAPI) were counted using 'Cell counter' plugin built into ImageJ (Rasband, W.S., ImageJ, U. S. National Institutes of Health, Bethesda, Maryland, USA, http://imagej.nih.gov/ij/, 1997-2014). For each well, the proportion of fluorescent marker-positive cells in each individual area was counted, and then averaged.

2.8 Cell viability assay

CellTiter-Glo® Luminescent Cell Viability Assay (Promega, Annex 6) was used. The manufacturer's protocol was followed (3/15 version; Supplementary Data, Appendix 15), with following modifications. Cells were grown in a standard tissue-culture-treated 96-well plate, with 100 µl of a complete cell culture medium per well. Following the addition of CellTiter-Glo® Reagent and the 10 minute incubation at RT, 150 µl of the reaction mixture was transferred from each well into a white LUMITRAC^{TM}200 96-well plate (Greiner Bio-One, Annex 1). The luminescence was recorded using GloMax® Microplate Reader (Promega, Annex 10).

2.9 Luciferase assay

2.9.1 *Renilla* luciferase – CHIKV

Dual-Glo® Luciferase Assay System (Promega, Annex 6) was used to determine the expression of RLuc in CHIKV-infected cells. The manufacturer's protocol was followed (9/11 version, Supplementary Data, Appendix 16), with following modifications. Cells were grown in a standard tissue-culture-treated 96-well plate, with 100 µl of a complete cell culture medium per well. After the addition of Dual-Glo® Luciferase Reagent the plate was incubated for 10 minutes at RT. Subsequently, Dual-Glo® Stop & Glo® Reagent was added and the plate was incubated for further 10 minutes at RT. Next, 150 µl of the reaction mixture was transferred from each well into white LUMITRAC^{TM}200 96-well plate which was subsequently sealed with MicroAmp® Optical Adhesive Film (Life Technologies Applied Biosystems®, Annex 2). In addition, a robust and waterproof adhesive tape was applied to the edges of the film to ensure that the plate is completely sealed. The luminescence was recorded using GloMax® Microplate Reader.

The presence of MicroAmp® Optical Adhesive Film was a biosecurity requirement as plates were moved between a CL3 laboratory and a CL2 laboratory, where the plate reader was located. The adhesive film reduced the recorded luminescence by approximately 10%. This effect was consistent across a wide range of RLuc concentration (data not shown).

2.9.2 *Renilla* luciferase – ChikRepl

Dual-Luciferase® Reporter Assay System (Promega, Annex 6) was used to determine the expression of RLuc in ChikRepl-transfected cells. The manufacturer's protocol was followed (6/11 version; Supplementary Data, Appendix 17). Cells were grown in 24-well plates and lysed using the Passive Lysis Buffer. Ten µl of the cell lysate was transferred into a white LUMITRAC^{TM}200 96-well plate. The luminescence was recorded using GloMax® Microplate Reader. Dual Injectors System was used to dispense 50 µl of both reagents per well.

2.9.3 *Gausia* luciferase – SFV

Dual-Luciferase® Reporter Assay System was used to determine the expression of GLuc in SFV-infected cells. The protocol outlined in 2.9.2 was followed, however, 10 µl of a cell culture supernatant and not cell-lysate was tested for each sample (GLuc is secreted into cell culture supernatant, lysis of cells is not required).

2.10 Transfection of nucleic acids into mammalian cells

FuGENE® 6 Transfection Reagent (Promega, Annex 6) was used to transfect DNA. Lipofectamine® 2000 Transfection Reagent (Invitrogen™ Life Technologies, Annex 6) was used to transfect DNA and RNA.

2.10.1 FuGENE® 6 Transfection Reagent (DNA)

The manufacturer's protocol was followed (4/11 version; Supplementary Data, Appendix 18). Cells to be transfected were grown in a 96-well plate, with 100 µl of a complete cell culture medium with no P/S per well. Cells were transfected with 200 ng of a DNA plasmid in 10 µl of DNA/FuGENE® 6 mixture per well. DNA:FuGENE® 6 ratio of 1:3 was used. Cells were incubated for 24-26 hours before being assayed. During this time the cell culture supernatant was not changed.

2.10.2 Lipofectamine® 2000 Transfection Reagent (DNA and RNA)

DNA was transfected following the manufacturer's protocol (July 2011 version; Supplementary Data, Appendix 19). Cells to be transfected were grown in a 6-well plate, with 2 ml of a complete cell culture medium with no P/S per well. Cells were transfected with 10 µg of DNA plasmids in 500 µl of DNA/Lipofectamine® 2000 mixture per well. DNA:Lipofectamine® 2000 ratio of 1:3 was used. The cell culture supernatant was not changed following the transfection.

RNA was transfected as outlined for DNA. For a 24-well plate, 0.8 µg of purified RNA (see 2.15.5) was transfected per well using RNA:Lipofectamine 2000 ratio of 1:3 in 100 µl of RNA/Lipofectamine® 2000 mixture. The cell culture supernatant was not changed following the transfection.

2.11 Polymerase Chain Reaction (PCR)

Venti 96-well Thermal Cycler (Life Technologies Applied Biosystems®, Annex 10) was used to amplify DNA via the conventional Polymerase Chain Reaction (PCR) using GoTaq® DNA Polymerase (Promega, Annex 6), Vent® DNA Polymerase (New England Biolabs, Annex 6) or Pfu DNA Polymerase (Promega, Annex 6). All reactions were performed in the final volume of 50 µl. The PCR reaction mixture universally included 1 µl of each primer at 10 µM concentration (Sigma-Aldrich® or Invitrogen™ Life Technologies), 1 µl of deoxynucleotide (dNTP) solution mixture at 10 mM concentration each (Bioline, Annex 6), 1 µl of a DNA template at less than 0.5 µg/µl concentration and nuclease-free water (Sigma-Aldrich®, Annex 6). Thin wall 0.2 µl tubes were used (Axygen, Annex 2).

For a new PCR protocol, the annealing temperature was initially tested at 2-3ºC below the higher of the two primer melting temperatures (T_m). If required, a range of annealing temperatures was subsequently tested, typically in 2 ºC or 3 ºC steps.

Details of all PCR primers and cycling conditions are located in Annex 12.

2.11.1 GoTaq® PCR

The manufacturer's protocol was followed (version 3/12; Supplementary Data, Appendix 20). The 5x Green GoTaq® Reaction Buffer was used.

2.11.2 Vent® PCR

The manufacturer's protocol was followed (Supplementary Data, Appendix 21). The Vent® polymerase was added at 0.5 µl (1 unit) per reaction. The PCR reaction was not supplemented with $MgSO_4$.

2.11.3 Pfu PCR

The manufacturer's protocol was followed (10/09 version; Supplementary Data, Appendix 22). The Pfu polymerase was added at 0.5 µl (1.25 units) per reaction.

2.11.4 Primer design

Eleven primer pairs were designed for control PCRs. In general, the designed primers were 18-22 bases long, had GC content of 52.4-61.1% and T_m of 51.1-58.6 ºC. Each primer of a pair had the same length, GC content and T_m. All primers were design manually by analysing the available sequences (or predicted sequences). Whenever possible, the primer pair was designed to amplify a fragment of clearly identifiable size (e.g. exactly 400 bp). Finally, all control primers were designed to anneal to the template at least 100 bases upstream or downstream of the sequence of interest (e.g. cloning site) so that the primers could be used for sequencing.

Fifteen primer pairs were designed to amplify a target sequence for cloning. Overall, the designed primers were 26-28 bases long, had GC content of 50-69.2 % and T_m of 61.1-67.4. All primers were composed of a core section of 17-19 bases that annealed to the target sequence (GC content of 41.2-66.7% and T_m of 42.2-54.9). This was followed by the sequence of a restriction site to be used for cloning and three random bases. The sequence of all cloning primers was dependent on the sequence of the restriction sites to be added in addition to the target sequence. Hence, variations in GC content and T_m between primers within a pair were occasionally large. The three random bases were used to minimise the differences in GC content and T_m between primers from one pair and to enhance the recognition of the cleavage site by a restriction enzyme.

Primer T_m was calculated using the Wallace formula (Wallace et al. 1979):

$$Tm = 64.9 + 41 * \frac{yG + zC - 16.4}{wA + xT + yG + zC}$$

Where w, x, y, z are the number of the bases A, T, G, C in the sequence, respectively.

2.11.5 Colony PCR

A GoTaq® PCR reaction mixture was set up and aliquoted into PCR tubes (see 2.11 and 2.11.1). No template DNA was added. Next, a sterile pipette tip was used to pick a single bacteria colony from an agar plate and dip it into a tube containing the PCR reaction mixture. Next, the tip was removed from the tube and used to streak a fresh agar plate containing the required selection antibiotic (see 2.19.1). Finally, PCR was run following the applicable protocol (see Annex 12). Samples were analysed by agarose gel electrophoresis (see 2.14).

2.11.6 Annealing of oligonucleotides

Long DNA oligonucleotides (78-81 bases) with 18 bases of a complementary sequence were annealed and extended using Vent® DNA polymerase. The standard protocol was modified. Both oligonucleotides were added at the concentration of 100 μM and the amount of dNTPs was doubled. The following cycling conditions were used:

Denaturation	–	95 ºC	– 2 min 30 sec	**x 1**
Annealing	–	55 ºC	– 2 min	**x 1**
Extension	–	72 ºC	– 5 min	**x 1**
4 ºC				∞

2.12 Reverse Transcription

First-strand cDNA was synthesised using SuperScript™ III Reverse Transcriptase (Invitrogen™ Life Technologies, Annex 6). The manufacturer's protocol was followed (December 2004 version; Supplementary Data, Appendix 23). The reaction was set up using 200 ng of purified RNA (see 2.15.4) and oligo$(dT)_{20}$. Finally, cDNA was treated with RNase H (Invitrogen™ Life Technologies, Annex 6).

2.13 Quantitative PCR (qPCR)

First-strand cDNA was synthesised using High Capacity cDNA Reverse Transcription Kit (Life Technologies, Annex 6) in Venti 96-well Thermal Cycler. The following reaction mixture in 15 μl final volume was set up for all samples:

- 10 x RT buffer – 1.5 µl
- Primer (0.5 µM stock) – 3 µl
- dNTPs – 0.15 µl
- RNase inhibitor – 0.19 µl
- MultiScribe^{TM} reverse transcriptase – 0.5 µl
- Nuclease-free water – up to the final volume of 15 µl
- RNA – 200 ng

Reverse transcription was completed using the following thermal cycling conditions:

16 ºC	– 30 min	**x 1**
42 ºC	– 30 min	**x 1**
85 ºC	– 2 min	**x 1**
4 ºC	– ∞	**x 1**

Quantitative PCR (qPCR) was performed using TaqMan® Universal PCR Master Mix (Life Technologies Applied Biosystems®, Annex 6) and Rotor-Gene 3000 Real-Time PCR Machine (Corbett Life Science Qiagen, Annex 10). The following reaction mixture in 20 µl final volume was set up for all samples, in triplicates:

- 2 x Universal Master Mix – 10 µl
- Primer-probe mix – 1 µl
- RT sample – 1.5 µl
- Nuclease-free water – up to final volume of 20 µl

Quantitative PCR was completed using the following thermal cycling conditions:

50 ºC	– 2 min	**x 1**
95 ºC	– 10 min	**x 1**
95 ºC **60 ºC**	– 15 sec – 1 min	**x 40**

2.14 Agarose gel electrophoresis

In brief, 1-3% w/v agarose gels were prepared by mixing Ultrapure™ Agarose (InvitrogenTM Life Technologies, Annex 6) and Tris Acetate-EDTA (TAE) buffer (Annex 11) in a glass beaker, and microwaving until the agarose was completely dissolved. Next, 5 µl of SYBR® Safe DNA Gel Stain (Life Technologies, Annex 6) was added per 100 ml of the gel and mixed well. Still hot gels were casted using a UV-transparent gel tray (15 x 10 cm, 15 x 15 cm or 15 x 25 cm) and a Mini-Gel Caster (Bio-Rad, Annex 10). Typically, 100 ml of a gel was prepared for the 15 x 10 cm trey. For trays of other sizes, the gel volume was adjusted accordingly. Combs with 15 and 20 wells were used. Solidified gels at RT were moved into Wide Mini-Sub® Cell GT Cell or Sub-Cell® GT Cell electrophoresis gel tanks (Bio-Rad, Annex 10) filled with TAE buffer. The buffer volume was subsequently adjusted to ensure that the gel was covered with the buffer, but only just.

Next, nucleic acid samples and either a 100 bp or a 1 kb DNA ladder (both Promega, Annex 6) were mixed with 6 x Blue/Orange Loading Dye (Promega, Annex 6). This was not performed for DNA samples amplified using GoTaq® DNA polymerase as the reaction buffer used already contained a loading dye (see 2.11.1). Finally, 5-40 µl of each sample or 6 µl of the chosen ladder was loaded per well. Electric current was applied using PowerPac™ Basic Power Supply (Bio-Rad, Annex 10). Typically, samples were analysed at 90 volts for 45 minutes to 2 hours.

Gels were visualised using DR89 Dark Reader blue transilluminator (Clare Chemical Research, Annex 10) or MultiImage Light Cabinet FluorChem HD2 (Alpha Innotech, Annex 10).

2.15 Nucleic acid isolation and purification

2.15.1 Measuring the concentration and purity of nucleic acids

The concentration and purity of eluted DNA and RNA samples were tested using NanoDrop™ (Thermo ScientificTM, Annex 10). If required, the integrity of samples was tested by agarose gel electrophoresis, as described in 2.14.

2.15.2 Isolation of cellular genomic DNA

DNeasy® Blood & Tissue Kit (Qiagen, Annex 8) was used. The manufacturer's protocol (spin-column) was followed (July 2006 version; Supplementary Data, Appendix 24). DNA was extracted from 1 x 10^6 of cultured cells. DNA was eluted with 200 µl of buffer AE. Purified samples were handled at RT and stored at -20 ºC.

2.15.3 Isolation of cellular total RNA

TRIzol® Reagent (Life Technologies Ambion™, Annex 6) was used. The manufacturer's protocol was followed (November 2010 version; Supplementary Data, Appendix 25). RNA was extracted from 1 x 10^6 cells. The RNA pellet was air dried for 5 minutes and resuspended in 50 µl of nuclease-free water (Sigma-Aldrich®, Annex 6). Purified RNA was handled on ice and stored at -80 ºC.

2.15.4 Isolation of Viral RNA

QIAamp Viral RNA Mini Kit (Qiagen, Annex 8) was used. The manufacturer's protocol (spin-column) was followed (June 2006 version; Supplementary Data, Appendix 26). RNA was extracted from 50 µl of cell culture supernatant and eluted with 60 µl of buffer AVE. Purified RNA was handled on ice and stored at -80 ºC.

2.15.5 Purification of RNA from enzymatic reactions

RNease® Mini Kit (Qiagen, Annex 8) was used. The manufacturer's protocol (spin-column) was followed (September 2010 version; Supplementary Data, Appendix 27). RNA was extracted from *in vitro* transcription reactions (see 2.3.3 and 2.4.3). On-column DNase digestion was performed using RNase-Free DNase Set (Qiagen, Annex 8). RNA was eluted with 30 µl of nuclease-free water. Purified RNA was handled on ice and stored at -80 ºC.

2.15.6 Purification of DNA from agarose gels

A sample of DNA was run on an agarose gel, as described in 2.14. Next, DNA was visualised using DR89 Dark Reader blue transilluminator. Required bands were removed from the gel using a disposable sterile scalpel (Swann-Morton, Annex 3) and put into DNase- and RNase-free 1.5mL screw cap microtubes (Sartsetdt, Annex

2). DNA was purified using NucleoSpin® Gel and PCR Clean-up (Macherey-Nagel, Annex 8). The manufacturer's protocol was followed (January 2012; Supplementary Data, Appendix 28). Purified DNA was handled at RT and stored at -20 ºC.

2.15.7 Purification of DNA extracted from enzymatic reactions

DNA from enzymatic reactions (PCR, restriction digest) was purified using NucleoSpin® Gel and PCR Clean-up following manufacturer's protocol (see 2.15.7).

2.15.8 Small-scale DNA plasmid propagation and isolation (Mini-prep)

A single colony was picked from an agar plate using a sterile pipette tip. It was used to inoculate 5 ml of LB broth (Annex 11) containing the appropriate selective antibiotic (See 2.19) in a universal bottle. Standard microbiological practices were followed. Next, the bacteria culture was incubated with shaking (250-300 RPM) at 37 ºC for 16 hours using InnOva^{TM} 4300 Incubator Shaker (New Brunswick, Annex 10). Finally, the plasmid DNA was isolated and purified using ISOLATE Plasmid Mini Kit (Bioline, Annex 8). The manufacturer's protocol was followed (1st edition; Supplementary Data, Appendix 29). DNA was eluted in 50 µl of the elution buffer. Purified DNA was handled at RT and stored at -20 ºC.

2.15.9 Large-scale DNA plasmid propagation and isolation (Maxi-prep)

A bacteria culture was prepared as described in 2.15.8 and incubated with shaking (250-300 RPM) at 37 ºC for 6-8 hours. Next, 0.5 ml of this culture was transferred into a sterile 1 litre glass conical flask containing 250 ml of either LB broth or Tryptone Soya Broth (Annex 11) containing the appropriate selective antibiotic (see 2.19). The culture was incubated with shaking (250-300 RPM) at 37 ºC for 16 or 40 hours, respectively. Finally, the plasmid DNA was isolated and purified using EndoFree® Plasmid Purification Maxi Kit (Qiagen, Annex 8). The manufacturer's protocol was followed (November 2005 version; Supplementary Data, Appendix 30) The DNA was resuspended in 0.1-1 ml of either endotoxin-free Buffer TE or DNase- and RNase-free water. Purified DNA was handled at RT and stored at -20 ºC.

2.16 DNA restriction digest

Restriction enzymes from Promega, New England Biolabs and Roche were used (see Annex 6). The activity of all restriction enzymes was expressed in units. One unit was defined as the amount of restriction enzyme required to fully digest 1 μg of bacteriophage lambda DNA in 1 hour. Each of the enzymes used had specific requirements for the optimal activity, including pH, enzyme cofactor(s), salt composition and ionic strength. Consequently, the reaction buffer that yielded the highest activity for the enzyme (all enzymes, if multiple used) was always chosen (typically 100%, no less than 75%). The final concentration of glycerol (typically part of a restriction enzyme diluent) was kept below 5% v/v. All DNA substrates were first purified as described in 2.15 and had A260/280 ratio of >1.8.

An analytical restriction digest was typically set up as outlined below and subsequently incubated for 2 hours at the required temperature (typically 37 ºC):

- Restriction enzyme(s) – 5-10 units, each
- Restriction Enzyme 10 x Buffer – 2 μl
- Acetylated BSA, 100 x (Promega, Annex 6) – 0.2 μl
- DNA – 0.5-1 μg
- Nuclease-free water – up to 20 μl final volume

The above setup was modified for a cloning restriction digest. In brief, 0.5-20 μg of a template DNA was used. The final volume of the reaction mixture depended on the amount of template DNA to be digested (10 μl per each 1 μg of DNA, and no less than 50 μl). The quantities of the buffer, BSA and water were adjusted accordingly.

Analytical restriction digests were analysed by agarose gel electrophoresis (see 2.14). Cloning restriction digests were purified as described in 2.15.7 or 2.15.6. The concentration and purity of eluted DNA was tested using NanoDrop™. Purified DNA was handled at RT and stored at -20 ºC.

2.17 DNA dephosphorylation

Cloning vectors linearized by a single restriction enzyme (or blunt-ended) were treated with Thermosensitive Alkaline Phosphatase (TSAP) (Promega, Annex 6) to remove 5' phosphate groups from DNA ends and thus prevent the recirculisation of linearized vectors during ligation. The following reaction mixture was set up:

- Linearized DNA – up to 5 µg
- TSAP – 0.5 µl per 1 µg of linearized DNA
- MULTI-CORE^{TM} 10 x Buffer – 5 µl
- Nuclease-free water – up to final volume of 50 µl

The reaction mixture was incubated at 37 ºC for 1 hour. Subsequently, TSAP was heat-inactivated at 74 ºC for 15 minutes. DNA was purified as described in 2.15.7.

2.18 DNA ligation

T4 DNA Ligase (New England Biolabs, Annex 6) was used. DNA was prepared by mixing a cloning vector and an insert at the molar ratio of 1 to 3 (100 ng total). The following reaction mixture was set up (T4 DNA Ligase was added last):

- 10 x T4 DNA Ligase Buffer (at RT) – 2 µl
- DNA – 100 ng
- T4 DNA Ligase – 1 µl
- Nuclease-free water – up to 20 µl final volume

The ligation mixture was incubated at RT for 3 hours. Next, it was either used to transform competent bacteria (see 2.19) or it was stored at -20ºC.

2.19 Transformation of competent bacteria with expression vectors

2.19.1 Preparation of selective LB agar plates

First, LB agar (Annex 11) was slowly melted in a microwave. Next, the melted agar was rocked at RT using SSM4 Sea-saw rocker (Stuart, Annex 10) until warm but cool enough to handle with unprotected hand. Inside a class II MBSC, a selective antibiotic was added. Ampicillin or kanamycin (both Sigma-Aldrich®, Annex 7)

were used at 100 µg/mL and 50 µg/mL final concentrations, respectively. The agar was mixed gently (to prevent formation of air bubbles) and then poured into 100 mm petri dishes at approximately 15 ml per dish. Finally, petri dishes were cooled to RT for approximately 30 minutes and then were stored at 4 ºC for up to 1 month.

2.19.2 SURE® 2 Supercompetent cells (Stratagene, Annex 7)

The manufacturer's protocol was followed (Supplementary Data, Appendix 32), however, 1.5 ml screw-cap microcentrifuge tubes were used instead of 14 ml round bottom tubes. Post-heat-shock, bacteria were diluted in 900 µl of SOC medium (Sigma-Aldrich®, Annex 7) and incubated at 37 ºC with shaking (225 RPM) for 1 hour using Thermomixer® Dry Block Heating Shakers (Eppendorf, Annex 10). Finally, the required volume of bacteria (based on anticipated transformation efficiency) was spread on selective LB agar plates (see 2.19.1) using disposable bacteria spreaders (Gosselin, Annex 2). Standard microbiological practices were followed. For volumes larger than 100 µl, bacteria were first pelleted by centrifugation at 4000 x g for 5 minutes and then resuspended in 50-100 µl of SOC medium. Plates were incubated for at least 16 hours at 37 ºC.

2.19.3 Subcloning Efficiency™ DH5α™ Competent Cells (Invitrogen™ Life Technologies, Annex 7)

The manufacturer's protocol was followed (January 2006 version; Supplementary Data, Appendix 32). Post-heat-shock, bacteria were diluted in 950 µl of SOC medium and incubated for 1 hour as described in 2.19.2. Finally, bacteria were spread on selective LB agar plates and incubated as described in 2.19.2.

2.20 DNA Sequencing

DNA was sequenced by Sanger dideoxy chain terminator method (Sanger et al. 1977). Commercially available services were used (GATC Biotech, MRC PPU DNA Sequencing and Services, and Source Bioscience). Purified PCR products and plasmids (circular and linearized) were sequenced. Samples and primers were prepared according to the recommendations of the service provider.

Sequences were aligned to a predicted reference sequence using ClustalW version 2 available at http://www.ebi.ac.uk/Tools/msa/clustalw2/ (Larkin et al. 2007, Goujon et al. 2010). Sequencing chromatograms were analysed using BioEdit Sequence Alignment tool version 7.1.3.0 (Hall, 1999) to confirm good sequence quality.

2.21 SFV *in vivo*

2.21.1 Mice

IFN-α/ß receptor knockout mice of A129/SvEv background (IFNAR mice) sourced from B&K Universal were used. Mice were maintained in the Biological Research Facility (BRF) at the University of Edinburgh School of Biomedical Sciences. Mice were maintained with environmental enrichment, a 12-hour light/dark cycle, and food and water *ad libitum*. Mice were acclimatised for a week prior to any experimental procedures. All experiments were carried out under the authority of a UK Home Office License.

2.21.2 Infection

Mice between the age of 4 and 5 weeks were injected intraperitoneally (IP) by Dr Rennos Fragkoudis, the Pirbright Institute. In brief, mice were immobilised and injected with 0.1 ml of virus inoculum diluted in PBSA at 5×10^3 PFU/animal using a 21 G needle (Terumo, Annex 3) inside a class I MBSC.

2.21.3 Sampling

Mice were euthanized by CO_2 overdose according to the Home Office guidelines with help from Dr Rennos Fragkoudis, the Pirbright Institute. Next, the animal fur was dampened with 70% ethanol. Pulling the abdominal skin with forceps, a small incision was made over the caudal half of the abdomen with scissors to expose the underlying abdominal wall. Care was taken to not pierce the abdominal wall while incising the skin. Next, lifting the abdominal wall with forceps, 5 mL of sterile Mg^{2+}- and Ca^{2+}-free PBS was injected into the caudal half of the peritoneal cavity using a 25 G needle, bevelled side up (Terumo, Annex 3). The entire body of the mouse was gently shaken by hand for approximately 10 seconds. PBS containing resident

peritoneal cells was aspirated using a 19 G needle (Terumo, Annex 3), inserted into the cranial half of the peritoneal cavity, bevelled side down. Cell suspension was stored on wet ice until processed further (see 2.21.6). Next, the abdominal cavity was opened using surgical scissors and the spleen was collected and placed into a bijoux tube containing 4% v/v neutral buffered formalin. Finally, using surgical scissors the skull was opened, the spinal cord was cut, and the brain was collected and placed into a bijoux tube containing 4% v/v neutral buffered formalin.

2.21.4 Processing of tissues and cryosectioning

Tissues for histology were kept in 4% v/v neutral buffered formalin for 72 hours. Next, tissues were submerged in 5 ml of 5% w/v sucrose solutions (Annex 11) for 1 hour, then in 5 ml of 10% w/v sucrose solution (Annex 11) for 1 hour, and finally in 5 ml of 20% w/v sucrose solution (Annex 11) overnight. The following day tissues were inspected to ensure that they sunk to the bottom of the sucrose solution. Next, the tissues were embedded in OCT Cryoembedding Matrix (Thermo Scientific™ Raymond Lamb, Annex 9) using Peel-A-Way Disposable Embedding Molds (Thermo Scientific™ Shandon™, Annex 2) and frozen using an isopentane (Sigma-Aldrich®, Annex 5) bath chilled to approximately -70 ºC with dry ice.

Tissues were sent to the Veterinary Pathology Unit at the University of Edinburgh for processing by Mr Neil MacIntyre. In brief, samples were sectioned into 8 μm thick sections using a cryomicrotome, placed on polylysine coated slides, and finally stored at -80 ºC.

2.21.5 Immunohistochemistry

Slides were removed from -80 ºC, placed in front of a fan and dried at RT for approximately 1 hour. Next, sections were immunostained as described in 2.6, with or without 0.3 % v/v Triton™ X-100 treatment step. The following antibodies were used: Rat anti-Mouse MARCO primary antibody (AbD Serotec®, Annex 9) at 1:200 dilution; Rat anti-Mouse CD169 primary antibody, Alexa Fluor® 647 conjugate (AbD Serotec®, Annex 9) at 1:100 dilution; Goat anti-Rat IgG secondary antibody, Alexa Fluor® 594 conjugate (Life Technologies, Annex 9) at 1:500 dilution.

2.21.6 Peritoneal macrophage flow cytometry

The suspension of peritoneal cells was centrifuged at 300 x g and 4 ºC for 10 minutes. One ml of the supernatant was frozen at -80 ºC. If required, cell pellet was resuspended in 10 ml of RBC lysis buffer (Annex 11) and incubated at RT for 10 minutes. Cells were washed twice with Mg^{2+}- and Ca^{2+}-free PBS by centrifugation at 300 x g and 4 ºC for 10 minutes, resuspended in 1 ml of Mg^{2+}-and Ca^{2+}-free PBS and mixed with 1 ml of 10% v/v neutral buffered formalin. Cells were fixed for 30 minutes at RT. Next, cells were centrifuged at 300 x g and 4 ºC for 10 minutes and then washed with Mg^{2+}- and Ca^{2+}-free PBS, as described above. Finally, cells were resuspended in 2 ml of FACS buffer (Annex 11), counted and stored at 4 ºC in dark.

The following day, 1 x 10^6 cells was resuspended in 100 µl of FACS buffer, and 1 µl of PE anti-mouse F4/80 antibody (Biolegend, Annex 9) or 1µl of PE Rat IgG2b, κ Isotype control (Biolegend, Annex 9) was added. Cell suspension was briefly vortexed and incubated in dark at RT for 30 minutes. Next, 1 ml of FACS buffer was added and the cells were centrifuged at 300 x g and RT for 5 minutes. Finally, cells were resuspended in 300 µl of Mg^{2+}- and Ca^{2+}-free PBS and analysed using BD FACSCalibur™ flow cytometer (BD, Annex 10). The data was analysed using FlowJo x 10.0.7 software (FlowJo, LLC).

2.22 CHIKV *in vivo*

The pathogenesis of a modified CHIKV was tested in a non-human primate model of the disease in collaboration with Dr Pierre Roques at the French Alternative Energies and Atomic Energy Commission (CEA), Division of Immuno-Virology, Fontenay-aux-Roses, France. The study was approved by the regional animal care and use committee (Comite Regional d'Ethique sur l'experimentation animal Ile de France Sud) in accordance with European directive 86/609/EEC.

Handling and sampling of live animals, infection and clinical observations were performed by Dr Pierre Roques with assistance from Division of Immuno-Virology staff and me. At the end of the study, animals were euthanized by a named veterinarian, and samples were collected by Dr Pierre Roques and me.

2.22.1 Animals

Naïve, adult (5-8 years old) male cynomolgus macaques (*Macaca fascicularis*) each weighing 8.0-8.5 kg were used. The animals were captive-bred in Mauritius, imported to France, and tested negative for simian immunodeficiency virus (SIV), simian T lymphotropic virus (STLV), herpes B virus, filovirus, simian type D retrovirus (SRV-1), simian retrovirus serotype 2 (SRV-2), measles virus, DENV and CHIKV. Animals had been previously infected experimentally with influenza A virus, however, they were confirmed to be seronegative for anti-CHIKV neutralising antibodies prior to infection with CHIKV. All animals were housed in single cages within a purpose-designed CL3 facility.

2.22.2 Infection

Animals were first sedated with 10 mg/kg of body mass ketamine chlorhydrate (Rhône Mérieux, Annex 5) injected intravenously (IV). Next, both wrists were shaved and the animals were inoculated sub-cutaneously (SC) on the upper part of the left wrist with 0.5 ml of virus inoculum in PBS at 1×10^6 PFU/animal.

2.22.3 Clinical observation

Animals were observed for overt signs of a disease such as loss of appetite and lethargy daily. Measurement of body temperature, body weight and wrist swelling (site of injection and contralateral) were performed at each time of sampling (2.22.4).

2.22.4 Sampling

Animals were sedated by ketamine chlorhydrate (see 2.22.2) before any sampling. Blood for haematology was collected on days -4, -1, 0 (prior to inoculation), 1, 2, 3, 4, 5, 7, 14, 18 (pre-euthanasia), 21, 28 and 35 (pre-euthanasia). Full haematology was performed using COULTER® HmX Hematology Analyzer (Beckman Coulter, Annex 10). Serum was collected on days -4, -1, 0 (prior to inoculation), 1, 3, 5, 7, 14, 18 (pre-euthanasia), 21, 28 and 35 (pre-euthanasia), aliquoted, and stored at -80 ºC. Plasma was collected on days -4, -1, 0 (prior to inoculation), 1, 2, 3, 4, 5, 7, 10, 14, 18 (pre-euthanasia), 21, 28 and 35 (pre-euthanasia), and stored at -80 ºC. PBMCs were collected on days -4, -1, 0 (prior to infection), 2, 4, 7, and 8, and stored in LN_2.

Animals were euthanized 18- or 35-days post-infection by IV injection of 10 mg/kg of body mass ketamine chlorhydrate followed by IV injection of 100 µg/kg of body mass sodium pentothal (Abbot Laboratories, Annex 5). During necropsy, a range of muscle, tendon, skin and lymph nodes samples were taken from around the site of infection, and contralateral. Samples were preserved in 10% v/v neutral buffered formalin for histology or snap-frozen using an isopropanol/dry ice bath for virus and RNA isolation. Spleen and liver samples were also collected, cut into smaller sections, and then preserved as described above.

2.22.5 Plasma viral RNA quantification (qPCR)

Viral RNA was isolated from 100 µl of EDTA-anticoagulated, cell-free plasma using NucleoSpin® 96 Virus Kit (Macherey-Nagel, Annex 8), in duplicates. The Manufacturer's protocol was followed (April 2014 version; Supplementary Data, Appendix 33). RNA was eluted in 100 µl of nuclease-free water and stored at -80 ºC. EDTA-anticoagulated, cell-free plasma of a CHIKV-uninfected macaque was used as the negative control. To generate a standard curve, CHIKV stock of known titre was first diluted in the plasma used for the negative control. Next, serial 10-fold dilutions were prepared.

Next, quantitative reverse transcriptase PCR was set up using SuperScript™ III One Step Quantitative RT-PCR System (Invitrogen Life Technologies, Annex 6). The manufacturer's protocol was followed (revision B.0; Supplementary Data, Appendix 34). For each sample, the following reaction mixture was prepared on ice in 25 µl final volume, in duplicates:

- SuperScript™ III reverse transcriptase/Platinum® Taq – 0.5 µl
- 2 x Reaction Mix – 12.5 µl
- Forward primer, 10 µM – 0.5 µl
- Reverse primer, 10 µM – 0.5 µl
- Probe, 10 µM – 0.5 µl
- RNase inhibitor (40U/µl) – 0.5 µl
- Purified RNA – 10 µl

Primers and probe used were designed by Laurent et al. (2007):

- Primer F1 – AAGCTCCGCGTCCTTTACCAAG
- Primer R1 – CCAAATGTCCTGGTCTTCCT
- Probe – [FAM]TCTCAACAGCTTGGTCACCGTT[TAM]

Reverse transcription and quantitative PCR were completed using ICycler IQ™ Real Time PCR with My IQ™ Real Time Module (Bio-Rad, Annex 10) and the following cycling conditions:

Reverse Transcription	–	56 ºC	– 30 min	**x 1**
Denaturation	–	95 ºC	– 5 min	**x 1**
Denaturation **Annealing and elongation**	– –	95 ºC 60 ºC	– 15 sec – 1 min	**x 35**
4 ºC				∞

2.23 Statistical analysis and data presentation

Within an experiment, all infections were done in triplicates (Chapter 3) or quadruplicates (Chapter 4 and 5). Data from a representative experiment out of 2-4 independent repeats (typically 3) are shown, unless specified otherwise.

Results were analysed using Mann-Whitney test, single-tailed. $P<0.05$ was accepted as indicating statistical significance. GraphPad Prism 5.0 (GraphPad Software Inc.) and Microsoft Excel 2010 (Microsoft) were used for analysis and graph preparation.

Chapter 3:

Interaction of Semliki Forest virus (SFV) with human monocyte-derived macrophages (MDMs)

Content:

3.1 Objectives

The intention for this part of the project was to investigate the interaction of human monocyte-derived macrophages (MDMs) with CHIKV. The role of cell debris from virus-infected cells in MDMs infection was of a particular interest. However, at the time of this study, the CL3 facility at the Roslin Institute was not yet available for use. Hence, proof-of-concept experiments were designed and completed using SFV.

There are no published studies investigating if SFV can infect human MDMs. However, several studies investigated if SFV could infect mouse macrophages. In 1976 van der Groen et al. demonstrated that peritoneal macrophages from OF_1 mice cultured *in vitro* can get productively infected with SFV strains V13 and A7. Oaten et al. (1980) showed that peritoneal macrophages from Swiss/A2G mice were productively infected with SFV strain A7(74) and L10 *in vivo* and *in vitro*. Finally, Fragkoudis et al. (2007) observed a population of virus-positive cells in spleen of SFV4-infected IFN-α/ß receptor knockout mice of A129/SvEv background (IFNAR mice), in marginal zones between the red pulp and white pulp. These areas are known to be rich in macrophages and dendritic cells.

The objectives for this part of the project were as follow:

1) To determine if purified SFV can infect human MDMs *in vitro*.

2) To determine if the presence of cell debris from SFV-infected human cell lines can affect the rate at which SFV infects human MDMs *in vitro*.

3) To determine if virus particles are required to infect MDMs with SFV.

4) To investigate properties of the cell debris from virus-infected human cell lines and the nature of the infectious material contained within.

3.2 Growing viruses and virus replicon particles

SFV4-steGFP and SFV4-3F-zsGreen were rescued, purified and titrated by Claudia Rückert, the University of Edinburgh, as described in 2.3.3 and 2.3.5. SFV1-3F-zsGreen replicon was rescued and purified as described in 2.4.3. SFV1-3F-zsGreen virus replicon particles (VRPs) were titrated as described in 2.4.4. VRP stock was confirmed negative for replication-competent virus following the protocol in 2.4.5.

SFV4-steGFP expressed enhanced green fluorescent protein (eGFP) (Cormack et al. 1996) as part of the virus structural polyprotein (Fragkoudis et al. 2007). The fluorescent marker was cleaved from the polyprotein co-translationally leading to its release into the cytoplasm of virus-infected cells. SFV4-3F-zsGreen and SFV1-3F-zsGreen VRPs were fundamentally identical in the non-structural region and they both expressed ZsGreen1 (commercially developed by Clontech, herein known as zsGreen) as a fusion protein with nsP3. Consequently, ZsGreen1 was localised to replication complexes in virus/VRP-infected cells leading to the characteristic foci of expression observed microscopically (Figure 3.7). SFV1-3F-zsGreen did not encode the structural genes in its genome and therefore VRP-infected cells could not produce virus/VRPs.

3.3 Can purified SFV infect human MDMs?

SFV4-steGFP was used to infect MDMs at multiplicity of infection (MOI) of 1, 50, 100, 500 and 1000 as described in 2.5.5. Twenty four hours post-infection, the percentage of infected (positive for eGFP) cells varied from 0 at MOI=1 to a peak value of only 0.06 % at MOI=500. Forty-eight hours post-infection, the percentage of infected cells was only marginally above the level of detection (LOD) of 0.01% for all MOIs tested. Data are summarised in Figure 3.1. Overall, MDMs did not infect readily with purified SFV4.

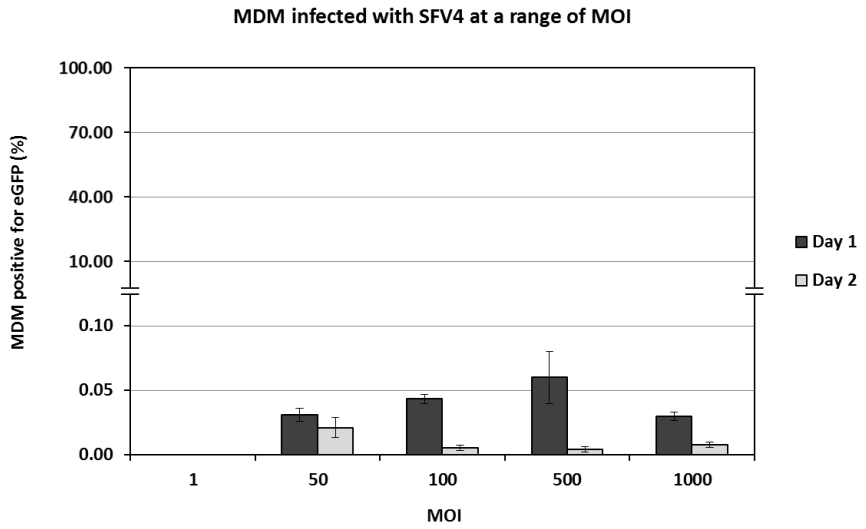

Figure 3.1. Infection of MDMs with purified SFV4-steGFP. Cells were observed for the expression of virus-encoded eGFP using Zeiss Observer.D1 inverted microscope 24- and 48-hours post-infection. MOI range of 1-1000 was tested. LOD=0.01%. Data expressed as mean +/- SD.

3.4 Can MDMs be transfected with virus or replicon genomic RNA?

A range of transfection and electroporation protocols was tested to investigate if MDMs positive for SFV or SF replicon genome replication can be obtained despite the low infection rate achieved with the purified virus. Genomic RNA of SFV4-3F-zsGreen (virus) and SFV1-3F-zsGreen (replicon) generated in 3.2 was used. Twenty four and forty eight hours post-transfection, MDMs were observed microscopically for expression of virus- and replicon-encoded zsGreen using Zeiss Observer.D1.

First, MDMs were transfected with Lipofectamine® 2000 Transfection Reagent. In brief, MDMs were harvested, counted and seeded into 96-well plates as described in 2.5.4. After 48 hours, the cell culture supernatant was replaced with a fresh one, and MDMs were transfected as described in 2.10.2. Unfortunately, no zsGreen-positive MDMs were observed at both time points.

Next, MDMs were electroporated using the Gene Pulser XcellTM Electroporation System. In brief, MDMs were harvested and counted as described in 2.5.4, and then electroporated as described in 2.3.3.1 (square wave protocol, 850 V, 4 msec pulse

length, 2 pulses with 5 second interval in between). In addition, the protocol was modified to follow the exponential decay parameters described by Smale (2010) and Ponsaerts et al. (2002) (250-300 V, 150-960 µF). Similarly to the transfection with Lipofectamine® 2000 Transfection Reagent, no zsGreen-positive MDMs were observed at both time points.

3.5 Can the presence of cellular debris from SFV-infected human cell lines affect the rate at which SFV infects human MDMs?

The ability of SFV4 to infect MDMs in presence of cellular debris from SFV4-infected human cell lines HeLa, 2fTGH and U4C was investigated. As discussed before, in 2011 Krejbich-Trotot et al. demonstrated that the presence of apoptotic debris from CHIKV-infected HeLa cells promoted the infection of primary murine macrophages, MM6- and Thp-1-PMA differentiated cells with CHIKV *in vitro*. Hence, HeLa cells were chosen for this study. HeLa are human cervix adenocarcinoma epithelial cells that have been used since 1951 (Gey et al. 1952). However, these cells are highly aberrant with respect to their genome and gene expression (Bottomley et al. 1969, Macville et al. 1999, Adey et al. 2013, Landry et al. 2013) and must be used with caution to study any complex biological processes. Consequently, 2fTGH and U4C cells were used in this study, in addition to HeLa.

2fTGH is a modified human fibrosarcoma cell line that is characterised by a competent IFN system. 2fTGH cells were generated by transfecting human fibrosarcoma cell line HT 1080 with a vector containing a selectable marker guanine phosphoribosyltransferase regulated by IFN-α (Pellegrini et al. 1989). The presence of the marker allowed selection of descendant cell lines containing a range of mutations in their IFN signalling pathway. U4C cell line is derived from one such mutant of 2fTGH cells. U4C cells lack JAK1 kinase and are therefore unresponsive to IFN-α/ß/γ (Kohlhuber et al. 1997). In addition, their innate immune response to double stranded RNA is defective. The use of U4C cells paired with the parental 2fTGH cells allowed to directly investigate if the presence of the competent IFN system in SFV-infected fibroblast cells can alter the capacity of cell debris derived from these cells to mediate infection of human MDMs with the virus.

To generate cellular debris, HeLa, 2fTGH and U4C cells were infected with SFV4-steGFP as described in 2.5.3. Seventy two hours post-infection, cells were inspected microscopically (Figure 3.2). All observed HeLa cells were positive for eGFP. Similarly, the majority of U4C cells was positive for eGFP. However, individual eGFP-negative U4C cells were also observed. The proportion of eGFP-positive 2fTGH cells was noticeably smaller, approximately a third of that observed for HeLa and U4C cells. The majority of cells expressing eGFP showed cytopathic effect (CPE) while little or no CPE was observed in eGFP-negative cells. Based on our current knowledge of alphavirus-induced cell death (see 1.4), the cellular debris were most likely composed of apoptotic debris. However, cell monolayers and the cellular debris were not investigated for the presence of markers of apoptosis (e.g. cleaved caspase 3) and markers of apoptotic debris (e.g. cell surface phosphatidylserine).

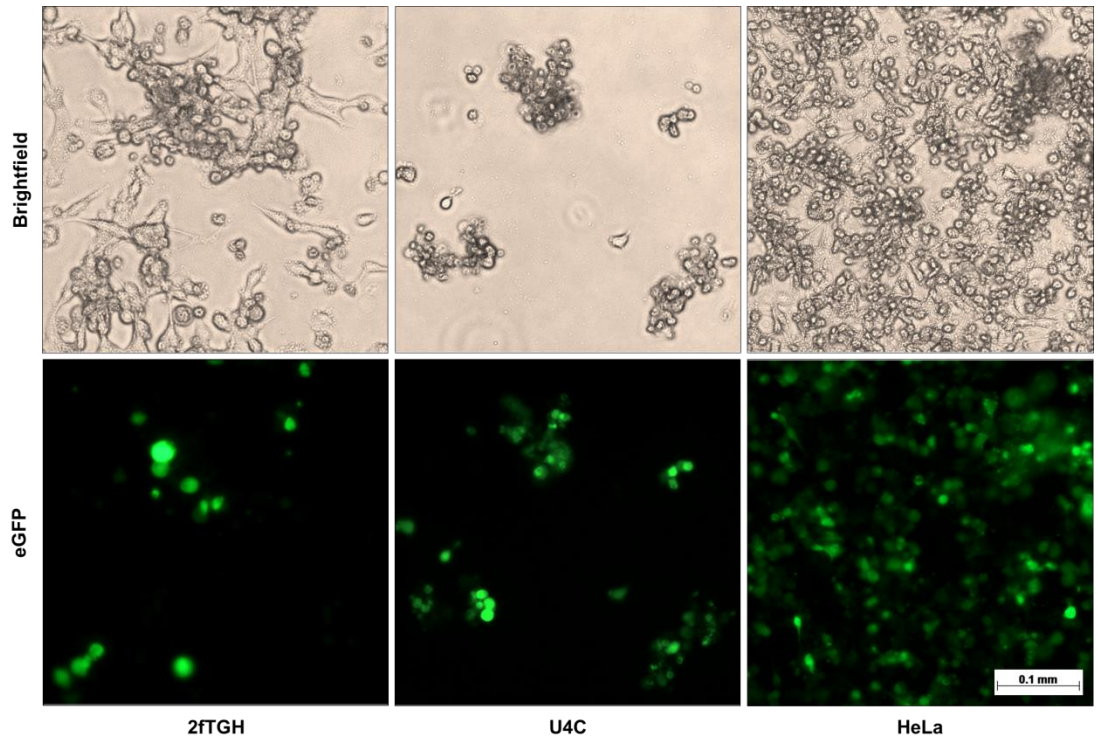

Figure 3.2. HeLa, 2fTGH and U4C cells infected with SFV4-steGFP. Cells were infected at MOI of 5 and incubated for 72 hours. Cells were observed for the expression of virus-encoded eGFP using Zeiss Observer.D1 inverted microscope.

Unclarified (containing cellular debris) and 0.2 μm-clarified supernatants were prepared as described in 2.5.3, diluted 1:10 in complete RPMI, and used to infect human MDMs as described in 2.5.4. The inoculum was not removed post-infection. Cells were incubated for 48 hours and inspected microscopically for the expression of virus-encoded eGFP every 24 hours. SFV4-steGFP titre in unclarified and 0.2 μm-clarified supernatants was measured as described in 2.3.5.

Infection of MDMs with unclarified supernatant from SFV4-steGFP-infected HeLa cells led to a significantly higher proportion of MDMs expressing eGFP in comparison to MDMs infected with the clarified supernatant 24- and 48-hours post-infection (33.0% vs 6.67% and 13% vs 4.33%, respectively) as shown in Figure 3.4c. Similar pattern was observed for MDMs infected with 2fTGH and U4C cells-derived supernatants (Figure 3.4a and Figure 3.4b, respectively). However, the overall number of eGFP-positive MDMs was lower when compared to MDMs infected with HeLa-derived supernatants (peak infection rate of 14.67% and 21% for 2fTGH- and U4C-derived supernatants, respectively). Importantly, in virus-infected cells eGFP was strongly expressed and was distributed across the cytoplasm and nucleus (Figure 3.3). Consequently, virus infected cells were differentiated from cells that simply engulfed cell debris containing eGFP with relative ease.

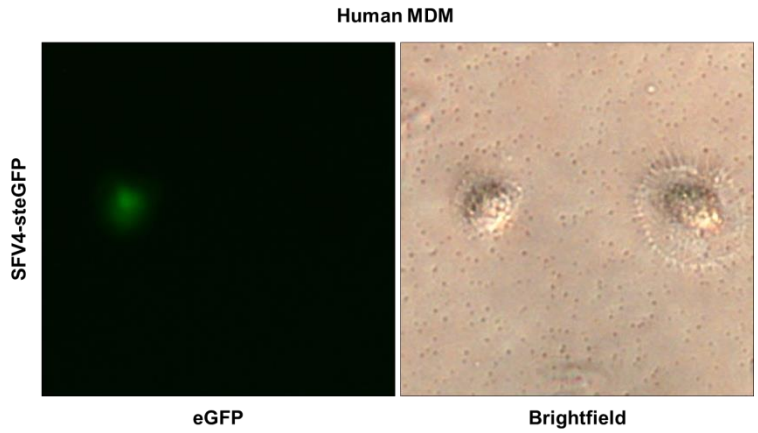

Figure 3.3. Human MDMs infected with SFV4-steGFP. MDMs were infected via 0.2 μm-clarified supernatant from SFV4-steGFP-infected HeLa cells and observed using Zeiss Observer.D1 microscope 48-hours post-infection.

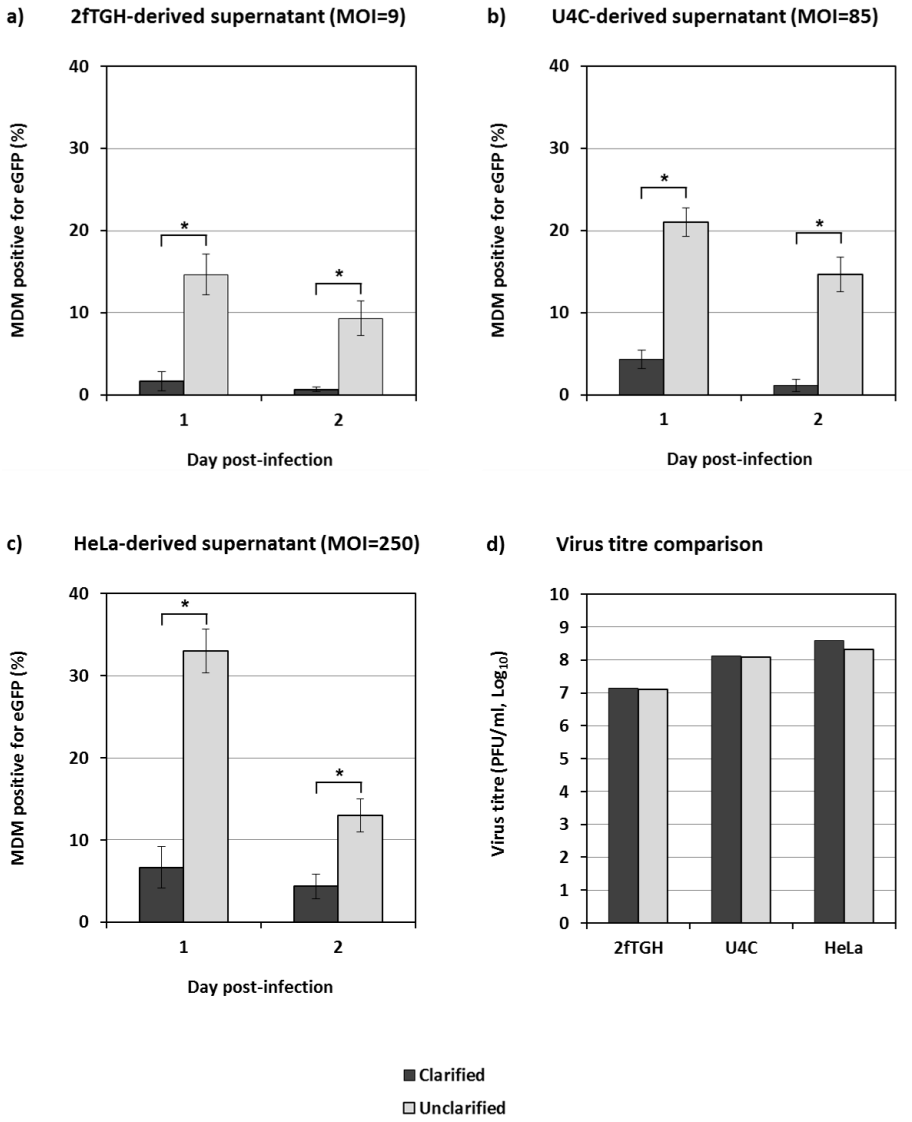

Figure 3.4. Infection of human MDMs with unclarified or 0.2 µm-clarified supernatants from SFV4-steGFP-infected 2fTGH, U4C and HeLa cells. (a-c) Cells were observed using Zeiss Observer.D1 inverted microscope 24- and 48-hours post-infection. LOD=0.01%. The MOIs at which MDMs were infected using 0.2 µm-clarified supernatants from HeLa, U4C and 2fTGH cells were approximately 250, 85 and 9, respectively. Data expressed as mean +/- SD; Mann-Whitney test, single-tailed; * $p<0.05$. (d) Supernatants used to infect MDMs on Day 0 were titrated on BHK-21 cells by plaque assay. LOD=12.5 PFU/ml.

There was no noteworthy difference between SFV4-steGFP titres measured in unclarified and 0.2 µm-clarified supernatants derived from HeLa, U4C and 2fTGH cells ($10^{8.33}$ vs $10^{8.60}$, $10^{8.08}$ vs $10^{8.13}$ and $10^{7.10}$ vs $10^{7.15}$ PFU/ml, respectively) as

shown in Figure 3.4d. However, there was a notable difference between titres measured in supernatants derived from different cells. The highest titre was observed in HeLa cells supernatant ($10^{8.33}$ - $10^{8.60}$ PFU/ml). The titre observed in U4C cells was approximately 3-fold lower ($10^{8.08}$ – $10^{8.13}$ PFU/ml) while the titre observed in 2fTGH cells was approximately 10-fold lower ($10^{7.10}$ – $10^{7.15}$ PFU/ml). Consequently, the MOI at which MDMs were infected with SFV4-steGFP varied substantially between supernatants derived from HeLa, U4C and 2fTGH cells (250, 85 and 9, respectively, for 0.2 μm-clarified supernatants). Interestingly, the proportion of MDMs positive for eGFP observed in this experiment was substantially higher than that observed when MDMs were infected with the purified virus at comparable MOIs (Figure 3.1). The design of both experiments was comparable.

2fTGH cells were more resistant to SFV4-steGFP infection than U4C and HeLa cells when exposed the same inoculum. Fever SFV4-steGFP-infected 2fTGH cells showed signs of virus infection, such as CPE or expression of virus-encoded eGFP. As a consequence, less cell debris was likely generated from 2fTGH cells in comparison to HeLa and U4C cells. However, the exact amount was not compared or quantified. In addition, SFV4-steGFP-infected 2fTGH cells released fewer virus particles into the cell culture supernatant. This overall reduction in the amount of infectious material generated by virus-infected 2fTGH cells was the most likely explanation for the difference in the infectivity of MDMs observed between 2fTGH- and U4C-derived supernatants. It seemed that the presence or absence of a competent IFN system in virus-infected human cells did not change the capacity of cell debris derived from these cells to infected human MDMs. Consequently, the effects that cell debris from HeLa-, 2fTGH- and U4C-infected cells had on human MDMs infection with SFV4-steGFP were fundamentally comparable. Importantly, this result was observed in spite of the notably different virus titres present in supernatants derived from different cells, as discussed above. As the overall effect was the most pronounced when HeLa cells-derived supernatants were used, it was decided that HeLa cells only would be used for the subsequent experiments.

3.6 Can presence of cell debris from uninfected cells promote infection of MDMs with SFV?

Cell debris from uninfected HeLa cells was generated as described in 2.5.6. Unclarified and 0.2 µm-clarified supernatants were prepared and added to human MDMs as described in 2.5.6. Next, purified SFV4-steGFP was added at MOI of 50. MDMs infected with purified virus alone at MOI of 50 were used as a control. The inoculum was not removed post-infection. Cells were incubated for 48 hour and inspected microscopically for the expression of virus-encoded eGFP every 24 hours.

Purified SFV4-steGFP infected less than 0.02% of MDMs within the first 24 hours and no eGFP-positive cells were observed 48-hours post infection (Figure 3.5). This was consistent with previous findings (Figure 3.1). Similar results were obtained when the purified virus was mixed with the 0.2 µm-clarified supernatant. In presence of the unclarified supernatant, the MDM infection rate increased four-fold. However, this still corresponded to less than 0.1% of eGFP-positive MDMs. The data indicated that presence of cell debris from uninfected cells was not itself sufficient to increase the rate at which SFV infects MDM to levels observed when cell debris derived from virus-infected cells was used (Figure 3.4).

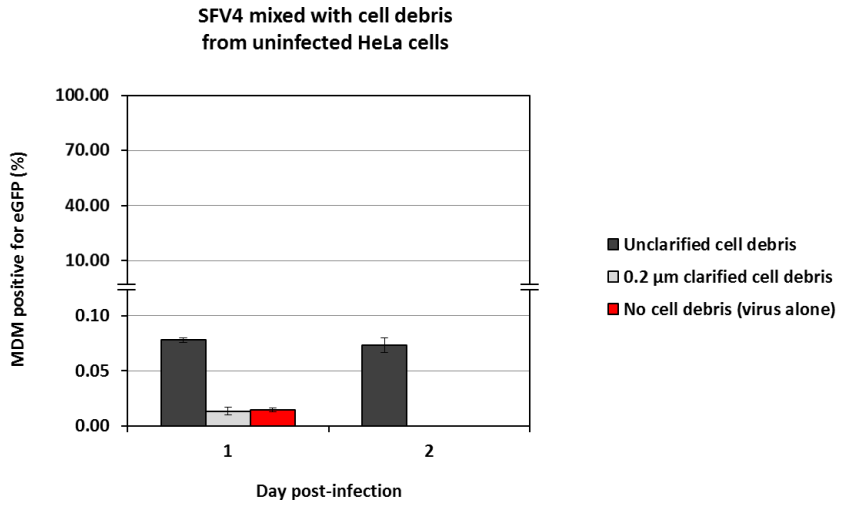

Figure 3.5. Infection of human MDMs with SFV4-steGFP at MOI of 50 mixed with cell debris from uninfected HeLa cells. Cells were observed for the expression of virus-encoded eGFP using Zeiss Observer.D1 inverted microscope 24- and 48-hours post-infection. LOD= 0.01%. Data expressed as mean +/- SD.

3.7 Can cell debris be infectious to MDMs in absence of virus particles?

Unclarified and 0.2 μm-, 0.45 μm- and 0.8 μm-clarified supernatants were prepared from HeLa cells infected with SFV4-3F-zsGreen and SFV1-3F-zsGreen VRP as described in 2.5.3. Supernatants were diluted 1:2 in complete RPMI and MDMs were infected as described in 2.5.4, on cover glasses. The inoculum was removed 6 hours post-infection, cells were washed with Mg^{2+} and Ca^{2}+-free PBS, and fresh complete RPMI was added. Cells were incubated for 48 hours. After 24 hours, live cells were inspected microscopically for the expression of virus/VRP-encoded zsGreen. After 48 hours, cells were fixed in 10% v/v neutral buffered formalin for 1 hour, washed three times in Mg^{2+} and Ca^{2}+-free PBS, mounted and inspected microscopically for the expression of virus/VRP-encoded zsGreen as described in 2.7.

Infections with unclarified supernatant derived from virus- and VRP-infected HeLa cells led to comparable numbers of MDMs positive for zsGreen 24 hours post-infection (32% and 29.67%, respectively). Data are summarised in Figure 3.6a. Clarification of the supernatant from virus-infected cells through a 0.2 μm filter reduced the proportion of zsGreen-positive MDMs to 4% (Figure 3.6d). The difference was statistically significant and consistent with previous findings for SFV4-steGFP (Figure 3.4c). Clarification of the supernatant from VRP-infected cells through a 0.2 μm filter reduced the proportion of zsGreen-positive MDMs to only 0.12% (Figure 3.6d). The reduction was significantly larger than that observed for the supernatant from virus-infected cells.

Remarkably, 48 hours post-infection the percentage of MDMs infected with the replicon via unclarified supernatant from VRP-infected cells doubled and reached the value of 72% (Figure3.6a). At the same time the number of MDMs infected with the virus via unclarified supernatant from virus-infected cells decreased to below 10%. The difference was statistically significant. Altogether, the above data suggested that virus particles were not required to infect MDMs via cell debris.

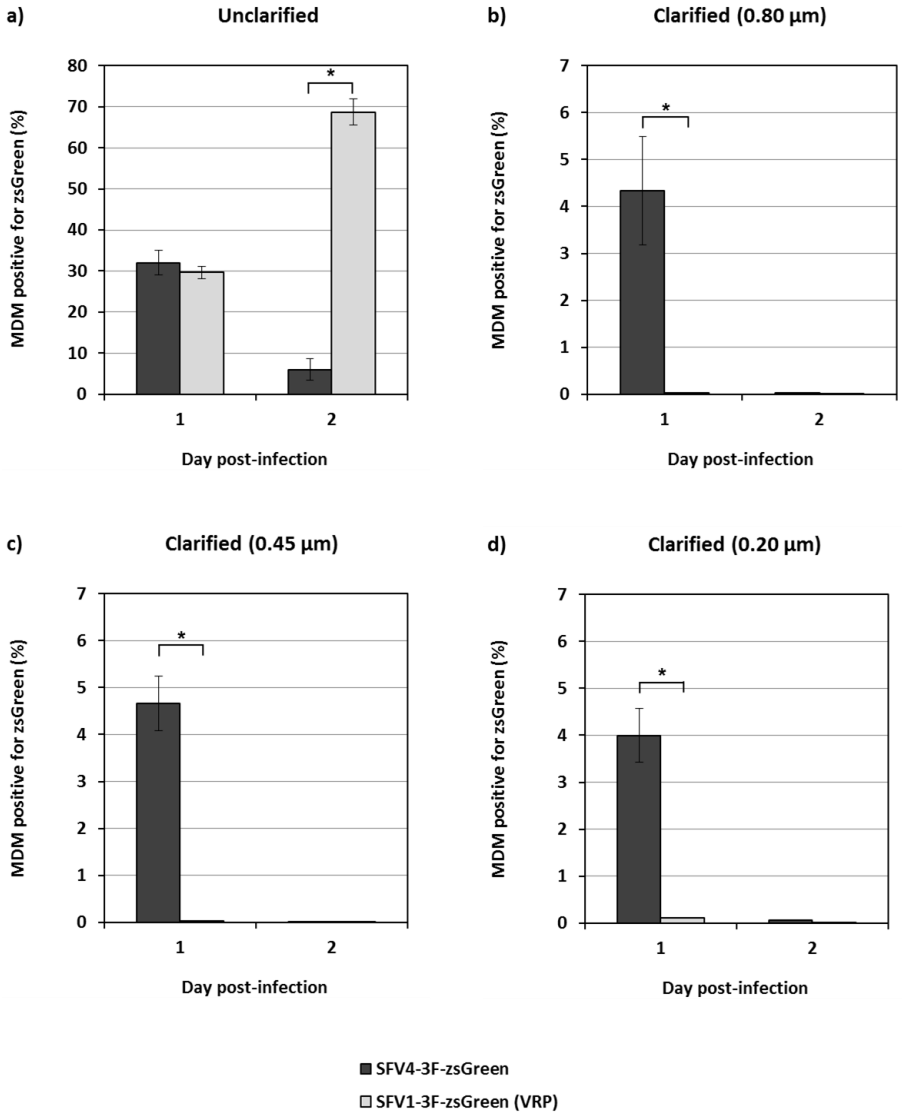

Figure 3.6. Infection of human MDMs with cell debris from SFV4-3F-zsGreen- and SFV1-3F-zsGreen VRP-infected HeLa cells. Cells were observed using Zeiss Observer.D1 inverted microscope 24-hours post-infection, and using Zeiss Axioskop 2 upright microscope 48-hours post-infection. LOD=0.01%. (a) Unclarified supernatant. (b-d) Supernatant clarified via 0.2 µm, 0.45 µm and 0.8 µm filters. Data expressed as mean +/- SD; Mann-Whitney test, single-tailed; * $p<0.05$.

Interestingly, microscopic observation of replicon-infected MDMs 48 hours post-infection showed no visual signs of CPE or any change in cell morphology in comparison to uninfected MDMs (Figure 3.7). At the same time, virus-infected MDMs were observed to round-up and often detach from the surface of plates. Importantly, HeLa, 2fTGH and U4C cells infected with SFV1-3F-zsGreen VRPs underwent apoptosis within 48 hours post infection (data not shown). Foci of zsGreen expression were clearly observed by fluorescent microscopy in both virus- and replicon-infected MDMs (Figure 3.7b), indicating the presence of active replication complexes in these cells.

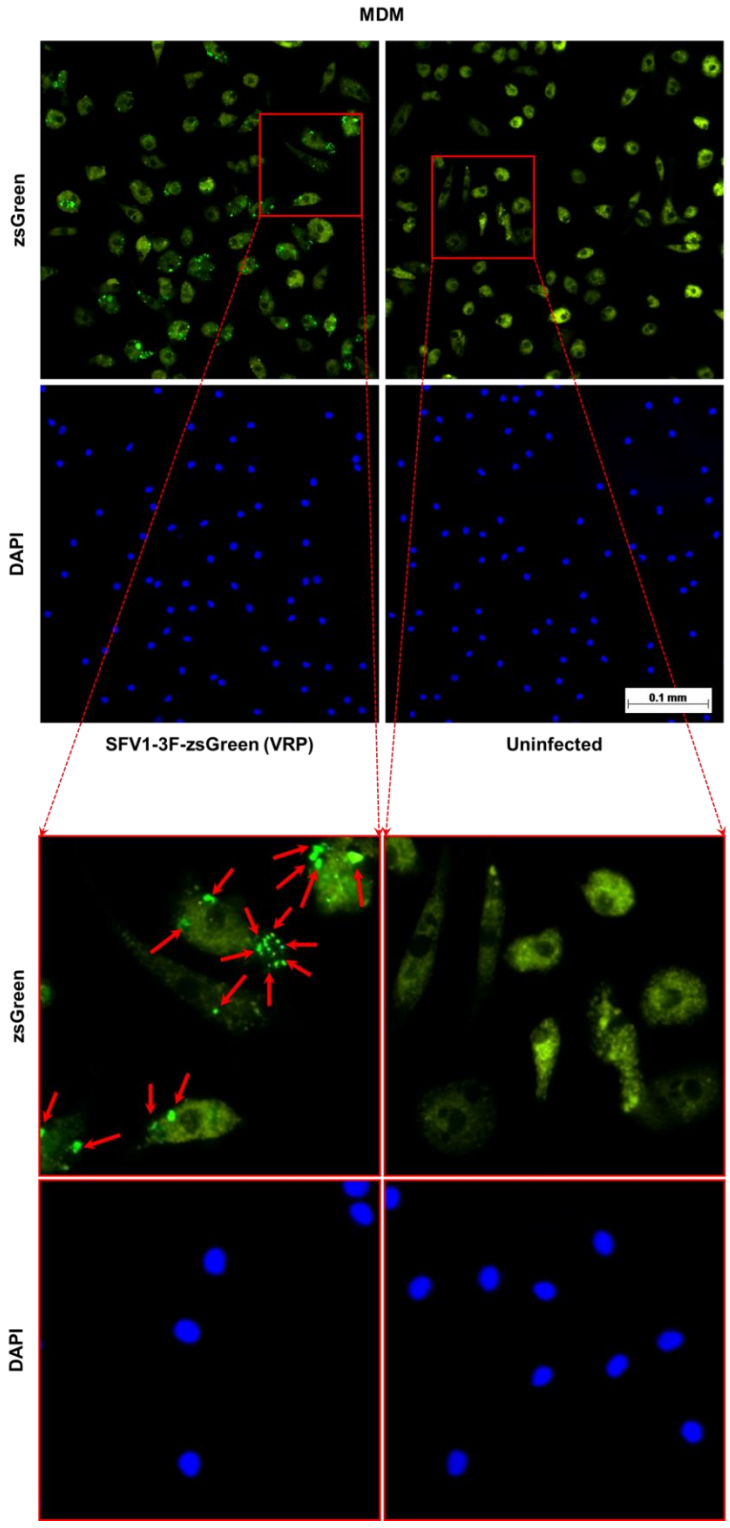

Figure 3.7. MDMs infected with SFV1-3F-zsGreen replicon via cell debris from VRP-infected HeLa cells. Cells were observed for the expression of replicon-encoded zsGreen using Zeiss Axioskop 2 upright microscope 48-hours post-infection. Cell nuclei were stained with DAPI. Red arrows indicate foci of zsGreen expression. Strong background auto-fluorescence of MDMs was observed.

3.8 What size of cell debris derived from SFV-infected cells facilitates the infection of human MDMs with the virus?

As described in the previous paragraph, MDMs were infected with 0.2 μm-, 0.45 μm- and 0.8 μm-clarified supernatant from virus- and VRP-infected HeLa cells. Overall, the clarification of a supernatant through 0.2 μm, 0.45 μm and 0.8 μm filters led to comparable numbers of zsGreen-positive MDMs (Figure 3.6b,c,d). The same pattern was observed for supernatants derived from virus- and VRP-infected cells. The results suggested that cell debris >0.8 μm in diameter was the primary carrier of infectious material.

3.9 Is infection of MDMs with SFV productive?

First, SFV4-steGFP thermal inactivation at 37 ºC was investigated. In brief, $10^{6.00}$ PFU of SFV4-steGFP was added to 1 ml of complete RPMI in a 24-well plate and incubated at 37 ºC for 4 days. Each day, 100 μl of virus was sampled and titrated. SFV4-steGFP demonstrated a linear correlation between the measured virus titre and the time of incubation at 37 ºC (Figure 3.8a). Approximately 80% of virus was inactivated every 24 hours.

Next, unclarified supernatant was prepared from HeLa cells infected with SFV4-steGFP as described in 2.5.3. The supernatant was diluted 1:10 in complete RPMI and MDMs were infected as described in 2.5.4, in 1 ml final volume per well. The inoculum was not removed post-infection. Cells were incubated for 72 hours. Successful infection of MDMs with SFV4-steGFP was confirmed microscopically. Every 24 hours, 100 μl of MDMs supernatant was collected and titrated.

Approximately 25-30% of MDMs expressed eGFP on day 1. A steady decrease in MDM supernatant virus titre was observed from day 0 to day 3 ($10^{6.82}$ PFU/ml to $10^{4.20}$ PFU/ml). The measured titres were at or below the expected titre calculated based on thermal inactivation (Figure 3.8b). The data suggested that MDM infection with SFV4-steGFP was either non-productive, or virus replication was below the limit of detection established by the thermal inactivation at 37 ºC.

This experiment had several notable limitations. Most significantly, the virus inoculum was not removed from the MDMs post-infection. As a consequence, the limit of detection of this assay was very high, as indicated by the thermal inactivation rate of SFV4-steGFP. It is possible that the SFV4-steGFP-infected MDMs were producing new virus particles at a low level, but the large amount of virus remaining in the supernatant post-infection made it impossible to detect. This experiment was designed to investigate production of virus progeny by a single population of MDMs that was infected at the same time. However, the continuous presence of the high titre virus in the MDM supernatant may have allowed an ongoing infection of new cells. This would result in a multiple-step growth curve rather than a single-step growth curve as the data would be a combination of the rate at which MDMs produce SFV4-steGFP and the virus transmission between cells within the culture. The limitations described above do not affect the primary finding that SFV4-steGFP-infected MDMs produce little or no virus. Permissive cells, such as BHK-21 cells, can produce >5,000 copies of the progeny virus from a single infected cell (see 4.13).

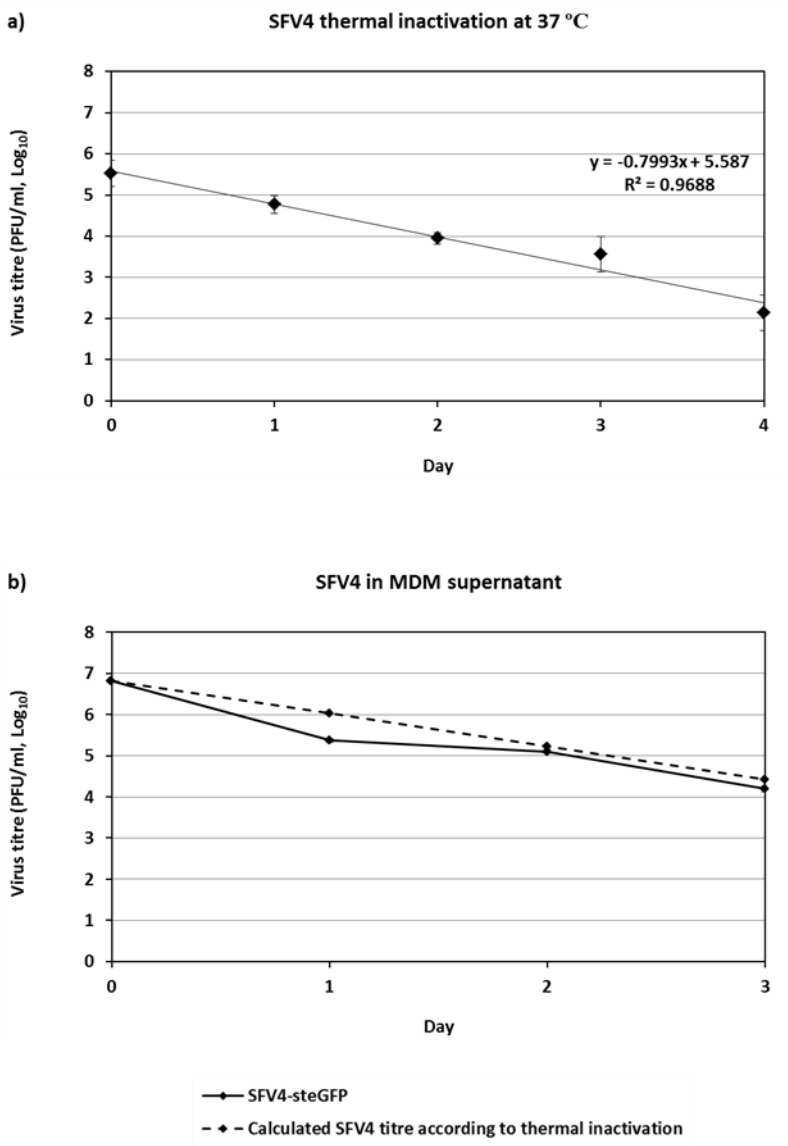

Figure 3.8. Production of virus progeny by SFV-4-steGFP-infected MDMs. (a) SFV4-steGFP thermal inactivation at 37 ºC. Linear regression (least squares) on individual data showed as mean +/- SD. (b) Measured SFV4-steGFP titres in the supernatant of virus-infected MDMs compared to the calculated SFV4-steGFP titre according to its thermal inactivation. Data showed as mean +/-SD.

3.10 Are intact replication complexes present in cell debris from virus- and VRP-infected cells?

Alphavirus replication complexes are very stable structures that remain active even during late stages of cell infection (Grimley et al. 1968, Kujala et al. 2001a, Kääriäinen et al. 2002, Spuul et al. 2010). Notably, the replication complex are stable enough to withstand cell-membrane disruption and immunoprecipitation (Barton et al. 1991, Kujala et al. 2001a). Cell debris from SFV4-3F-zsGreen-, SFV4-steGFP- and SFV1-3F-zsGreen VRP-infected HeLa cells was observed by transmission electron microscopy (TEM) to investigate if they retained intact SFV replication complexes that could potentially act as an infectious material.

Sections of cell debris from virus- and VRP-infected HeLa cells confirmed the presence of substantially fragmented cells with no identifiable nucleus, and the presence of apoptotic bodies (Figure 3.9). All these were hallmarks of the late stage apoptosis (Elmore 2007). There was no notable difference between the cell debris generated by eSFV4-steGFP, SFV4-3F-zsGreen and SFV1-3F-zsGreen VRP.

Detailed analysis of the cell debris sections revealed that intact replication complexes were indeed present within the cell debris derived from SFV4-steGFP-, SFV4-3F-zsGreen- and SFV1-3F-zsGreen VRP-infected HeLa cells (Figure 3.10). The size of observed replication complexes varied between 0.5 μm and 1.25 μm, and was within the expected range (Grimley et al. 1968, Froshauer et al. 1988). Interestingly, little or no virus particles were observed within the cell debris from virus-infected HeLa cells.

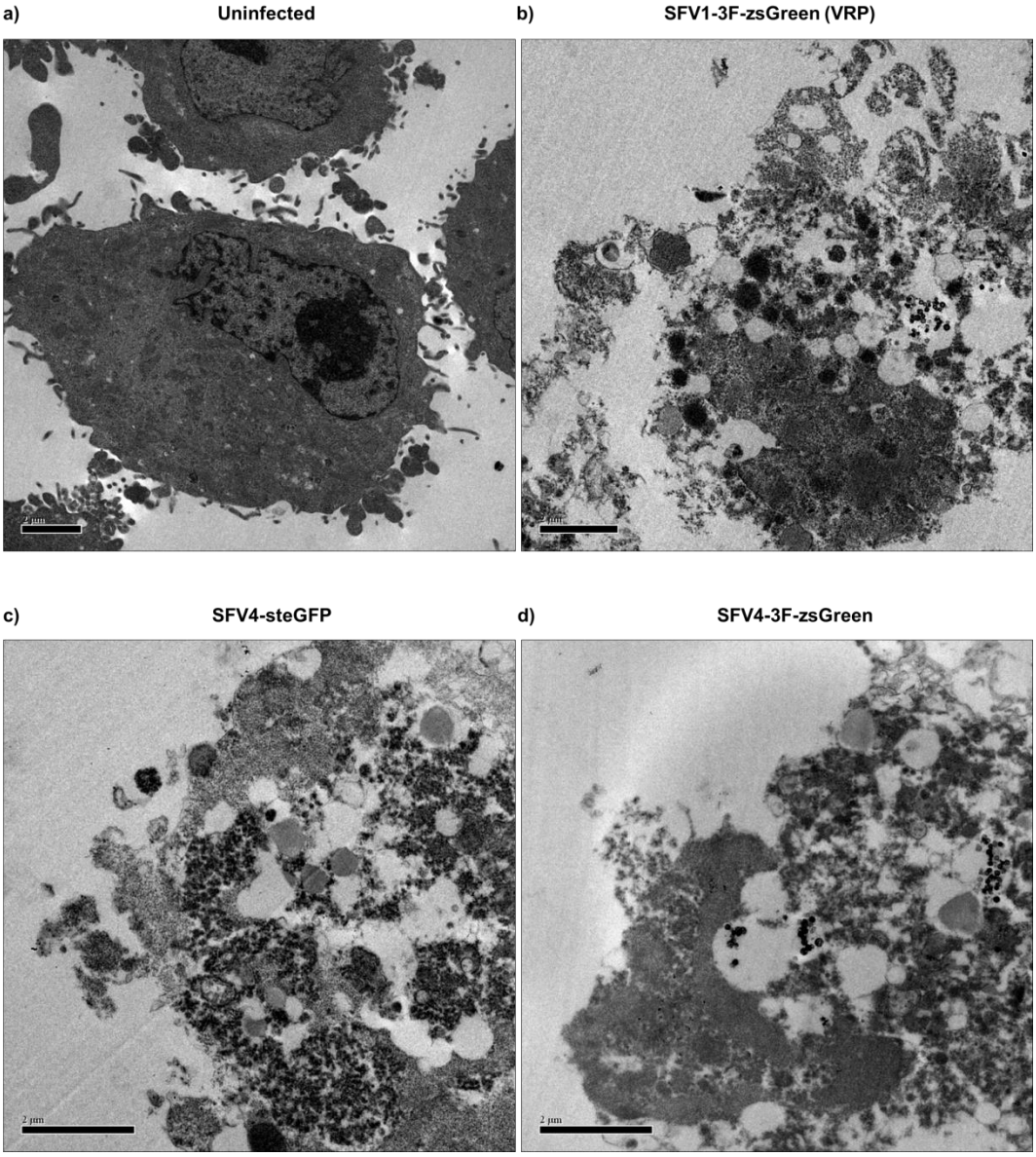

Figure 3.9. Transmission electron microscopy of cell debris from virus- and VRP-infected HeLa cells 3 days post-infection. (a) Uninfected HeLa cells collected by trypsinisation. (b) Cell debris from SFV1-3F-zsGreen VRP-infected HeLa cells (c) Cell debris from SFV4-steGFP-infected HeLa cells. (d) Cell debris from SFV4-3F-zsGreen-infected HeLa cells. Scale bars equal to 2.0 µm.

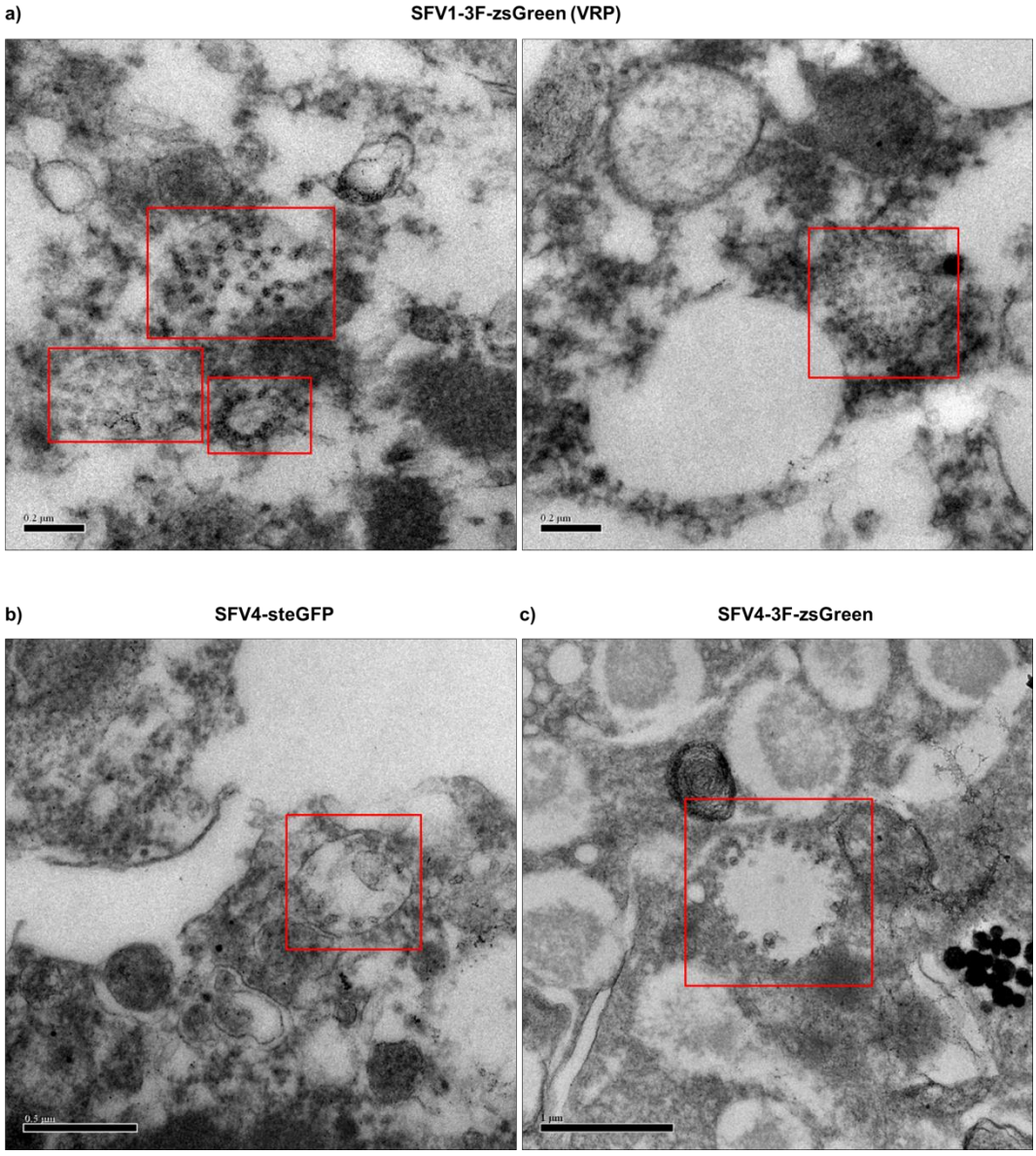

Figure 3.10. Transmission electron microscopy of SFV replication complexes present in cell debris from virus- and VRP-infected HeLa cells 3 days post-infection. (a) Cell debris from SFV1-3F-zsGreen VRP-infected HeLa cells. (b) Cell debris from SFV4-steGFP-infected HeLa cells. (c) Cell debris from SFV4-3F-zsGreen-infected HeLa cells. Red squares mark the location of replication complexes. Photos were analysed independently by Dr Tero Ahola, the University of Helsinki. Scale bars equal to (a) 0.2 µm, (b) 0.5 µm and (c) 1.0 µm.

3.11 Discussion

The principal hypothesis behind this part of the project was that human monocyte derived macrophages (MDMs) can be infected with SFV by a novel mechanism involving apoptotic debris from virus-infected cells. To date there has been no evidence in the literature to suggest that SFV can infect human macrophages *in vitro*.

The work presented in this chapter was preliminary. The long-term aim was to confirm these findings with CHIKV and to investigate the interaction of CHIKV and human MDMs in much greater detail. This would include in depth characterisation of apoptotic cell debris, CHIKV replication in MDMs and cellular responses to virus infection in MDMs. However, during the second year of the project its scope changed and the intended CHIKV experiments were not completed.

Despite the preliminary nature of this work, several **key findings** were made:

1. Human MDMs are refractory to infection with purified SFV but can be infected via cell debris from SFV-infected HeLa, 2fTGH and U4C cells.

2. The SFV infectious material was contained within cell debris derived from SFV-infected HeLa, 2fTGH and U4C cells.

3. Intact SFV replication complexes were identified within the HeLa cell debris 72-hours post SFV or VRP infection.

4. Cell debris derived from uninfected cells do not promote MDM infection in presence of a high-titre purified virus.

5. Presence of infectious SFV particles is not required to infect human MDMs via cell debris derived from SFV-infected HeLa, 2fTGH and U4C cells.

6. Genomic and subgenomic promoters of SFV are active in SFV-infected MDMs.

The data presented in this chapter are the first evidence to demonstrate that SFV can infect human macrophages *in vitro*. Interestingly, purified SFV4-steGFP failed to infect human MDMs at MOIs of 1, 50, 100, 500 and 1000. SFV-permissive cells such as BHK-21 are readily infected at MOIs as low as 0.001. Importantly, cell debris from HeLa, 2fTGH and U4C cells infected with SFV were all successful in establishing a notable SFV infection in MDMs. The virus load in the inoculum containing the cell debris had no major effect on the MDM infection rate. What is more, cell debris derived from uninfected cells did not promote MDM infection in presence of a high-titre purified SFV. The above data were consistent with findings by Krejbich-Trotot et al. (2011) for CHIKV. They suggested that MDMs are not infected with SFV via receptor-mediated endocytosis and that presence of infectious SFV particles in the cell supernatant is not required to infect MDMs. Infection of macrophages via cellular debris derived from virus-infected cells might be more widespread amongst alphaviruses and is not just restricted to CHIKV.

Infection of MDMs using HeLa-derived apoptotic debris produced with VRPs provided further insight into the nature of the SFV material infectious to MDMs. It showed that the presence of infectious virus particles within the cell debris was not required to infect MDMs. The SFV material infectious to MDMs was contained primarily within apoptotic debris of >0.8 μm. It was either viral genomic RNA in the cytoplasm or viral genomic RNA associated with replication complexes. It is likely that macrophages are infected by the virus material contained within apoptotic debris via phagosomes. This mechanism of infection may protect virus from antibodies, facilitate its spread to neighbouring cells and promote persistent infection *in vivo*. However, the exact mechanism remains unclear.

Human mRNAs are relatively stable inside a cell, with a mean half-life of approximately 7 hours (Tani et al. 2012). Thomas et al. (2015) demonstrated that during apoptosis cellular mRNAs are rapidly degraded. Human mRNAs and alphavirus genomic RNAs share similar structure. Hence, it is likely that virus genomic RNAs in the cytoplasm of apoptotic cells are also degraded. Hence, the presence of full-length virus RNA in the cytoplasm of apoptotic debris must be

investigated. Presence of intact virus replication complexes in apoptotic debris from virus- and VRP-infected HeLa cells was confirmed by transmission electron microscopy. These structures should be sufficiently stable to protect viral RNA contained within the spherules from degradation during apoptosis (Grimley et al. 1968, Kujala et al. 2001a, Kääriäinen et al. 2002, Spuul et al. 2010). However, it is not known if replication complexes present within apoptotic debris are indeed active. Further studies must address this by immunoprecipitation of replication complexes from apoptotic debris and then measuring their activity (Barton et al. 1991, Kujala et al. 2001b, Kallio et al. 2013)

As discussed previously, there is an ongoing debate as to the sensitivity of human macrophages to CHIKV (Schwartz et al. 2010). The data obtained in this chapter support the hypothesis that the differences observed by some may be due to the quality of the virus inoculum used. The presence of apoptotic debris in a cell-culture-derived virus inoculum that was not suitably purified (e.g. by ultracentrifugation via a sucrose gradient) could promote infection of macrophages with the virus. This must always be considered when designing new experimental protocols.

Expression of SFV-encoded fluorescent markers driven by both genomic and subgenomic promoters of the virus was observed in SFV4-3F-zsGreen- and SFV4-steGFP-infected MDMs, respectively. This finding suggested that in SFV-infected MDMs non-structural and structural proteins of the virus are produced. Consequently, SFV infection of human MDMs may be productive. SFV replicates to very high titres in HeLa, 2fTGH and U4C cells. By contrast, no virus production was observed in MDMs infected with SFV4-steGFP via cell debris. However, the experimental design prohibited detection of low-level virus replication. It is possible that small amounts of virus progeny are released from SFV-infected MDMs. This would be consistent with previously reported infections of primary mouse macrophages with SFV (van der Groen et al. 1976, Oaten et al. 1980). Interestingly, CHIKV infection of human MDMs can also be productive *in vitro*. (Sourisseau et al. 2007, Labadie et al. 2010).

Visual observation of MDMs showed that upon infection with SFV they round-up, detach from the surface of plates, and likely undergo apoptosis. By contrast, replicon-infected MDMs do not seem to demonstrate any morphological changes within the same time frame. The above observation should be confirmed by a cell viability assay and by inspecting MDMs for hallmarks of apoptosis, such as cleaved caspase-3, -8 and -9. The morphological dissimilarity described above may explain the difference in MDM infectivity via apoptotic debris produced by virus and by VRPs observed 48 hours post-infection (Figure 3.6a). Most likely, a comparable and high number of MDMs was initially infected with both. However, while the virus-infected MDMs were removed from the cell monolayer, the replicon-infected MDMs remained in the cell monolayer. This would suggest that apoptotic debris is very effective at facilitating MDM infection with SFV. Barry et al. (2010) established that SFV envelope glycoproteins trigger the unfolded protein response of the ER that accelerates apoptotic cell death. Based on the above data, it is possible that in persistently infected macrophages CHIKV/SFV replication is maintained at a low level with little or no structural proteins being produced. This should be investigated further using modified viruses and replicons that encode marker genes under control of both genomic and subgenomic promoters. The relative expression of marker genes driven by both promoters in virus/VRP-infected MDMs could be measured over an extended period of time, and compared to that observed in a fibroblast infection.

Alphaviruses can infect both dividing and non-dividing cells (Sourisseau et al. 2007). However, outcome of an alphavirus infection often depends on a maturation state of the cell. Upon infection of mammalian epithelial or fibroblast cells a rapid shutoff of host cell transcription and translation is typically observed (Jaffar-Bandjee et al. 2009, Krejbich-Trotot et al. 2011). Subsequently, cells undergo apoptosis. However, terminally differentiated cells, such as mature vertebrate neurons, often do not undergo apoptosis when infected with SFV (Fleming 1977, Fazakerley et al. 1993, Oliver et al. 1997, 1998, Allsopp et al. 2000). It is possible that at least in some cases the maturation state of CHIKV-infected macrophage may promote persistence by inhibiting apoptosis. This must be investigated in further detail.

As discussed in 1.4, alphavirus infection of mammalian cells triggers apoptosis both *in vitro* and *in vivo*. It is safe to assume that the cellular debris derived from HeLa, 2fTGH and U4C cells were indeed apoptotic bodies. The analysis of Hela cell debris by a transmission electron microscope confirmed the presence of hallmarks of late-stage apoptosis, such as nuclear fragmentation. However, a detailed analysis of the cell debris was not performed.

As mentioned at the beginning of this discussion, the work presented in this chapter was preliminary. However, many of the findings were intriguing and more detailed studies should be planned to investigate them in more depth.

Future work should include:

1. Confirmation of data obtained for SFV with CHIKV in human MDMs and human fibroblasts;
2. Characterisation of virus-induced cell debris;
    - size fractioning (gradient centrifugation);
    - identification of the cell debris population that contains the SFV material infectious to MDMs (size fractioning combined with bioassays);
    - expression of apoptotic markers (immunostaining);
    - protein composition (proteomics);
    - transcriptome composition (transcriptomics);
    - presence of viral genomic RNA (PCR, qPCR);
    - presence and localisation of virus particles and virus replication complexes (immunostaining, marker genes, electron microscopy);
    - protein composition (proteomics; virus encoding a marker);
    - purification of replication complexes (gradient centrifugation, immunoprecipitation);
    - measuring the activity of replication complexes;
    - inactivation of unprotected RNA within virus-induced cell debris (treatment with RNAses);
3. Characterisation of virus replication in monocytes, MDMs and Thp-1 cells
    - time course of viral RNA replication (qPCR; 3H-uridine labelling);

- time course of virus protein production (Western blot, 35S-labelled methionine, expression of a virus-encoded marker gene);
- time course of production (release) of infectious virus particles (plaque assay, expression of a virus-encoded marker gene, qPCR);
- differential expression of virus proteins from the genomic and subgenomic promoters (reporter virus encoding two marker genes, one under control of the genomic promoter and one under control of the subgenomic promoter);
- formation of replication complexes (electron microscopy);
- cell death (immunostaining for markers of apoptosis, cell viability assays).

Chapter 4:

Restricting alphavirus replication in haematopoietic cells by incorporating a miR-142-3P recognition elements into the virus genome: proof-of-concept studies using Semliki Forest virus

Content:

4.1 Objectives

As mentioned previously, the scope of the PhD project presented in this thesis changed following the completion of work described in Chapter 3. The new objective was to investigating the role of monocyte and macrophage infection with CHIKV in the nonhuman primate model of chikungunya virus disease. This shift was largely dictated by the availability of tools and resources at the time.

The new objective was addressed by harnessing endogenous miR-142-3P to restrict virus replication in haematopoietic cells. In context of cynomolgus macaque infection with CHIKV this effectively means restricting CHIKV replication in monocytes and macrophages as other haematopoietic cells are not readily infected with the virus (Labadie et al. 2010). The cell-specific restriction of virus replication was attempted by incorporation of a recognition element (RE) with multiple copies of target sequences fully complementary to miR-142-3P into the genome of CHIKV.

The work presented in this chapter includes generation of resources and tools required to undertake this project, and proof-of-concept experiments completed using SFV. The work presented in Chapter 5 includes generation of miR-142-3P-targeted CHIKV and investigation of its pathogenesis in the nonhuman primate model of CHIKV disease.

The specific objectives for this part of the project were as follow:

1) To design and generate a recognition element for miR-142-3P, and a suitable control.

2) To incorporate miR-142-3P recognition element into the genome of Semliki Forest virus.

3) To investigate if replication of Semliki Forest virus encoding miR-142-3P recognition element is attenuated in haematopoietic cells.

4) To design, generate and characterise Hek 293 cells that can express miR-142-3P under control of the tetracycline-inducible promoter.

5) To investigate if replication of Semliki Forest virus encoding miR-142-3P recognition element is attenuated in Hek 293 cells that express miR-142-3P, but not in Hek 293 cells that do not express miR-142-3P.

6) To design and generate a panel of pcDNA^{TM}3.1+ plasmids that express miR-142-3P.

7) To investigate if replication of Semliki Forest virus encoding miR-142-3P recognition element is attenuated in cells transfected with pcDNA3.1+ expressing miR-142-3P, but not in cells transfected with control plasmids.

8) To investigate the stability of miR-142-3P RE in Semliki Forest virus genome during serial passage on BHK-21 cells.

9) To investigate if Semliki Forest virus encoding miR-142-3P recognition element is attenuated *in vivo* in IFN-α/ß receptor knockout mice.

4.2 Designing miR-142-3P recognition element (RE)

Three miRNA recognition elements (REs) were designed for this study: miR-142-3P RE, miR-142-3P Antisense RE and miRNA RE Control. Their sequences are provided in Annex 15. The three REs shared a common design (Figure 4.1a). In brief, they were designed as a cassette encoding a 5' multiple cloning site (MCS), 4 copies of the miR-142-3P target sequence (TS) separated from each other by 4-nucleotide spacers, and a 3' MCS (Figure 4.1a). The overall RE design was optimised for cloning into both SFV4 and ICRES1 clones, as described later.

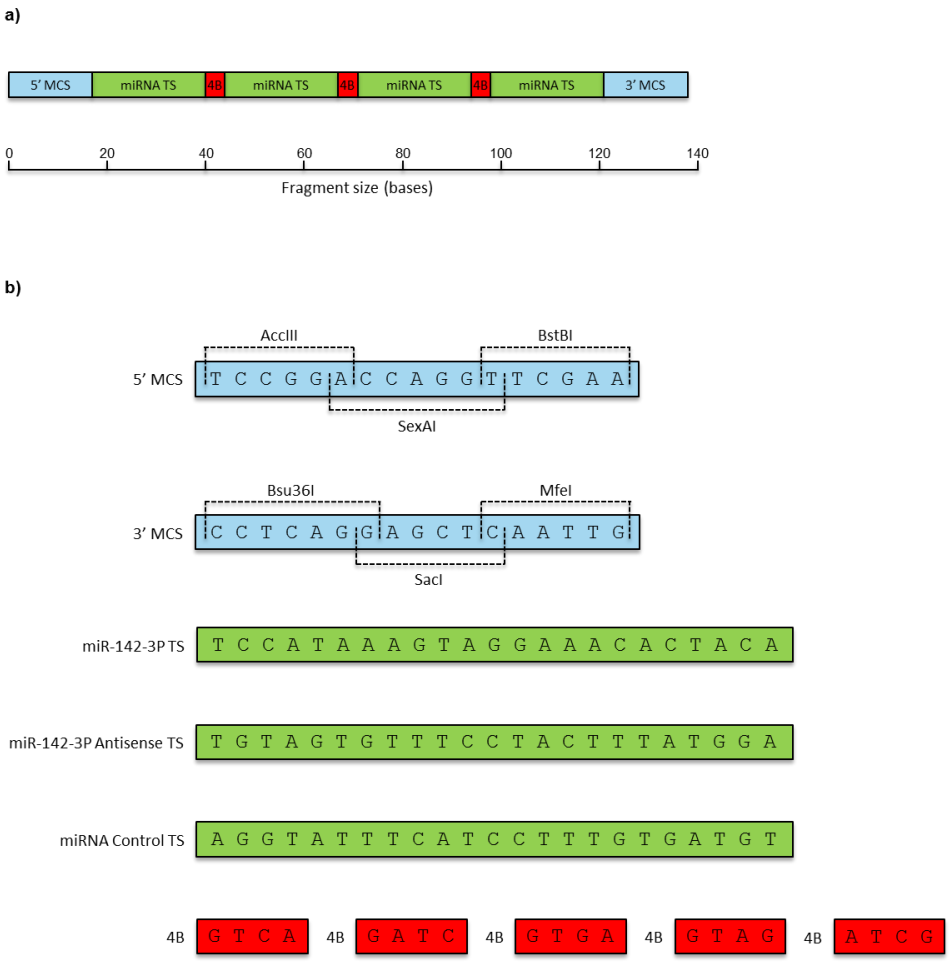

Figure 4.1. Design of the miRNA REs. (a) Common design shared by all miRNA REs: 5' multiple cloning site (MCS), 4 copies of the target sequence (TS) separated from each other by 4 nucleotide spacers, 3' MCS. (b) Details of each component of the miRNA RE cassette. Three out of five different 4-nucleotide spacers (4B) were used in each cassette.

Both 5’ and 3’ multiple cloning sites were identical in all miRNA REs. The primary difference between the three REs was the type of the target sequence (TS) present in the cassette (Figure 4.1b):

1. **miR-142-3P RE** – miR-142-3P TS, the reverse complement of miR-142-3P (perfect target). In an alphavirus encoding this RE, the virus genome would be targeted for degradation in all cells that express miR-142-3P.

2. **miR-142-3P Antisense RE** – miR-142 Antisense TS, the reverse complement of miR-142-3P TS. In an alphavirus encoding this RE, the virus antigenome (-ve strand, replication intermediate) would be targeted for degradation in all cells that express miR-142-3P.

3. **miRNA RE Control** – Control TS, reverse sequence of miR-142-3P Antisense TS (3’ to 5’ sequence but in 5’ to 3’ orientation). In an alphavirus encoding this RE, neither the virus genome nor the virus antigenome would be targeted for degradation in cells that express miR-142-3P. This construct was used as the control for miR-142-3P RE and miR-142-3P Antisense RE.

All miRNA REs were designed to be incorporated into coding and non-coding regions of SFV and CHIKV genomes. Consequently, the size of all REs was such that they would not cause a frameshift mutation when inserted into an open reading frame (i.e. divisible by three). None of the REs contained stop codons in the +1 frame. To fulfil the above requirements, five different 4-nucleotide spacers were used (Figure 4.1b). Furthermore, three additional bases were inserted into miR-142-3P RE (two following 5’ MCS and one prior to 3’ MCS). Consequently, the size of miR-142-3P RE was 141 bp while the size of miR-142-3P Antisense RE and miRNA RE Control was 138 bp.

The 5’ and 3’ MCSs were 17 base pairs long and contained 3 rare restriction sites, each (Figure 4.1b). The MCSs were not intended to be used for cloning of a RE into the genomes of SFV or CHIKV. Instead, they were designed to act as a universal primer annealing site. This approach ensured that any restriction sites required for cloning could be added to all miRNA REs by a single PCR (the same set of primers and the same cycling conditions). Also, the entire miRNA RE cassette would always remain intact in all viruses, irrespective of the restriction sites used for cloning.

AccIII, MfeI and SacI restriction sites were not present in ICRES1 icDNAs or chikungunya replicons. All restriction sites incorporated into the miRNA REs MCSs were already present in SFV4 icDNAs.

Finally, SacI and Bsu36I restriction sites were incorporated into the 3’ MCS to allow easy-to-interpret control digests of ICRES1 and SFV4 icDNAs, respectively. In brief, a miRNA RE could be inserted into the coding region of the alphavirus non-structural polyprotein, between the nsP3 and nsP4. This locus had been used previously to successfully insert marker genes into the genomes of SFV and CHIKV (e.g. SFV4-3F-zsGreen, ICRES1-3F-zsGreen). At this location an insert would be cloned into the virus genome via a single restriction site, XhoI in SFV4 and SpeI in ICRES1. However, the use of a single restriction site for the cloning could result in the miRNA RE integrating into the virus genome in either of the two possible orientations, only one of which would yield a fully functional construct. In SFV4, Bsu36I restriction site was present in two genomic locations. One of them was close to the discussed cloning site. A control digest with Bsu36I would yield fragments that are different in the size by 114 bp depending on the insert orientation and small enough to clearly separate on an agarose gel (Figure 4.2a). Similar was true for ICRES1 control digests performed with SacI and AgeI (Figure 4.2b).

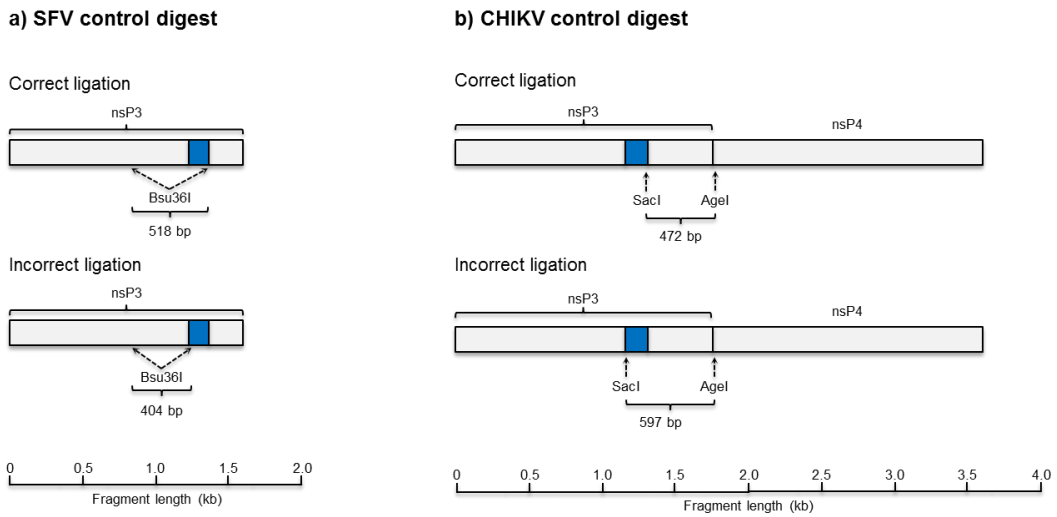

Figure 4.2. SFV and CHIKV control digest design. Diagrams represent the genomic locations of SFV and CHIKV corresponding to the nsP3 and nsP4. (a) Bsu36I digest of SFV4 icDNA with a miRNA RE element inserted in between nsP3 and nsP4 would yield a fragment of 518 bp in case of the correct ligation and a fragment of 404 bp in case of the incorrect ligation. (b) SacI and AgeI double digest of ICRES1 clone with a miRNA RE element inserted in between nsP3 and nsP4 would yield a fragment of 472 bp in case of the correct ligation and a fragment of 597 bp in case of the incorrect ligation.

4.3 Generating miRNA REs

Each of the three miRNA REs was synthesised in a form of two 78-81 bp long oligonucleotides with 18 bases of a complementary sequence as outlined in Table 4.1. Next, 1 µl of each oligonucleotides at 100 µM concentration were annealed and extended using Vent® DNA polymerase as described in 2.11.6 and outlined in Figure 4.3. Double-stranded products were run on a 3% agarose gel as described in 2.14. Finally, the bands of the required size (138-141 bp) were purified from the gel following 2.15.6.

Table 4.1. Oligonucleotides used to generate the miRNA recognition elements used in this project. The underlined sequence indicates the complementarity region.

Recognition element	Oligonucleotide name	Oligonucleotide sequence
miR-142-3P RE	miR-142-3P RE For	TCCGGACCAGGTTCGAATCTCCATAAAGTAGGAAACACTACAGTCATCCATAAAGTAGGAAACACTACAGATCTCCAT
	miR-142-3P RE Rev	CAATTGAGCTCCTGAGGTTGTAGTGTTTCCTACTTTATGGACGATTGTAGTGTTTCCTACTTTATGGAGATCTGTAGTGTT
miR-142-3P Antisense RE	Antisense RE For	TCCGGACCAGGTTCGAATGTAGTGTTTCCTACTTTATGGAGTGATGTAGTGTTTCCTACTTTATGGAGATCTGTAGTG
	Antisense RE Rev	CAATTGAGCTCCTGAGGTCCATAAAGTAGGAAACACTACACGATTCCATAAAGTAGGAAACACTACAGATCTCCATAA
miRNA RE Control	Control RE For	TCCGGACCAGGTTCGAAAGGTATTTCATCCTTTGTGATGTGTGAAGGTATTTCATCCTTTGTGATGTCTAGAGGTATT
	Control RE Rev	CAATTGAGCTCCTGAGGACATCACAAAGGATGAAATACCTCGATACATCACAAAGGATGAAATACCTCTAGACATCAC

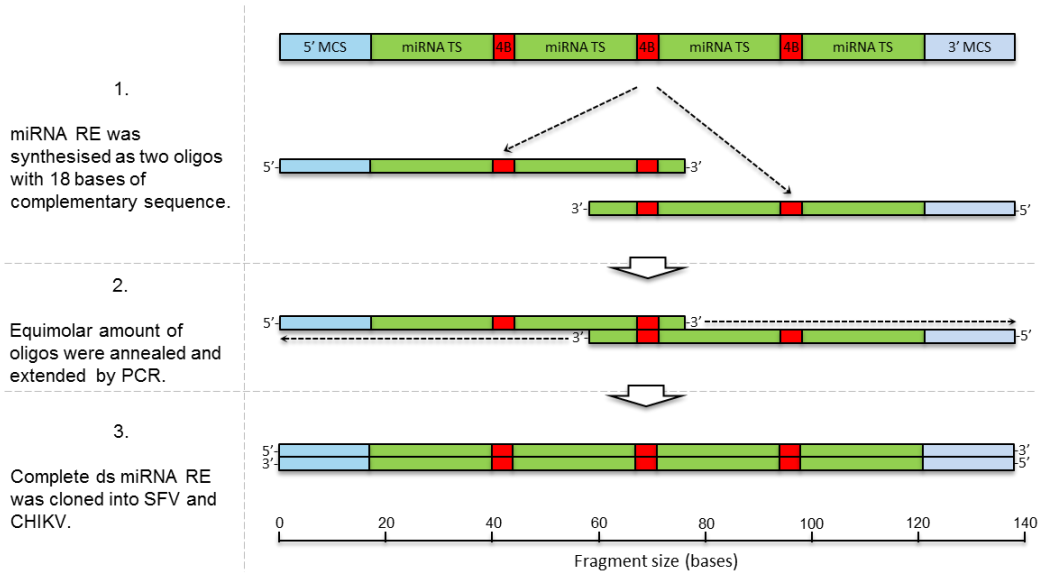

Figure 4.3. Generation of a miRNA RE. Two oligonucleotides with 18 bases of a complementary sequence were aligned and extended using Vent® polymerase.

4.4 Incorporating miRNA REs into the genome of SFV

SFV4-3H-zsGreen-2SG-GLuc icDNA was modified by incorporation of miRNA REs into its genome (Figure 4.4). In this construct, zsGreen was inserted into the 3' terminus of the nsP3 gene. This marker gene was cleaved from the non-structural polyprotein post-translationally leading to its released into the cytoplasm of virus-infected cells. Furthermore, a cassette encoding a duplicated SFV subgenomic promoter and *Gaussia* luciferase (GLuc) was inserted between ApaI and BamHI sites into the 3' UTR of SFV, directly downstream of the structural polyprotein stop codon. ß-globin intron was present in the capsid region to disrupt a cryptic *E.coli* promoter. It was removed from the virus genome during its replication (Dr Rennos Fragkoudis, the Pirbright Institute, personal communication). Finally, SFV4-3H-zsGreen-2SG-GLuc was cloned into the icDNA under control of the CMV promoter.

In brief, miRNA REs were incorporated into the 3' UTR of SFV4-3H-zsGreen-2SG-GLuc in place of the GLuc as outlined in Figure 4.5. This position is known to be genetically stable in SFV (Prof Andres Merits, the University of Tartu, personal communication). The resulting SFV4 clones would maintain zsGreen as a marker gene and should be small and stable enough to be used *in vitro* and *in vivo*. The cloning procedure is detailed in Annex 17.

SFV4 constructs encoding miR-142-3P RE, miR-142-3P Antisense RE and miRNA RE Control were called SFV4-3H-zsGreen-miR-142-3P RE, SFV4-3H-zsGreen-miR-142-3P Antisense RE and SFV4-3H-zsGreen-miRNA RE Control, respectively. Altogether, these viruses were named SFV4-3H-zsGreen-miRNA RE. Their sequences are provided in Supplementary Data, Appendix 1.

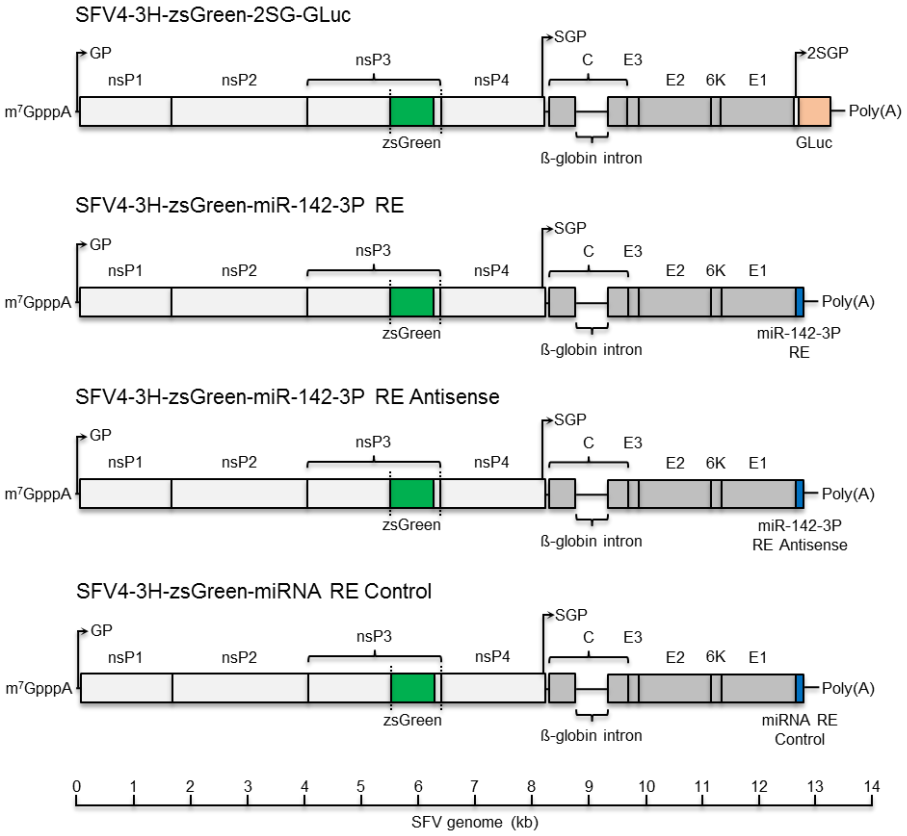

Figure 4.4. Schematic representation of SFV4-3H-zsGreen-miRNA RE clones. miRNA REs were inserted into the 3' UTR of the virus, between ApaI and BamHI restriction sites. Parental virus, SFV4-3H-zsGreen-2SG-GLuc, is shown at the top. nsP – non-structural protein; GP – genomic promoter; SGP – subgenomic promoter; 2SGP – duplicated subgenomic promoter; C – capsid; E1-E3 – envelope glycoproteins; GLuc – *Gaussia* luciferase; vertical dashed line – protein cleavage sites; Poly(A) – Poly(A) tail; m^7GpppA – 5' CAP; RE – recognition element.

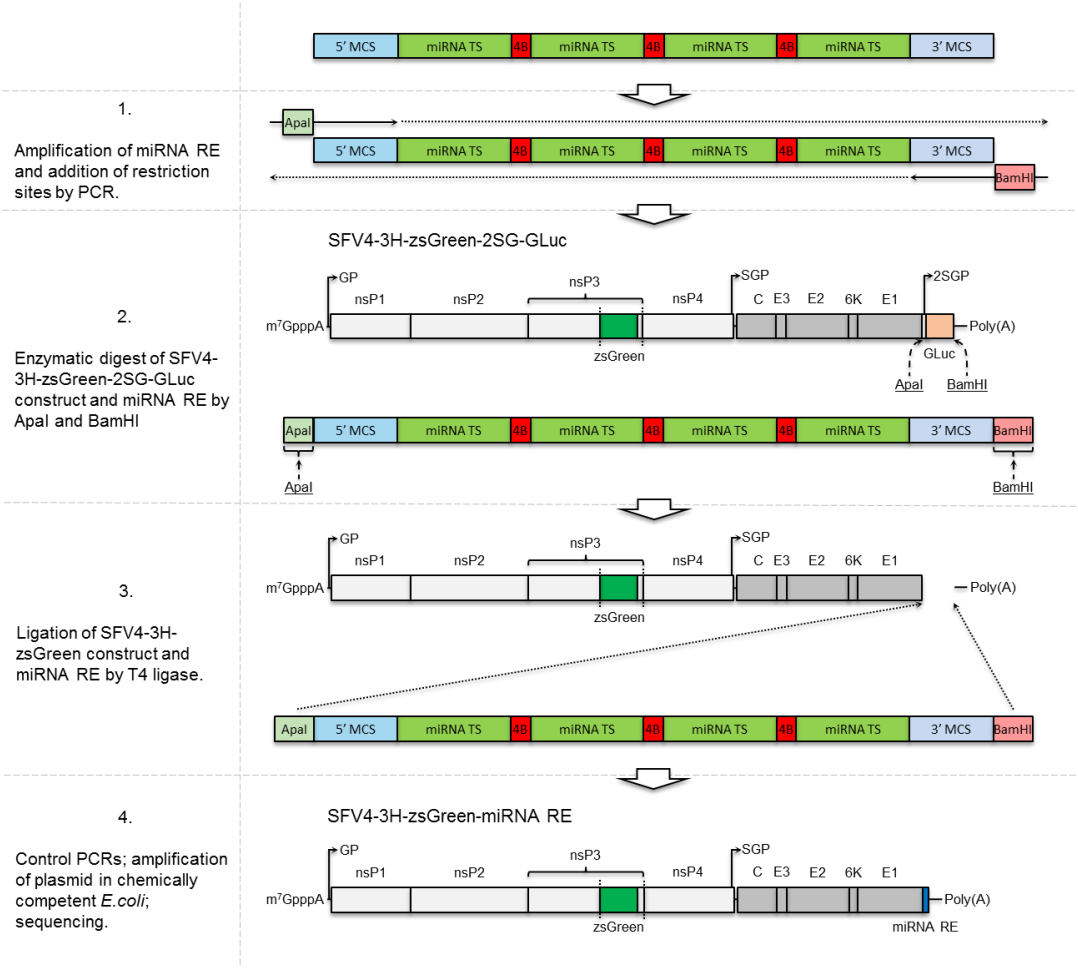

Figure 4.5. Incorporation of a miRNA RE into the genome of SFV4-3H-zsGreen-2SG-GLuc. Simplified structure of SFV4-3H-zsGreen-2SG GLuc is presented. nsP-non-structural protein; GP – genomic promoter; SGP – subgenomic promoter; 2SGP – duplicated subgenomic promoter; C – capsid; E1-E3 – envelope glycoproteins; GLuc – *Gaussia* luciferase; vertical dashed line – protein cleavage sites; Poly(A) – Poly(A) tail; m^7GpppA – 5' CAP; RE – recognition element; MCS – multiple cloning site; 4B – 4-nucleotide spacer; TS – target sequence.

4.5 Growing SFV-3H-zsGreen-miRNA RE clones

SFV4-3H-zsGreen-miRNA RE constructs were successfully rescued from icDNAs as described in 2.3.3.2. Virus stock (clarified cell culture supernatant) was titrated following the protocol outlined in 2.3.5. Expression of zsGreen in icDNA-electroporated cells was confirmed microscopically 24 hours post-electroporation.

4.6 Will SFV4-3H-zsGreen-miR-142-3P RE be attenuated in haematopoietic IC-21 cells but not in fibroblast BHK-21 cells?

The following proof-of-concept experiment was completed only once due to reasons explained later. First, BHK-21 cells and haematopoietic IC-21 cells were infected with all three SFV4-3H-zsGreen-miRNA RE clones at MOI of 0.01 and 100, respectively, in 24-well plates. The protocol described in 2.5.1 was followed. Twenty hours post-infection cells were fixed with 10% v/v neutral buffered formalin, washed with PBS and observed microscopically for the expression of virus-encoded zsGreen.

The microscopic inspection of IC-21 and BHK-21 cells revealed a complete absence of zsGreen expression. Hence, cells were immunostained for SFV nsP3 as described in 2.6. Positive staining was observed in virus-infected but not in uninfected cells. The proportion of virus-infected cells was calculated as described in 2.7.4.

Similar proportion of BHK-21 cells was infected with all the three viruses (Figure 4.6b). Approximately 45% of IC-21 cells were infected with SFV4-3H-zsGreen-miRNA RE Control (figure 4.6a). This was comparable to the infection rate observed for SFV4-3H-zsGreen-miR-142-3P Antisense RE. Importantly, less than 1% of IC-21 cells infected with the virus encoding miR-142-3P RE were positive for SFV nsP3. This corresponded to a statistically significant 99% reduction in the number of virus-positive cells relative to the control virus (Figure 4.7). These results suggested that the presence of miR-142-3P target sequences in the genome of SFV4 but not in the antigenome would efficiently restrict virus-replication in haematopoietic cells.

The lack of zsGreen expression in all SFV4-3H-zsGreen-miRNA RE clones was very surprising as the marker gene was clearly produced during virus rescue (see 4.5). Varjak et al. (2010) reported a presence of a functional degradation signal within the C-terminal region of SFV nsP3 that significantly accelerated degradation of RLuc in a chimeric reporter assay. Its exact role in virus replication is not well understood. However, it is believed that in a replication of an unmodified virus the nsP3 is stabilised by individual components of the viral replicase. It is also possible that SFV replication can inhibit nsP3 degradation. The zsGreen in SFV4-3H-

zsGreen-2SG-GLuc construct was fused with C-terminal amino acids of the nsP3. Most likely, the presence of the degradation signal led to rapid destruction of the virus-encoded zsGreen within hours post-translation. The zsGreen did not have sufficient time to accumulate or mature, causing the lack of detectable fluorescent signal during microscopic analysis. This effect may perhaps be more pronounced in cells where SFV replicates slower (potentially IC-21) in comparison to cells where SFV replicates very quickly (e.g. BHK-21). This may explain why zsGreen was clearly observed during production of virus stock in BHK-21 cells. As the SFV4-3H-zsGreen-miRNA RE clones were not fully functional it was decided that they would not be used in subsequent experiments. Instead, the three miRNA REs were cloned into other SFV4 constructs as described in 4.7.

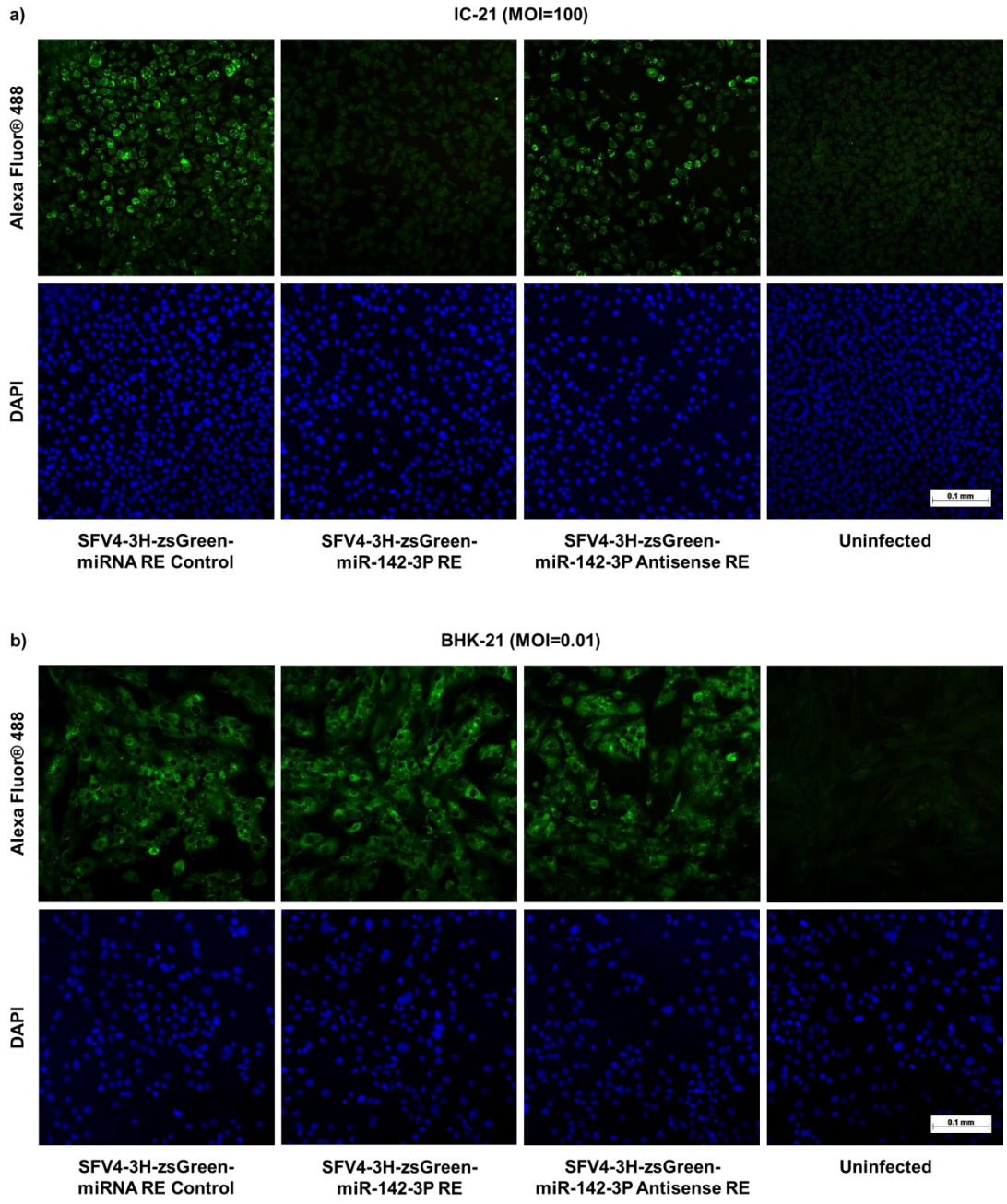

Figure 4.6. Infection of IC-21 and BHK-21cells with SFV4-3H-zsGreen-miRNA RE constructs. IC-21 (a) and BHK-21 (b) cells were infected at MOI of 100 and 0.01, respectively, with SFV4-3H-zsGreen-miR-142-3P RE, SFV4-3H-zsGreen-miR-142-3P Antisense RE and SFV4-3H-zsGreen-miRNA RE Control. Cells were incubated for 20 hours, fixed with 10% v/v neutral buffered formalin, immunostained for SFV nsP3 (Alexa Fluor ® 488-conjugated secondary antibody), mounted with VECTASHIELD mounting medium containing DAPI and inspected using Zeiss Axioskop 2 upright microscope.

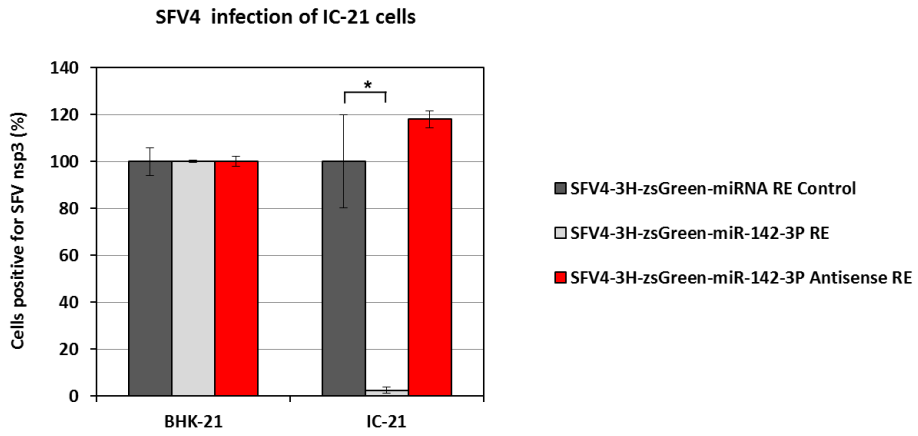

Figure 4.7. Infection of IC-21 and BHK-21 cells with SFV4-3H-zsGreen-miRNA RE constructs. IC-21 and BHK-21 cells were infected at MOI of 100 and 0.01, respectively, with SFV4-3H-zsGreen-miR-142-3P RE, SFV4-3H-zsGreen-miR-142-3P Antisense RE and SFV4-3H-zsGreen-miRNA RE Control. Cells were incubated for 20 hours, fixed, immunostained for SFV nsP3, mounted and inspected using Zeiss Axioskop 2 upright microscope. The proportion of nsP3-positive cells was calculated. The results were normalised to the infection in BHK-21 cells and to SFV4-3H-zsGreen miRNA RE Control virus. Data expressed as relative mean +/- relative SD; Mann-Whitney test, single-tailed; * $p<0.05$.

4.7 Generating SFV4-3F-zsGreen-miRNA RE and SFV4-3F-zsGreen-2SG-GLuc-miRNA RE constructs

SFV4-3F-zsGreen-2SG-GLuc was modified to incorporate miRNA REs in its genome. In this construct, zsGreen was expressed as a fusion protein with the nsP3. Consequently, in virus-infected cells zsGreen was localised to replication complexes in the cytoplasm. Furthermore, a cassette encoding a duplicated SFV subgenomic promoter and GLuc was inserted between ApaI and BamHI sites in the 3' UTR as described previously for SFV4-3H-zsgreen-2SG-GLuc. Finally, SFV4-3F-zsGreen-2SG-GLuc was cloned into the icDNA under control of the CMV promoter.

Two virus panels were generated based on SFV4-3F-zsGreen-2SG-GLuc. In the first one, all three miRNA REs were cloned into the 3' UTR of the virus, directly downstream of the GLuc, between NotI and PmeI restriction sites (Figure 4.8). The resulting viruses were designed to study the replication of SFV encoding miR-142-

3P RE *in vitro*. In the second panel, GLuc was replaced by miR-142-3P RE and miRNA RE Control (Figure 4.9). Based on the preliminary data obtained using SFV4-3H-zsGreen-miR-142-3P Antisense RE (see 4.6) it was decided that miR-142-3P Antisense RE would not be used. The overall design was similar to that of SFV4-3H-zsGreen-miRNA RE constructs (see 4.4). The resulting SFV4 clones would maintain a functional zsGreen as a marker gene and should be small and stable enough to use *in vivo*. The cloning procedure is detailed in Annex 18.

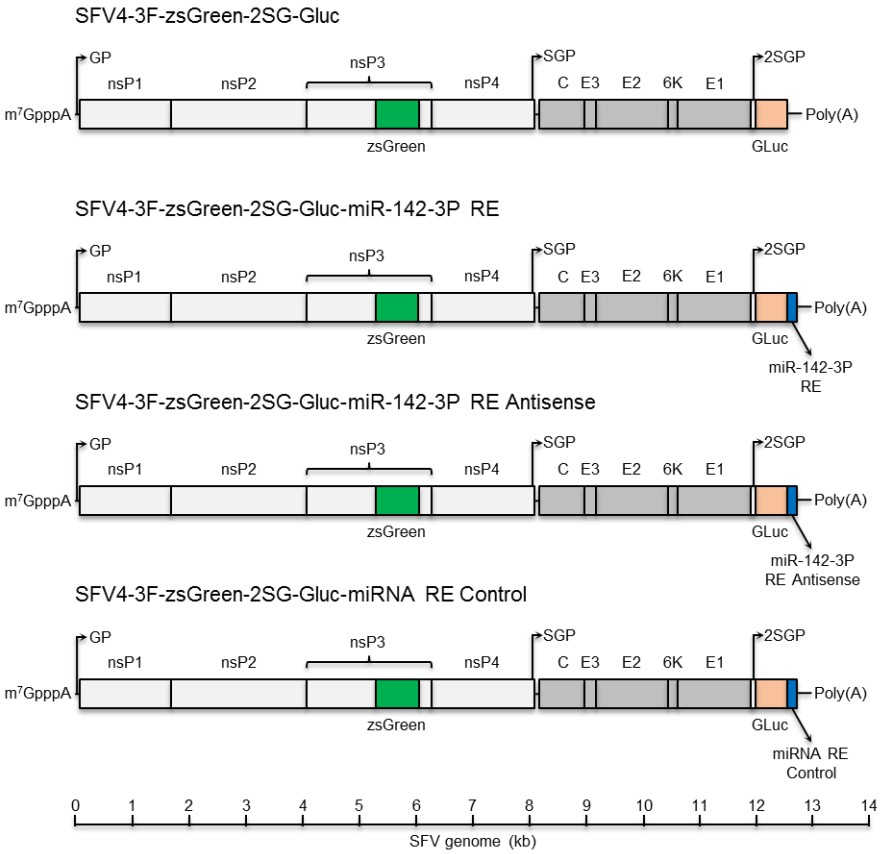

Figure 4.8. Schematic representation of SFV4-3F-zsGreen-2SG-GLuc miRNA RE clones. miRNA REs were inserted into the 3' UTR of the virus, downstream of the GLuc, between NotI and PmeI restriction sites. Parental virus, SFV4-3F-zsGreen-2SG-GLuc, is shown at the top. nsP – non-structural protein; GP – genomic promoter; SGP – subgenomic promoter; 2SGP – duplicated subgenomic promoter; C – capsid; E1-E3 – envelope glycoproteins; GLuc – *Gaussia* luciferase; Poly(A) – Poly(A) tail; m^7GpppA – 5' CAP; RE – recognition element.

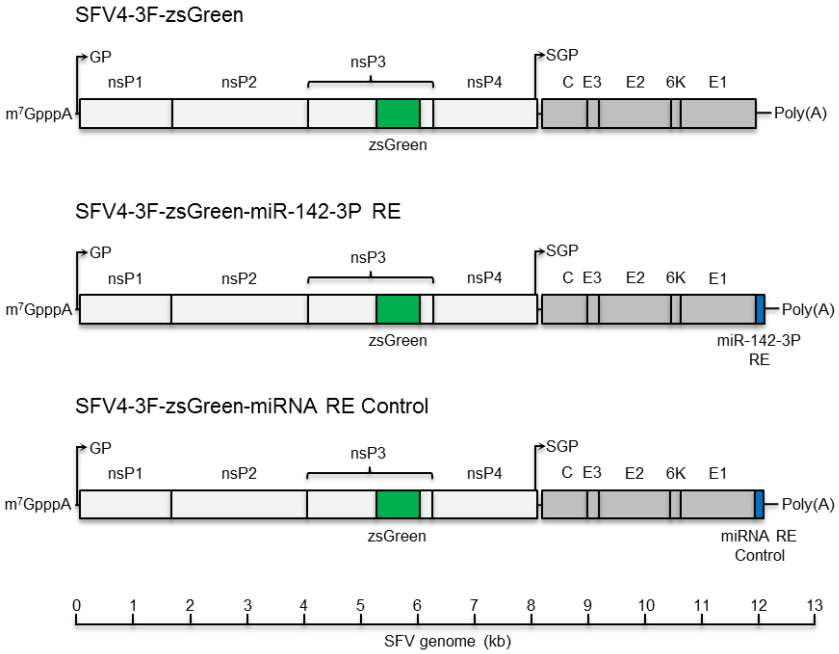

Figure 4.9. Schematic representation of SFV4-3F-zsGreen-miRNA RE clones. miRNA REs were inserted into the 3' UTR of the virus. Parental virus, SFV4-3F-zsGreen, is shown at the top. nsP – non-structural protein; GP – genomic promoter; SGP – subgenomic promoter; C – capsid; E1-E3 – envelope glycoproteins; Poly(A) – Poly(A) tail; m^7GpppA – 5' CAP; RE – recognition element.

SFV4-3F-zsGreen-2SG-GLuc constructs encoding miR-142-3P RE, miR-142-3P Antisense RE and miRNA RE Control were called SFV4-3F-zsGreen-2SG-GLuc-miR-142-3P RE, SFV4-3F-zsGreen-2SG-GLuc-miR-142-3P Antisense RE and SFV4-3F-zsGreen-2SG-GLuc-miRNA RE Control, respectively. Altogether, these viruses were named SFV4-3F-zsGreen-2SG-GLuc-miRNA RE. Their sequences are provided in Supplementary Data, Appendix 1.

SFV4-3F-zsGreen constructs encoding miR-142-3P RE and miRNA RE Control were called SFV4-3F-zsGreen-miR-142-3P RE and SFV4-3F-zsGreen-miRNA RE Control, respectively. Altogether, these viruses were named SFV4-3F-zsGreen-miRNA RE. Their sequences are provided in Supplementary Data, Appendix 1.

4.8 Growing SFV encoding miR-142-3P RE and functional marker genes zsGreen and GLuc

SFV4-3F-zsGreen-2SG-GLuc, SFV4-3F-zsGreen-miRNA RE and SFV4-3F-zsGreen-2SG-GLuc-miRNA RE constructs were successfully rescued from icDNAs as described in 2.3.3.2. Virus stock (clarified cell culture supernatant) was titrated following the protocol outlined in 2.3.5. Expression of zsGreen in icDNA-electroporated cells was confirmed microscopically 24 hours post-electroporation.

4.9 Will the presence of miR-142-3P RE affect the rate at which SFV can replicate in fibroblast BHK-21 cells?

Replication of SFV4 (wt), SFV4-3F-zsGreen, SFV4-3F-zsGreen-2SG-GLuc, SFV4-3F-zsGreen-miRNA RE and SFV4-3F-zsGreen-2SG-GLuc-miRNA RE constructs in BHK-21 cells was investigated by completing one-step growth curves. In brief, cells were infected at MOI of 10 to ensure an infection rate close to 100%. Virus replication was tested by plaque assay (and GLuc, if applicable) every 2-4 hours, for 24 hours. The protocol described in 2.3.7 was followed.

The results shown in Figure 4.10a suggested that incorporation of marker genes into the genome of SFV had a negative effect on virus replication. This was observed at all time-points but it was the most pronounced within the first 12 hours post-infection. The effect was amplified when multiple marker genes were used. This could be due to size of modified viruses (larger genome would replicate slower) or due to disruptions made in the virus genome during cloning.

Incorporation of a miRNA RE into SFV4 genome did not itself affect virus replication. This was observed in SFV4-3F-zsGreen-miRNA RE constructs (Figure 4.10b) and in SFV4-3F-zsGreen-2SG-GLuc-miRNA RE constructs (Figure 4.10c,d).

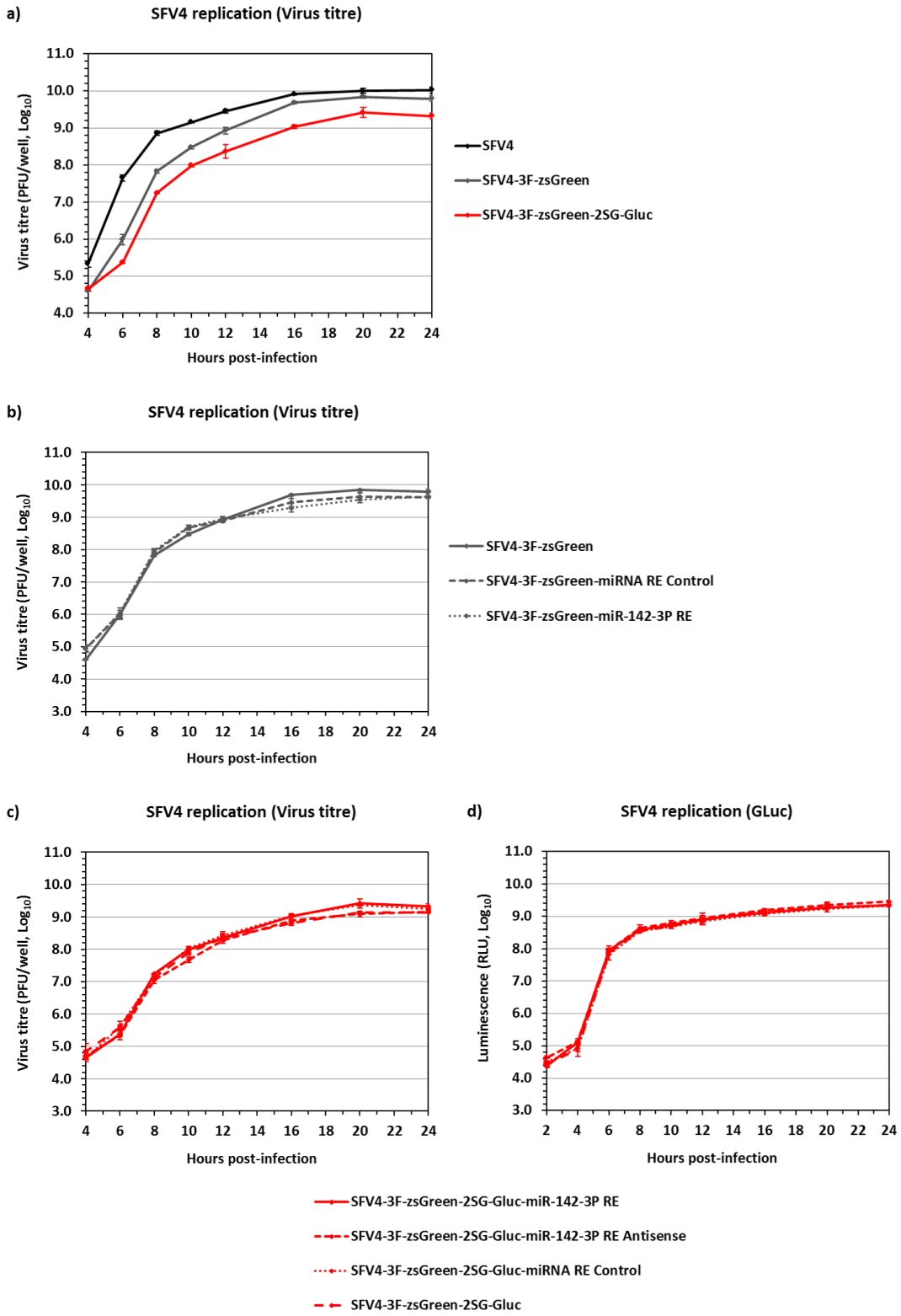

Figure 4.10. SFV4 one-step growth curves. BHK-21 cells were infected at MOI of 10 and incubated for 24 hours. The cell supernatant was sampled every 2 hours for the first 12 hours, and then every 4 hours. Samples were tested by plaque assay (a,b,c) or by GLuc assay (d). Data expressed as mean +/- SD.

The size of plaques produced by SFV4 (wt), SFV4-3F-zsGreen, SFV4-3F-zsGreen-2SG-GLuc, SFV4-3F-zsGreen-miRNA RE and SFV4-3F-zsGreen-2SG-GLuc-miRNA RE constructs on BHK-21 cells was investigated using Zeiss AxioVision 4.8 digital image processing software. All viruses were plaqued as described in 2.3.5, at the same time and on the same BHK-21 cells.

The observed plaque sizes (Figure 4.11, 4.12) mirrored the pattern identified by one-step growth curves (Figure 4.10). SFV4 (wt) produced the largest plaques (2.28 mm, SD=0.06) with the most distinctive edge. The size of SFV4-3F-zsGreen plaques was reduced by approximately 21% (1.80 mm, SD=0.08) in comparison to SFV4 (wt). The reduction was statistically significant ($P<0.05$). The size of SFV4-3F-zsGreen-2SG-GLuc was reduced even further, by 32% (1.32 mm, SD=0.06) in comparison to SFV4 (wt). The reduction was statistically significant ($P<0.05$) with respect to both SFV4 (wt) and SFV4-3F-zsGreen. Importantly, incorporation of a miRNA RE into a virus genome did not itself affect the size of plaques produced by this virus. With the exception of SFV4 (wt), all viruses generated plaques that had uneven, serrated edges. All viruses were characterised by a homogenous plaque population.

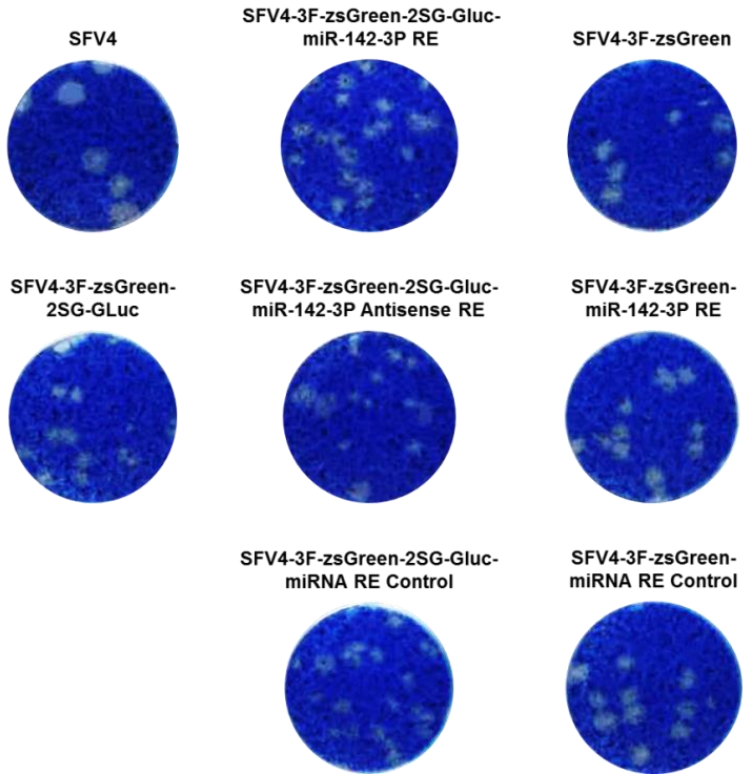

Figure 4.11. Plaques generated by different SFV4 clones. Cells were incubated for 48 hours with CMC-based semi-solid overlay, fixed with 10% v/v neutral buffered formalin for 1 hour and then stained with 0.1% toluidine blue.

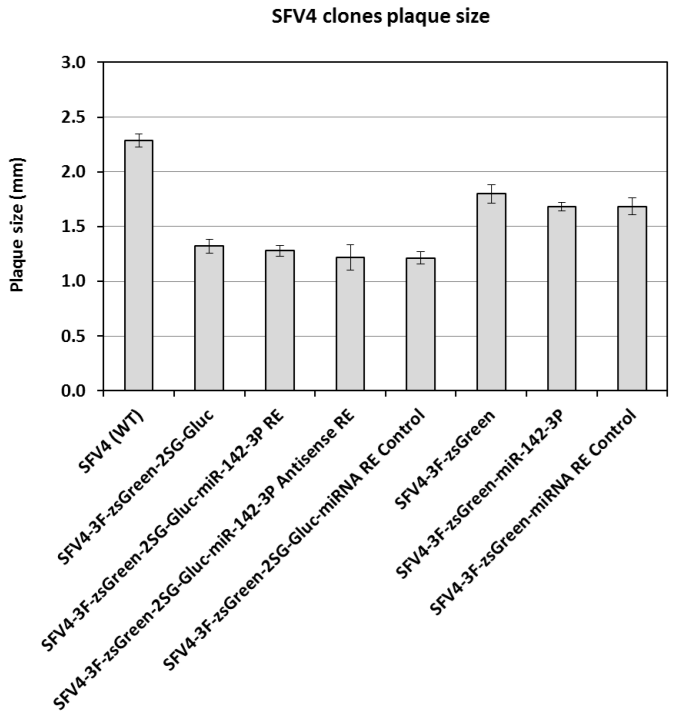

Figure 4.12. Size of plaques generated by different SFV4 clones. The size of plaques was measured using Zeiss AxioVision 4.8 digital image processing software. Data expressed as mean of random 20 individual plaques +/- SD.

4.10 Will SFV4-3F-zsGreen-2SG-GLuc-miR-142-3P RE be attenuated in haematopoietic IC-21 cells but not in fibroblast BHK-21 cells?

SFV4-3F-zsGreen-2SG-GLuc-miR-142-3P RE, SFV4-3F-zsGreen-2SG-GLuc-miR-142-3P Antisense RE and SFV4-3F-zsGreen-2SG-GLuc-miRNA RE Control were used to infect BHK-21 cells at MOI of 0.005, and IC-21 cells at MOIs of 10 and 100, in 24-well plates. The protocol outlined in 2.5.1 was followed. Fifty µl of the supernatant from IC-21 cells was collected 1.5 hours post-infection (samples from replicate wells were pooled). Twenty hours post-infection supernatants from virus-infected cells were collected and cells were observed microscopically for the expression of virus-encoded zsGreen. Virus titres and GLuc levels were measured as described in 2.3.5 and 2.9.3, respectively.

The replication of the three viruses in IC-21 cells could not be accurately measured by a plaque assay due to high levels of virus remaining in cell supernatants post-infection (up to 10^5 PFU/ml). Twenty hours post-infection, virus titres from IC-21 cells infected with SFV4-3F-zsGreen-2SG-GLuc-miR-142-3P Antisense RE and SFV4-3F-zsGreen-2SG-GLuc-miRNA RE Control were higher (up 10^6 PFU/ml) and comparable to each other suggesting active replication of both viruses in these cells. However, the amount of virus present in the supernatant of IC-21 cells infected with SFV4-3F-zsGreen-2SG-GLuc-miR-142-3P RE was close to the titre calculated according to the SFV4 thermal inactivation (see Figure 3.8). This suggested that the full attenuation of SFV4-3F-zsGreen-2SG-GLuc-miR-142-3P RE in IC-21 cells could not be measured by a plaque assay in this experiment.

GLuc encoded by all three viruses allowed simple but indirect measurement of virus replication. In BHK-21 cells, all three viruses replicated to the same extent (Figure 4.13). In IC-21 cells, viruses encoding miRNA RE Control and miR-142-3P Antisense RE replicated to comparable levels. However, the measured replication of SFV4-3F-zsGreen-2SG-GLuc-miR-142-3P RE was reduced by over 99% with respect to the control virus at both MOIs. The difference was statistically significant. The above data was fully supported by observation of virus-infected cells under a microscope. A pattern similar to that shown in Figure 4.7 was observed.

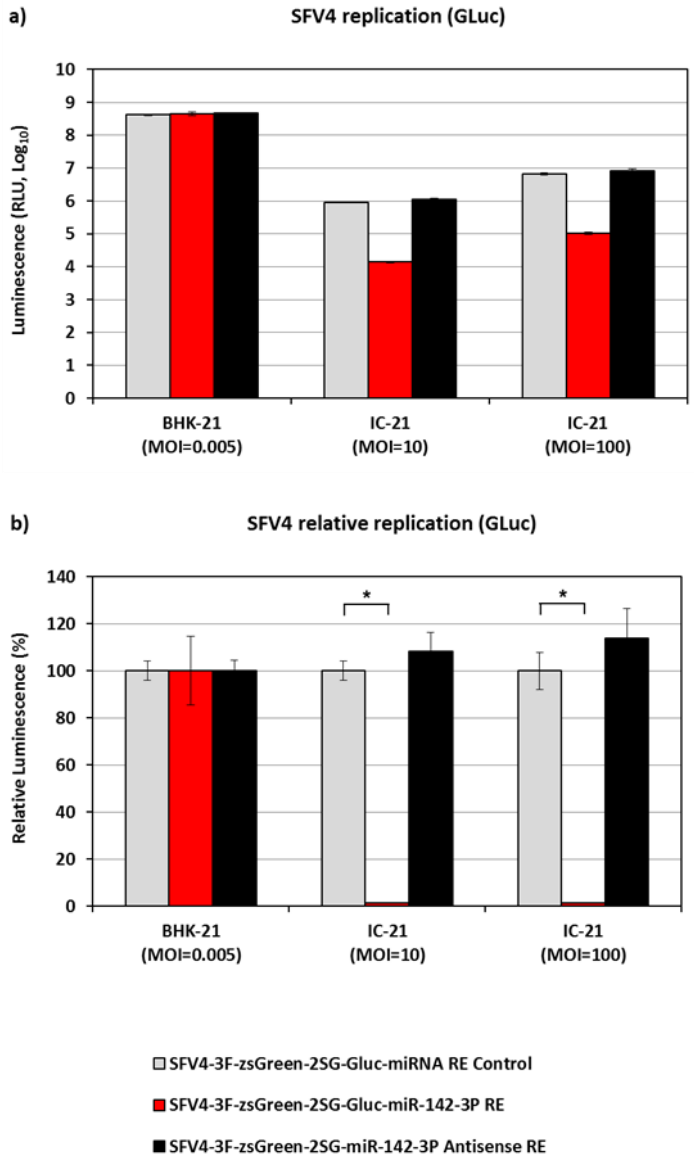

Figure 4.13. Replication of SFV4-3H-zsGreen-miRNA RE clones in IC-21 and BHK-21 cells. BHK-21 cells were infected at MOI of 0.005. IC-21 cells were infected at MOI of 10 and 100. GLuc was measured in the supernatant from virus-infected cells 20 hours post-infection. (a) Raw data expressed as mean +/- SD. (b) Results normalised to the infection in BHK-21 cells and to SFV4-3F-zsGreen-2SG-GLuc-miRNA RE Control virus. Data expressed as relative mean +/- relative SD; Mann-Whitney test, single-tailed; * $p<0.05$.

4.11 Designing, generating and characterising Hek 293 cells that express miR-142-3P under control of the hybrid CMV/TetO$_2$ promoter

Stable cell lines that can express miR-142-3P under control of the hybrid CMV/TetO$_2$ promoter were generated using Flp-In^{TM} T-Rex^{TM} System. Non-haematopoietic Flp-In^{TM} T-Rex^{TM} 293 cells were used. They did not express any notable levels of miR-142-3P and they were susceptible to infection by SFV and CHIKV. These cells were designed and generated to confirm that the attenuation of SFV4 clones encoding miR-142-3P RE in haematopoietic IC-21 cells observed in 4.6 and 4.10 was solely due to the action of miR-142-3P.

The Flp-In^{TM} T-Rex^{TM} System is described below. Flp-In^{TM} T-Rex^{TM} 293 cells contain a single stably integrated minimal (34 bp) Flp Recombination Target (FRT) site at a transcriptionally active genomic locus. The FRT site is located immediately downstream of ATG initiation codon of lacZ-Zeocin^{TM} fusion gene under the control of the SV40 early promoter. In addition, Tet repressor (TetR) is expressed under control of the human cytomegalovirus (CMV) immediate early enhancer/promoter from a different genomic locus. Next, gene of interest (GOI) is cloned into pcDNA^{TM}5/FRT/TO expression vector under control of the hybrid CMV/TetO$_2$ promoter. In addition, the pcDNA^{TM}5/FRT/TO plasmid encodes the hygromycin resistance gene which lacks a promoter and a start codon but includes a FRT sequence in its 5' end. Upon co-transfection of pcDNA^{TM}5/FRT/TO containing the GOI and pOG44 (plasmid expressing Flp recombinase) into the Flp-In^{TM} T-Rex^{Tm} 293 cells, the pcDNA^{TM}5/FRT/TO construct is integrated into the cell genome via Flp-mediated homologous recombination between FRT sites in the cell genome and the pcDNA^{TM}5/FRT/TO. During this process the FRT sites are maintained and the SV40 early promoter and ATG initiation codon of the lacZ-Zeocin^{TM} fusion gene are donated to hygromycin resistance gene thus inactivating the lacZ-Zeocin^{TM} fusion gene. Consequently, stable clones expressing the GOI are resistant to hygromycin but are sensitive to Zeocin^{TM} and lack the ß-galactosidase activity. The CMV/TetO$_2$ promoter upstream of the GOI consists of the CMV immediate early enhancer/promoter followed by two copies of 19 nucleotide *tet* operator 2 (TetO$_2$, 5'-TCCCTATCAGTGATAGAGA-3') separate by a 2 base pair spacer. Each TetO$_2$

can bind two molecules of the TetR homodimer that is constitutively expressed in Flp-In™ T-Rex™ 293 cells thus repressing the transcription of the GOI. However, upon addition of tetracycline, the antibiotic binds to the TetR and changes its conformation leading to its dissociation from $TetO_2$ and induction of GOI transcription. Consequently, the activity of the CMV promoter driving the expression of the GOI can be regulated by presence of tetracycline.

The genomic locus of miR-142-3P on human chromosome 17 has been characterised in human K562 cells by Sun et al. (2010). The transcription start site of the miR-142 primary transcript was located 308 bases upstream from the 5' end of the miR-142 precursor. A polyA signal was located 730 bases downstream of the transcription start site. A schematic representation of the miR-142-3P locus (HSA17:5640719-56409349[-]) is located in Figure 4.14.

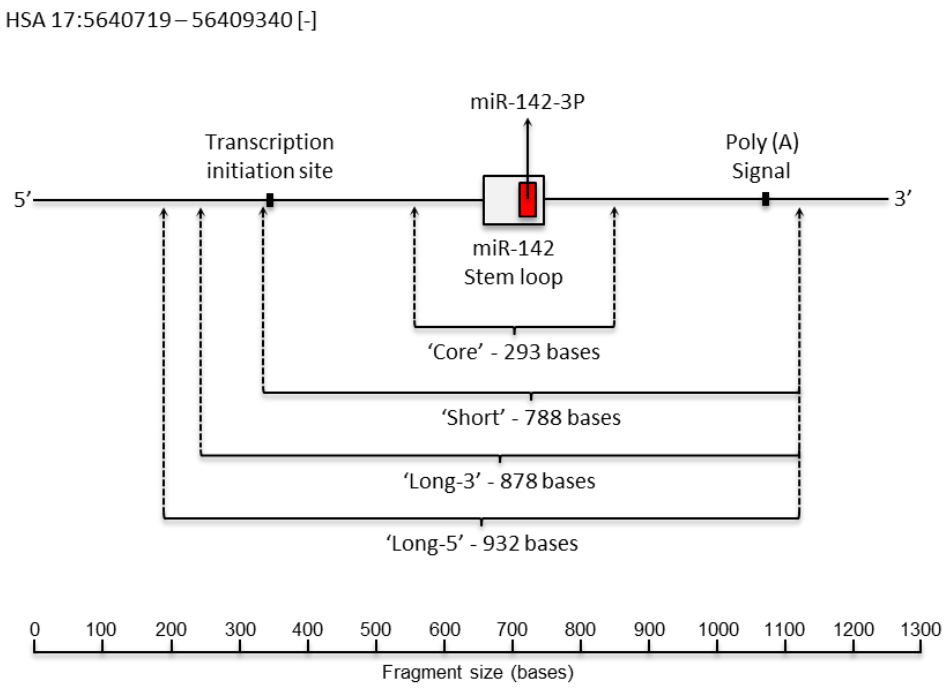

Figure 4.14. Schematic representation of miR-142-3P locus on human chromosome 17. Locations of the transcription start site of the miR-142 primary transcript, miR-142 stem loop, miR-142-3P and a polyA signal located on human chromosome 17 (HSA17:5640719-56409340[-]) are shown. Fragments of genomic sequence cloned into Flp-In™ T-Rex™ 293 cells are indicated.

In brief, Flp-In™ T-Rex™ 293 cells were modified by inserting a sequence from the genomic locus of miR-142-3P into their genome, under control of the hybrid CMV/$TetO_2$ promoter. Four different constructs were designed (Figure 4.14). Their complete sequences are provided in Annex 16.

1. **miR-142 'Core'** – 293 nucleotide fragment encompassing 103 bp upstream of miR-142 stem loop to 103 bp downstream of miR-142 stem loop.

2. **miR-142 'Short'** – 788 nucleotide fragment encompassing 8 bp upstream of the transcription start site of miR-142 primary transcript to 50 bp downstream of poly(A) signal.

3. **miR-142 'Long-3'** – 878 nucleotide fragment encompassing 98 bp upstream of the transcription start site of miR-142 primary transcript to 50 bp downstream of poly(A) signal.

4. **miR-142 'Long-5'** - 932 nucleotide fragment encompassing 152 bp upstream of the transcription start site of miR-142 primary transcript to 50 bp downstream of poly(A) signal.

The cloning details are provided in Annex 19. The resulting cell lines were called Hek 293 miR-142 'Core', Hek 293 miR-142 'Short', Hek 293 miR-142 'Long-3', Hek 293 miR-142 'Long-5' and Hek 293 Control. Six clones of each cell line were sub-cultured.

The expression of miR-142-3P was assayed by qPCR in two clones of each cell line. First, each clone was seeded into a 6-well plate at 5 x 10^5 cells/well in duplicates. Doxycycline (an analogue of tetracycline) was added to one well from each pair at 1 μg/ml final concentration. Cells were incubated for exactly 24 hours. Next, total RNA was extracted using TRIzol® reagent as described in 2.15.3. The expression of miR-142-3P per 200 ng of RNA was measured using TaqMan® miR-142-3P Assay (Life Technologies Applied Biosystems®, Annex 6) as described in 2.13.

The qPCR amplification curves were analysed visually (Figure 4.15). All cell lines (with the exception of Hek 293 Control) expressed miR-142-3P following the addition of doxycycline (DOX). One of the highest expressions of miR-142-3P following induction with DOX was observed in Hek 293 miR-142 'Core' cell line. This was an interesting finding. It suggested that the expression cassette encoded by the Flp-In™ T-Rex™ 293 cells can efficiently transcribe the miR-142-3P gene in the absence of any promoters or control elements present upstream of the miR-142 primary transcript. In addition, the 293 nucleotide fragment encompassing 103 bp upstream of miR-142 stem loop to 103 bp downstream of miR-142 stem loop must contain all elements required by the cellular miRNA machinery to process the pri-miRNA into the mature miR-142-3P.

Evidence of background expression of miR-142-3P was observed in all cell lines (with the exception of Hek 293 Control) induced with DOX. This was not unexpected as promoters based on *tet* operator 2 ($TetO_2$) had been shown before to be leaky (Senkel et al. 2009). Interestingly, Hek 293 miR-142 'Core' cells demonstrated one of the lowest background expressions of miR-142-3P. It is possible that the lack of any promoters normally found upstream of the miR-142 primary transcript may contribute to the tight control of pri-mRNA expression by the *tet* operator 2 in Flp-In™ T-Rex™ 293 cells. As a result of the above findings, Hek 293 miR-142 'Core' cells were chosen for further characterisation.

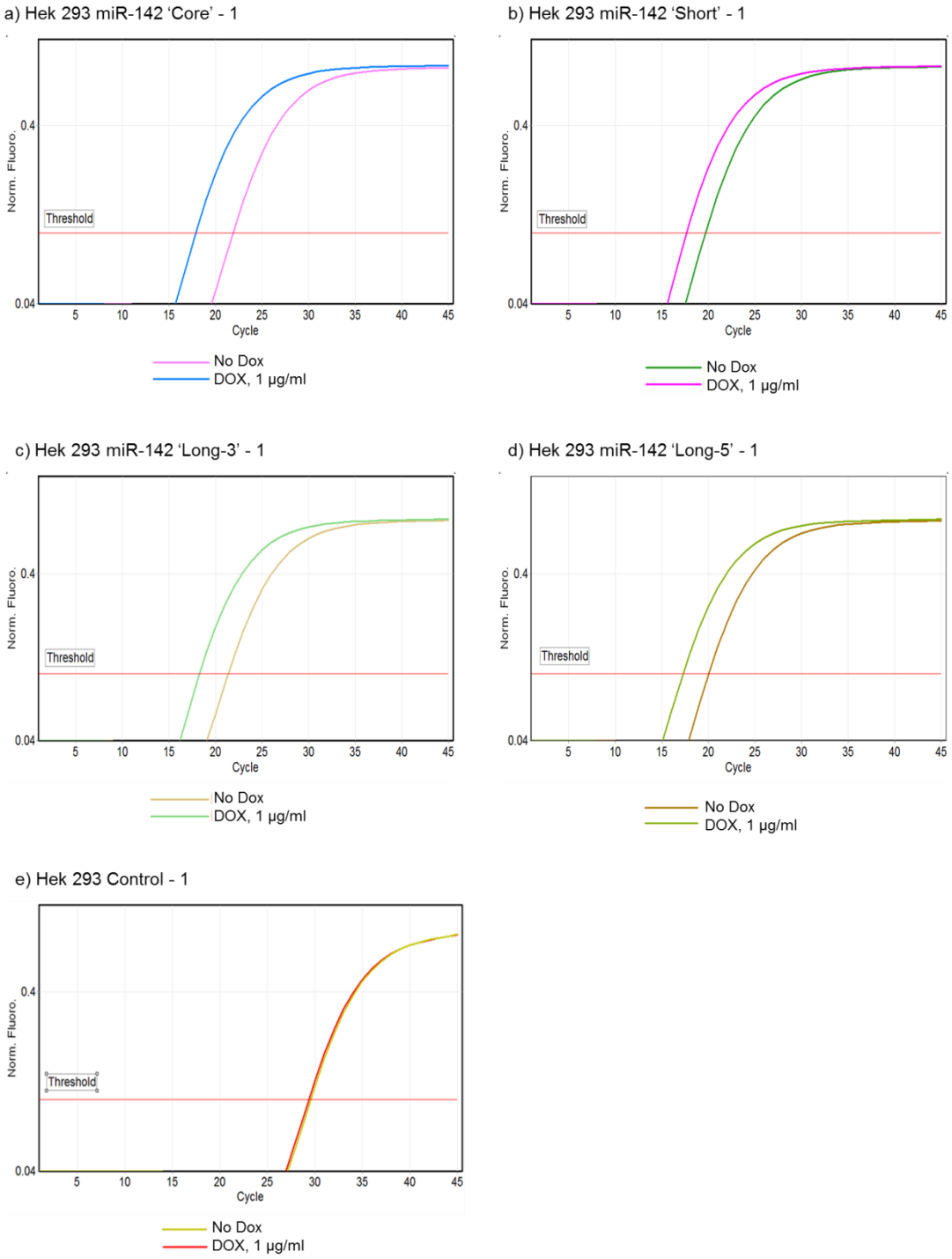

Figure 4.15. Relative expression of miR-142-3P in modified Flp-In™ T-Rex™ 293 cells. qPCR amplification curves from one clone of each cell lines are shown. Cells were induced or not with DOX at 1µg/ml final concentration for 24 hours prior to RNA extraction. X-axis – qPCR cycle number. Y-axis – Normalised fluorescence. The same threshold was used in a,b,c,d and e.

The expression of miR-142-3P was assessed by qPCR in all clones of Hek 293 miR-142 'Core' cell line following the protocol described above. The qPCR amplification curves were analysed visually (Figure 4.16). No notable difference was observed between the 6 clones. Consequently, clone 1 was chosen for further analysis and the resultant cell line was renamed as Hek 293 miR-142. Finally, Hek 293 Control and Hek 293 miR-142 cell lines were expanded and frozen in LN_2 as described in 2.2.11. The LN_2 master stock of both cell lines was assigned Passage number 0.

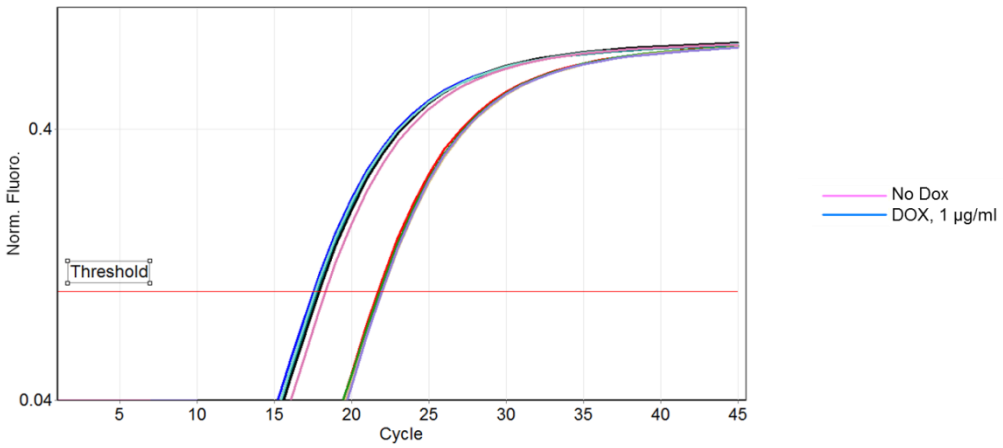

Figure 4.16. Relative expression of miR-142-3P in 6 clones of Hek 293 miR-142 'Core'. No notable difference was observed. Clone 1 was chosen for further analysis and the resultant cell line was renamed Hek 293 miR-142.

The expression of miR-142-3P relative to miR-16 was subsequently measured in Hek 293 miR-142 (+/- DOX), Hek 293 (+/- DOX), BHK-21, 3T3, Thp-1 (not treated with PMA) and IC-21 cells, in biological triplicates. Hek 293 miR-142 cells (+/- DOX) and Hek 293 Control cells (+/- DOX) were prepared as described above. The other cell lines were harvested, counted and then 1 x 10^6 of cells was pelleted by centrifugation for 5 min at 200 x g and RT. Total RNA was extracted using TRIzol® reagent as described in 2.15.3. The expression of miR-142-3P and miR-16 was measured using TaqMan® miR-142-3P Assay and TaqMan® miR-16 Assay, respectively (both Life Technologies Applied Biosystems®, Annex 6). The protocol described in 2.13 was followed.

The qPCR data are summarised in Figure 4.17. The relative levels of miR-142-3P were up to 10,000 higher in haematopoietic cells IC-21 and Thp-1 than in fibroblast cell lines 3T3 and BHK-21. High levels of miR-142-3P RE in human Thp-1 cells and in mouse IC-21 cells confirmed that this miRNA is conserved in humans and mice. As expected, the level of miR-142-3P expression in Hek 293 Control cells was low and not dependent on the induction with DOX. As expected, a strong background expression of the miRNA was observed in Hek 293 miR-142 cells not induced with DOX. Importantly, following the induction with DOX the expression of miR-142-3P in Hek 293 miR-142 cells increased over 14-fold and was only slightly smaller than that observed in Thp-1 and IC-21 cells.

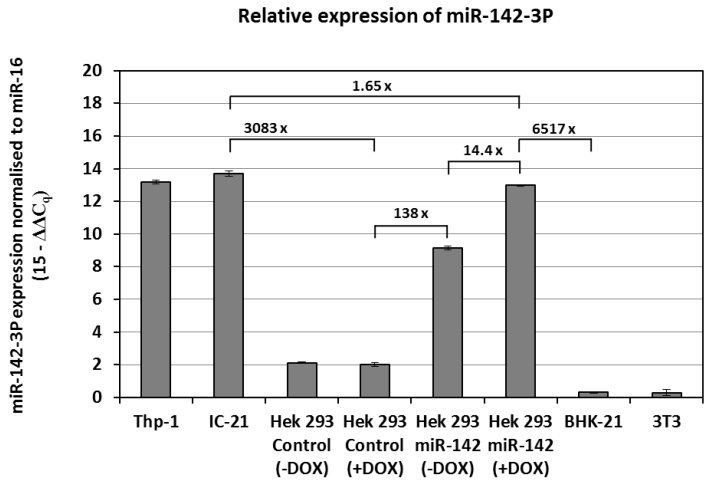

Figure 4.17. miR-142-3P expression normalised to miR-16 in a range of haematopoietic and non-haematopoietic cell lines. Data expressed as $15\text{-}\Delta\Delta C_q$, mean of 3 biological replicates +/- SD. Hek 293 miR-142 (+DOX) and Hek 293 Control (+DOX) cells were induced with DOX at 1μg/ml final concentration for 24 hours prior to RNA extraction. Dox – doxycycline; C_q – quantification cycle.

In all subsequent experiments, Hek 293 miR-142 and Hek 293 Control cells were treated with DOX at 100 ng/ml. This concentration of DOX was sufficient to fully induce the expression of miR-142-3P in Hek 293 miR-142 cells (data not shown).

Susceptibility of Hek 293 miR-142 and Hek 293 Control cells to SFV was investigated. In brief, both cell lines were harvested, counted and seeded into 24-well plates (with or without DOX at 100 ng/ml final concentration) as described in 2.5.1. After 24 hours of incubation, cells were infected with SFV4-3F-zsGreen-2SG-GLuc-miRNA RE Control at MOI of 0.1 and 1 as described in 2.5.1. Twenty hours post-infection the supernatant from virus-infected cells was collected. Virus titres and GLuc levels were measured as described in 2.3.5 and 2.9.3, respectively.

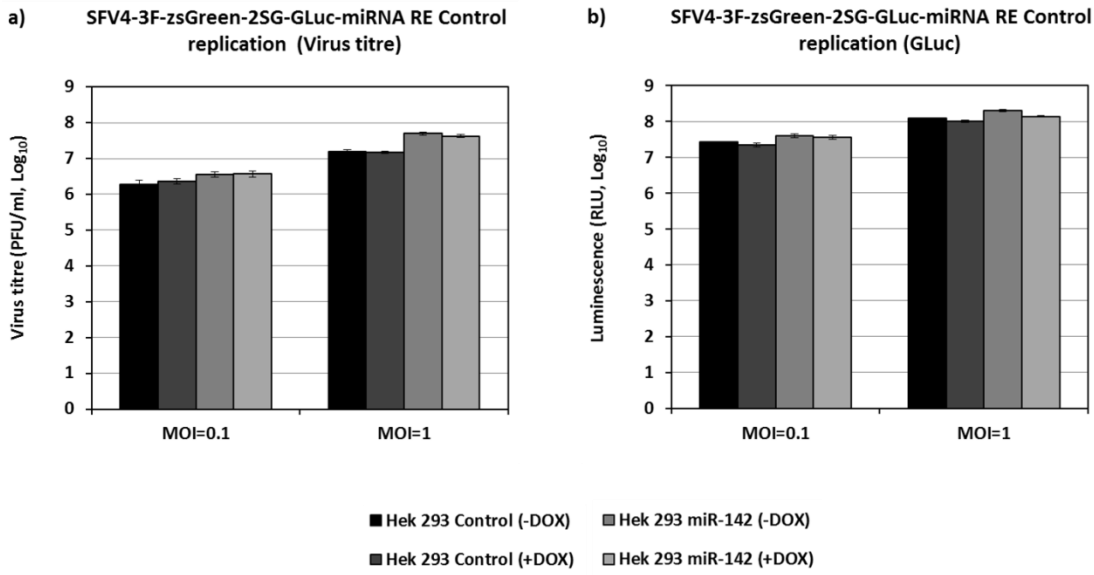

Figure 4.18. Infection of Hek 293 miR-142 and Hek 293 Control cells with SFV4-3F-zsgreen-2SG-miRNA RE Control. Hek 293 miR-142 (+DOX) and Hek 293 Control (+DOX) cells were induced with DOX at 100 ng/ml final concentration for 24 hours prior to infection. Cells were infected at MOI of 0.1 and 1. Data expressed as mean +/- SD.

As shown in Figure 4.18, SFV4-3F-zsGreen-2SG-GLuc successfully infected Hek 293 miR-142 and Hek 293 Control cells. Interestingly, the virus replicated marginally better in Hek 293 miR-142 cells than in Hek 293 Control cells. This difference was more pronounced when cells were infected at the higher MOI. Similar results were observed for CHIKV (data not shown). Overall, treatment of cells with doxycycline did not change the susceptibility of these cells to the control virus.

4.12 Will SFV encoding miR-142-3P RE be attenuated in non-haematopoietic cells expressing miR-142-3P?

Hek 293 miR-142 and Hek 293 Control cells were harvested, counted and seeded into 24-well plates (with or without DOX at 100 ng/ml final concentration) as described in 2.5.1. After 24 hours of incubation, cells were infected with SFV4-3F-zsGreen-2SG-miR-142-3P RE, SFV4-3F-zsGreen-2SG-GLuc-miR-142-3P Antisense and SFV4-3F-zsGreen-2SG-GLuc-miRNA RE Control at MOI of 0.1 and 1 as described in 2.5.1. Twenty hours post-infection the supernatant from virus infected cells was collected and the cells were observed microscopically for the expression of virus-expressed zsGreen. Virus titres and GLuc levels were measured as described in 2.3.5 and 2.9.3, respectively.

In Hek 293 Control cells that were either induced with DOX or not, all three viruses replicated to the same extent at both MOIs as demonstrated by both virus production (Figure 4.19) and by GLuc expression (Figure 4.20). This confirmed that the pre-treatment of cells with DOX in itself did not selectively alter virus replication. Replication of all three viruses in Hek 293 miR-142 cells not induced with DOX was comparable to that observed in Hek 293 Control cells, suggesting that the background expression of miR-142-3P (see Figure 4.17) was not sufficient to alter the replication of any of these viruses. In Hek 293 miR-142 cells that were pre-treated with DOX, the replication of viruses encoding miRNA RE Control and miR-142-3P Antisense RE was not affected. However, the measured replication of SFV4-3F-zsGreen-2SG-GLuc-miR-142-3P RE was reduced by over 95% with respect to the control virus at both MOIs. This was demonstrated by virus production (Figure 4.19) and by GLuc expression (Figure 4.20). In both assays the observed attenuation of SFV was statistically significant. The above results were fully supported by observation of virus-infected cells under the microscope. Altogether, the above data confirmed that the replication of SFV4 encoding miR-142-3P target sequences in its genome but not in its antigenome was attenuated in cells that express miR-142-3P.

The close correlation between production of viable virus particles and expression of virus-encoded GLuc observed in Figures 4.19 and 4.20 suggested that miR-142-3P

attenuated SFV4-3F-zsGreen-2SG-GLuc-miR-142-3P RE by interfering with the replication of its RNA genome during early stages of infection. As described in 1.3.2, alphavirus RNA is replicated inside replication complexes that shield it from cellular factors. Once replication complexes are established and matured, large amounts of newly synthesised viral RNA are released into the cytoplasm. At this stage, alphavirus RNA encoding a miRNA RE would quickly saturate the cellular miRNA machinery and render it non-effective. Consequently, the alphavirus RNA encoding a miRNA RE may be the most vulnerable to targeting by cellular miRNAs immediately after the nucleocapsid disassembly, when the unprotected genomic RNA is released into the cytoplasm. However, relatively high background levels of miRNA expression may be required to efficiently degrade alphavirus RNA during the brief period before the replication complexes are established. This was supported by the lack of attenuation of SFV4-3F-zsGreen-2SG-miR-142-3P RE in Hek 293 miR-142 cells not induced with DOX which demonstrated a background expression of miR-142-3P (138-fold higher than those observed in Hek 293 Control cells).

The pre-treatment of Hek 293 miR-142 cells with DOX led to only 14-fold increase in the expression of miR-142-3P in comparison to cells that were not induced. However, the effect of this moderate increase in miR-142-3P expression on SFV4-3F-zsGreen-2SG-GLuc-miR-142-3P RE replication was significant. The relationship between the levels of miR-142-3P expression and the attenuation of SFV4 encoding the miR-142-3P RE was further investigated using Hek 293 miR-142-3P cells induced with a range of DOX concentrations. In brief, Hek 293 miR-142 cells were harvested, counted and seeded into 24-well plates with increasing amounts of DOX (0-1000 ng/ml, 0.2 ng/ml or 10-fold steps) as described in 2.5.1. After 24 hours of incubation, cells were infected with SFV4-3F-zsGreen-2SG-miR-142-3P RE and SFV4-3F-zsGreen-2SG-GLuc-miRNA RE Control at MOI of 1 as described in 2.5.1. Twenty hours post-infection the cells were observed microscopically for the expression of virus-encoded zsGreen. The supernatant from virus infected cells was collected, and cellular RNA was extracted as described in 2.15.3. Virus titres and GLuc levels were measured as described in 2.3.5 and 2.9.3, respectively.

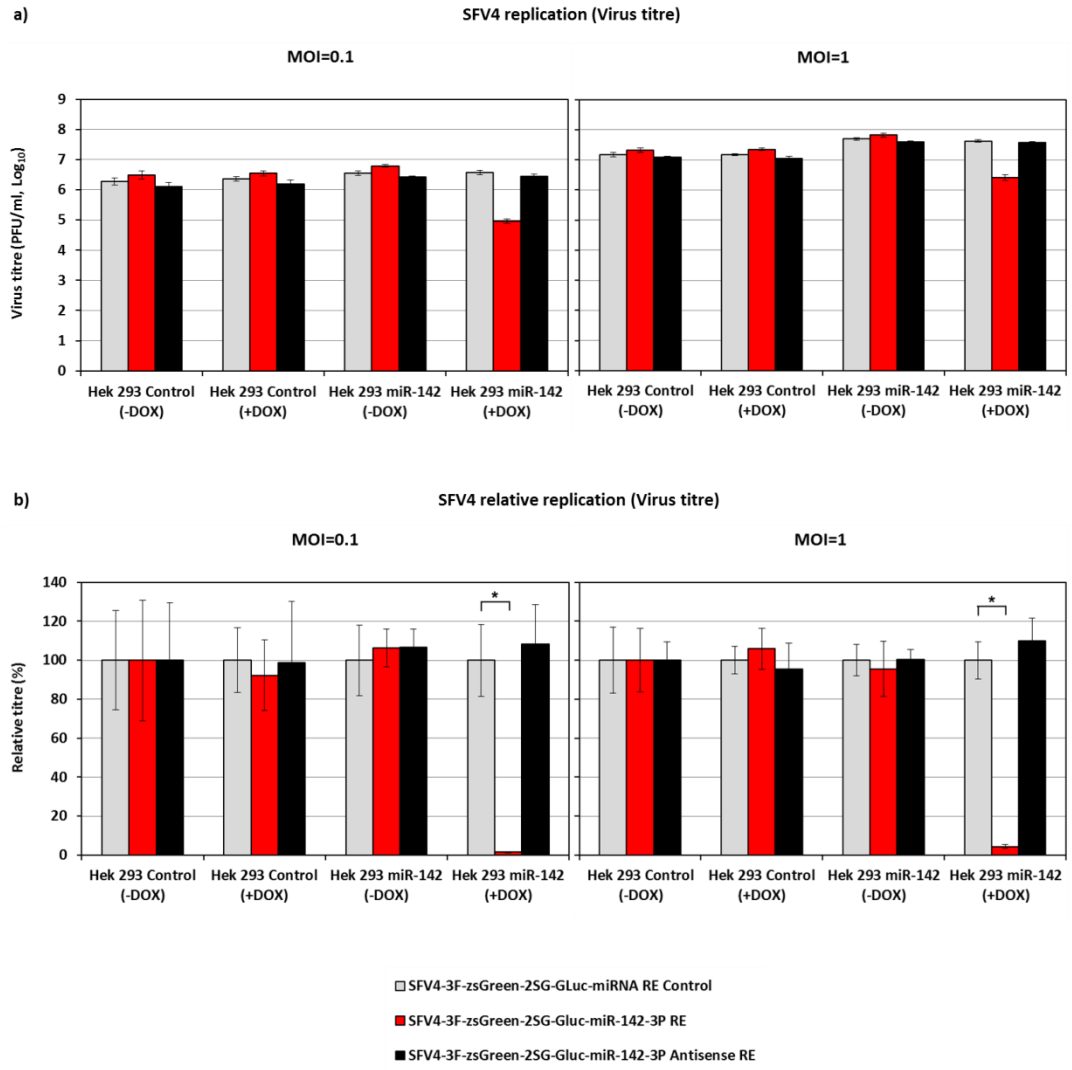

Figure 4.19. Virus production in SFV4-3F-zsGreen-2SG-GLuc-miRNA RE-infected Hek 293 miR-142 and Hek 293 Control cells. Hek 293 miR-142 (+DOX) and Hek 293 Control (+DOX) cells were induced with DOX at 100 ng/ml final concentration for 24 hours prior to infection. Cells were infected at MOI of 0.1 and 1. (a) Raw data expressed as mean +/- SD. (b) Results normalised to the infection in Hek 293 Control (-DOX) cells and to SFV4-3F-zsGreen-2SG-GLuc-miRNA RE Control virus. Data expressed as relative mean +/- relative SD; Mann-Whitney test, single-tailed; * $p<0.05$.

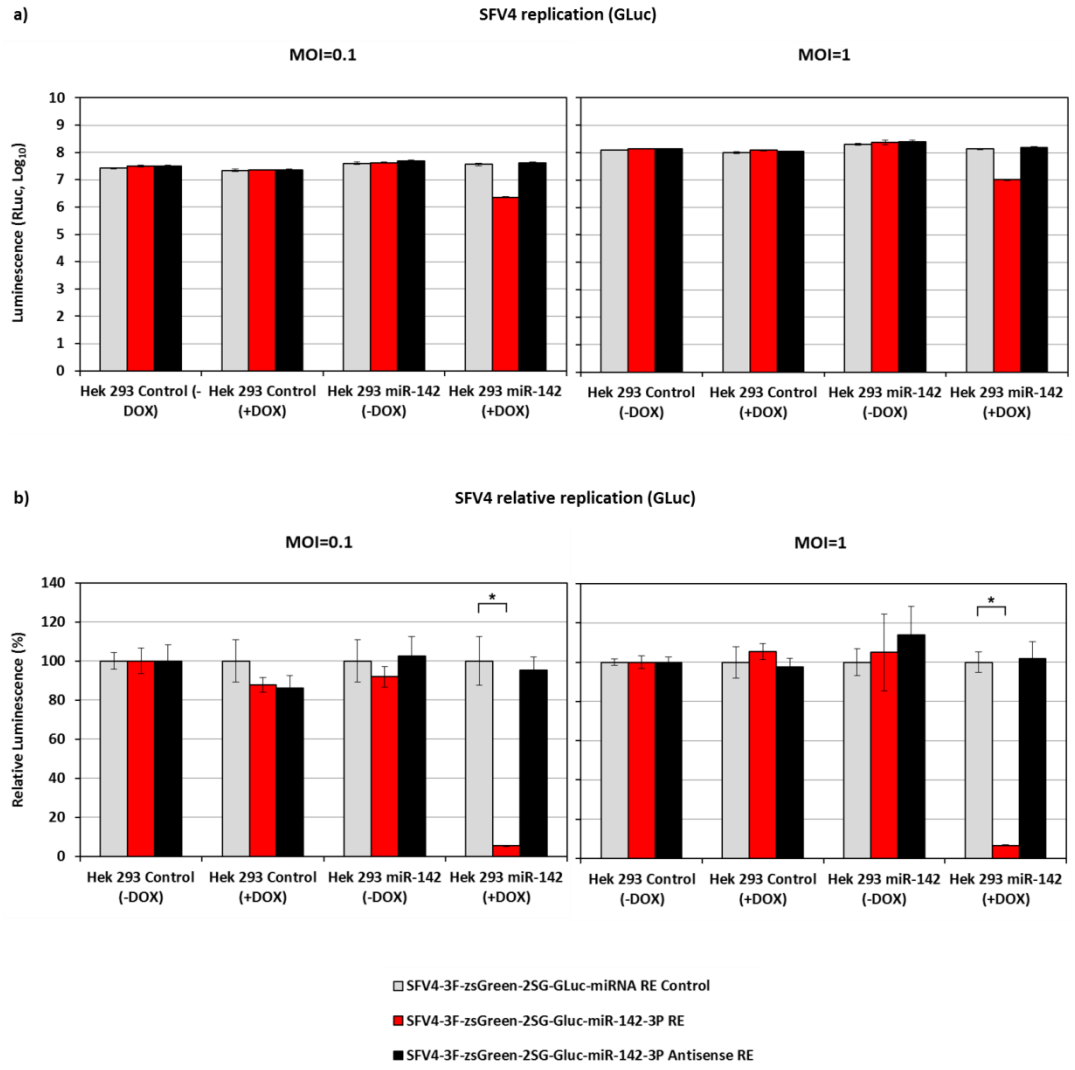

Figure 4.20. GLuc production in SFV4-3F-zsGreen-2SG-GLuc-miRNA RE-infected Hek 293 miR-142 and Hek 293 Control cells. Hek 293 miR-142 (+DOX) and Hek 293 Control (+DOX) cells were induced with DOX at 100 ng/ml final concentration for 24 hours prior to infection. Cells were infected at MOI of 0.1 and 1. (a) Raw data expressed as mean +/- SD. (b) Results normalised to the infection in Hek 293 Control (-DOX) cells and to SFV4-3F-zsGreen-2SG-GLuc-miRNA RE Control virus. Data expressed as relative mean +/- relative SD; Mann-Whitney test, single-tailed; * $p<0.05$.

The induction of Hek 293 miR-142-3P cells with DOX did not affect the replication of SFV4-3F-zsGreen-2SG-GLuc-miRNA RE Control as demonstrated by both virus production (Figure 4.21a) and by GLuc expression (Figure 4.21c). This confirmed that the pre-treatment of cells with DOX in itself did not affect SFV replication. SFV4-3F-zsGreen-2SG-GLuc-miR-142-3P RE was attenuated when Hek 293 miR-142 cells were pre-treated with DOX at concentration of above 0.1 ng/ml. The maximum effect was achieved with DOX at concentrations of above 10 ng/ml. This was demonstrated by both virus production (Figure 4.21a) and GLuc expression (Figure 4.21c). The extent of virus attenuation observed in this experiment was comparable to that shown in Figure 4.19 (virus production) and Figure 4.20 (GLuc expression). A more detailed analysis revealed that the majority of virus attenuation took place when Hek 293 miR-142 cells were induced with DOX at a narrow range of concentrations between 0.4 and 1.2 ng/ml. Again, this was confirmed by virus production (Figure 4.21b) and by GLuc expression (Figure 4.21d).

At the time of writing this thesis the relative levels of miR-142-3P expression in Hek 293 miR-142-3P cells generated during this experiment were not yet tested. Hence, it was impossible to investigate the exact correlation between levels of miR-142-3P and SFV4-3F-zsGreen-2SG-GLuc-miR-142-3P RE replication. However, the sharp decrease in the virus replication observed when Hek 293 miR-142 cells were pre-treated with DOX at the concentration range of 0.4-1.2 ng/ml may further indicate that a threshold level of a miRNA expression is required to efficiently degrade viral RNA before replication complexes can be established. It is also possible that the CMV/$TetO_2$ driving the transcription of miR-142-3P pri-miRNA becomes active at this very specific concentration of DOX.

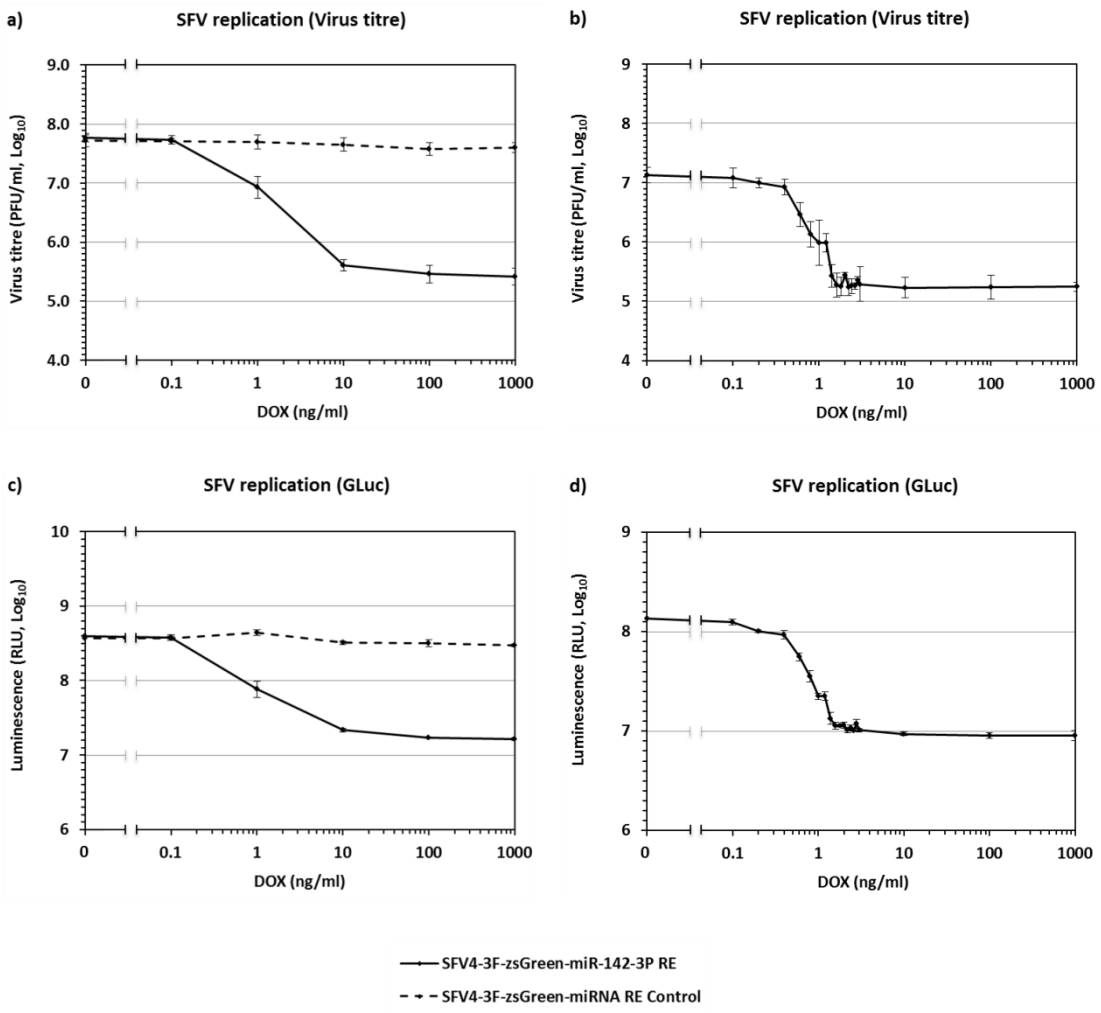

Figure 4.21. Attenuation of SFV4-3F-zsGreen-2SG-GLuc-miR-142-3P RE and SFV4-3F-zsGreen-2SG-GLuc-miRNA RE Control in HEK 293 miR-142 cells induced with DOX at concentrations ranging from 0 to 1000 ng/ml. a) Comparison of both viruses (virus production). b) Comparison of both viruses (GLuc expression). c) Detailed analysis of SFV4-3F-zsGreen-2SG-GLuc-miR-142-3P RE attenuation (virus production). d) Detailed analysis of SFV4-3F-zsGreen-2SG-GLuc-miR-142-3P RE attenuation (GLuc expression). Data expressed as mean +/- SD.

4.13 Designing and generating pcDNA^{TM}3.1+ plasmids that express miR-142-3P in non-haematopoietic cell lines

When Hek 293 miR-142 and Hek 293 Control cells were designed it was uncertain whether they would work. Hence, a panel of pcDNA^{TM}3.1+ expression plasmids was generated in parallel to allow transient expression of miR-142-3P in non-haematopoietic cells. The multiple cloning sites in pcDNA^{TM}3.1+ vector and pcDNATM5/FRT/TO vector were identical. All constructs used to generate Hek 293 miR-142 cells (miR-142 'Core', 'Short', 'Long-3' and 'Long-5') were cloned into pcDNA^{TM}3.1+ as described in 4.11. The sequencing results for the chosen clones are provided in Supplementary Data, Appendix 11. The resulting plasmids were called pcDNA3.1+ miR-142 'Core', pcDNA3.1+ miR-142 'Short', pcDNA3.1+ miR-142 'Long-3' and pcDNA3.1+ miR-142 'Long-5', respectively. Their sequences are provided in Supplementary Data, Appendix 5.

In addition, pcDNA3.1+ miR-142 'Core' and pcDNA3.1+ miR-142 'Short' were further modified to co-express a marker gene mCherry. The resulting constructs were called pcDNA3.1+ miR-142 'Core' mCherry and pcDNA3.1+ miR-142 'Short' mCherry. Plasmid sequences are provided in Supplementary Data, Appendix 5. The cloning details are provided in Annex 20. The expression of mCherry in plasmid-transfected cells was confirmed microscopically (Figure 4.22). The expression of miR-142-3P in plasmid-transfected cells was not measure.

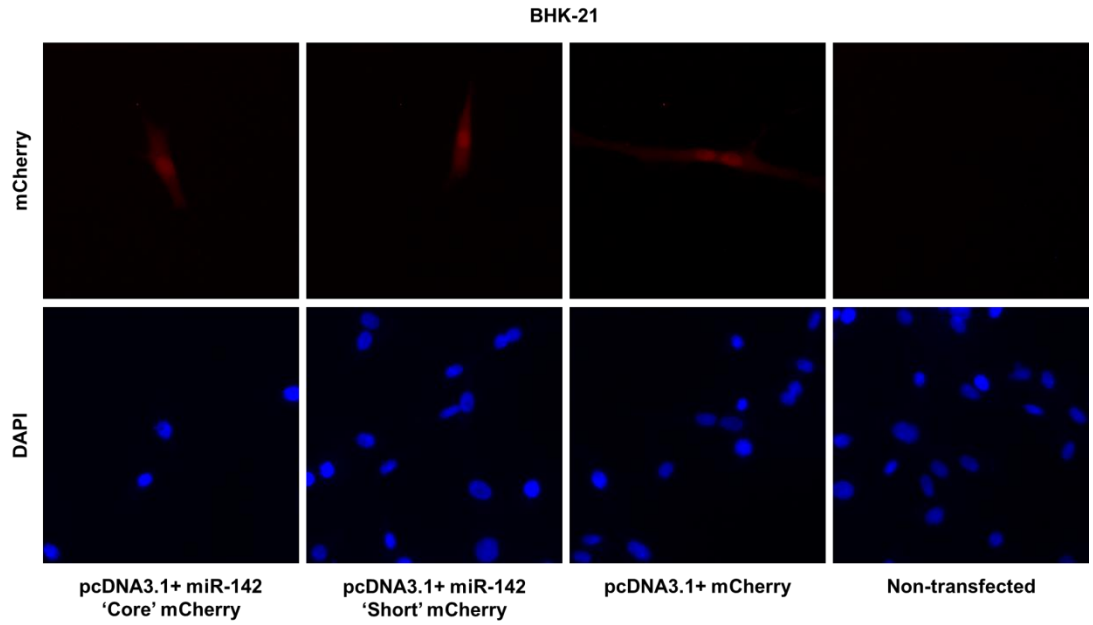

Figure 4.22. Expression of mCherry in BHK-21 cells transfected with the panel of cloned pcDNA3.1+ plasmids encoding mCherry. Cells were observed 24 hours post-transfection using Zeiss Axioskop 2 upright microscope. Cell nuclei were stained with DAPI.

4.14 Will SFV encoding miR-142-3P RE be attenuated in cells transfected with pcDNA^{TM}3.1+ plasmids expressing miR-142-3P, but not in cells transfected with control plasmids?

The following experiment was completed only once. Hek 293T cells were harvested, counted, and seeded into 96-well plates at 2.5 x 10^4 cells per well as described in 2.5.1. Complete medium with no P/S was used. After 24 hours of incubation, cells were transfected with all plasmids generated in 4.13 using FuGENE® 6 as described in 2.10.1. Unmodified pcDNA^{TM}3.1+ was transfected as a control. Twenty-four hours post-transfection, cells were inspected microscopically for the expression of mCherry, and then infected with SFV4-3F-zsGreen-2SG-GLuc-miR-142-3P and SFV4-3F-zsGreen-2SG-GLuc-miRNA RE Control at MOI of 0.1. Twenty hours post-infection the supernatant from virus infected cells was collected. GLuc levels were measured as described in 2.9.3.

As shown in Figure 4.23, both viruses replicated to the same levels in Hek 293T cells transfected with control plasmids (pcDNA^{TM}3.1+ and pcDNA3.1+ mCherry). In all Hek 293T cells transfected with pcDNA3.1+ plasmid modified to express miR-142-3P, the measured replication of SFV4-3F-zsGreen-2SG-GLuc-miR-142-3P RE was significantly reduced with respect to the control virus. Overall, the above results were consistent with previous observations on IC-21 and Hek 293 miR-142 cells.

In cells transfected with pcDNA3.1+ miR-142-3P 'Core' plasmid, the replication of SFV4-3F-zsGreen-2SG-GLuc-miR-142-3P RE was reduced by 90%. The attenuation of this virus was less prominent in cells transfected with pcDNA3.1+ miR-142-3P 'Short', pcDNA3.1+ miR-142-3P 'Long-3' and pcDNA3.1+ miR-142-3P 'Long-5' plasmids (83%, 75% and 76%, respectively). Notably, there was a clear relationship between the extent of virus attenuation and the length of the miR-142-3P construct expressed by the plasmid. In brief, the shorter the construct, the more attenuated virus replication was. Furthermore, cells transfected with plasmids expressing miR-142-3P were less permissive to virus replication than cells transfected with plasmids co-expressing the same miR-142-3P construct and mCherry. The difference in measured virus replication was 2-fold for the pair of miR-142-3P 'Core' plasmids, and 2.5-fold for the pair of miR-142-3P 'Short' plasmids.

The attenuation of SFV4-3F-zsGreen-2SG-GLuc-miR-142-3P RE in cells transfected with pcDNA3.1+ miR-142-3P 'Core' plasmid was not as high as that observed on Hek 293 miR-142 cells induced with DOX (Figure 4.20). However, the efficacy of plasmid transfection was only 75-80% (as indicated by expression of mCherry in pcDNA3.1+ mCherry-transfected cells). The observed variation in the capacity of different plasmids to attenuate SFV4-3F-zsGreen-2SG-GLuc-miR-142-3P RE replication may have resulted from notably different plasmid sizes (see Annex 12).

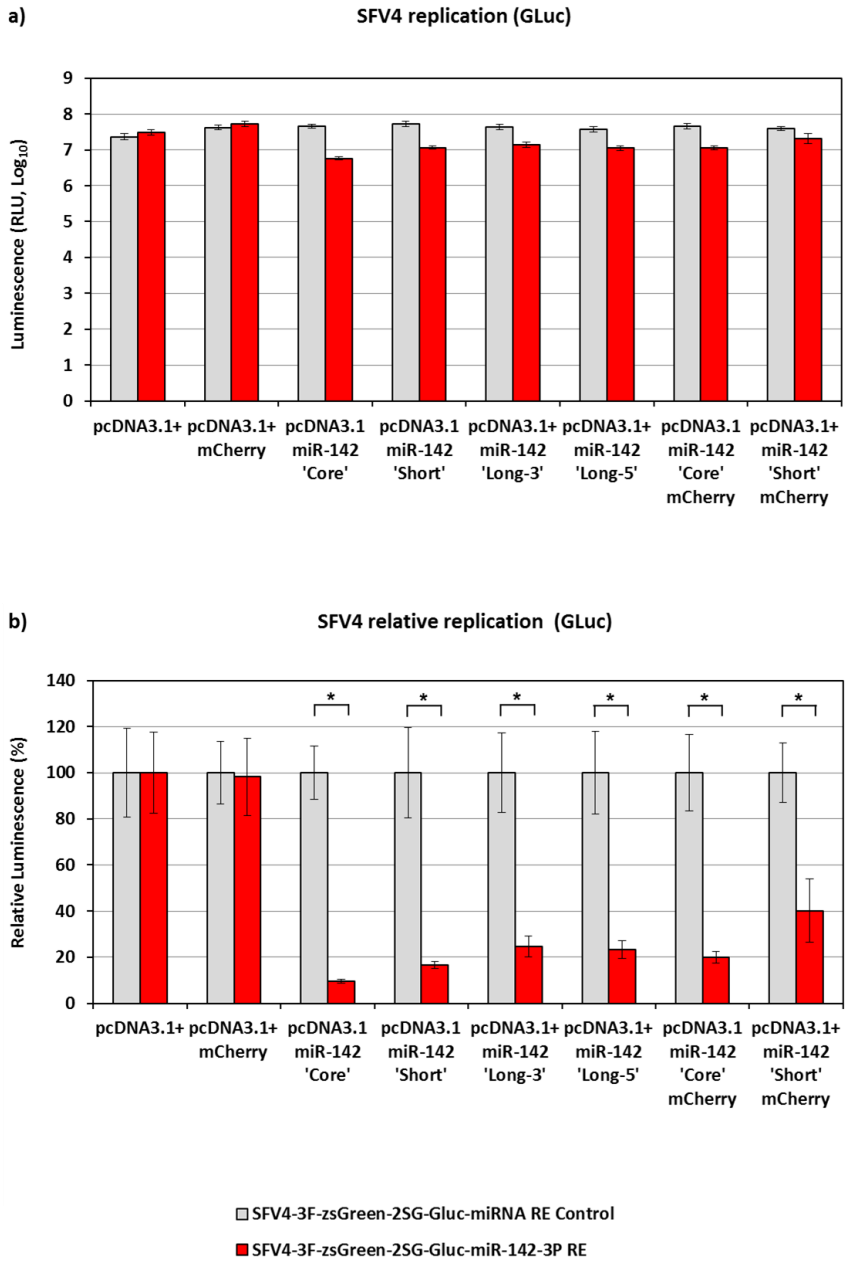

Figure 4.23. Replication of SFV4-3F-zsGreen-2SG-GLuc in Hek 293T cells transfected with pcDNA3.1+ plasmids expressing miR-142-3P. Transfected cells were infected at MOI of 0.1. (a) Raw data expressed as mean +/- SD. (b) Results normalised to the infection in cells transfected with pcDNA^{TM}3.1+ and to SFV4-3F-zsGreen-2SG-GLuc-miRNA RE Control virus. Data expressed as relative mean +/- relative SD; Mann-Whitney test, single-tailed; * $p<0.05$.

4.15 Designing a functional bioassay to test the stability of miR-142-3P RE in SFV genome using Hek 293 cells modified to express miR-142-3P

A bioassay in the form of a modified plaque assay was designed to assess the stability of miR-142-3P RE inserted into the genome of SFV and CHIKV. In principle, a virus encoding miR-142-3P RE was titrated on Hek 293 miR-142 cells (+DOX) and on Hek 293 Control cells (+DOX). The two titres were compared and the fraction of virus unable to form plaques in presence of miR-142-3P was calculated. This assay did not investigate the stability of a miR-142-3P RE at the molecular level. The complete protocol is described in 2.3.6.

Hek 293 miR-142 and Hek 293 Control cells were not strongly adherent. However, cells seeded into 6-well plates were more robust than cells seeded into 24- or 12-well plates. Hence, the assay was optimised for 6-well plates. To investigate the optimal number of cells needed to seed plates, Hek 293 miR-142 and Hek 293 Control cells were plated at 2 x 10^6, 2.5 x 10^6 and 3 x 10^6 cells/well with 100 ng/ml DOX and incubated for 24 hours. Next, cells were fixed with 10% v/v neutral buffered formalin, cell nuclei were stained with DAPI and monolayers were inspected microscopically. Cells seeded at 2.5 x 10^6 cells/well showed the best balance between an under confluent monolayer and formation of cell clumps (Figure 4.24).

To optimise the incubation time post-infection, cells were seeded at 2.5 x 10^6 cells/well with 100 ng/ml of DOX and incubated for 24 hours. Next, the cell supernatant was removed and 3 ml of semi-solid overlay (see 2.3.6) was added. After 24-, 48- and 72-hours incubation cells were fixed with 10% v/v neutral buffered formalin, cell nuclei were stained with DAPI and monolayers were inspected microscopically. The optimal incubation time was identified as 48 hours as longer incubation led to a notable deterioration of Hek 293 miR-142 and Hek 293 Control cells monolayers (Figure 4.25).

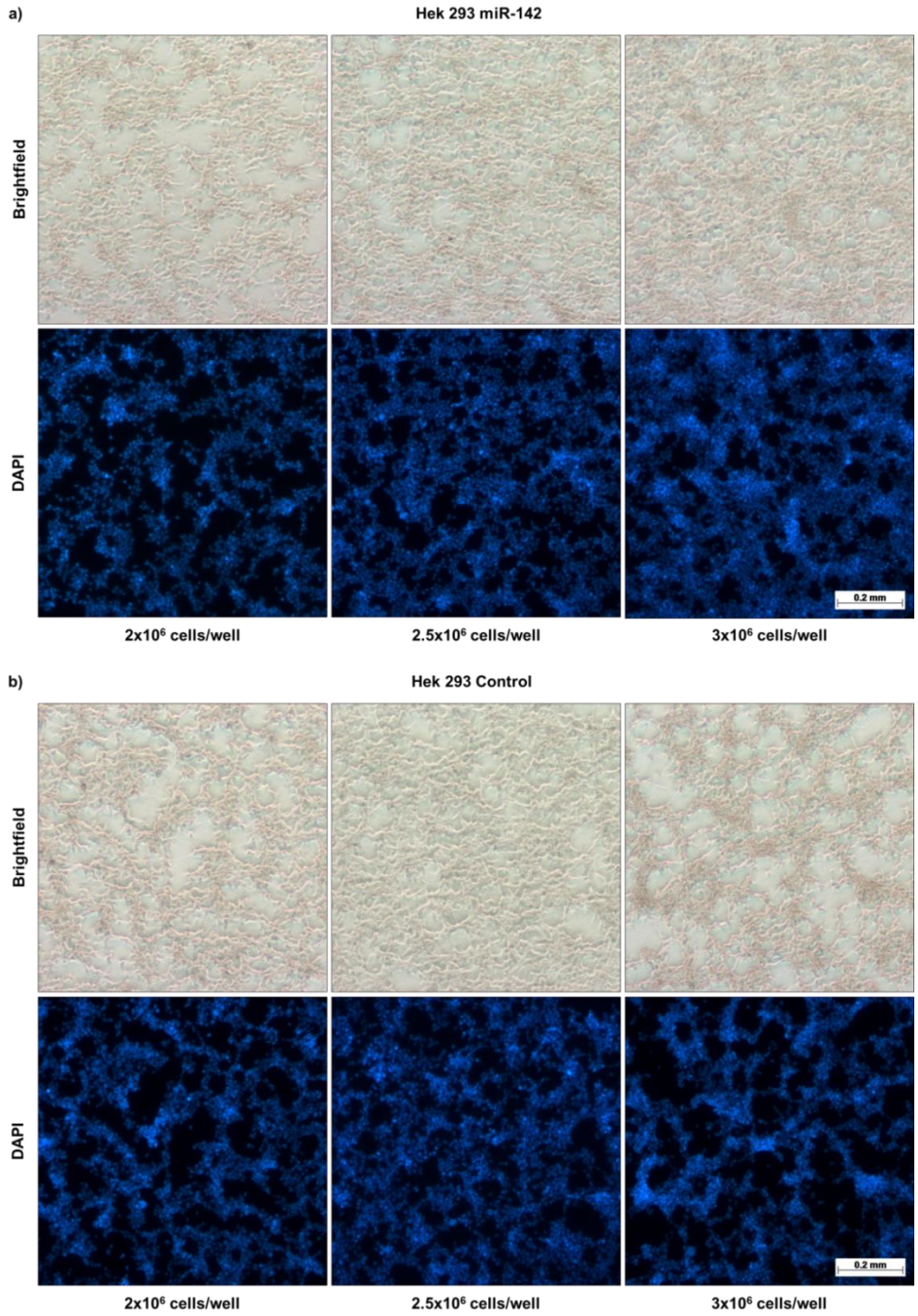

Figure 4.24. Hek 293 miR-142 stability bioassay - optimising the seeding density. Cells were seeded at 2 x 10^6, 2.5 x 10^6 and 3 x 10^6 cells/well with 100 ng/ml doxycycline. Cells were inspected microscopically 24 hours later. Cell nuclei were stained with DAPI.

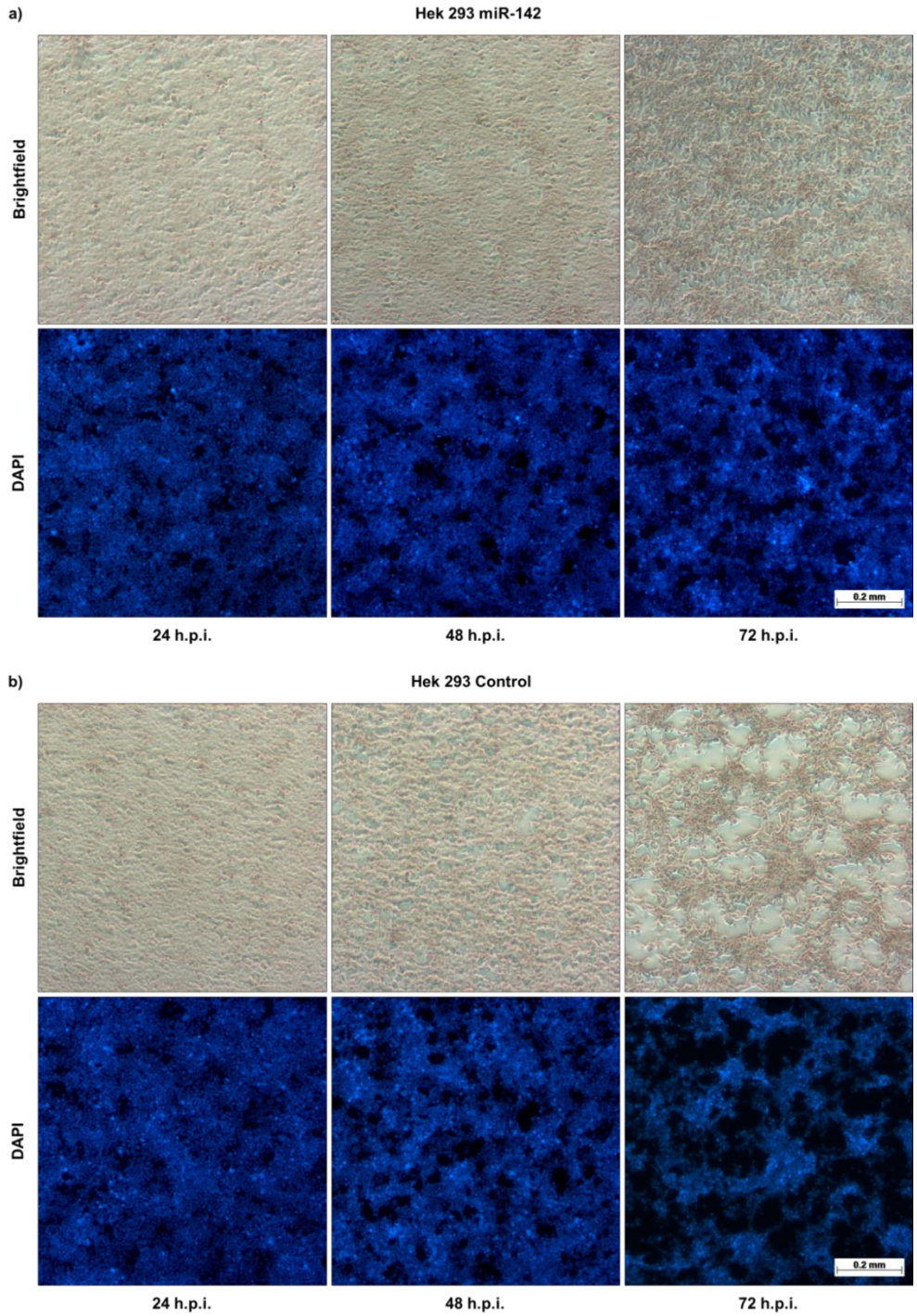

Figure 4.25. Hek 293 miR-142 stability bioassay - optimising the incubation time post-infection. Cells were seeded at 2.5 x 10^6 cells/well with 100 ng/ml of doxycycline. After 24 hours, the cell supernatant was removed and 3 ml of semi-solid overlay was added. Cells were inspected microscopically after 24-, 48- and 72-hours of incubation. Cell nuclei were stained with DAPI.

To investigate the formation of SFV plaques, Hek 293 miR-142 and Hek 293 Control cells were seeded at 2.5 x 10^6 cells/well with 100 ng/ml of DOX and incubated for 24 hours. Next, cells were infected with 650 µl of SFV4-3F-zsGreen per well and incubated at room temperature for 90 minutes. The volume of virus inoculum was sufficient to completely cover cell monolayers and therefore minimise the need to rock plates. Next, 3 ml of a semi-solid overlay with 100 ng/ml of DOX was added. After 24, 48 and 72 hours cells were fixed with 10% v/v neutral buffered formalin. Cell nuclei were stained with DAPI and monolayers were inspected microscopically for the expression of virus-encoded zsGreen or stained with 0.1% toluidine blue. The virus did not form large-enough plaques to allow counting by eye (Figure 4.26). Microscopical inspection of cell monolayers revealed that SFV4-3F-zsGreen formed plaques of comparable sizes on both Hek 293 miR-142 and Hek 293 Control cells (Figures 4.27 and 4.28). All plaques were very small. Twenty four hours post-infection the average size of a plaque was only 0.1 mm in diameter. This increased to only 0.2 and 0.25 mm in diameter 48 and 72 hours post-infection, respectively.

To investigate formation of plaques by a virus encoding miR-142-3P RE in the presence of miR-142-3P, the protocol described above was followed. However, Hek 293 miR-142 and Hek 293 Control cells were infected with both SFV4-3F-zsGreen and SFV4-3F-zsGreen-miR-142-3P RE. Plates were incubated 48 hours post-infection. The results are summarised in Figures 4.29 and 4.30. SFV4-3F-zsGreen and SFV4-3F-zsGreen-miR-142-3P RE produced plaques of comparable sizes on Hek 293 Control cells (0.20 mm and 0.17 mm in diameter, respectively). Plaques formed by SFV4-3F-zsGreen on Hek 293 miR-142 cells were similar in size to those formed on Hek 293 Control cells (0.19 mm in diameter). Not surprisingly, SFV4-3F-zsGreen-miR-142-3P RE did not plaque readily on Hek 293 miR-142-3P cells. Plaques were only observed at low virus dilutions and they were smaller than that witnessed on Hek 293 Control cells. In addition, two distinctive plaque phenotypes were present. Small plaques were on average 0.4 mm in diameter. However, any foci of infection larger than 8 cells were counted as a plaque. Larger plaques were on average 0.1 mm in diameter. Virus capable on forming plaques on Hek 293 miR-142 cells induced with DOX must have lost or significantly mutated the miR-142-3P RE.

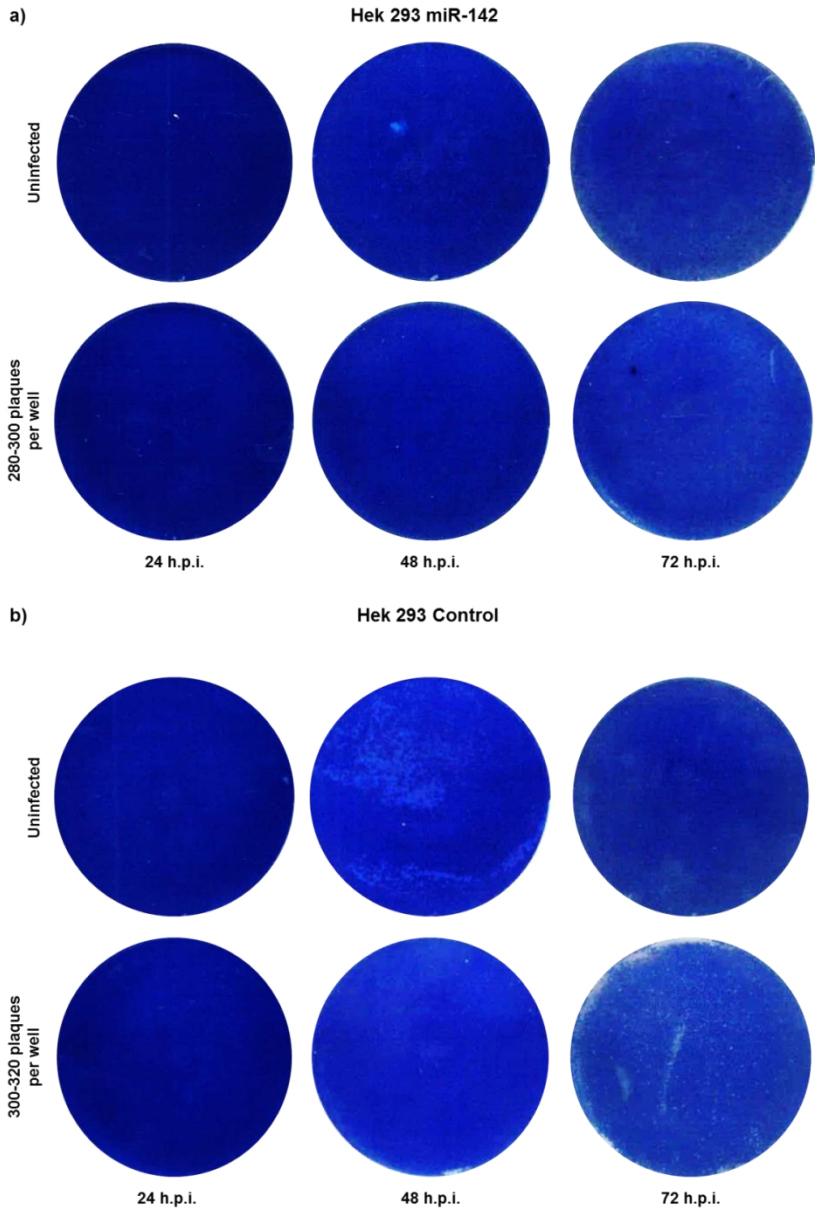

Figure 4.26. Hek 293 miR-142 stability bioassay – formation of virus plaques observed visually. Cells were seeded at 2.5 x 10^6 cells/well with 100 ng/ml of doxycycline. After 24 hours, cells were infected with SFV4-3F-zsGreen and a semi-solid overlay was added. Cells were fixed with 10% v/v neutral buffered formalin and stained with 0.1% toluidine blue 24, 48 and 72 hours post-infection. Uninfected cell monolayers and cell monolayers containing 280-320 plaques per well (confirmed microscopically) were compared.

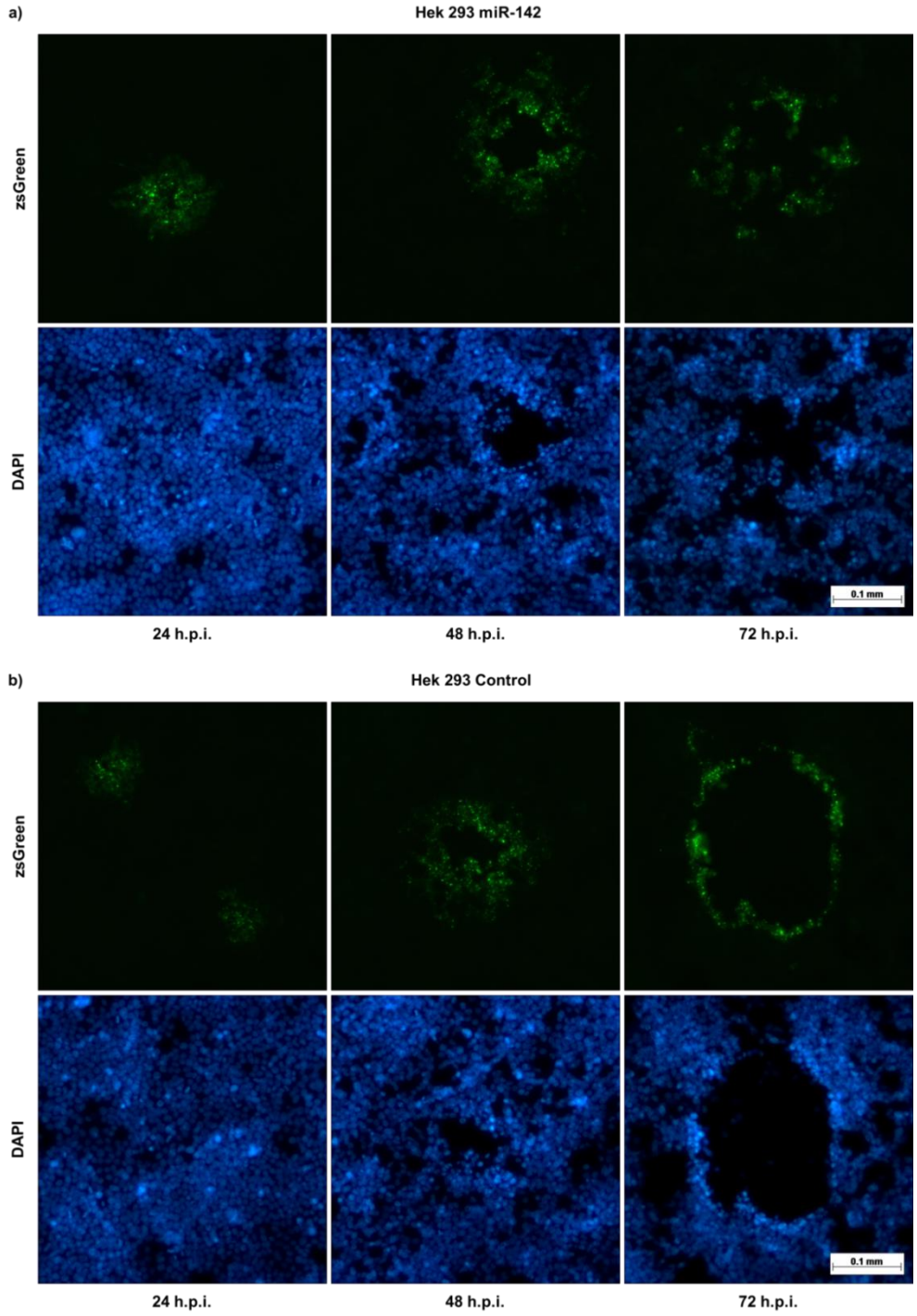

Figure 4.27. Hek 293 miR-142 stability bioassay - formation of virus plaques observed microscopically. Cells were seeded at 2.5 x 10^6 cells/well with 100 ng/ml of doxycycline. After 24 hours, cells were infected with SFV4-3F-zsGreen and a semi-solid overlay was added. The formation of plaques was observed microscopically after 24, 48 and 72 hours of incubation. Cell nuclei were stained with DAPI.

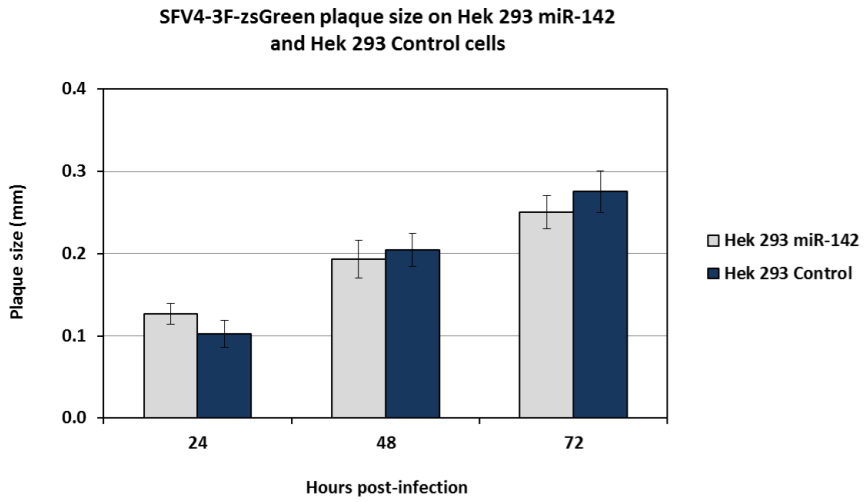

Figure 4.28. Hek 293 miR-142 stability bioassay – plaque size. Cells were seeded at 2.5 x 10^6 cells/well with 100 ng/ml of doxycycline. After 24 hours, cells were infected with SFV4-3F-zsGreen and a semi-solid overlay was added. The formation of plaques was observed microscopically after 24, 48 and 72 hours of incubation. The size of SFV4-3F-zsGreen plaques was measured using Zeiss AxioVision 4.8 digital image processing software. Data expressed as mean of random 20 individual plaques +/- SD.

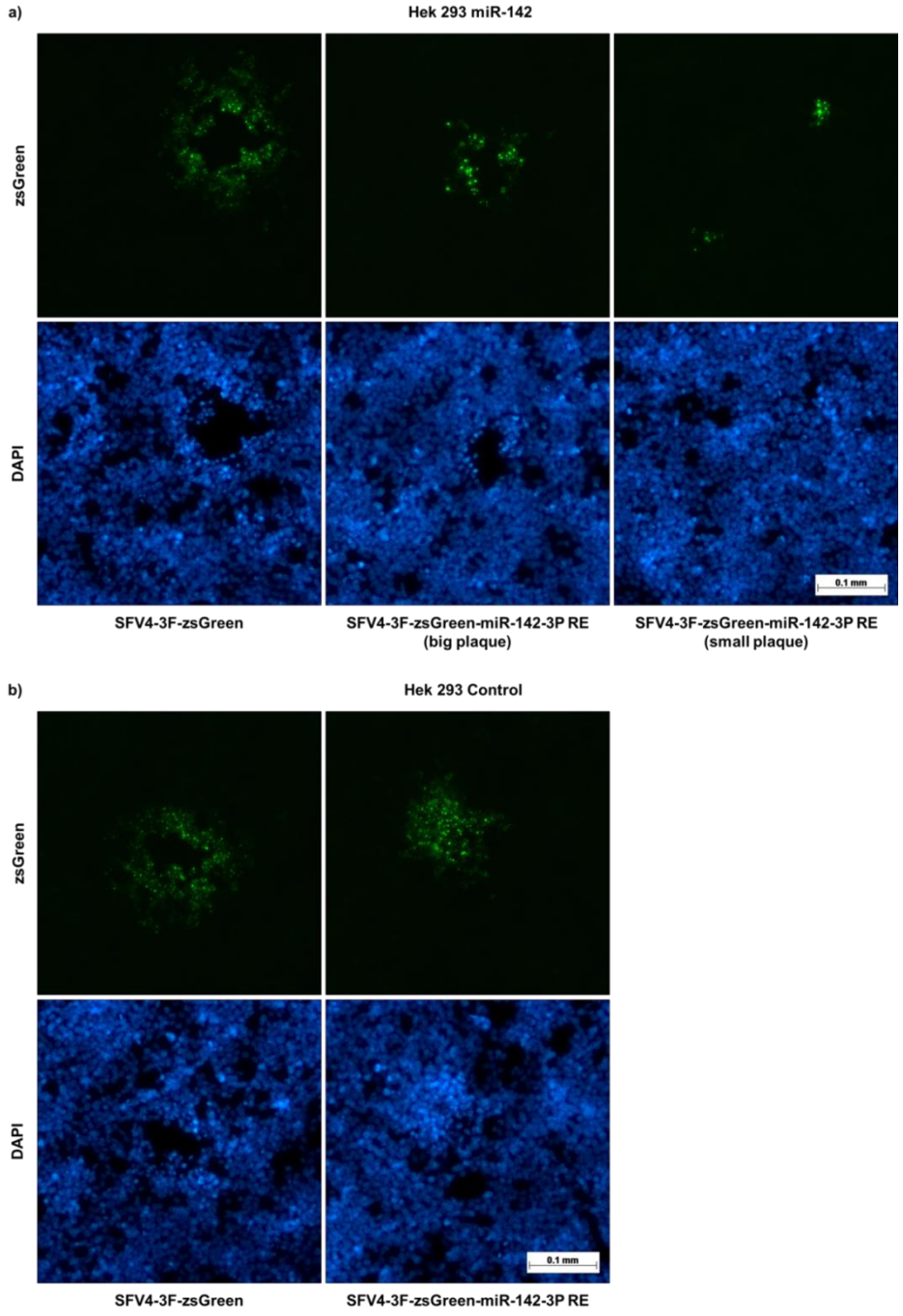

Figure 4.29. Hek 293 miR-142 stability bioassay – formation of plaques by a virus encoding miR-142-3P RE. Cells were seeded at 2.5 x 10^6 cells/well with 100 ng/ml of doxycycline. After 24 hours, cells were infected with SFV4-3F-zsGreen and SFV4-3F-zsGreen-miR-142-3P RE, and a semi-solid overlay was added. The formation of plaques was observed microscopically 48 hours post-infection. Cell nuclei were stained with DAPI.

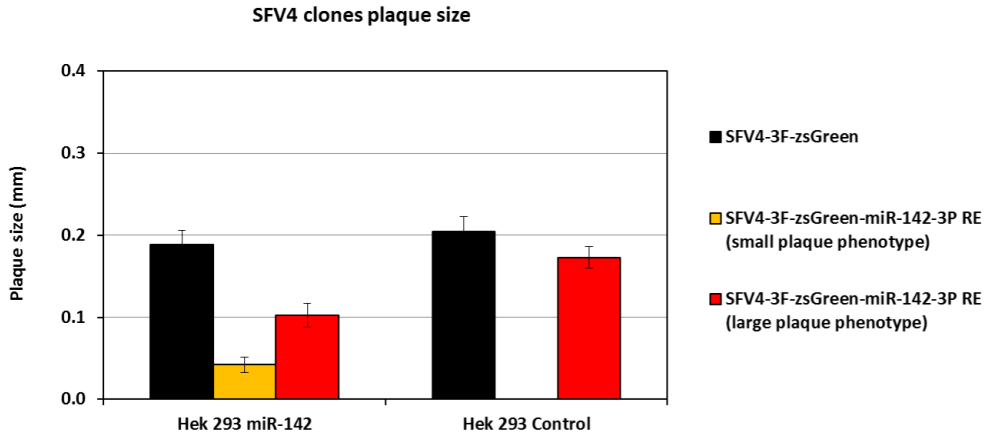

Figure 4.30. Hek 293 miR-142 stability bioassay – formation of plaques by a virus encoding miR-142-3P RE. Cells were seeded at 2.5 x 10^6 cells/well with 100 ng/ml of doxycycline. After 24 hours, cells were infected with SFV4-3F-zsGreen and a semi-solid overlay was added. The formation of plaques was observed microscopically after 24, 48 and 72 hours of incubation. The size of SFV4-3F-zsGreen plaques was measured using Zeiss AxioVision 4.8 digital image processing software. Data expressed as mean of random 20 individual plaques +/- SD.

4.16 Will miR-142-3P RE be stable in the genome of SFV that has been passaged *in vitro* on BHK-21 cells?

The genetic stability of miR-142-3P RE incorporated into the genome of SFV4-3F-zsGreen-miR-142-3P RE was investigated *in vitro*. The virus was passaged 5 times on BHK-21 cells at two distinct MOIs. The virus was passaged in absence of the selective pressure from miR-142-3P. The detailed protocol is described in 2.3.4.

For the 'high' MOI passage, BHK-21 cells were first infected with SFV4-3F-zsGreen-miR-142-3P RE at MOI of 0.1. Next, the virus-infected BHK-21 cells were incubated for 48 hours. Then, the cell culture supernatant containing BHK-21-derived progeny of SFV4-3F-zsGreen-miR-142-3P RE was collected (Passage 1 stock). Next, 1 µl of the collected supernatant was used to infect fresh BHK-21. The remaining supernatant was frozen at -80 ºC. As previously, the virus-infected

BHK-21 cells were incubated for 48 hours. Subsequently, the BHK-21 cell culture supernatant containing new BHK-21-derived virus progeny was collected (Passage 2 stock). This procedure was repeated for each consecutive virus passage.

For the 'low' MOI passage, the procedure described above was followed. However, the initial infection of BHK-21 cells was done at MOI of 0.001. All subsequent infections of BHK-21 cells were completed using 1 µl of the supernatant from the previous passage that had been diluted 1 in 100 in PBSA. Retrospective titration on BHK-21 cells of all collected samples revealed that the 'low' MOI was equal to 0.01-0.05 while the 'high' MOI was equal to 1-5.

The genetic stability of miR-142-3P RE in the passaged SFV4-3F-zsGreen-miR-142-3P RE was investigated using the bioassay developed in 4.15. The detailed protocol is available in 2.3.6. Each passage stock of SFV4-3F-zsGreen-miR-142-3P RE was titrated on both Hek 293 miR-142 cells (+DOX) and Hek 293 Control cells (+DOX). In principle, all viable SFV4-3F-zsGreen-miR-142-3P RE was able to form plaques on Hek 293 Control cells. However, only virus that had lost or significantly mutated the miR-142-3P RE was capable of forming plaques on Hek 293 miR-142 cells induced with DOX.

To calculate the fraction of virus unable to form plaques in presence of miR-142-3P, the virus titre obtained on Hek 293 miR-142 cells was compared to the virus titre obtained on the Hek 293 Control cells for each passage stock of the virus. The results were expressed as a proportion of the total virus population present in the sample that was unable to form plaques in presence of miR-142-3P. Hence, a virus that was completely unable to plaque on Hek 293 miR-142 cells induced with DOX would have a stability of 100% while a virus that was not at all attenuated on Hek 293 miR-142 cells induced with DOX would have a stability of 0%. The results were normalised to SFV4-3F-zsGreen to account for any differences in the infectivity of Hek 293 miR-142 and Hek 293 Control cells that may have been present at the time of the assay.

Remarkably, 3.09% of infectious virus particles present in SFV4-3F-zsGreen-miR-142-3P RE unpassaged stock were able to form plaques in the presence of miR-142-3P (Figure 4.31). This proportion was much higher than anticipated. With each consecutive passage, the stability of the virus was gradually and markedly reduced. After 5 passages only 80.15-83.06% of the virus particles were still inhibited by the expression of miR-142-3P. Altogether, the above data suggested that the SFV4-3F-zsGreen-miR-142-3P RE was not a genetically stable construct.

Surprisingly, the stability of SFV4-3F-zsGreen-miR-142-3P RE was not affected by the MOI at which the virus was passaged. In a high MOI infection the majority of cells in a monolayer are infected at once and therefore a single cycle of infection takes place. In a low MOI infection, multiple cycles of virus replication are required to infect all cells. Hence, a virus passaged at a low MOI should effectively undergo more cycles of replication than a virus passaged at high MOI, increasing the likelihood of mutants arising. BHK-21 cells are very permissive to infection with SFV. It is possible that the difference in the inoculum dose of SFV was not substantial enough to differentiate the two groups.

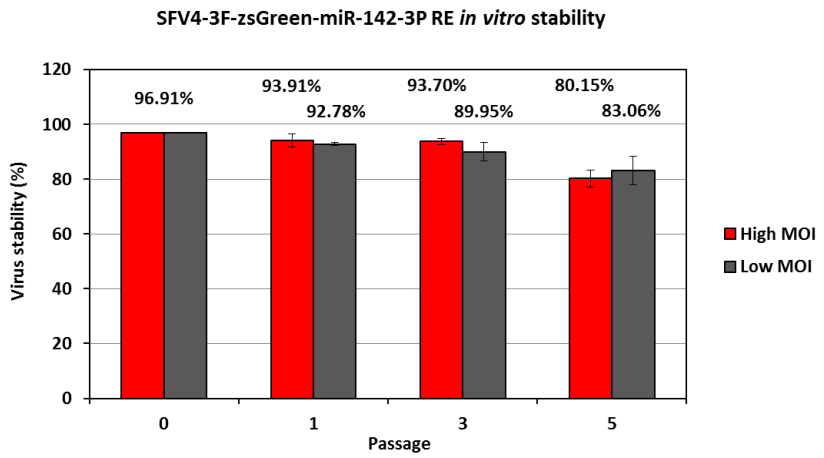

Figure 4.31. SFV4-3F-zsGreen-miR-142-3P RE stability *in vitro*. The virus was passaged on BHK-21 cells at high MOI (estimated at 1-5) or at low MOI (estimated at 0.01-0.05). Virus stability (%) was defined as the proportion of the total virus population that was unable to form plaques in presence of miR-142-3P. Data expressed as relative mean +/- relative SD.

4.17 Will SFV encoding miR-142-3P RE be attenuated *in vivo* in IFN-α/ß receptor knockout mice?

As mentioned earlier, Fragkoudis et al. (2007) observed a population of virus-positive cells in spleen of SFV4-infected IFN-α/ß receptor knockout mice of A129/SvEv background (IFNAR mice), in marginal zones between the red pulp and white pulp. These areas are known to be rich in macrophages and dendritic cells. Hence, the pathogenesis of SFV4-3F-zsGreen-miR-142-3P RE and SFV4-3F-zsGreen-miRNA RE Control viruses was investigated in IFNAR mice in a pilot proof-of-concept experiment, as described below.

In brief, 7 IFNAR mice were divided into two groups of 3 animals each, and 1 group of 1 animal. The two groups of 3 animals were inoculated with either SFV4-3F-zsGreen-miR-142-3P RE (group B) or with SFV4-3F-zsGreen-miRNA RE Control (group C) at 5 x 10^3 PFU/animal. The protocol outlined in 2.21.2 was followed. The one animal in the last group was inoculated with PBSA only (group A).

Animals were euthanized 28 hours post-infection. Peritoneal macrophages, brain and spleen were collected from all animals as described in 2.21.3. One ml of peritoneal wash was collected as described in 2.21.6 and tested for virus load following 2.3.5. Virus titre in the peritoneal cavity was calculated based on the assumption that 50 µl of peritoneal fluid was initially present in each animal. The stability of miR-142-3P RE in SFV4-3F-zsGreen-miR-142-3P RE recovered from peritoneal wash was assessed as described in 2.3.6. Brain and spleen samples were processed and sectioned using a cryomicrotome as described in 2.21.4. Spleen sections were immunostained for murine macrophage cell surface receptors CD169 and Macrophage receptor with collagenous structure (MARCO) as described in 2.21.5. Sections were imaged using confocal microscopy as described in 2.7.2. Peritoneal F4/80-positive cells were analysed by flow cytometry as described in 2.21.6.

All virus-infected animals demonstrated a high viral load in the peritoneal cavity (Figure 4.32a). The titre ranged from $10^{7.88}$ to $10^{10.38}$ PFU/ml in animals infected with SFV4-3F-zsGreen-miRNA RE Control and from $10^{8.18}$ to $10^{9.68}$ PFU/ml in

animals infected with SFV4-3F-zsGreen-miR-142-3P RE. There was no overall difference between the two groups.

Virus isolated from all animals infected with SFV4-3F-zsGreen-miR-142-3P RE demonstrated reduced stability in comparison to the inoculum (Figures 4.31 and 4.32b). The stability observed in animals B1 and B2 (84.84% and 88.80%, respectively) was comparable to the stability of this virus observed after 5 passages on BHK-21 cells *in vitro* in absence of the selective pressure from miR-142-3P (Figure 4.31). On the other hand, only 65% of virus isolated from animal B3 was unable to form plaques in presence of miR-142-3P.

Stability of any RNA virus construct is dependent on many factors, including the size of an insert, the nature of an insert, the location of an insert within a virus genome, presence of a selective pressure, individual characteristics of infected cells, virus titre and physiological conditions. Most of these factors are relatively easy to control during an *in vitro* passage of a virus. Consequently, stability data from an *in vitro* passage of a virus are often very clear, with individual replicates behaving in a similar fashion as shown in Figure 4.31. Replication of a virus *in vivo* is a much more complex process. Many of the conditions listed above may vary from one infected animal to another. In addition, the availability of permissive cells is large, allowing many rounds of virus replication. As a result, stability of an RNA virus observed *in vivo* can be much more variable than that observed *in vitro*. It is difficult to dissect why the virus isolated from animal B3 was less stable than viruses isolated from the other two animals. Cells of the haematopoietic lineage are not the primary site of SFV replication in mice. Hence, a virus encoding miR-142-3P RE would not normally be exposed to a significant selective pressure from the presence of miR-142-3P. However, if by chance SFV4-3F-zsGreen-miR-142-3P RE was exposed to miR-142-3P early during infection, it could accelerate the loss of miR-142-3P RE from the virus genome, or its mutation. The results from animals B1 and B2 may suggest, however, that *in vitro* passaging of a virus can provide some indication of its *in vivo* stability. Unfortunately, the limited number of animals available in this study does not allow to draw any definite conclusions.

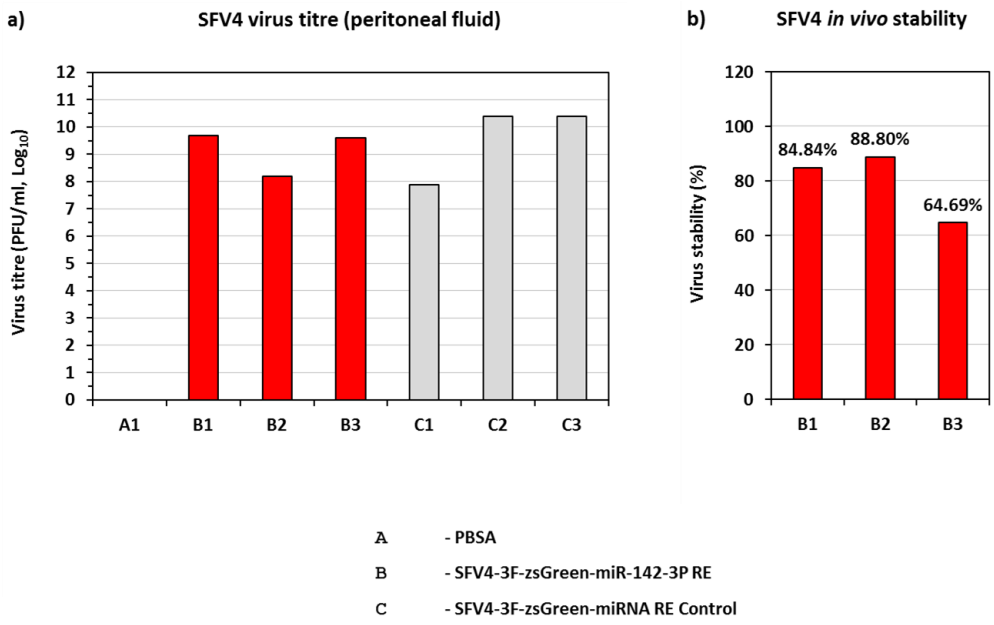

Figure 4.32. Analysis of virus isolated from the peritoneal cavity of virus-infected IFNAR mice. (a) Titre of virus present in the peritoneal cavity. (b) Stability of the virus present in the peritoneal cavity expressed as the proportion of the total virus population unable to form plaques in presence of miR-142-3P (in %).

The analysis of F4/80-positive peritoneal macrophages by flow cytometry showed no zsGreen-positive cells in either of the two cohorts of virus-infected animals. Data are not shown.

MARCO and CD169 are cell surface receptors expressed in murine splenic marginal zone macrophages (Ito et al. 1999, Prestwood et al. 2012). However, all immunostainings of spleen sections using anti-mouse CD169 and anti-mouse MARCO primary antibodies failed. Due to lack of available time the immunostaining protocol was not optimised. Without any troubleshooting data available, it was difficult to hypothesise why the immunostainings failed.

Nevertheless, when spleen sections were imaged by confocal microscopy a difference was observed between animals infected with SFV4-3F-zsGreen-miR-142-3P RE and the control virus (Figures 4.33 and 4.34). In spleen sections from animals infected with SFV4-3F-zsGreen-miRNA RE Control, there was a visible population

of zsGreen-positive cells in what was presumed to be marginal zones between the red pulp and the white pulp. The spleen sections were not stained with haematoxylin and eosin as this would interfere with the signal from zsGreen. However, the white pulp of spleen typically has a higher cell density than the surrounding areas of spleen. This could be observed as a localised increase in the concentration of DAPI-stained nuclei. Hence, marginal zones were identified as zones immediately surrounding areas of localised increase in the concentration of DAPI-stained nuclei. The number of zsGreen positive cells per 1000 of total cells present in this region of spleen varied between 18.80 and 34.45 in individual animals (Figure 4.34). Based on previous findings by Fragkoudis et al. (2007) it is likely that these cells were splenic macrophages. However, their identity was not confirmed by immunostaining for macrophage-specific markers due to technical issues described previously.

Most importantly, almost no zsGreen-positive cells were observed in marginal zones of spleens from animals infected with SFV4-3F-zsGreen-miR-142-3P RE (Figures 4.33 and 4.34). As those animals experience similar viraemia to animals infected with SFV4-3F-zsGreen-miRNA RE Control (Figure 4.32a), the difference was tissue-specific and not systemic. However, the relative replication of the two viruses was not investigated in other tissues permissive to SFV infection, such as pancreas. Interestingly, the attenuation of virus replication observed in these cells was present in spite of the loss of virus stability described in Figure 4.32b. It is possible that cells in marginal zones of spleen were infected early during infection, when the virus stability was still relatively high. It is also possible that any attenuation of virus replication, even partial, had a notable effect on virus replication in these cells.

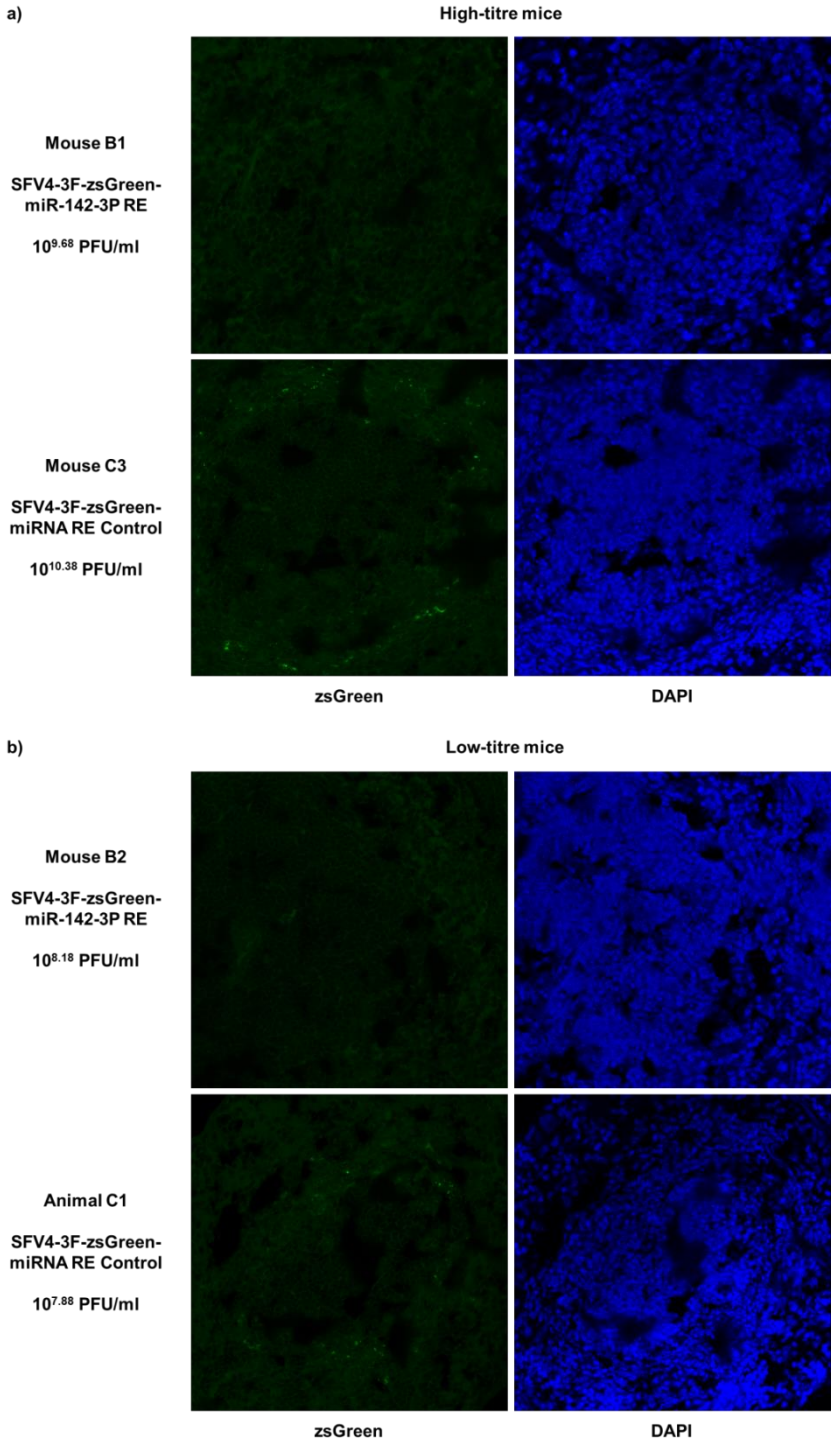

Figure 4.33. Sections of spleens from SFV4-infected IFNAR mice collected 28 hours post-infection. Representative comparison of marginal zones in spleen sections from animals infected with SFV4-3F-zsGreen-miR-142-3P RE and the control virus. (a) Sections from animals that had high virus load in the peritoneum. (b) Sections from animals that had low virus load in the peritoneum. Sections were imaged by Dr Pippa Hawes, the Pirbright Institute, using Leica TCS SP5 confocal microscope.

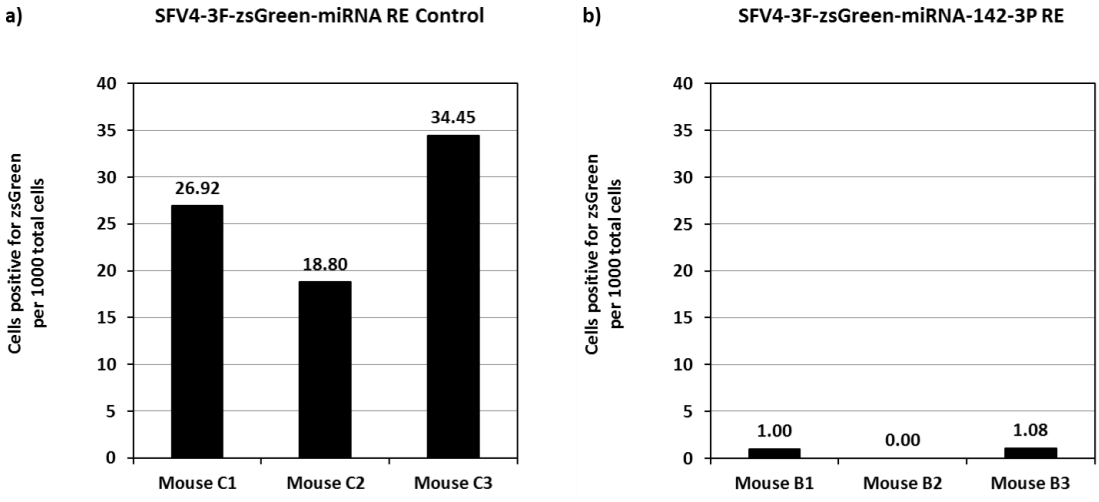

Figure 4.34. Prevalence of zsGreen positive cells in sections of spleens from SFV4-infected IFNAR mice collected 28 hours post-infection. Number of zsGreen positive cells and DAPI-stained nuclei was counted in 10 high power fields. Data represented as the number of cells positive for zsGreen per 1000 total cells.

4.18 Discussion

The principal objective of the work presented in this chapter was to harness endogenous haematopoietic-specific miR-142-3P to restrict replication of Semliki Forest virus in monocytes and macrophages. The cell-specific restriction of virus replication was attempted by incorporation of a recognition element (RE) with multiple copies of a target sequences fully complementary to miR-142-3P into the genome of SFV.

The work presented in this chapter laid foundation to the objective of Chapter 5, which was to investigating the role of monocyte and macrophage infection with CHIKV in the nonhuman primate model of chikungunya virus disease. It included generation of resources and tools required to undertake this project, and proof-of-concept experiments completed using SFV.

Key findings:

1. Two RE for miR-142-3P, and one control RE, were successfully designed, generated and cloned into genomes of multiple SFV clones.

2. Hek 293 cell line that expressed miR-142-3P under control of the tetracycline-inducible hybrid CMV/TetO2 promoter was designed and generated.

3. Presence of target sequences to miR-142-3P in the genome (but not antigenome) of SFV restricted replication of this virus in all cells expressing miR-142-3P.

4. Replication of SFV encoding the RE for miR-142-3P was restricted in haematopoietic cells not only *in vitro*, but also *in vivo*.

5. SFV encoding a RE for miR-142-3P was reverting slowly to its non-attenuated phenotype following serial passage on BHK-21 cells and *in vivo*. However, it was sufficiently stable to demonstrate a difference in pathogenesis *in vivo*.

Three miRNA REs were successfully designed and generated. Any of the three miRNA REs was inserted into the 3' UTR of the virus, directly downstream of the structural polyprotein ORF. In SFV, this position is typically stable (Tsetsarkin et al. 2006, Prof Andres Merits, the University of Tartu, personal communication). Furthermore, it corresponds to a common location of a miRNA target sequence in a cellular mRNA.

Replication of SFV encoding miR-142-3P target sequences in its genome was significantly restricted in mouse macrophage IC-21 cells, but not in fibroblast BHK-21 cells. The extent of virus attenuation was comparable or better to that observed by Pham et al. (2012) in a similar study on dengue virus. The restriction of virus replication was further confirmed in non-haematopoietic Hek 293 cells modified to express miR-142-3P, and in non-haematopoietic Hek 293T cells transfected with plasmids expressing miR-142-3P. The above data clearly demonstrated that the attenuation of SFV encoding miR-142-3P RE in cells expressing miR-142-3P was specifically due to the action of miR-142-3P and that the presence of a miR-142-3P RE had no effect on virus replication in non-haematopoietic cells.

Interestingly, the presence of miR-142-3P target sequences in the antigenome of the virus had no effect on virus replication in presence of miR-142-3P. Most likely, the SFV antigenome is shielded from cellular miRNAs and the cellular silencing machinery by virus replication complexes (Kallio et al. 2013). In fact, the number of alphavirus antigenomes corresponds to the total number of replication complex spherules present in a virus-infected cell (Dr Tero Ahola, the University of Tartu, personal communication). This suggests that all copies of an alphavirus antigenome are associated with replication complexes in virus-infected cells and are therefore protected from degradation via cellular miRNAs. Based on the above data, miR-142-3P Antisense RE was not incorporated into the genome of CHIKV for the subsequent experiments presented in Chapter 5.

SFV encoding miR-142-3P RE was progressively reverting to a non-attenuated phenotype following serial passage on BHK-21 cells. After 5 passages only 80% of the virus was still unable to form plaques in presence of miR-142-3P. The above data suggested that SFV4-3F-zsGreen-miR-142-3P RE was not a genetically stable construct. However, these findings were similar to other studies that used a cellular miRNA to restrict virus tissue tropism (Pham et al. 2012, Heiss et al. 2012). The molecular mechanism responsible for the reversion of the virus to a non-attenuated phenotype was not investigated.

In a pilot study, the replication of SFV encoding miR-142-3P RE was investigated in IFN-α/ß receptor knockout mice of A129/SvEv background (IFNAR mice). In these animals, SFV encoding miR-142-3P RE and the control virus replicated to comparable titres. In spleen sections from animals infected with the control virus, there was a visible population of zsGreen-positive cells in marginal zones between the white pulp and the red pulp. These cells were most likely macrophages, however, this was not confirmed by immunostaining for macrophage-specific markers due to technical issues. The above observation was consistent with previous findings by Fragkoudis et al. (2007). Significantly, almost no zsGreen-positive cells were observed in marginal zones of spleens from animals infected with SFV4 encoding the RE for miR-142-3P. This suggests that this virus was restricted in haematopoietic cells not only *in vitro*, but also *in vivo*. The *in vivo* stability of SFV4-3F-zsGreen-miR-142-3P RE was much more variable than that observed *in vitro*. However, it was sufficient to demonstrate a difference in pathogenesis in IFNAR mice.

As mentioned previously, some of the work presented in this chapter was continued in Chapter 5 with CHIKV. However, more detailed studies should be planned to investigate some of the findings presented in this chapter.

Future work should include:

1. In-depth characterisation of Hek 293 miR-142 cells;
    - Expression of miR-142-3P following induction with variable concentration of DOX (qPCR);

- Time course of miR-142-3P expression following induction with DOX;
- Cell line stability over time;

2. Characterisation of miR-142-3P levels produced in cells transfected with plasmids expressing miR-142-3P;
3. In-depth characterisation of SFV4-3F-zsGreen-miR-142-3P RE population that reverted to a non-attenuated phenotype;
    - Deep sequencing of the virus population;
    - Plaque purification of individual virus clones;
4. Optimisation of the protocols used to immunostain splenic macrophages;
5. Detailed characterisation of SFV4-3F-zsGreen-miR-142-3P RE pathogenesis in IFNAR mice;
    - Six animals per group per sampling time point;
    - Two time points at which animals are sacrificed and samples are collected, 24 and 40 hours post-infection;
    - Collection of blood for virus titration and the assessment of virus stability;
    - Collection of multiple organs (spleen, brain, kidneys, pancreas and hart) for virus titration, RNA extraction and immunohistopathology;
    - Analysis of virus replication in different tissues (plaque assay, qPCR, immunohistopathology);
    - Analysis of peritoneal macrophages for the presence of virus (FACS, immunohistopathology).

Chapter 5:

Investigating the role of monocyte and macrophage infection with chikungunya virus in the non-human primate model of chikungunya virus disease.

Contents:

5.1 Objectives

The objectives for this part of the project were as follow:

1) To incorporate miR-142-3P recognition element into the genome of chikungunya replicons and chikungunya virus.

2) To investigate if chikungunya replicon encoding miR-142-3P recognition element is attenuated in cells that express miR-142-3P.

3) To investigate if chikungunya virus encoding miR-142-3P recognition element is attenuated in haematopoietic cells.

4) To investigate if chikungunya virus encoding miR-142-3P recognition element is attenuated in Hek 293 cells that express miR-142-3P, but not in Hek 293 cells that do not express miR-142-3P.

5) To investigate if chikungunya virus encoding miR-142-3P recognition element is attenuated in cells transfected with pcDNA3.1+ expressing miR-142-3P, but not in cells transfected with control plasmids.

6) To investigate the stability of miR-142-3P RE in chikungunya virus genome during serial passage on BHK-21 cells.

7) To investigate if chikungunya virus encoding miR-142-3P recognition element is attenuated *in vivo* in cynomolgus macaques.

5.2 Incorporating miRNA REs into chikungunya replicons

Chikungunya VRPs provided a useful tool to study chikungunya virus attenuation *in vitro*. Importantly, chikungunya VRPs could be handled at containment level (CL) 2 while replication-competent chikungunya virus had to be handled at CL3.

Two panels of chikungunya replicons were cloned. First one was based on ChikRepl-3F-zsGreen-SG-mCherry (Figure 5.1). In this construct, zsGreen was expressed as a fusion protein with the nsP3. Hence, in replicon-infected cells zsGreen was localised to replication complexes in the cytoplasm. In addition, a second marker gene mCherry was inserted after the non-structural ORF between AvrII and PmeI sites, under control of the CHIKV subgenomic promoter. To generate the panel of replicons, miR-142-3P RE and miRNA RE Control were inserted between AvrII and PmeI sites in place of mCherry. The cloning procedure is detailed in Annex 21.

Replicons encoding miR-142-3P RE and miRNA RE Control were called ChikRepl-3F-zsGreen-miR-142-3P RE and ChikRepl-3F-zsGreen-miRNA RE Control, respectively. Their sequences are provided in Supplementary Data, Appendix 4.

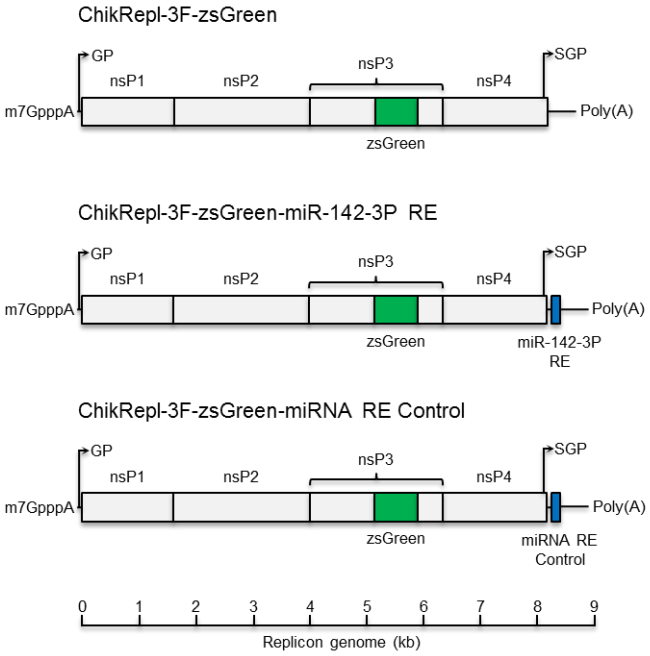

Figure 5.1. Schematic representation of ChikRepl-3F-zsGreen-miRNA RE clones. miRNA REs was inserted after the non-structural ORF, between AvrII and PmeI restriction sites. nsP – non-structural protein; GP – genomic promoter; SGP – subgenomic promoter; Poly(A) – Poly(A) tail; m^7GpppA – 5' CAP; RE – recognition element.

The second panel of chikungunya replicons was based on ChikRepl-3F-RLuc-SG-FLuc (Figure 5.2). In this construct, *Renilla* luciferase (RLuc) was expressed as a fusion protein with the nsP3. Consequently, in replicon-infected cells RLuc was localised to replication complexes in the cytoplasm. However, fusion of RLuc to nsP3 did not inhibit RLuc activity. Furthermore, *Firefly* luciferase (FLuc) was inserted after the non-structural ORF between AvrII and PmeI sites, under control of the CHIKV subgenomic promoter. To generate the panel of replicons, miR-142-3P RE and miRNA RE Control were inserted between AvrII and PmeI sites in place of FLuc. The protocol described earlier was followed.

Resulting replicons encoding miR-142-3P RE and miRNA RE Control were called ChikRepl-3F-RLuc-miR-142-3P RE and ChikRepl-3F-RLuc-miRNA RE Control, respectively. Their sequences are provided in Supplementary Data, Appendix 4.

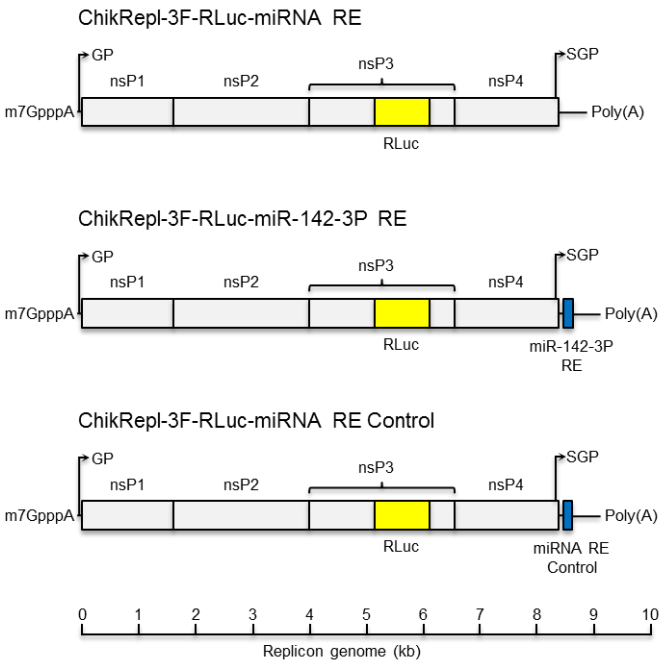

Figure 5.2. Schematic representation of ChikRepl-3F-RLuc-miRNA RE clones. miRNA RE was inserted after the non-structural ORF, between AvrII and PmeI restriction sites. nsP – non-structural protein; GP – genomic promoter; SGP – subgenomic promoter; Poly(A) – Poly(A) tail; m^7GpppA – 5' CAP; RE – recognition element.

5.3 Growing chikungunya VRPs

ChikRepl-3F-zsGreen, ChikRepl-3F-zsGreen-miR-142-3P RE and ChikRepl-3F-zsGreen-miRNA RE Control replicons were successfully rescued as described in 2.4.3. However, a replication-competent virus was identified in all VRP stocks following the protocol in 2.4.5. The replicon rescue was attempted twice more, however, each time a replication-competent virus was isolated. Hence, the decision was made to not use VRPs in the subsequent experiments (with the exception of 5.4).

All plasmids and molecular biology reagents used to generate the VRPs were confirmed to be free of full-length virus icDNA by PCR. The generation of the replication-competent virus was likely a consequence of recombination between the replicon RNA and the two helper RNAs. Split-helper systems used to rescue VRPs are specifically designed to minimise the likelihood of this happening. The theoretical frequency of producing a replication-competent virus using the SFV split-

helper system was calculated to be $<1.9 \times 10^{-13}$ (Smerdou et al., 1999). This frequency is not known for the chikungunya split-helper system. Some of its design features may unexpectedly promote the recombination. The analysis of plasmid sequences revealed that there is a relative large complementarity between individual components of the system. Molecular analysis of the replication-competent virus may provide information necessary to identify the way by which it was generated.

5.4 Will a chikungunya replicon encoding miR-142-3P RE be attenuated in non-haematopoietic cells expressing miR-142-3P?

This experiment was completed only once due to reasons explained in 5.3. First, Hek 293 miR-142 and Hek 293 Control cells were harvested, counted and seeded into 24-well plates in complete DMEM with no P/S (with or without DOX at 100 ng/ml final concentration) as described in 2.5.1. After 24 hours of incubation, cells were transfected with ChikRepl-3F-RLuc, ChikRepl-3F-RLuc-miR-142-3P RE and ChikRepl-3F-RLuc-miRNA RE Control replicons as described in 2.4.3 (generation of replicon RNA), 2.15.5 (RNA purification) and 2.10.2 (transfection using Lipofectamine® 2000). Twenty four hours post-infection the levels of replicon-expressed RLuc were measured as described in 2.9.2.

In Hek 293 Control cells that were either induced with doxycycline or not, all three replicons replicated to the same extent as demonstrated by the expression of RLuc (Figure 5.3). In Hek 293 miR-142 cells not induced with DOX, the replication of the control replicons ChikRepl-3F-RLuc and ChikRepl-3F-RLuc-miRNA RE Control was not affected. However, the measured replication of ChikRepl-3F-RLuc-miR-142-3P RE was reduced by over 60% with respect to ChikRepl-3F-RLuc-miRNA RE Control. The difference was statistically significant. In Hek 293 miR-142 cells induced with DOX a similar pattern was observed. However, the measured replication of ChikRepl-3F-RLuc-miR-142-3P RE was reduced by over 80% with respect to ChikRepl-3F-RLuc-miRNA RE Control. Interestingly, attenuation of SFV4-3F-zsGreen-2SG-GLuc-miR-142-3P RE on Hek 293 miR-142 cells not induced with DOX was never observed (Figure 4.19, Figure 4.20).

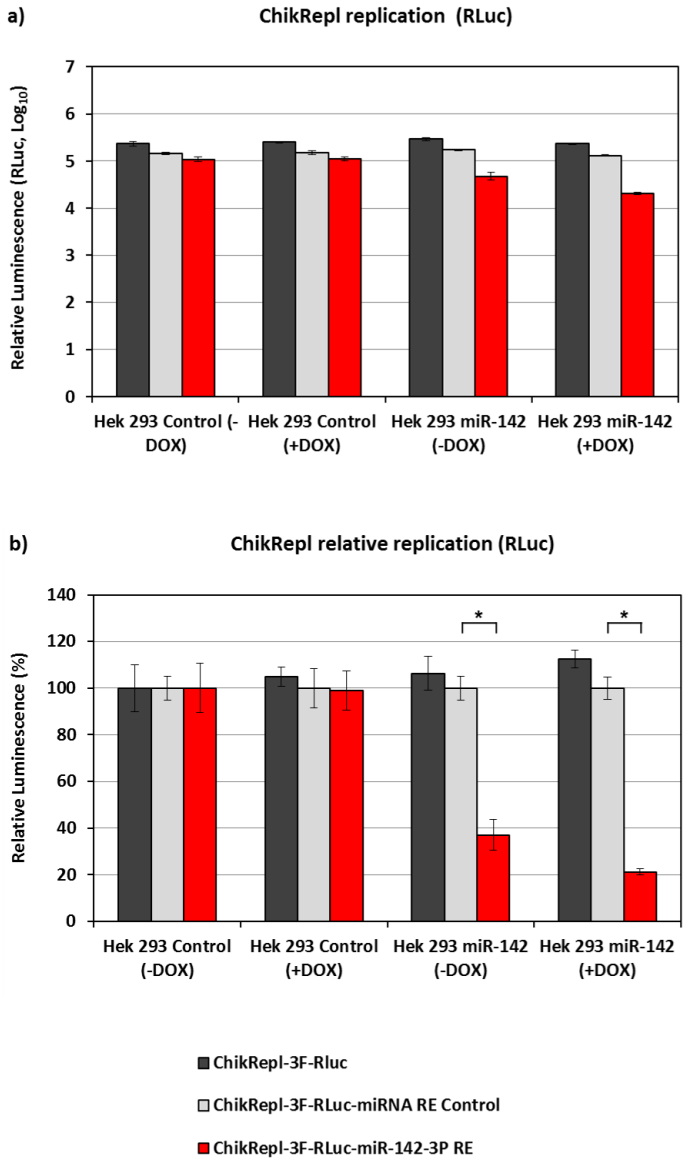

Figure 5.3. RLuc expression in ChikRepl-3F-RLuc-miRNA RE-transfected Hek 293 miR-142 and Hek 293 Control cells. Hek 293 miR-142 (+DOX) and Hek 293 Control (+DOX) cells were induced with DOX at 100 ng/ml final concentration for 24 hours prior to infection. Replicon RNA was transfected using Lipofectamine® 2000. (a) Raw data expressed as mean +/- SD. (b) Results normalised to the replication in Hek 293 Control (-DOX) cells and to ChikRepl-3F-RLuc-miRNA RE Control replicon. Data expressed as relative mean +/- relative SD; Mann-Whitney test, single-tailed; * $p<0.05$.

5.5 Incorporating miRNA REs into CHIKV

Two panels of chikungunya viruses that mirrored the replicon designs were cloned. First one was based on ICRES1-3F-zsGreen-2SG-mCherry. In this virus, zsGreen was expressed as a fusion protein with the nsP3 and mCherry was inserted after the non-structural ORF between AvrII and PmeI sites, under control of the CHIKV subgenomic promoter. The subgenomic promoter was duplicated downstream of mCherry to drive the expression of the structural polyprotein. In brief, miR-142-3P RE and miRNA RE Control were inserted between AvrII and PmeI sites (Figure 5.4, Figure 5.5). The protocol described in 5.2 was followed, however, the colony PCR was completed using a different set of primers (Annex 12, protocol 4).

Resulting CHIKV encoding miR-142-3P RE and miRNA RE Control were called ICRES1-3F-zsGreen-miR-142-3P RE and ICRES1-3F-zsGreen-miRNA RE Control, respectively. Their sequences are provided in Supplementary Data, Appendix 2.

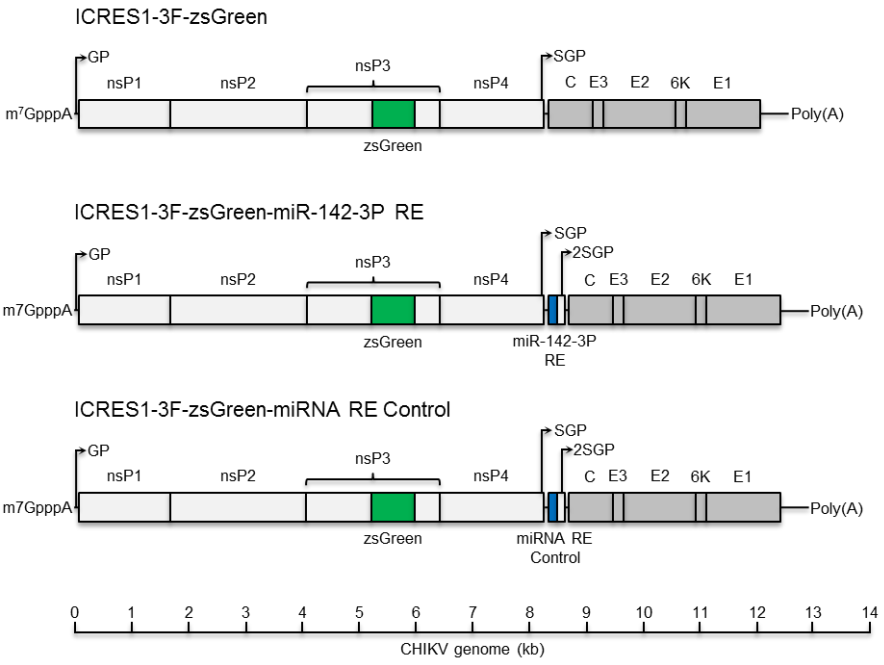

Figure 5.4. Schematic representation of ICRES1-3F-zsGreen-miRNA RE clones. miRNA RE was inserted after the non-structural ORF, between AvrII and PmeI restriction sites. nsP – non-structural protein; Poly(A) – Poly(A) tail; GP – genomic promoter; SGP – subgenomic promoter; m^7GpppA – 5' CAP.

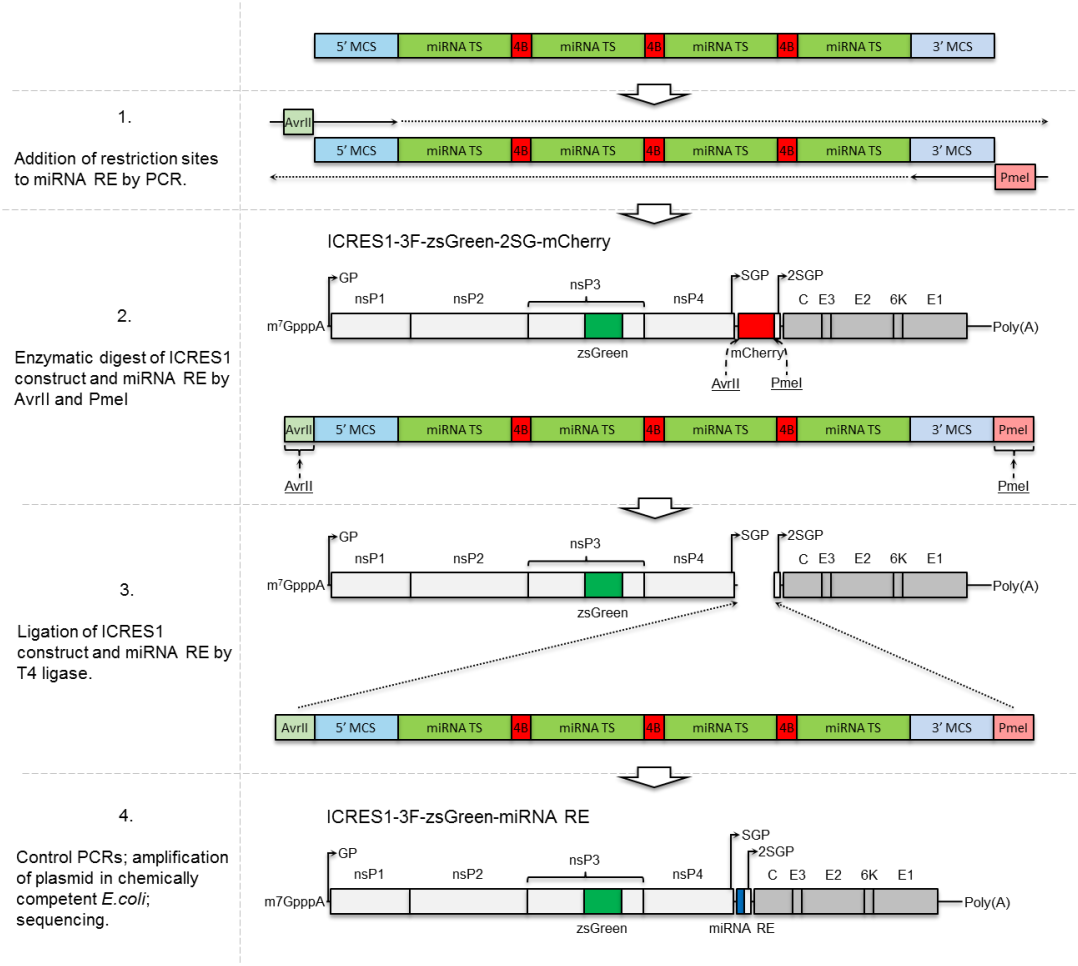

Figure 5.5. Incorporation of a miRNA RE into the genome of ICRES-3F-zsGreen-2SG-mCherry. nsP-non-structural protein; GP – genomic promoter; SGP – subgenomic promoter; 2SGP – duplicated subgenomic promoter; C – capsid; E1-E3 – envelope glycoproteins; vertical dashed line – protein cleavage sites; Poly(A) – Poly(A) tail; m^7GpppA – 5' CAP; RE – recognition element; MCS – multiple cloning site; 4B – 4-nucleotide spacer; TS – target sequence.

The second panel of CHIKV was based on ICRES-3F-RLuc-2SG-FLuc (Figure 5.6). In this construct, RLuc was expressed as a fusion protein with the nsP3 and FLuc was inserted after the non-structural ORF between AvrII and PmeI sites, under control of the CHIKV subgenomic promoter. The fusion of RLuc to nsP3 did not inhibit RLuc activity. In brief, miR-142-3P RE and miRNA RE Control were inserted between AvrII and PmeI sites in place of FLuc. The protocol described earlier was followed.

Resulting CHIKV encoding miR-142-3P RE and miRNA RE Control were called ICRES1-3F-RLuc-miR-142-3P RE and ICRES1-3F-RLuc-miRNA RE Control, respectively. Their sequences are provided in Supplementary Data, Appendix 2.

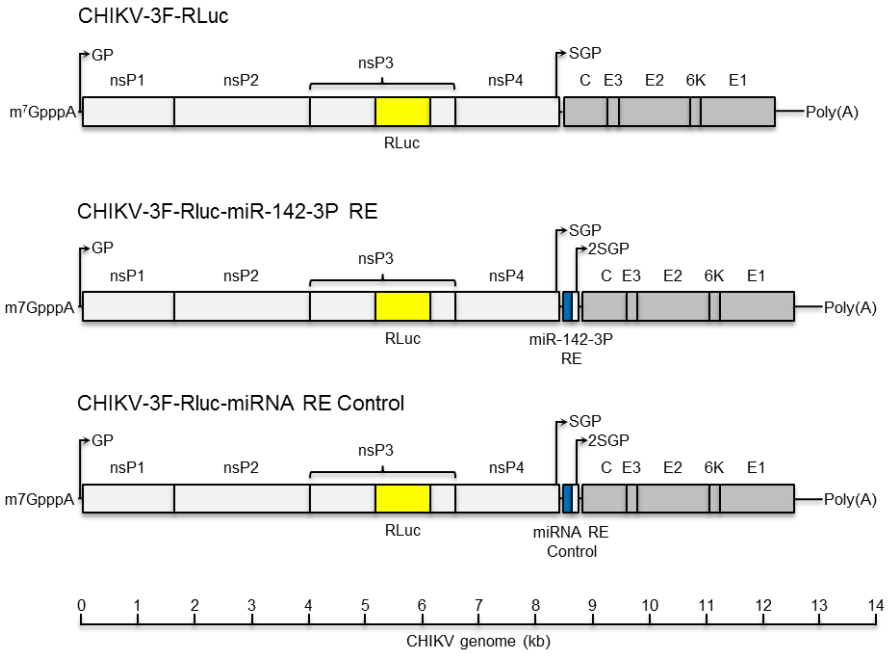

Figure 5.6. Schematic representation of ICRES1-3F-RLuc-miRNA RE clones. miRNA RE was inserted after the non-structural ORF, between AvrII and PmeI restriction sites. nsP – non-structural protein; GP – genomic promoter; SGP – subgenomic promoter; Poly(A) – Poly(A) tail; m^7GpppA – 5' CAP; RE – recognition element.

5.6 Growing CHIKV clones

ICRES1-3F-zsGreen, ICRES1-3F-zsGreen-miR-142-3P RE, ICRES1-3F-zsGreen-miRNA RE Control, ICRES1-3F-zsGreen-2SG-mCherry, ICRES1-3F-RLuc, ICRES1-3F-RLuc-miR-142-3P RE, ICRES1-3F-RLuc-miRNA RE Control, ICRES1-3F-RLuc-2SG-FLuc and ICRES1 (wt) were successfully rescued from icDNAs as described in 2.3.3.1. Virus stock (purified by ultracentrifugation through a 20% w/v sucrose cushion) was titrated following the protocol outlined in 2.3.5.

5.7 Will the presence of miR-142-3P RE affect the rate at which CHIKV can replicate in fibroblast BHK-21 cells?

Replication of ICRES1-3F-zsGreen, ICRES1-3F-zsGreen-miR-142-3P RE, ICRES1-3F-zsGreen-miRNA RE Control, ICRES1-3F-zsGreen-2SG-mCherry, ICRES1-3F-RLuc, ICRES1-3F-RLuc-miR-142-3P RE, ICRES1-3F-RLuc-miRNA RE Control, ICRES1-3F-RLuc-2SG-FLuc and ICRES1 (wt) was investigated by completing one-step growth curves. In brief, cells were infected at MOI of 10 to ensure an infection rate close to 100%. Virus replication was tested by plaque assay every 2-4 hours, for 24 hours. The protocol described in 2.3.7 was followed.

The results shown in Figure 5.7a suggested that incorporation of marker genes into the genome of ICRES1 had a negative effect on virus replication. This was observed at all time-points. The effect was amplified when multiple marker genes were used. Interestingly, viruses expressing RLuc as a fusion protein with nsP3 were replicating slower than corresponding viruses expressing zsGreen (Figure 5.7a). This difference was likely related to the size of both marker proteins, and their genes. RLuc (36 kDa) is a larger protein than zsGreen (25 kDa). When fused to nsP3, both markers can affect the processing of the non-structural polyprotein into its individual components, formation of replication complexes and activity of the virus replicase. However, the larger RLuc has the capacity to cause more steric hindrance than zsGreen and therefore affect the formation, maturation and activity of the virus replicase more significantly than zsGreen. In addition, the RLuc gene is 240 nucleotides longer than the zsGreen gene. Typically, the speed of virus genome replication is proportionally reduced as the length of the inserted gene increases. Notably, the size-dependent attenuation of a virus is not always evident *in vivo*. However, it may lead to decreased replication and pathogenicity. Hence, CHIKV constructs encoding zsGreen should be used in preference to constructs encoding RLuc *in vivo*.

Incorporation of a miRNA RE into ICRES1 genome did not itself affect virus replication. This was observed in ICRES1-3F-zsGreen-miRNA RE constructs (Figure 5.7b) and in ICRES1-3F-RLuc-miRNA RE constructs (Figure 5.7c).

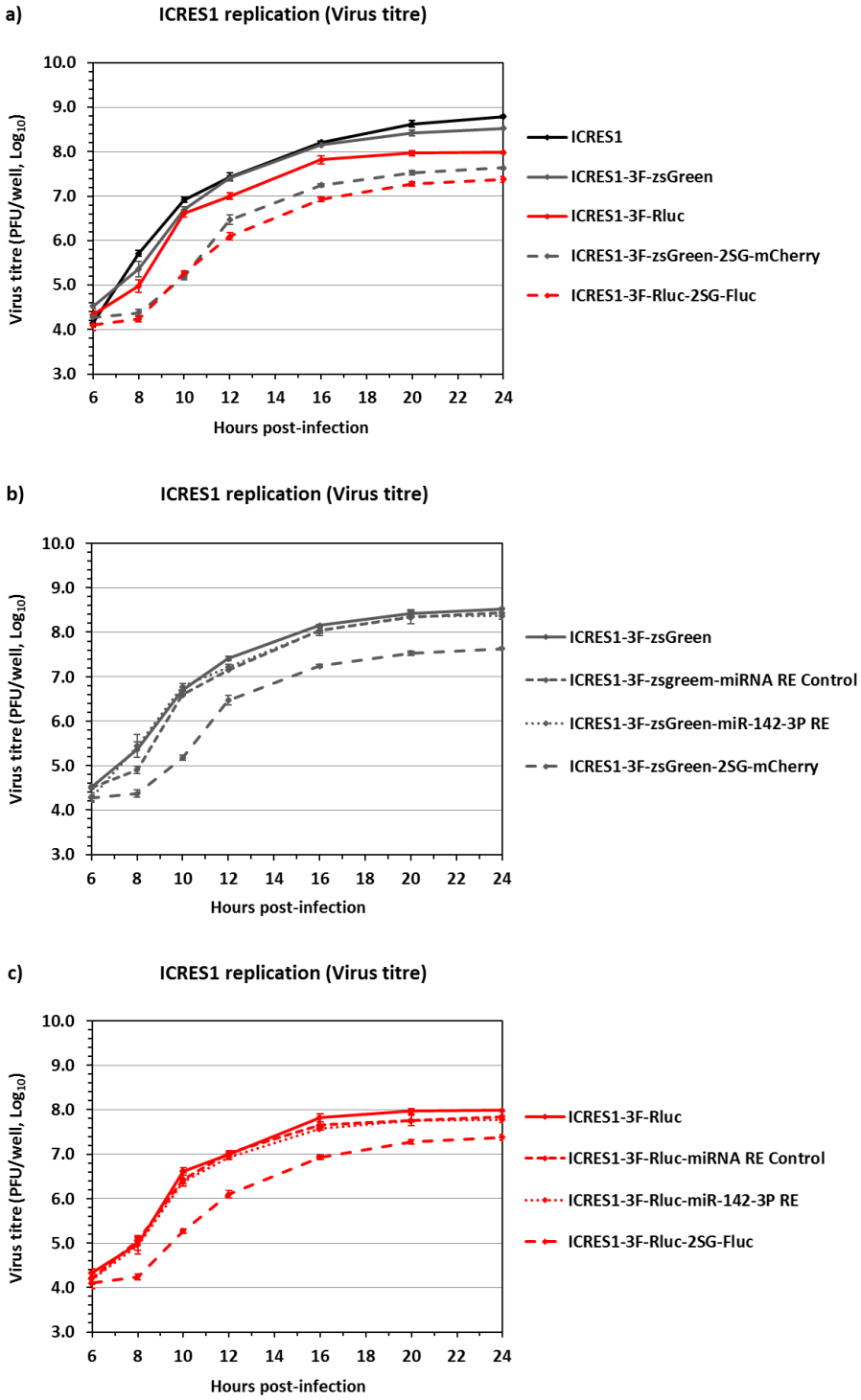

Figure 5.7. ICRES1 one-step growth curves. BHK-21 cells were infected at MOI of 10 and incubated for 24 hours. The cell supernatant was sampled every 2 hours for the first 12 hours, and then every 4 hours. Samples were tested by plaque assay. Data expressed as mean +/- SD.

The size of plaques produced by ICRES1-3F-zsGreen, ICRES1-3F-zsGreen-miR-142-3P RE, ICRES1-3F-zsGreen-miRNA RE Control, ICRES1-3F-zsGreen-2SG-mCherry, ICRES1-3F-RLuc, ICRES1-3F-RLuc-miR-142-3P RE, ICRES1-3F-RLuc-miRNA RE Control, ICRES1-3F-RLuc-2SG-FLuc and ICRES1 (wt) was investigated. All viruses were plaqued as described in 2.3.5, at the same time and on the same BHK-21 cells.

As shown in Figures 5.8 and 5.9, ICRES1 (wt) produced plaques of the largest size (2.74 mm, SD=0.10). However, the size of plaques formed by ICRES1-3F-zsGreen (2.62 mm, SD=0.13), ICRES1-3F-zsGreen-miR-142-3P RE (2.57 mm, SD=0.10), ICRES1-3F-zsGreen-miRNA RE Control (2.54 mm, SD=0.12), ICRES1-3F-RLuc-miR-142-3P RE (2.63 mm, SD=0.15) and ICRES1-3F-RLuc-miRNA RE Control (2.53 mm, SD=0.14) was only mildly reduced. Plaques of significantly smaller sizes were produced by ICRES1-3F-zsGreen-2SG-mCherry (2.04 mm, SD=0.15) and ICRES1-3F-RLuc-2SG-FLuc (1.19 mm, SD=0.04). This observation was consistent with one-step growth curves. Importantly, incorporation of a miRNA RE into a virus genome did not itself affect the size of plaques produced by this virus.

Interestingly, ICRES1-3F-RLuc yielded a mixed population of plaques (Figures 5.8 and 5.9). Large plaques (20% of the total population) were comparable in size (2.61 mm, SD=0.05) to those formed by ICRES1-3F-zsGreen, ICRES1-3F-zsGreen-miR-142-3P RE, ICRES1-3F-zsGreen-miRNA RE Control, ICRES1-3F-RLuc-miR-142-3P RE, ICRES1-3F-RLuc-miRNA RE Control and ICRES1 (wt). Small plaques (80% of the total population) were comparable in size (1.36 mm, SD=0.21) to those formed by ICRES1-3F-RLuc-2SG-FLuc. To exclude the possibility of virus cross-contamination, ICRES1-3F-RLuc icDNA was purified and re-grown as described in 2.19.2 and 2.15.9. Fresh virus stock was generated from the new icDNA as described in 2.3.3. However, the new stock of ICRES1-3F-RLuc was still characterised by the mixed plaque phenotype. This finding suggested that there could be an inherent molecular issue with this particular CHIKV construct that resulted in production of two slightly different virus populations during virus rescue. Molecular differences between these two populations of ICRES1-3F-RLuc were not characterised.

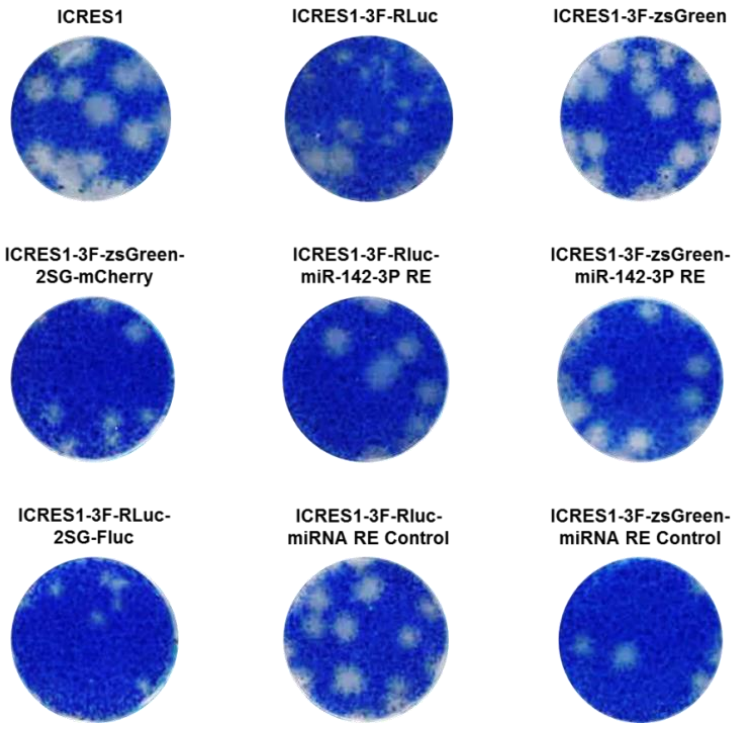

Figure 5.8. Plaques generated by different ICRES1 clones. Cells were incubated for 72 hours with CMC-based semi-solid overlay, fixed with 10% v/v neutral buffered formalin for 1 hour and then stained with 0.1% toluidine blue.

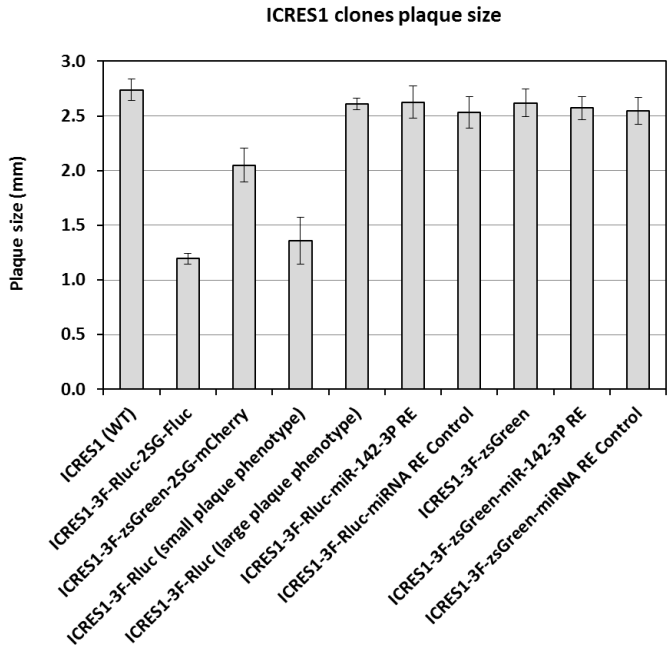

Figure 5.9. Size of plaques generated by different ICRES1 clones. The size of plaques was measured using Zeiss AxioVision 4.8 digital image processing software. Data expressed as mean of random 20 individual plaques +/- SD.

5.8 Will ICRES1-3F-RLuc-miR-142-3P RE be attenuated in haematopoietic IC-21 and Thp-1 cells but not in fibroblast 3T3 and NHDF cells?

ICRES1-3F-RLuc-miR-142-3P RE and the control virus were used to infect IC-21 cells at MOI of 100 and 1000, Thp-1 cells (PMA-induced) at MOI of 100 and 1000, 3T3 cells at MOI of 1 and NHDF cells at MOI of 1, in 96-well plates. The above cells were selected to provide a panel of species-matched fibroblast and macrophage cell lines (human Thp-1 and NHDF, mouse IC-21 and 3T3). The protocol outlined in 2.5.1 was followed. Twenty hours post-infection, RLuc levels were measured as described in 2.9.1.

RLuc encoded by all three viruses allowed simple but indirect measurement of virus replication. In 3T3 and NHDF cells, the two viruses replicated to comparable levels (Figure 5.10). The minor differences observed were most likely due to inaccurate titration of the virus stock. In IC-21 cells infected at MOI of 100 and 1000, the replication of ICRES1-3F-RLuc-miR-142-3P RE was reduced with respect to the control virus by approximately 90% and 98%, respectively. The difference was statistically significant. In Thp-1 cells, an almost identical effect was observed. The results clearly demonstrated that the replication of ICRES1 encoding miR-142-3P target sequences in its genome was attenuated in haematopoietic cells. The results were consistent with previous findings for SFV.

.

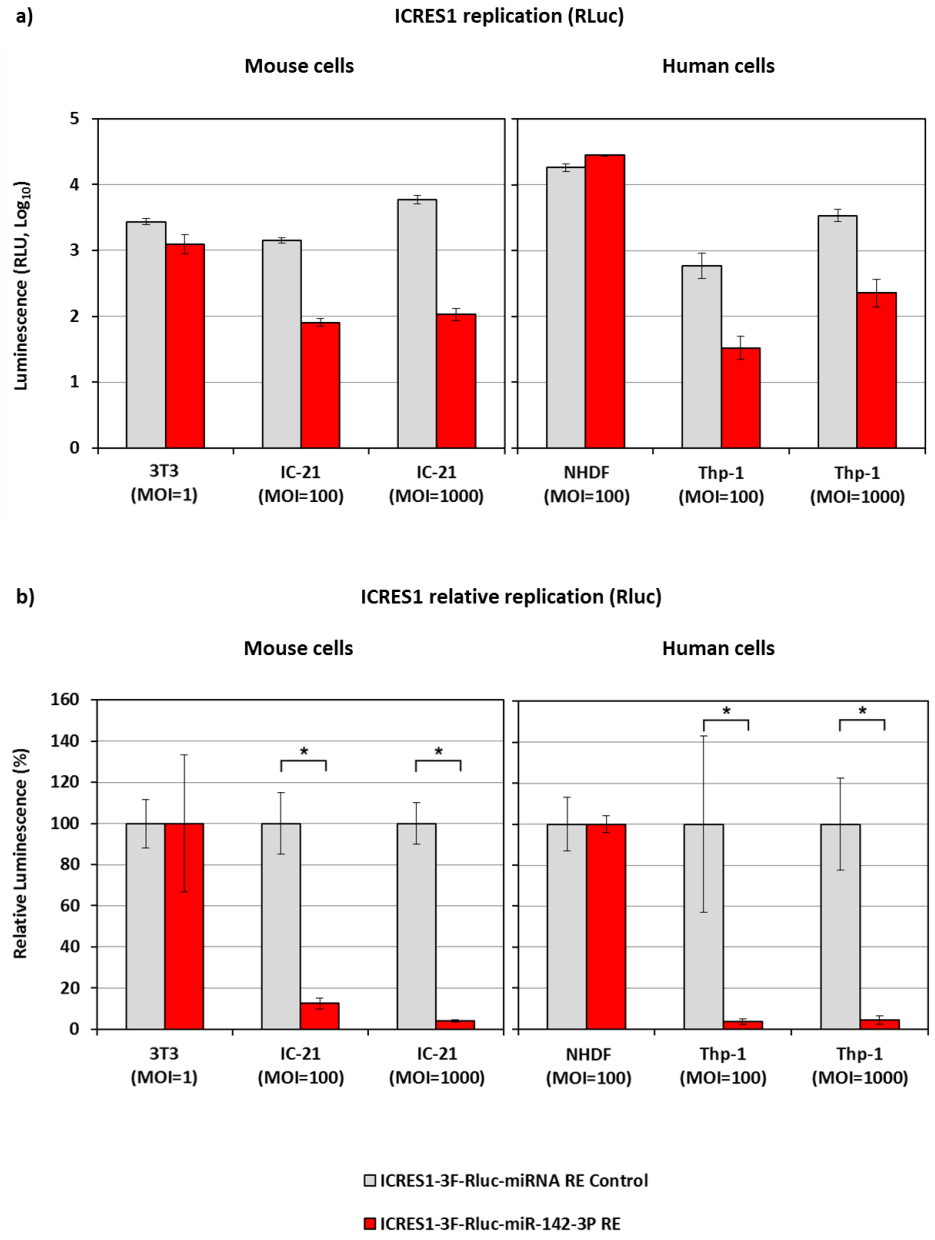

Figure 5.10. Replication of ICRES1-3F-RLuc-miRNA RE clones in IC-21, Thp-1, 3T3 and NHDF cells. IC-21 and Thp-1 cells (PMA-induced) were infected at MOI of 100 and 1000. 3T3 and NHDF cells were infected at MOI of 1 and 100, respectively. RLuc was measured 20 hours post-infection. (a) Raw data expressed as mean +/- SD. (b) Virus replication in IC-21 or Thp-1 cells was normalised to virus replication in 3T3 or NHDF cells, respectively. The resulting relative replication of ICRES1-3F-RLuc-miR-142-3P RE was normalised to the relative replication of ICRES-3F-RLuc-miRNA RE Control. Data expressed as relative mean +/- relative SD; Mann-Whitney test, single-tailed; * $p<0.05$.

5.9 Will CHIKV encoding miR-142-3P RE be attenuated in non-haematopoietic cells expressing miR-142-3P?

Hek 293 miR-142 and Hek 293 Control cells were harvested, counted and seeded into 24-well plates and into 96-well plates (with or without DOX at 100 ng/ml final concentration) as described in 2.5.1. After 24 hours of incubation, cells were infected at MOI of 1 and 10 with ICRES1-3F-zsGreen-miR-142-3P RE and ICRES1-3F-zsGreen-miRNA RE Control (24-well plates), and with ICRES1-3F-RLuc-miR-142-3P RE and ICRES1-3F-RLuc-miRNA RE Control (96-well plates). Twenty hours post-infection the supernatant from cells infected with ICRES1-3F-zsGreen-miRNA RE viruses was collected. Cells were observed microscopically for the expression of virus-encoded zsGreen. Virus load was measures as described in 2.3.5. Furthermore, RLuc levels were measured in ICRES1-3F-RLuc-miRNA RE-infected cells as described in 2.9.1.

In Hek 293 Control cells that were either induced with doxycycline or not, all viruses replicated to the same extent as demonstrated by both virus production (Figure 5.11) and by RLuc expression (Figure 5.12). In Hek 293 miR-142 cells not induced with DOX, the replication of viruses encoding miR-142-3P RE was reduced by 20-30% with respect to the control viruses as demonstrated by both virus production and by RLuc expression. This effect suggested that the background expression of miR-142-3P present in these cells may have been sufficient to partially affect replication of CHIKV encoding miR-142-3P RE. In Hek 293 miR-142 cells induced with DOX, the replication of ICRES1-3F-zsGreen-miR-142-3P RE and ICRES1-3F-RLuc-miR-142-3P RE was reduced by statistically significant 99% and 90%, respectively, as demonstrated by virus production and by RLuc expression.

The above results were fully supported by observation of virus-infected cells under the microscope (data not shown). Altogether, the above data confirmed that the replication of ICRES1 encoding miR-142-3P target sequences in its genome was attenuated in cells that express miR-142-3P. The results were in agreement with previous findings for SFV.

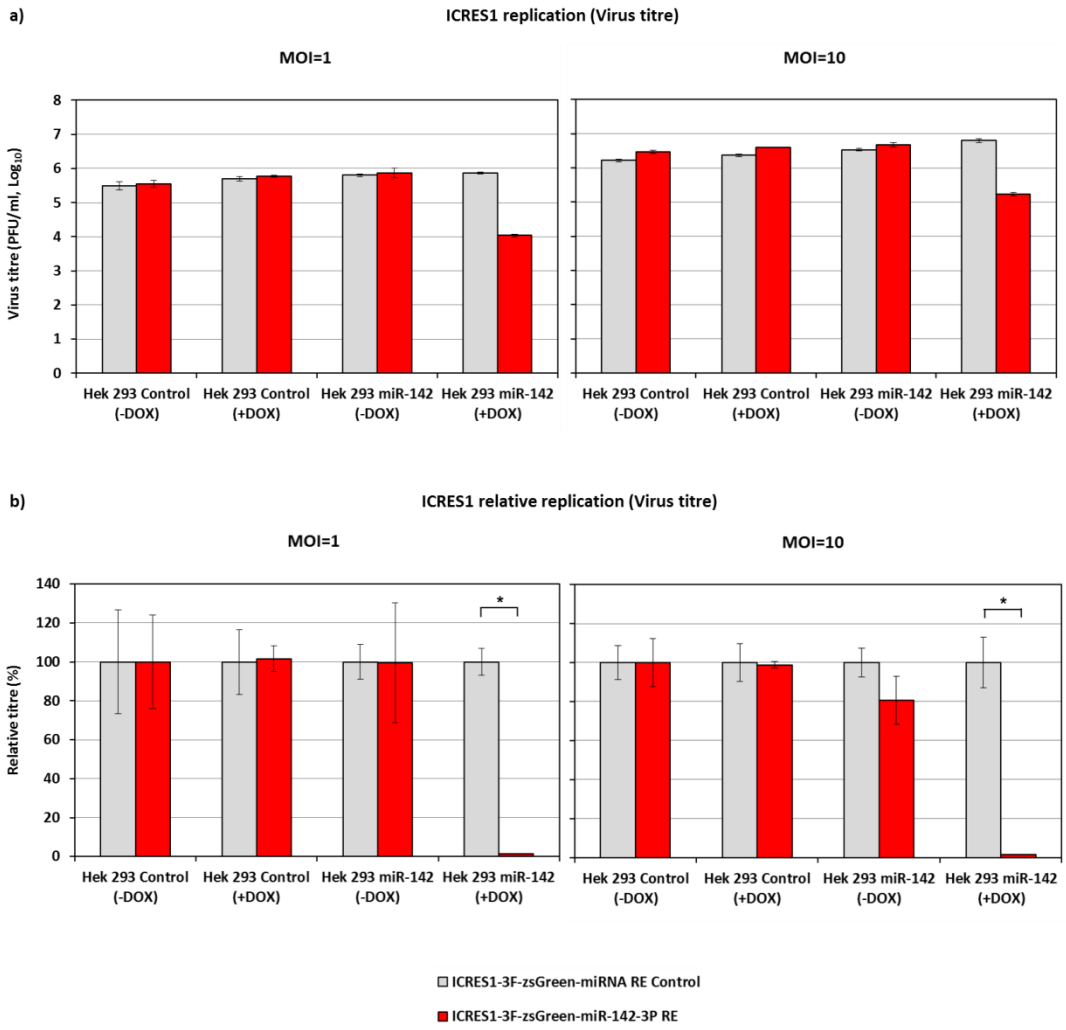

Figure 5.11. Virus production in ICRES1-zsGreen-miRNA RE-infected Hek 293 miR-142 and Hek 293 Control cells. Hek 293 miR-142 (+DOX) and Hek 293 Control (+DOX) cells were induced with DOX at 100 ng/ml final concentration for 24 hours prior to infection. Cells were infected at MOI of 1 and 10. (a) Raw data expressed as mean +/- SD. (b) Results normalised to the infection in Hek 293 Control (-DOX) cells and to ICRES1-3F-zsGreen-miRNA RE Control virus. Data expressed as relative mean +/- relative SD; Mann-Whitney test, single-tailed; * $p<0.05$.

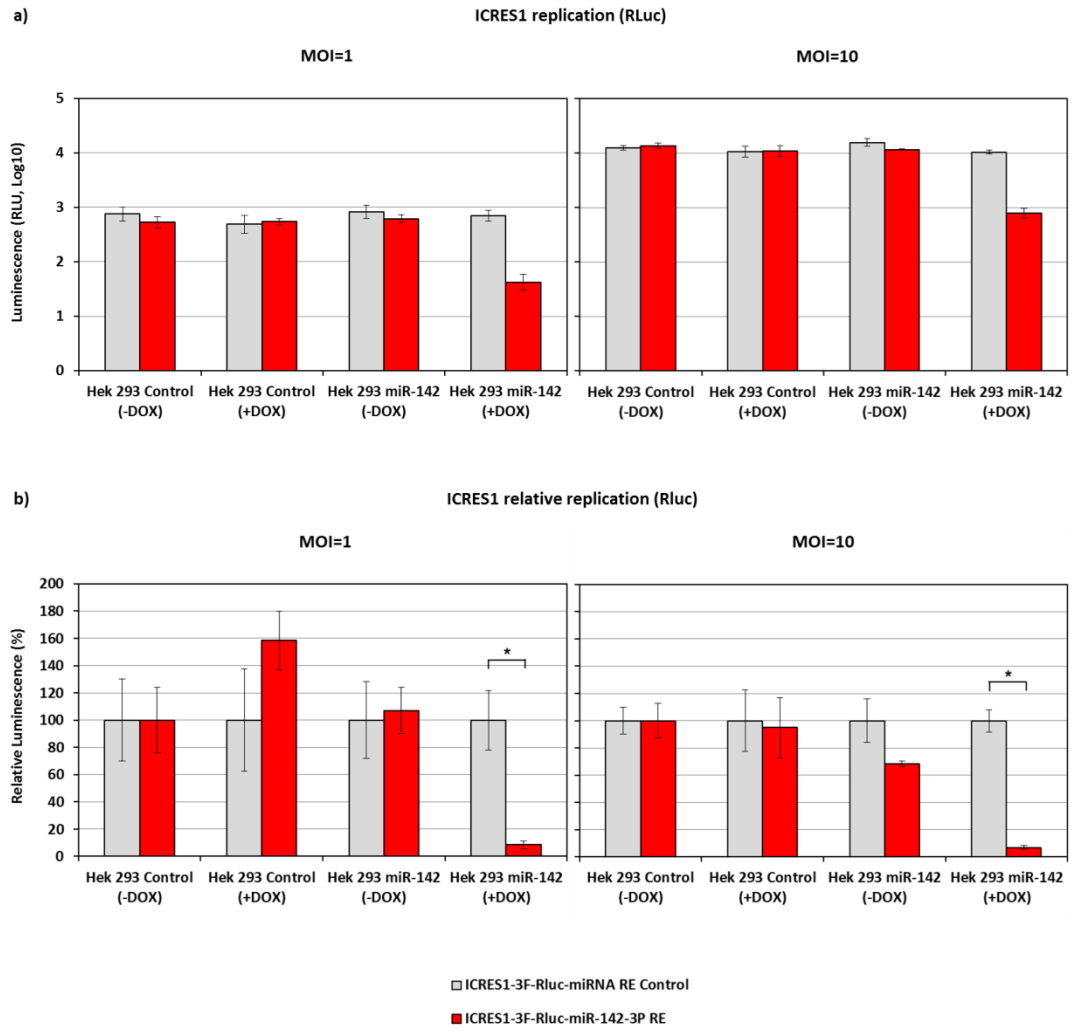

Figure 5.12. RLuc expression in ICRES1-3F-RLuc-miRNA RE-infected Hek 293 miR-142 and Hek 293 Control cells. Hek 293 miR-142 (+DOX) and Hek 293 Control (+DOX) cells were induced with DOX at 100 ng/ml final concentration for 24 hours prior to infection. Cells were infected at MOI of 1 and 10. (a) Raw data expressed as mean +/- SD. (b) Results normalised to the infection in Hek 293 Control (-DOX) cells and to ICRES1-3F-RLuc-miRNA RE Control virus. Data expressed as relative mean +/- relative SD; Mann-Whitney test, single-tailed; * $p<0.05$.

The relationship between the levels of miR-142-3P expression and the attenuation of CHIKV encoding miR-142-3P RE was further investigated using Hek 293 miR-142-3P cells induced with a range of DOX concentrations. In brief, Hek 293 miR-142 cells were harvested, counted and seeded into 96-well and 24-well plates with increasing amounts of DOX (0-1000 ng/ml, 0.2 ng/ml or 10-fold steps) as described in 2.5.1. After 24 hours of incubation, cells were infected at MOI of 10 with ICRES1-3F-zsGreen-miR-142-3P RE (24-well plates), and with ICRES1-3F-RLuc-miR-142-3P RE (96-well plates). Cellular RNA was extracted from uninfected cells (24-well plates) as described in 2.15.3. Twenty hours post-infection the supernatant from cells infected with ICRES1-3F-zsGreen-miR-142-3P RE was collected. Cells were observed microscopically for the expression of virus-encoded zsGreen and the virus load was measures as described in 2.3.5. Furthermore, RLuc levels were measured in ICRES1-3F-RLuc-miR-142-3P RE-infected cells as described in 2.9.1.

ICRES1 clones encoding miR-142-3P RE were attenuated when Hek 293 miR-142 cells were pre-treated with DOX at concentration higher than 0.1 ng/ml (Figure 5.13). The majority of virus attenuation took place when Hek 293 miR-142 cells were induced with DOX at a narrow range of concentrations between 0.4 and 1.0 ng/ml. This was observed by virus production (Figure 5.13a) and by RLuc expression (Figure 5.13b). The extent of virus attenuation observed in this experiment was comparable to that shown in Figure 5.11 (virus production) and Figure 5.12 (RLuc expression). Importantly, the results mirrored exactly the behaviour of SFV4-3F-zsGreen-2SG-GLuc-miR-142-3P observed in an equivalent experiment (Figure 4.21). At the time of writing this thesis the relative levels of miR-142-3P expression in Hek 293 miR-142-3P cells generated during this experiment were not yet tested. Hence, it was impossible to investigate the exact correlation between levels of miR-142-3P and the replication of ICRES1 clones encoding miR-142-3P RE. However, the similarity between data obtained for SFV and CHIKV suggested that miR-142-3P restricted replication of both SFV and CHIKV in a similar fashion.

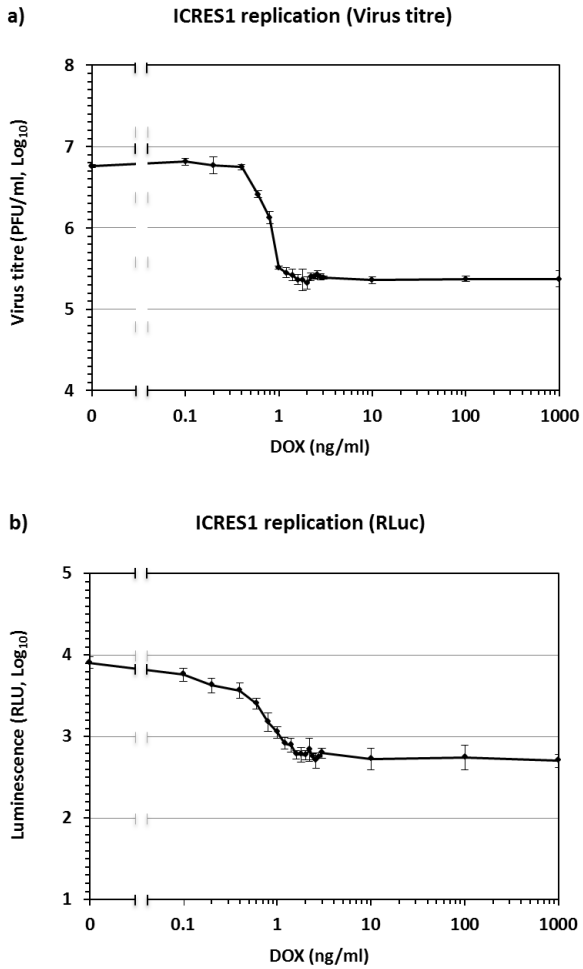

Figure 5.13. Attenuation of ICRES1-3F-zsGreen-miR-142-3P RE and ICRES1-3F-RLuc-miR-142-3P RE in HEK 293 miR-142 cells induced with DOX at concentrations ranging from 0 to 1000 ng/ml. a) Detailed analysis of ICRES1-3F-zsGreen-miR-142-3P RE attenuation (virus production). d) Detailed analysis of ICRES1-3F-RLuc-miR-142-3P RE attenuation (RLuc expression). Data expressed as mean +/- SD.

5.10 Will CHIKV encoding miR-142-3P RE be attenuated in cells transfected with pcDNA^{TM}3.1+ plasmids expressing miR-142-3P, but not in cells transfected with control plasmids?

The following experiment was completed only once. Hek 293T cells were harvested, counted, and seeded into 96-well plates at 2.5 x 10^4 cells per well as described in 2.5.1. Complete medium with no P/S was used. After 24 hours of incubation, cells were transfected with all plasmids generated in 4.13 using FuGENE® 6 as described in 2.10.1. Unmodified pcDNA^{TM}3.1+ was transfected as a control. Twenty-four hours post-transfection, cells were inspected microscopically for the expression of mCherry, and then infected with ICRES1-3F-zsGreen-miR-142-3P and ICRES1-3F-zsGreen-miRNA RE Control at MOI of 0.1. Twenty hours post-infection the RLuc levels in virus-infected cells were measured as described in 2.9.1.

As shown in Figure 5.14, both viruses replicated to the same levels in Hek 293T cells transfected with pcDNA^{TM}3.1+. In all Hek 293 cells transfected with pcNDA3.1+ modified to express miR-142-3P, the measured replication of SFV4-3F-zsGreen-2SG-GLuc-miR-142-3P RE was significantly reduced with respect to the control virus. Overall, the attenuation of ICRES1-3F-zsGreen-miR-142-3P RE was not as high as that observed on Hek 293 miR-142 cells induced with doxycycline. However, the efficacy of plasmid transfection was only 75% (as indicated by expression of mCherry in pcDNA3.1+ mCherry-transfected cells). The above results were consistent with previous observations on IC-21 and Hek 293 miR-142 cells.

Interestingly, the results did not fully mirror the behaviour of SFV4-3F-zsGreen-2SG-GLuc-miR-142-3P RE observed in an equivalent experiment (Figure 4.23). Most notably, the attenuation of CHIKV replication was less pronounced than the attenuation of SFV. In addition, the extent of SFV attenuation varied in cells transfected with different plasmids. This was not observed in this experiment. As both experiments were performed only once, it is difficult to discuss why the differences were present. It is likely that they may have resulted from small variations in the experimental conditions that were not suitably controlled for.

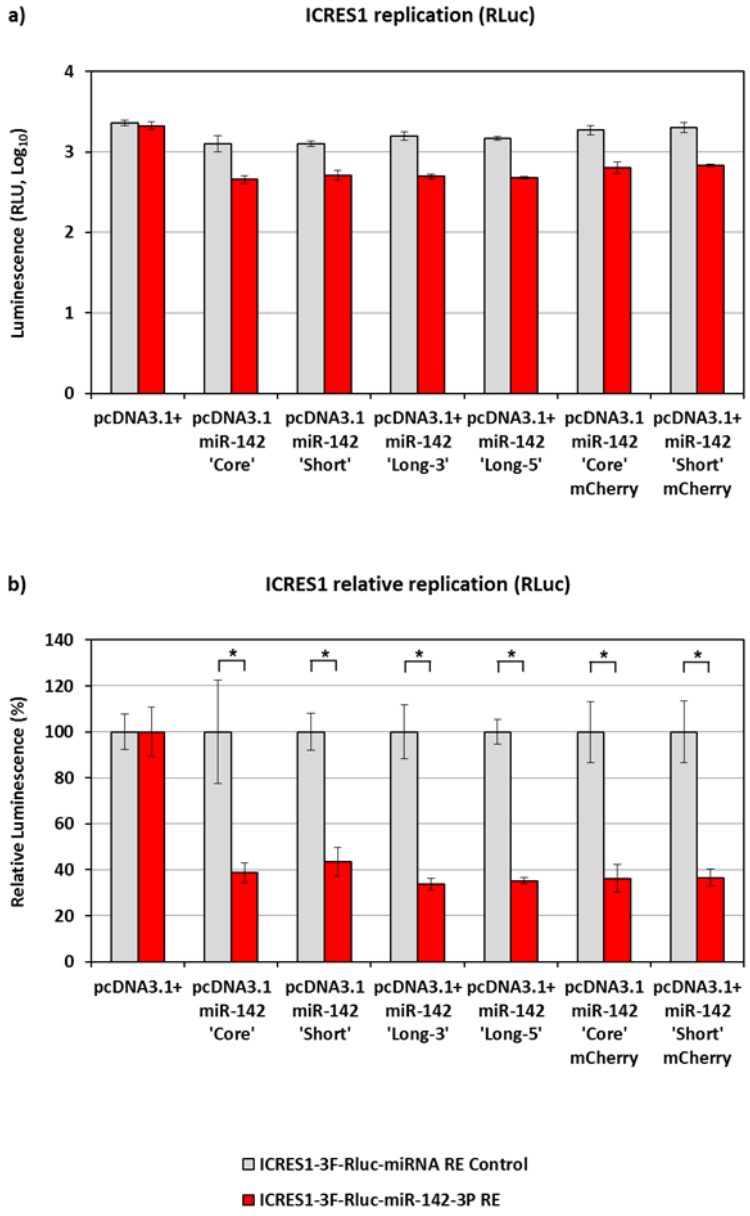

Figure 5.14. Replication of ICRES1-3F-RLuc-miRNA RE in Hek 293T cells transfected with pcDNA3.1+ plasmids expressing miR-142-3P. Transfected cells were infected at MOI of 0.1. (a) Raw data expressed as mean +/- SD. (b) Results normalised to the infection in cells transfected with pcDNA^{TM}3.1+ and to ICRES1-3F-zsGreen-miRNA RE Control virus. Data expressed as relative mean +/- relative SD; Mann-Whitney test, single-tailed; * $p<0.05$.

5.11 Will miR-142-3P RE be stable in the genome of CHIKV that has been passaged *in vitro* on BHK-21 cells?

The genetic stability of miR-142-3P RE incorporated into the genome of ICRES1-3F-zsGreen-miR-142-3P RE was investigated *in vitro*. The virus was passaged 5 times on BHK-21 cells at a 'high' MOI. The virus was passaged in absence of the selective pressure from miR-142-3P. The results were expressed as a proportion of the total virus population present in the sample that was unable to form plaques in presence of miR-142-3P. Detailed description of this experiment is located in 4.16.

Interestingly, only 0.2% of ICRES1-3F-zsGreen-miR-142-3P RE stock virus (inoculum) was able to form plaques in the presence of miR-142-3P (Figure 5.15). The stability of ICRES1-3F-zsGreen-miR-142-3P RE did not change significantly between passages 0 (inoculum) and 5. After 10 passages, almost 95% of the virus was still unable to form plaques in presence of miR-142-3P. The results indicated that ICRES1-3F-zsGreen-miR-142-3P was genetically stable in the absence of a selective pressure from miR-142-3P.

The above findings were notably different from the stability of SFV4-3F-zsGreen-miR-142-3P RE observed in an equivalent experiment (Figure 4.31). With each consecutive passage, the stability of SFV4-3F-zsGreen-miR-142-3P RE was gradually and markedly reduced. After 5 passages only 80.15% of the virus particles were still inhibited by the expression of miR-142-3P. Consequently, SFV4-3F-zsGreen-miR-142-3P RE was not considered to be a genetically stable construct. In spite of that, the replication of SFV4-3F-zsGreen-miR-142-3P RE was restricted in haematopoietic cells not only *in vitro*, but also *in vivo*. Altogether, the above findings strongly suggested that ICRES1-3F-zsGreen-miR-142-3P RE was sufficiently stable to be tested in the non-human primate model of CHIKV disease.

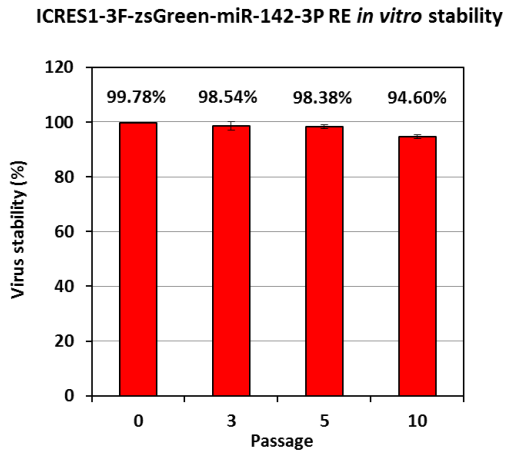

Figure 5.15. ICRES1-3F-zsGreen-miR-142-3P RE stability *in vitro*. The virus was passaged on BHK-21 cells at high MOI (estimated at 1-5). Virus stability (%) was defined as the proportion of the total virus population that was unable to form plaques in presence of miR-142-3P. Data expressed as relative mean +/- relative SD.

5.12 Investigating the role of monocyte and macrophage infection with CHIKV in the non-human primate model of chikungunya disease

Two adult cynomolgus macaques (see 2.22.1) were inoculated with 10^6 PFU of ICRES1-3F-zsGreen-miR-142-3P RE as described in 2.22.2. No control group was included, historic data (published and unpublished) were used for comparison. Animals were observed for clinical signs of disease as described in 2.22.3. Whole blood, PBMC, plasma and serum samples were collected as described in 2.22.4. Viral load in plasma was evaluated by qPCR as described in 2.22.5. Animals 31065 and 30856 were euthanised 18 and 35 days post-infection, respectively. During necropsy, samples from muscles, tendons, lymph nodes, liver, spleen, skin and joint tissue were collected as described in 2.22.4.

Both animals were successfully infected with CHIKV (Figure 5.16). The peak viraemia of approximately 10^6 CHIKV genome copy number per ml of plasma was observed on Day 2 post-infection. No virus was detected in the plasma of infected animals from Day 4 post-infection. The above results were notably different from

published kinetics of CHIKV replication in cynomolgus macaques (Labadie et al. 2010). Typical viraemia in cynomolgus macaques infected with a comparable dose of CHIKV lasted up to 7 days post-infection. The peak viral load of 10^8-10^9 CHIKV genome copy number per ml of plasma was typically observed 2 days post-infection. Altogether, the above results indicated that CHIKV encoding a marker gene zsGreen and a recognition element for miR-142-3P was attenuated in the non-human primate model of chikungunya virus disease. Unfortunately, at the time of writing this thesis no further data are available.

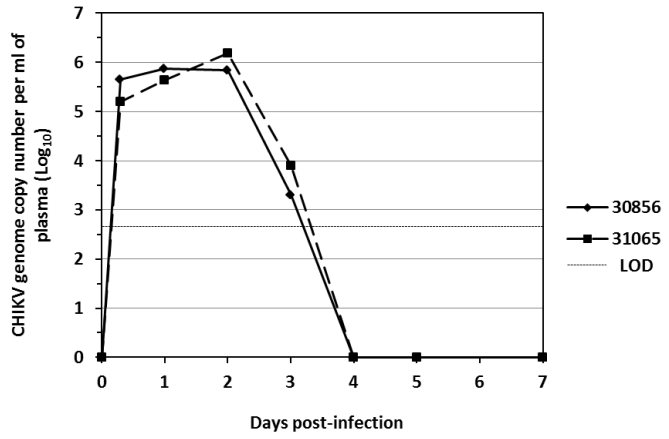

Figure 5.16. CHIKV infection in adult cynomolgus macaques. Two adult macaques were infected with 10^6 PFU of ICRES1-3F-zsGreen-miR-142-3P RE. Viral load in plasma was evaluated by qPCR. LOD=500 CHIKV genome copy number per ml of plasma.

5.13 Discussion

The principal objective of the work presented in this chapter was to generate CHIKV that was restricted in monocytes and macrophages but could replicate normally in other cells and tissues. This virus was used to investigate the role of monocyte and macrophage infection with CHIKV in the non-human primate model of chikungunya virus disease.

Key findings:

1. Presence of target sequences to cellular miR-142-3P in the genome of CHIKV restricted replication of this virus in all cells expressing miR-142-3P.

2. CHIKV encoding the RE for miR-142-3P was shown to be stable *in vitro* following serial passage on BHK-21 cells in the absence of selective pressure from miR-142-3P.

3. The pathogenesis of CHIKV encoding the RE for miR-142-3P was investigated in the non-human primate model of chikungunya virus disease. Preliminary data indicated that CHIKV encoding the RE for miR-142-3P was attenuated in cynomolgus macaques.

Replication of CHIKV encoding miR-142-3P target sequences in its genome was significantly restricted in haematopoietic IC-21 and Thp-1 cells, but not in fibroblast 3T3 and NHDF cells. The restriction of virus replication was further confirmed in non-haematopoietic Hek 293 cells modified to express miR-142-3P and in non-haematopoietic Hek 293T cells transfected with plasmids expressing miR-142-3P. The above data were in full agreement with previous findings for SFV.

In CHIKV, miR-142-3P RE or miRNA RE Control were inserted into the J region of the virus. This overall design was different to that of SFV. However, in CHIKV this position was believed to be more genetically stable than the 3' UTR (Tsetsarkin et al. 2006, Prof Andres Merits, the University of Tartu, personal communication). Indeed, the stability of CHIKV was superior to that observed for SFV. After 5

passages, over 98% of the virus was still unable to form plaques in presence of miR-142-3P. This was reduced to 95% after 10 passages. The above data suggested that ICRES1-3F-zsGreen-miR-142-3P RE was genetically stable in absence of the selective pressure from miR-142-3P. Importantly, non-haematopoietic fibroblasts and myoblasts are the primary sites of CHIKV replication *in vivo*. Hence, the majority of virus observed in the plasma of infected humans and animals is produced in absence of selective pressure from miR-142-3P. Consequently, this virus was expected to be relatively stable *in vivo*.

Both cynomolgus macaques were successfully infected with the modified CHIKV. Consequently, this study represents the first successful attempt to directly study the importance of monocyte and macrophage infection with CHIKV in the non-human primate model of the disease. Both animals demonstrated very comparable viraemia that lasted approximately 3 days. The duration of viraemia was 3-4 days shorter than expected based on historic data (Labadie et al. 2010). The peak viraemia of 10^6 CHIKV genome copy number per ml of plasma was observed on day 2 post-infection. It was approximately 2 $\log_{10}$ lower than expected based on historic data (Labadie et al. 2010).

The above results suggested that CHIKV encoding a recognition element for miR-142-3P was attenuated in the non-human primate model of chikungunya virus disease. None of the *in vitro* experiments indicated that the modified virus was attenuated in non-haematopoietic cells. Hence, the observed attenuation was likely due to restriction of virus replication in monocytes and macrophages. It is possible that an initial infection of monocytes circulating the in the blood is required to efficiently disseminated CHIKV. Similar role of monocytes in human CHIKV infection was proposed by Her et al. (2010). At the time of writing this thesis no further data were available.

Cynomolgus macaque model of CHIKV infection is very complex. Restriction of CHIKV tissue tropism does not simply promote survival of infected animals. Hence, a large proportion of disease-associated markers must be investigated to fully assess

the role of monocyte and macrophage infection with CHIKV in cynomolgus macaques. These include antibody responses, cytokine expression profiles, chemokine expression profiles, growth factors expression profiles, haematology, clinical observation, T cell responses and tissue immunohistochemistry. Fortunately, good historic data exist (published and unpublished) that can be used as the reference.

The results of this study will provide a valuable and unique insight into the mechanism of CHIKV pathogenesis in non-human primates, and in humans. However, a significant amount of further work is needed to complete this work:

1. Characterisation of ICRES1-3F-zsGreen-miR-142-3P RE replication in peripheral blood mononuclear cells (FACS, immunohistochemistry, qPCR, plaque assay);
2. Analysis of virus replication in collected tissues (muscles, tendons, skin, cartlidge, liver, spleen, lymph nodes) (immunohistochemistry, plaque assay, qPCR);
3. Characterisation of cytokine expression profiles (IFN-γ, IL-2, IL-4, IL-5, IL-13, IL-17, TNF-α, IL-1ra, IL1β, IL-6, IL-8, IL-10);
4. Characterisation of chemokine expression profiles (MIP-1α, MIP-1β);
5. Characterisation of growth factor profiles (e.g. GM-CSF);
6. Characterisation of T-cell responses (e.g. IFN-γ ELISPOT) ;
7. Characterisation of antibody responses;
8. Analysis of virus stability throughout the viraemia.

Chapter 6:

Concluding remarks

The immunobiology of viral arthritides is complex and not well understood. Virus replication or presence of a pathogen (or pathogen-derived material) may induce innate or adaptive immune responses that mediate cell damage (Suhrbier et al. 2009). Virus infections have been proposed to induce autoimmune responses (Suhrbier et al. 2009). This can be achieved via molecular mimicry or activation of self-reactive lymphocytes by inflammatory conditions at the site of infection. It is possible that phagocytosis of apoptotic debris containing virus material by antigen-presenting cells leads to robust and uncontrolled immune response that induces autoimmunity against self-antigens present in apoptotic debris (Krejbich-Trotot et al. 2011). Autoimmune response can also be induced by presence of viral antigens and nucleic acids in affected joints (Suhrbier et al. 2009). Cell damage is then usually mediated by adaptive immune response against viral antigen, which may cause inflammation and long-term arthritis. Interestingly, double stranded RNA (dsRNA), which is an intermediate in alphavirus replication, may stimulate inflammation when present in synovial fluid (Bokarewa et al. 2008). CHIKV dsRNA, however, is not normally observed in synovial fluid in patients suffering from arthritis (Grivard et al., 2007).

In this study, the interaction of human MDMs with SFV was investigated. The results demonstrated that human MDMs are refractory to infection with purified SFV but can be infected via apoptotic debris from virus-infected cells. Importantly, virus particles are not required to infect human MDMs via apoptotic debris from virus-infected cells. The SFV infectious material contained within apoptotic debris is viral genomic RNA either in the cytoplasm or associated with replication complexes.

Macrophages are one of the major cell populations that infiltrates joint tissue in polyarthritis (Assunção-Miranda et al. 2010). They are part of innate and adaptive immune responses that are activated in response to virus infection. As described previously, proinflammatory factors associated with CHIKV arthralgia/arthritis include MCP-1, IL-6, IL-8, IFN-α, IL-6, IL-12 and GM-CSF (Hoarau et al. 2010, Chow et al. 2011). These cytokines and chemokines suggest that rheumatic disease is associated at least in part with macrophage recruitment and activation (Suhrbier & Mahalingam, 2009). Furthermore, long-term presence of IgM and elevated levels of

IL-12 and IFN-α suggests that CHIKV virus infection might be persistence in PBMC (Hoarau et al. 2010). Lack of increased levels of TNF-α is surprising. It is possible, however, that TNF-α is expressed locally, at the site of inflammation. It has been suggested that chronic infection of macrophages by some viruses affects their differentiation, which results in an alternative phenotype different from M1/M2 characteristics that contributes to tissue fibrosis (Hoarau et al. 2010). This has not yet been investigated in detail.

In this study, the role of monocyte and macrophage infection with CHIKV was investigated. The tissue tropism of CHIKV was restricted by insertion of target sequences to haematopoietic-specific miR-142-3P into the virus genome. Replication of modified CHIKV was restricted in haematopoietic cells and the virus was shown to be very stable *in vitro*. The pathogenesis of CHIKV encoding the RE for miR-142-3P was investigated in the cynomolgus macaque model of CHIKV disease. At the time of writing this thesis the majority of samples were not yet analysed. Once available, the results of this study will provide a valuable insight into CHIKV pathogenesis in non-human primates, and in humans.

References

1. Adams JM., Cory S. The Bcl-2 protein family: arbiters of cell survival. *Science* 1998; 281:1322–1326.

2. Adey A., Burton JN., Kitzman JO., Hiatt JB., et al. The haplotype-resolved genome and epigenome of the aneuploid HeLa cancer cell line. *Nature* 2013; 500:207–211.

3. Ahola T., Laakkonen P., Vihinen H., Kääriäinen L. Critical residues of Semliki Forest virus RNA capping enzyme involved in methyltransferase and guanylyltransferase-like activities. *J. Virol.* 1997; 71:392–397.

4. Akahata W., Yang Z., Andersen H., Sun S., et al. A virus-like particle vaccine for epidemic chikungunya virus protects nonhuman primates against infection. *Nat. Med.* 2010; 16:334–338.

5. Aliperti G., Schlesinger M. Evidence for an autoprotease activity of Sindbis virus capsid protein. *Virology* 1978; 90:366–369.

6. Allsopp TE., Fazakerley JK. Altruistic cell suicide and the specialized case of the virus-infected nervous system. *Trends Neurosci.* 2000; 23:284–290.

7. Amor S., Scallan MF., Morris MM., Dyson H., et al. Role of immune responses in protection and pathogenesis during Semliki Forest virus encephalitis. *J. Gen. Virol.* 1996; 77:281–291.

8. Antalis TM., Linn ML., Donnan K., Mateo L., et al. The serine proteinase inhibitor (serpin) plasminogen activation inhibitor type 2 protects against viral cytopathic effects by constitutive interferon alpha/beta priming. *J. Exp. Med.* 1998; 187:1799–1811.

9. Arpino C., Curatolo P., Rezza G. Chikungunya and the nervous system: what we do and do not know. *Rev. Med. Virol.* 2009; 19:121–129.

10. Assunção-Miranda I., Bozza MT. Pro-Inflamatory response resulting from Sindbis virus infection of human macrophages: implications for the pathogenesis of viral arthritis. *J. Med. Virol.* 2010; 82:164–174.

11. Assunção-Miranda I., Cruz-Oliveira C., Da Poian AT. Molecular mechanisms involved in the pathogenesis of alphavirus-induced arthritis. *Biomed Res. Int.* 2013; 2013:973516.

12. Atasheva S., Gorchakov R., English R., Frolov I., et al. Development of Sindbis viruses encoding nsP2/GFP chimeric proteins and their application for studying nsP2 functioning. *J. Virol.* 2007; 81:5046–5057.

13. Atkins GJ. The pathogenesis of alphaviruses. *ISRN Virol.* 2013; 2013:1–22.

14. Balachandran S., Roberts PC., Kipperman T., Bhalla KN., et al. Alpha/beta interferons potentiate virus-induced apoptosis through activation of the FADD/Caspase-8 death signaling pathway. *J. Virol.* 2000; 74:1513–1523.

15. Balluz I., Glasgow G., Killen H., Mabruk M., et al. Virulent and avirulent strains of Semliki Forest virus show similar cell tropism for the murine central nervous system but differ in the severity and rate of induction of cytolytic damage. *Neuropathol. Appl. Neurobiol.* 1993; 19:233–239.

16. Barnes D., Kunitomi M., Vignuzzi M., Saksela K., et al. Harnessing endogenous miRNAs to control virus tissue tropism as a strategy for developing attenuated virus vaccines. *Cell Host Microbe* 2008; 4:239–248.

17. Barry G., Fragkoudis R., Ferguson MC., Lulla A., et al. Semliki Forest virus-induced endoplasmic reticulum stress accelerates apoptotic death of mammalian cells. *J. Virol.* 2010; 84:7369–7377.

18. Bartel DP. MicroRNAs: genomics, biogenesis, mechanism, and function. *Cell* 2004; 116:281–297.

19. Barton DJ., Sawicki SG., Sawicki DL. Solubilization and immunoprecipitation of alphavirus replication complexes. *J. Virol.* 1991; 65:1496–1506.

20. Baskerville S., Bartel DP. Microarray profiling of microRNAs reveals frequent coexpression with neighboring miRNAs and host genes. *RNA* 2005; 11:241–247.

21. Berglund P., Sjöberg M., Garoff H., Atkins G., et al. Semliki Forest virus expression system: production of conditionally infectious recombinant particles. *Biotechnology (N Y)* 1993; 11:916–920.

22. Bernard KA., Klimstra WB., Johnston RE. Mutations in the E2 glycoprotein of Venezuelan equine encephalitis virus confer heparan sulfate interaction, low morbidity, and rapid clearance from blood of mice. *Virology* 2000; 276:93–103.

23. Bernard E., Solignat M., Gay B., Chazal N., et al. Endocytosis of chikungunya virus into mammalian cells: role of clathrin and early endosomal compartments. *PLoS One* 2010; 5:e11479.

24. Bick MJ., Carroll J-WN., Gao G., Goff SP., et al. Expression of the zinc-finger antiviral protein inhibits alphavirus replication. *J. Virol.* 2003; 77:11555–11562.

25. Bissels U., Wild S., Tomiuk S., Hafner M., et al. Combined characterization of microRNA and mRNA profiles delineates early differentiation pathways of CD133+ and CD34+ hematopoietic stem and progenitor cells. *Stem Cells* 2011; 29:847–857.

26. Bokarewa M., Tarkowski A., Lind M., Dahlberg L., et al. Arthritogenic dsRNA is present in synovial fluid from rheumatoid arthritis patients with an erosive disease course. *Eur. J. Immunol.* 2008; 38:3237–3244.

27. Bonatti S., Migliaccio G., Blobel G., Walter P. Role of signal recognition particle in the membrane assembly of Sindbis viral glycoproteins. *Eur. J. Biochem.* 1984; 140:499–502.

28. Bottomley R., Trainer A., Griffin M. Enzymatic and chromosomal characterization of HeLa variants. *J. Cell Biol.* 1969; 41:806–815.

29. Bouquillard E., Combe B. A report of 21 cases of rheumatoid arthritis following chikungunya fever. A mean follow-up of two years. *Join Bone Spine* 2009; 76:654–657.

30. Bradish CJ., Allner K., Maber HB. The virulence of original and derived strains of Semliki Forest virus for mice, guinea-pigs and rabbits. *J. Gen. Virol.* 1971; 12:141–160.

31. Brault AC., Foy B., Myles K., Kelly L., et al. Infection patterns of O'nyong nyong virus in the malaria-transmitting mosquito, Anopheles gambiae. *Insect Mol. Biol.* 2004; 13:625–635.

32. Brown BD., Venneri MA., Zingale A., Sergi Sergi L., et al. Endogenous microRNA regulation suppresses transgene expression in hematopoietic lineages and enables stable gene transfer. *Nat. Med.* 2006; 12:585–591.

33. Bushati N., Cohen S. MicroRNA functions. *Annu Rev Dev Cell Dev Biol* 2007; 23:175–205.

34. Byrnes AP., Griffin DE. Binding of Sindbis virus to cell surface heparan sulfate. *J. Virol.* 1998; 72:7349–7356.

35. Caley I., Betts M., Davies N., Swanstrom R., et al. Venezuelan equine encephalitis virus vectors expressing HIV-1 proteins: vector design strategies for improved vaccine efficacy. *Vaccine* 1999; 17:3124–3135.

36. Cavrini F., Gaibani P., Pierro AM., Rossini G., et al. Chikunguny: an emerging and spreading arthropod-borne viral disease. *J Inf Dev Ctries* 2009; 3:744–752.

37. Cecconi F., Alvarez-Bolado G., Meyer BI., Roth KA., et al. Apaf1 (CED-4 homolog) regulates programmed cell death in mammalian development. *Cell* 1998; 94:727–737.

38. Chaaithanya IK., Muruganandam N., Sundaram SG., Kawalekar O., et al. Role of proinflammatory cytokines and chemokines in chronic arthropathy in CHIKV infection. *Viral Immunol.* 2011; 24:265–271.

39. Chang L-J., Dowd KA., Mendoza FH., Saunders JG., et al. Safety and tolerability of chikungunya virus-like particle vaccine in healthy adults: a phase 1 dose-escalation trial. *Lancet* 2014; 384:2046–2052.

40. Chareonsirisuthigul T., Kalayanarooj S., Ubol S. Dengue virus (DENV) antibody-dependent enhancement of infection upregulates the production of anti-inflammatory cytokines, but suppresses anti-DENV free radical and pro-inflammatory cytokine production, in THP-1 cells. *J. Gen. Virol.* 2007; 88:365–375.

41. Chen J., Miller D., Katow S., Frey T. Expression of the rubella virus structural proteins by an infectious Sindbis virus vector. *Arch. Virol.* 1995; 140:2075–2084.

42. Chen C., Li L., Lodish H., Bartel D. MicroRNAs modulate hematopoietic lineage differentiation. *Science* 2004; 303:83–86.

43. Chen Y-B., Seo SY., Kirsch DG., Sheu T-T., et al. Alternate functions of viral regulators of cell death. *Cell Death Differ.* 2006; 13:1318–1324.

44. Chen K., Rajewsky N. The evolution of gene regulation by transcription factors and microRNAs. *Nat Rev Genet* 2007; 8:93–103.

45. Cheng RH., Kuhn RJ., Olson NH., Rossmann MG., et al. Nucleocapsid and glycoprotein organization in an enveloped virus. *Cell* 1995; 80:621–630.

46. Cheng EH., Levine B., Boise LH., Thompson CB., et al. Bax-independent inhibition of apoptosis by Bcl-XL. *Nature* 1996; 379:554–556.

47. Chow A., Her Z., Ong EKS., Chen J., et al. Persistent arthralgia induced by chikungunya virus infection is associated with interleukin-6 and granulocyte macrophage colony-stimulating factor. *J. Infect. Dis.* 2011; 203:149–157.

48. Colin A., Faideau M., Dufour N., Auregan G., et al. Engineered lentiviral vector targeting astrocytes in vivo. *Glia* 2009; 57:667–679.

49. Colmenero P., Berglund P., Kambayashi T., Biberfeld P., et al. Recombinant Semliki Forest virus vaccine vectors: the route of injection determines the localization of vector RNA and subsequent T cell response. *Gene Ther.* 2001; 8:1307–1314.

50. Cormack B., Valdivia R., Falkow S. FACS-optimized mutants of the green fluorescent protein (GFP). *Gene* 1996; 173:33–38.

51. Couderc T., Chrétien F., Schilte C., Disson O., et al. A mouse model for chikungunya: young age and inefficient type-I interferon signaling are risk factors for severe disease. *PLoS Pathog.* 2008; 4:e29.

52. Couderc T., Lecuit M. Focus on chikungunya pathophysiology in human and animal models. *Microbes Infect.* 2009; 11:1197–1205.

53. Danial NN., Korsmeyer SJ. Cell death: critical control points. *Cell* 2004; 116:205–219.

54. Das T., Jaffar-Bandjee MC., Hoarau JJ., Krejbich-Trotot P., et al. Chikungunya fever: CNS infection and pathologies of a re-emerging arbovirus. *Prog. Neurobiol.* 2010; 91:121–129.

55. Das PK., Merits A., Lulla A. Functional cross-talk between distant domains of chikungunya virus non-structural protein 2 is decisive for its RNA-modulating activity. *J. Biol. Chem.* 2014; 289:5635–5653.

56. Davis N., Willis L., Smith J., Johnston R. In vitro synthesis of infectious Venezuelan equine encephalitis virus RNA from a cDNA clone: analysis of a viable deletion mutant. *Virology* 1989; 171:189–204.

57. de Andrade DC., Jean S., Clavelou P., Dallel R., et al. Chronic pain associated with the chikungunya fever: long lasting burden of an acute illness. *BMC Infect. Dis.* 2010; 10:31.

58. Deuber SA., Pavlovic J. Virulence of a mouse-adapted Semliki Forest virus strain is associated with reduced susceptibility to interferon. *J. Gen. Virol.* 2007; 88:1952–1959.

59. Dhanwani R., Khan M., Bhaskar ASB., Singh R., et al. Characterization of chikungunya virus infection in human neuroblastoma SH-SY5Y cells: role of apoptosis in neuronal cell death. *Virus Res.* 2012; 163:563–572.

60. Ding M., Schlesinger M. Evidence that Sindbis virus nsP2 is an autoprotease which processes the virus nonstructural polyprotein. *Virology* 1989; 171:280–284.

61. Djuranovic S., Nahvi A., Green R. MiRNA-mediated gene silencing by translational repression followed by mRNA deadenylation and decay. *Science* 2012; 336:237–240.

62. Doench J. Specificity of microRNA target selection in translational repression. *Gene Dev* 2004; 18:504–511.

63. Dryga S., Dryga O., Schlesinger S. Identification of mutations in a Sindbis virus variant able to establish persistent infection in BHK cells: the importance of a mutation in the nsP2 gene. *Virology* 1997; 228:74–83.

64. Dupuis-Maguiraga L., Noret M., Brun S., Grand R Le., et al. Chikungunya disease: infection-associated markers from the acute to the chronic phase of arbovirus-induced arthralgia. *PLoS Negl. Trop. Dis.* 2012; 6:e1446.

65. Edge RE., Falls TJ., Brown CW., Lichty BD., et al. A let-7 microRNA-sensitive vesicular stomatitis virus demonstrates tumor-specific replication. *Mol. Ther.* 2008; 16:1437–1443.

66. Elmore S. Apoptosis: a review of programmed cell death. *Toxicol. Pathol.* 2007; 35:495–516.

67. Everett H., McFadden G. Apoptosis: an innate immune response to virus infection. *Trends Microbiol.* 1999; 7:160–165.

68. Fazakerley JK., Pathak S., Scallan M., Amor S., et al. Replication of the A7(74) strain of SFV in neurons. *Viral Immunol.* 1993; 195:627–637.

69. Fazakerley JK. Pathogenesis of Semliki Forest virus encephalitis. *J. Neurovirol.* 2002; 8 Suppl 2:66–74.

70. Fazakerley JK. Semliki Forest virus infection of laboratory mice: a model to study the pathogenesis of viral encephalitis. *Arch. Virol. Suppl.* 2004; 18:179–190.

71. Feng C., Tan M., Sun W., Shi Y., et al. Attenuation of the influenza virus by microRNA response element in vivo and protective efficacy against 2009 pandemic H1N1 virus in mice. *Int. J. Infect. Dis.* 2015; 38:146-152.

72. Ferguson MC., Saul S., Fragkoudis R., Weisheit S., et al. The ability of the encephalitic arbovirus Semliki Forest virus to cross the blood brain barrier is determined by the charge of the E2 glycoprotein. *J. Virol.* 2015; 89:7536–7549.

73. Fleming P. Age-dependent and strain-related differences of virulence of Semliki Forest virus in mice. *J. Gen. Virol.* 1977; 37:93–105.

74. Flipse J., Wilschut J., Smith J. Molecular mechanisms involved in antibody-dependent enhancement of dengue virus infection in humans. *Traffic* 2013; 14:25–35.

75. Fragkoudis R., Breakwell L., McKimmie C., Boyd A., et al. The type I interferon system protects mice from Semliki Forest virus by preventing widespread virus dissemination in extraneural tissues, but does not mediate the restricted replication of avirulent virus in central nervous system neurons. *J. Gen. Virol.* 2007; 88:3373–3384.

76. Frolov I., Hoffman T., Pragai B., Dryga S., et al. Alphavirus-based expression vectors: strategies and applications. *Proc. Natl. Acad. Sci. U.S.A.* 1996; 93:11371–11377.

77. Frolov I., Agapov E., Hoffman TA., Prágai BM., et al. Selection of RNA replicons capable of persistent noncytopathic replication in mammalian cells. *J. Virol.* 1999; 73:3854–3865.

78. Frolov I., Garmashova N., Atasheva S., Frolova EI. Random insertion mutagenesis of Sindbis virus nonstructural protein 2 and selection of variants incapable of downregulating cellular transcription. *J. Virol.* 2009; 83:9031–9044.

79. Frolova E., Frolov I., Schlesinger S. Packaging signals in alphaviruses. *J. Virol.* 1997; 71:248–258.

80. Frolova E., Gorchakov R., Garmashova N., Atasheva S., et al. Formation of nsP3-specific protein complexes during Sindbis virus replication. *J. Virol.* 2006; 80:4122–4134.

81. Frolova EI., Gorchakov R., Pereboeva L., Atasheva S., et al. Functional Sindbis virus replicative complexes are formed at the plasma membrane. *J. Virol.* 2010; 84:11679–11695.

82. Froshauer S., Kartenbeck J., Helenius A. Alphavirus RNA replicase is located on the cytoplasmic surface of endosomes and lysosomes. *J. Cell Biol.* 1988; 107:2075–2086.

83. García-Arriaza J., Cepeda V., Hallengärd D., Sorzano CÓS., et al. A novel poxvirus-based vaccine, MVA-CHIKV, is highly immunogenic and protects mice against chikungunya infection. *J. Virol.* 2014; 88:3527–3547.

84. Gardner J., Anraku I., Le TT., Larcher T., et al. Chikungunya virus arthritis in adult wild-type mice. *J. Virol.* 2010; 84:8021–8032.

85. Gardner CL., Ebel GD., Ryman KD., Klimstra WB. Heparan sulfate binding by natural Eastern equine encephalitis viruses promotes neurovirulence. *Proc. Natl. Acad. Sci. U.S.A.* 2011; 108:16026–16031.

86. Gardner CL., Choi-Nurvitadhi J., Sun C., Bayer A., et al. Natural variation in the heparan sulfate binding domain of the eastern equine encephalitis virus E2 glycoprotein alters interactions with cell surfaces and virulence in mice. *J. Virol.* 2013; 87:8582–8590.

87. Gardner CL., Hritz J., Sun C., Vanlandingham DL., et al. Deliberate attenuation of chikungunya virus by adaptation to heparan sulfate-dependent infectivity: a model for rational arboviral vaccine design. *PLoS Negl. Trop. Dis.* 2014; 8:e2719.

88. Garmashova N., Gorchakov R., Frolova E., Frolov I. Sindbis virus nonstructural protein nsP2 is cytotoxic and inhibits cellular transcription. *J. Virol.* 2006; 80:5686–5696.

89. Garmashova N., Gorchakov R., Volkova E., Paessler S., et al. The Old World and New World alphaviruses use different virus-specific proteins for induction of transcriptional shutoff. *J. Virol.* 2007; 81:2472–2484.

90. Garmashova N., Atasheva S., Kang W., Weaver SC., et al. Analysis of Venezuelan equine encephalitis virus capsid protein function in the inhibition of cellular transcription. *J. Virol.* 2007; 81:13552–13565.

91. Garoff H., Frischauf A., Simons K., Lehrach H., et al. Nucleotide sequence of cDNA coding for Semliki Forest virus membrane glycoproteins. *Nature* 1980; 288:236–241.

92. Garoff H., Huylebroeck D., Robinson A., Tillman U., et al. The signal sequence of the p62 protein of Semliki Forest virus is involved in initiation but not in completing chain translocation. *J. Cell Biol.* 1990; 111:867–876.

93. Gay B., Bernard E., Solignat M., Chazal N., et al. pH-dependent entry of chikungunya virus into Aedes albopictus cells. *Infect. Genet. Evol.* 2012; 12:1275–1281.

94. Gey G., Coffman W., Kubicek M. Tissue culture studies of the proliferative capacity of cervical carcinoma and normal epithelium. *Cancer Res.* 1952; 12:264–265.

95. Glanville N., Ranki M., Morser J., Kääriäinen L., et al. Initiation of translation directed by 42S and 26S RNAs from Semliki Forest virus in vitro. *Proc. Natl. Acad. Sci. U.S.A.* 1976; 73:3059–3063.

96. Glasgow GM., Sheahan BJ., Atkins GJ., Wahlberg JM., et al. Two mutations in the envelope glycoprotein E2 of Semliki Forest virus affecting the maturation and entry patterns of the virus alter pathogenicity for mice. *Virology* 1991; 185:741–748.

97. Glasgow GM., Mcgee MM., Sheahan BJ., Atkins GJ. Death mechanisms in cultured cells infected by Semliki Forest virus. *J Gen.Virol* 1997; 78(7):1559–1563.

98. Glasgow GM., McGee MM., Tarbatt CJ., Mooney DA., et al. The Semliki Forest virus vector induces p53-independent apoptosis. *J. Gen. Virol.* 1998; 79:2405–2410.

99. Gomez de Cedrón M., Ehsani N., Mikkola ML., Garcia JA., et al. RNA helicase activity of Semliki Forest virus replicase protein NSP2. *FEBS Lett.* 1999; 448:19–22.

100. Gorchakov R., Frolova E., Frolov I., Cells V. Inhibition of transcription and translation in Sindbis virus-infected cells. *J. Virol.* 2005; 79:9397–9409.

101. Gottfried E., Kunz-Schughart LA., Weber A., Rehli M., et al. Expression of CD68 in non-myeloid cell types. *Scand. J. Immunol.* 2008; 67:453–463.

102. Gottwein E., Cai X., Cullen BR. A novel assay for viral microRNA function identifies a single nucleotide polymorphism that affects Drosha processing. *J. Virol.* 2006; 80:5321–5326.

103. Gough PJ., Gordon S., Greaves DR. The use of human CD68 transcriptional regulatory sequences to direct high-level expression of class A scavenger receptor in macrophages in vitro and in vivo. *Immunology* 2001; 103:351–361.

104. Goujon M., McWilliam H., Li W., Valentin F., et al. A new bioinformatics analysis tools framework at EMBL-EBI. *Nucleic Acids Res.* 2010; 38:W695–W699.

105. Grakoui A., Levis R., Raju R., Huang H V., et al. A cis-acting mutation in the Sindbis virus junction region which affects subgenomic RNA synthesis. *J. Virol.* 1989; 63:5216–5227.

106. Grandadam M., Caro V., Plumet S., Thiberge JM., et al. Chikungunya virus, southeastern France. *Emerg. Infect. Dis.* 2011; 17:910–913.

107. Grandgirard D., Studer E., Monney L., Belser T., et al. Alphaviruses induce apoptosis in Bcl-2-overexpressing cells: evidence for a caspase-mediated, proteolytic inactivation of Bcl-2. *EMBO J.* 1998; 17:1268–1278.

108. Griffin DE., Hardwick JM. Regulators of apoptosis on the road to persistent alphavirus infection. *Annu. Rev. Microbiol.* 1997; 51:565–592.

109. Grimley PM., Berezesky IK., Friedman RM. Cytoplasmic structures associated with an arbovirus infection: loci of viral ribonucleic acid synthesis. *J. Virol.* 1968; 2:1326–1338.

110. Grimley PM., Friedman RM. Arboviral infection of voluntary striated muscles. *J. Virol.* 1970; 122:45–52.

111. Grivard P., Le Roux K., Laurent P., Fianu A., et al. Molecular and serological diagnosis of chikungunya virus infection. *Pathol Biol (Paris)* 2007; 55(10):490-494.

112. van der Groen G., Vanden Berghe D., Pattyn S. Interaction of mouse peritoneal macrophages with different arboviruses in vitro. *J. Gen. Virol.* 1976; 34:353–361.

113. de Groot RJ., Hardy WR., Shirako Y., Strauss JH. Cleavage-site preferences of Sindbis virus polyproteins containing the non-structural proteinase. Evidence for temporal regulation of polyprotein processing in vivo. *EMBO J.* 1990; 9:2631–2638.

114. de Groott RJ., Rümenapf T., Kuhn RJ., Strauss EG., et al. Sindbis virus RNA polymerase is degraded by the N-end rule pathway. *Proc. Natl. Acad. Sci. U.S.A.* 1991; 88:8967–8971.

115. Guo H., Ingolia N., Weissman J., Bartel D. Mammalian microRNAs predominantly act to decrease target mRNA levels. *Nature* 2010; 466:835–840.

116. Hahn YS., Strauss EG., Strauss JH. Mapping of RNA-temperature-sensitive mutants of Sindbis virus: assignment of complementation groups A, B, and G to nonstructural proteins. *J. Virol.* 1989; 63:3142–3150.

117. Hall T. BioEdit: a user-friendly biological sequence alignment editor and analysis program for Windows 95/98/NT. *Nucleic Acids Symp. Ser.* 1999; 41:95–98.

118. Hallengärd D., Lum F-M., Kümmerer BM., Lulla A., et al. Prime-boost immunization strategies against chikungunya virus. *J. Virol.* 2014; 88:13333–13343.

119. Hamer D., Chen L. Chikungunya: establishing a new home in the Western hemisphere. *Ann Intern Med* 2014; 161:827–828.

120. Hardy WR., Strauss JH. Processing the nonstructural polyproteins of Sindbis virus: nonstructural proteinase is in the C-terminal half of nsP2 and functions both in cis and in trans. *J. Virol.* 1989; 63:4653–4664.

121. He L., Hannon G. MicroRNAs: small RNAs with a big role in gene regulation. *Nat Rev Genet* 2004; 5:522–531.

122. Heil ML., Albee A., Strauss JH., Kuhn RJ. An amino acid substitution in the coding region of the E2 glycoprotein adapts Ross River virus to utilize heparan sulfate as an attachment moiety. *J. Virol.* 2001; 75:6303–6309.

123. Heiss BL., Maximova OA., Pletnev AG. Insertion of microRNA targets into the flavivirus genome alters its highly neurovirulent phenotype. *J. Virol.* 2011; 85:1464–1472.

124. Heiss BL., Maximova OA., Thach DC., Speicher JM., et al. MicroRNA targeting of neurotropic flavivirus: effective control of virus escape and reversion to neurovirulent phenotype. *J. Virol.* 2012; 86:5647–5659.

125. Henderson BE., Metselaar D., Kirya GB., Timms GL. Investigations into yellow fever virus and other arboviruses in the northern regions of Kenya. *Bull. World Health Organ.* 1970; 42:787–795.

126. Her Z., Kam Y-W., Lin RTP., Ng LFP. Chikungunya: a bending reality. *Microbes Infect.* 2009; 11:1165–1176.

127. Her Z., Malleret B., Chan M., Ong EKS., et al. Active infection of human blood monocytes by chikungunya virus triggers an innate immune response. *J. Immunol.* 2010; 184:5903–5913.

128. Higashi N., Matsumoto A., Tabata K., Nagatomo Y. Electron microscope study of development of chikungunya virus in green monkey kidney stable (VERO) cells. *Virology* 1967; 33:55–69.

129. Higgs S., Oray C., Myles K., Beaty B. Infecting larval arthropods with a chimeric, double subgenomic Sindbis virus vector to express genes of interest. *Biotechniques* 1999; 27:908–911.

130. Hoarau J-J., Jaffar Bandjee M-C., Krejbich-Trotot P., Das T., et al. Persistent chronic inflammation and infection by chikungunya arthritogenic alphavirus in spite of a robust host immune response. *J. Immunol.* 2010; 184:5914–5927.

131. Hume DA., Ross IL., Himes SR., Sasmono RT., et al. The mononuclear phagocyte system revisited. *J. Leukoc. Biol.* 2002; 72:621–627.

132. Hume DA. The mononuclear phagocyte system. *Curr. Opin. Immunol.* 2006; 18:49–53.

133. Ito S., Naito M., Kobayashi Y., Takatsuka H., et al. Roles of a macrophage receptor with collagenous structure (MARCO) in host defense and heterogeneity of splenic marginal zone macrophages. *Arch Histol Cytol.* 1999; 62:83–95.

134. Jackson AC., Rossiter JP. Apoptotic cell death is an important cause of neuronal injury in experimental Venezuelan equine encephalitis virus infection of mice. *Acta Neuropathol.* 1997; 93:349–353.

135. Jaffar-Bandjee MC., Das T., Hoarau JJ., Krejbich-Trotot P., et al. Chikungunya virus takes centre stage in virally induced arthritis: possible cellular and molecular mechanisms to pathogenesis. *Microbes Infect.* 2009; 11:1206–1218.

136. Jan JT., Griffin DE. Induction of apoptosis by Sindbis virus occurs at cell entry and does not require virus replication. *J. Virol.* 1999; 73:10296–10302.

137. Jin P., Wang E., Ren J., Childs R., et al. Differentiation of two types of mobilized peripheral blood stem cells by microRNA and cDNA expression analysis. *J. Transl. Med.* 2008; 6:39.

138. Joe AK., Foo HH., Kleeman L., Levine B. The transmembrane domains of Sindbis virus envelope glycoproteins induce cell death. *J Virol* 1998; 72:3935–3943.

139. Johnson DC., Schlesinger MJ., Elson EL. Photobleaching recovery measurements reveal differences in envelopment of Sindbis and vesicular stomatitis viruses. *Cell* 1981; 23:423–431.

140. Joubert P-E., Werneke SW., de la Calle C., Guivel-Benhassine F., et al. Chikungunya virus-induced autophagy delays caspase-dependent cell death. *J. Exp. Med.* 2012; 209:1029–1047.

141. Judith D., Mostowy S., Bourai M., Gangneux N., et al. Species-specific impact of the autophagy machinery on chikungunya virus infection. *EMBO Rep.* 2013; 14:534–544.

142. Kääriäinen L., Soderlund H. Structure and replication of alpha-viruses. *Curr Top Microbiol Immunol* 1978; 82:15–69.

143. Kääriäinen L., Ahola T. Functions of alphavirus nonstructural proteins in RNA replication. *Prog. Nucleic Acid Res. Mol. Biol.* 2002; 71:187–222.

144. Kallio K., Hellström K., Balistreri G., Spuul P., et al. Template RNA length determines the size of replication complex spherules for Semliki Forest virus. *J. Virol.* 2013; 87:9125–9134.

145. Kamer G., Argos P. Primary structural comparison of RNA-dependent polymerases from plant, animal and bacterial viruses. *Nucleic Acids Res.* 1984; 12:7269–7282.

146. Kamrud KI., Coffield VM., Owens G., Goodman C., et al. In vitro and in vivo characterization of microRNA-targeted alphavirus replicon and helper RNAs. *J. Virol.* 2010; 84:7713–7725.

147. Karlsson G., Liljeström P. Live viral vectors: Semliki Forest virus. *Methods Mol Med* 2003; 87:69–82.

148. Kaur P., Thiruchelvan M., Lee RCH., Chen H., et al. Inhibition of chikungunya virus replication by harringtonine, a novel antiviral that suppresses viral protein expression. *Antimicrob. Agents Chemother.* 2013; 57:155–167.

149. Kelly EJ., Hadac EM., Greiner S., Russell SJ. Engineering microRNA responsiveness to decrease virus pathogenicity. *Nat. Med.* 2008; 14:1278–1283.

150. Kelly EJ., Nace R., Barber GN., Russell SJ. Attenuation of vesicular stomatitis virus encephalitis through microRNA targeting. *J. Virol.* 2010; 84:1550–1562.

151. Kelvin AA., Banner D., Silvi G., Moro ML., et al. Inflammatory cytokine expression is associated with chikungunya virus resolution and symptom severity. *PLoS Negl. Trop. Dis.* 2011; 5:e1279.

152. Kepp O., Senovilla L., Galluzzi L., Panaretakis T., et al. Viral subversion of immunogenic cell death. *Cell Cycle* 2009; 8:860–869.

153. Keränen S., Kääriäinen L. Functional defects of RNA-negative temperature-sensitive mutants of Sindbis and Semliki Forest viruses. *J. Virol.* 1979; 32:19–29.

154. Kerr J., Wyllie A., Currie A. Apoptosis: a basic biological phenomenon with wide-ranging implications in tissue kinetics. *Br. J. Cancer* 1972; 26:239–257.

155. Khan AH., Morita K., Parquet M del C., Hasebe F., et al. Complete nucleotide sequence of chikungunya virus and evidence for an internal polyadenylation site. *J. Gen. Virol.* 2002; 83:3075–3084.

156. Kielian M., Chanel-Vos C., Liao M. Alphavirus entry and membrane fusion. *Viruses* 2010; 2:796–825.

157. Kiiver K., Merits A., Sarand I. Novel vectors expressing anti-apoptotic protein Bcl-2 to study cell death in Semliki Forest virus-infected cells. *Virus Res.* 2008; 131:54–64.

158. Kim J., Dittgen T., Nimmerjahn A., Waters J., et al. Sindbis vector SINrep(nsP2S726): a tool for rapid heterologous expression with attenuated cytotoxicity in neurons. *J. Neurosci. Methods* 2004; 133:81–90.

159. Kim DY., Firth AE., Atasheva S., Frolova EI., et al. Conservation of a packaging signal and the viral genome RNA packaging mechanism in alphavirus evolution. *J. Virol.* 2011; 85:8022–8036.

160. Kinne RW., Bräuer R., Stuhlmüller B., Palombo-Kinne E., et al. Macrophages in rheumatoid arthritis. *Arthritis Res* 2000; 2:189–202.

161. Klimstra WB., Ryman KD., Johnston RE. Adaptation of Sindbis virus to BHK cells selects for use of heparan sulfate as an attachment receptor. *J. Virol.* 1998; 72:7357–7366.

162. Klimstra WB., Heidner HW., Johnston RE. The furin protease cleavage recognition sequence of Sindbis virus PE2 can mediate virion attachment to cell surface heparan sulfate. *J. Virol.* 1999; 73:6299–6306.

163. Klimstra WB., Nangle EM., Smith MS., Yurochko AD., et al. DC-SIGN and L-SIGN can act as attachment receptors for alphaviruses and distinguish between mosquito cell- and mammalian cell-derived viruses. *J. Virol.* 2003; 77:12022–12032.

164. Kohlhuber F., Rogers NC., Watling D., Feng J., et al. A JAK1 / JAK2 chimera can sustain alpha and gamma interferon responses. *Mol. Cell. Biol.* 1997; 17:695–706.

165. Koscianska E., Starega-Roslan J., Krzyzosiak W. The role of Dicer protein partners in the processing of microRNA precursors. *PLoS One* 2011; 6:e28548.

166. Krakauer DC., Payne RJ. The evolution of virus-induced apoptosis. *Proc. Biol. Sci.* 1997; 264:1757–1762.

167. Krejbich-Trotot P., Denizot M., Hoarau J-J., Jaffar-Bandjee M-C., et al. Chikungunya virus mobilizes the apoptotic machinery to invade host cell defenses. *FASEB J.* 2011; 25:314–25.

168. Krejbich-Trotot P., Gay B., Li-Pat-Yuen G., Hoarau J-J., et al. Chikungunya triggers an autophagic process which promotes viral replication. *Virol. J.* 2011; 8:432.

169. Kroemer G., Galluzzi L., Brenner C. Mitochondrial membrane permeabilization in cell death. *Physiol. Reveiw* 2007; 87:99–163.

170. Kujala P., Ikäheimonen A., Ehsani N., Vihinen H., et al. Biogenesis of the Semliki Forest virus RNA replication complex. *J. Virol.* 2001; 75:3873–3884.

171. Kumar S., Jaffar-Bandjee M-C., Giry C., Connen de Kerillis L., et al. Mouse macrophage innate immune response to chikungunya virus infection. *Virol. J.* 2012; 9:313.

172. Kuo S-C., Chen Y-J., Wang Y-M., Tsui P-Y., et al. Cell-based analysis of chikungunya virus E1 protein in membrane fusion. *J. Biomed. Sci.* 2012; 19:44.

173. Kurokawa M., Kornbluth S. Caspases and kinases in a death grip. *Cell* 2009; 138:838–854.

174. Kwanhian W., Lenze D., Alles J., Motsch N., et al. MicroRNA-142 is mutated in about 20% of diffuse large B-cell lymphoma. *Cancer Med.* 2012; 1:141–155.

175. Laakkonen P., Ahola T., Kääriäinen L. The effects of palmitoylation on membrane association of Semliki Forest virus RNA capping enzyme. *J. Biol. Chem.* 1996; 271:28567–28571.

176. Laakkonen P., Auvinen P., Kujala P., Kääriäinen L. Alphavirus replicase protein NSP1 induces filopodia and rearrangement of actin filaments. *J. Virol.* 1998; 72:10265–10269.

177. Labadie K., Larcher T., Joubert C., Mannioui A., et al. Chikungunya disease in nonhuman primates involves long-term viral persistence in macrophages. *J. Clin. Invest.* 2010; 120:894–906.

178. Lagos-Quintana M., Rauhut R., Lendeckel W., Tuschl T. Identification of novel genes coding for small expressed RNAs. *Science* 2001; 294:853-858.

179. Lagos-Quintana M., Rauhut R., Yalcin A., Meyer J., et al. Identification of tissue-specific microRNAs from mouse. *Curr. Biol.* 2002; 12:735–739.

180. Lagrange B., Martin RZ., Droin N., Aucagne R., et al. A role for miR-142-3p in colony-stimulating factor 1-induced monocyte differentiation into macrophages. *Biochim. Biophys. Acta* 2013; 1833:1936–1946.

181. Lai E. Micro RNAs are complementary to 39 UTR sequence motifs that mediate negative post-transcriptional regulation. *Nat Genet* 2002; 30:363–364.

182. Lanciotti RS., Ludwig ML., Rwaguma EB., Lutwama JJ., et al. Emergence of epidemic O'nyong-nyong fever in Uganda after a 35-year absence: genetic characterization of the virus. *Virology* 1998; 252:258–268.

183. Landry JJM., Pyl PT., Rausch T., Zichner T., et al. The genomic and transcriptomic landscape of a HeLa cell line. *G3* 2013; 3:1213–1224.

184. Langlois RA., Varble A., Chua MA., García-Sastre A., et al. Hematopoietic-specific targeting of influenza A virus reveals replication requirements for induction of antiviral immune responses. *Proc. Natl. Acad. Sci. U.S.A.* 2012; 109:12117–12122.

185. Lani R., Hassandarvish P., Chiam CW., Moghaddam E., et al. Antiviral activity of silymarin against chikungunya virus. *Sci. Rep.* 2015; 5:11421.

186. Larkin MA., Blackshields G., Brown NP., Chenna R., et al. Clustal W and Clustal X version 2.0. *Bioinformatics* 2007; 23:2947–2948.

187. Lau N., Lim L., Weinstein E., Bartel D. An abundant class of tiny RNAs with probable regulatory roles in Caenorhabditis elegans. *Science* 2001; 294:858–862.

188. Laurent P., Le Roux K., Grivard P., Bertil G., et al. Development of a sensitive real-time reverse transcriptase PCR assay with an internal control to detect and quantify chikungunya virus. *Clin. Chem.* 2007; 53:1408–1414.

189. Lavergne A., de Thoisy B., Lacoste V., Pascalis H., et al. Mayaro virus: complete nucleotide sequence and phylogenetic relationships with other alphaviruses. *Virus Res.* 2006; 117:283–290.

190. Leber MF., Bossow S., Leonard VHJ., Zaoui K., et al. MicroRNA-sensitive oncolytic measles viruses for cancer-specific vector tropism. *Mol. Ther.* 2011; 19:1097–1106.

191. Lee Y., Kim M., Han J., Yeom K-H., et al. MicroRNA genes are transcribed by RNA polymerase II. *EMBO J.* 2004; 23:4051–4060.

192. Lee T-C., Lin Y-L., Liao J-T., Su C-M., et al. Utilizing liver-specific microRNA-122 to modulate replication of dengue virus replicon. *Biochem. Biophys. Res. Commun.* 2010; 396:596–601.

193. Lemm JA., Rümenapf T., Strauss EG., Strauss JH., et al. Polypeptide requirements for assembly of functional Sindbis virus replication complexes: a model for the temporal regulation of minus- and plus-strand RNA synthesis. *EMBO J.* 1994; 13:2925–2934.

194. Leung JY-S., Ng MM-L., Chu JJH. Replication of alphaviruses: a review on the entry process of alphaviruses into cells. *Adv. Virol.* 2011; 2011:249640.

195. Levine B., Huang Q., Isaacs JT., Reed JC., et al. Conversion of lytic to persistent alphavirus infection by the bcl-2 cellular oncogene. *Nature* 1993; 361:739–742.

196. Levis R., Schlesinger S., Huang H V. Promoter for Sindbis virus RNA-dependent subgenomic RNA transcription. *J. Virol.* 1990; 64:1726–1733.

197. Lewis J., Wesselingh SL., Griffin DE., Hardwick JM. Alphavirus-induced apoptosis in mouse brains correlates with neurovirulence. *J. Virol.* 1996; 70:1828–1835.

198. Lewis B., Burge C., Bartel D. Conserved seed pairing, often flanked by adenosines, indicates that thousands of human genes are microRNA targets. *Cell* 2005; 120:15–20.

199. Liao R., Sun J., Zhang L., Lou G., et al. MicroRNAs play a role in the development of human hematopoietic stem cells. *J. Cell. Biochem.* 2008; 104:805–817.

200. Lidbury BA., Rulli NE., Suhrbier A., Smith PN., et al. Macrophage-derived proinflammatory factors contribute to the development of arthritis and myositis after infection with an arthrogenic alphavirus. *J. Infect. Dis.* 2008; 197:1585–1593.

201. Ligon BL. Reemergence of an unusual disease: the chikungunya epidemic. *Semin. Pediatr. Infect. Dis.* 2006; 17:99–104.

202. Liljeström P., Lusa S., Huylebroeck D., Garoff H. In vitro mutagenesis of a full-length cDNA clone of Semliki Forest virus : the small 6,000-molecular-weight membrane protein modulates virus release. *J. Virol.* 1991; 65:4107–4113.

203. Liljeström P., Garoff H. A new generation of animal cell expression vectors based on the Semliki Forest virus replicon. *Nat. Biotechnol.* 1991; 9:1356–1361.

204. Lim L., Lau N., Garrett-Engele P., Grimson A., et al. Microarray analysis shows that some microRNAs downregulate large numbers of target mRNAs. *Nature* 2005; 433:769–773.

205. Lim PJ., Chu JJH. A polarized cell model for chikungunya virus infection: entry and egress of virus occurs at the apical domain of polarized cells. *PLoS Negl. Trop. Dis.* 2014; 8:e2661.

206. Linn M., Aaskov J., Suhrbier A. Antibody-dependent enhancement and persistence in macrophages of an arbovirus associated with arthritis. *J. Gen. Virol.* 1996; 77:407–411.

207. Lopez S., Yao J., Kuhn RJ., Strauss EG., et al. Nucleocapsid-glycoprotein interactions required for assembly of alphaviruses. *J. Virol.* 1994; 68:1316–1323.

208. Lu YE., Cassese T., Kielian M. The cholesterol requirement for Sindbis virus entry and exit and characterization of a spike protein region involved in cholesterol dependence. *J. Virol.* 1999; 73:4272–4278.

209. Lu J., Getz G., Miska EA., Alvarez-Saavedra E., et al. MicroRNA expression profiles classify human cancers. *Nature* 2005; 435:834–838.

210. Lu X., Li X., He Q., Gao J., et al. miR-142-3p regulates the formation and differentiation of hematopoietic stem cells in vertebrates. *Cell Res.* 2013; 23:1356–1368.

211. Lulla A., Lulla V., Merits A. Macromolecular assembly-driven processing of the 2/3 cleavage site in the alphavirus replicase polyprotein. *J. Virol.* 2012; 86:553–565.

212. Lulla V., Karo-Astover L., Rausalu K., Merits A., et al. Presentation overrides specificity: probing the plasticity of alphaviral proteolytic activity through mutational analysis. *J. Virol.* 2013; 87:10207–10220.

213. Lund E., Guttinger S., Calado A., Dahlberg J., et al. Nuclear export of microRNA precursors. *Science* 2004; 303:3011–3016.

214. Lundstrom K., Pralong W., Martinou JC. Anti-apoptotic effect of Bcl-2 overexpression in RIN cells infected with Semliki Forest virus. *Apoptosis* 1997; 2:189–191.

215. Lundstrom K., Schweitzer C., Rotmann D., Schneider E., et al. Semliki Forest virus vectors: efficient vehicles for in vitro and in vivo gene delivery. *FEBS Lett.* 2001; 504:99–103.

216. Lv M., Zhang X., Jia H., Li D., et al. An oncogenic role of miR-142-3p in human T-cell acute lymphoblastic leukemia (T-ALL) by targeting glucocorticoid receptor-α and cAMP/PKA pathways. *Leukemia* 2012; 26:769–777.

217. Macville M., Schro E., Padilla-Nash H., Keck C., et al. Comprehensive and definitive molecular cytogenetic characterization of HeLa cells by spectral karyotyping. *Cancer Res.* 1999; 59:141–150.

218. Malvy D., Ezzedine K., Mamani-Matsuda M., Autran B., et al. Destructive arthritis in a patient with chikungunya virus infection with persistent specific IgM antibodies. *BMC Infect. Dis.* 2009; 9:200.

219. Mancini EJ., Clarke M., Gowen BE., Rutten T., et al. Cryo-electron microscopy reveals the functional organization of an enveloped virus, Semliki Forest virus. *Mol. Cell* 2000; 5:255–266.

220. Mateo L., Linn L., Mccoll R., Cross S., et al. An arthrogenic alphavirus induces monocyte chemoattractant protein-1 and interleukin-8. *Intervirology* 2000; 60:55–60.

221. Mathiot CC., Grimaud G., Garry P., Bouquety JC., et al. An outbreak of human Semliki Forest virus infections in Central African Republic. *Am. J. Trop. Med. Hyg.* 1990; 42:386–393.

222. McInerney GM., Smit JM., Liljeström P., Wilschut J. Semliki Forest virus produced in the absence of the 6K protein has an altered spike structure as revealed by decreased membrane fusion capacity. *Virology* 2004; 325:200–206.

223. Melancon P., Garoff H. Reinitiation of translocation in the Semiki Forest virus structural polyprotein: identification of the signal for the El glycoprotein. *EMBO J.* 1986; 5:1551–1560.

224. Merits A., Vasiljeva L., Ahola T., Kääriäinen L., et al. Proteolytic processing of Semliki Forest virus-specific non-structural polyprotein by nsP2 protease. *J. Gen. Virol.* 2001; 82:765–773.

225. Messaoudi I., Vomaske J., Totonchy T., Kreklywich CN., et al. Chikungunya virus infection results in higher and persistent viral replication in aged rhesus macaques due to defects in anti-viral immunity. *PLoS Med.* 2013; 7:e2343.

226. Moriishi K., Koura M., Matsuura Y. Induction of Bad-mediated apoptosis by Sindbis virus infection: involvement of pro-survival members of the Bcl-2 family. *Virology* 2002; 292:258–271.

227. Morrison TE., Whitmore AC., Shabman RS., Lidbury BA., et al. Characterization of Ross River virus tropism and virus-induced inflammation in a mouse model of viral arthritis and myositis. *J. Virol.* 2006; 80:737–749.

228. Mukhopadhyay S., Zhang W., Gabler S., Chipman PR., et al. Mapping the structure and function of the E1 and E2 glycoproteins in alphaviruses. *Structure* 2006; 14:63–73.

229. Murphy F., Harrison A., Collin W. The role of extraneural arbovirus infection in the pathogenesis of encephalitis. An electron microscopic study of Semliki Forest virus infection in mice. *Lab Invest* 1970; 22:318–328.

230. Murphy A-M., Sheahan B., Atkins G. Induction of apoptosis in Bcl-2-expressing rat prostate cancer cells using the Semliki Forest virus vector. *Int. J. Cancer* 2001; 94:572–578.

231. Myles KM., Kelly CLH., Ledermann JP., Powers AM. Effects of an opal termination codon preceding the nsP4 gene sequence in the O'nyong-nyong virus genome on Anopheles gambiae infectivity. *J. Virol.* 2006; 80:4992–4997.

232. Narita M., Shimizu S., Ito T., Chittenden T., et al. Bax interacts with the permeability transition pore to induce permeability transition and cytochrome c release in isolated mitochondria. *Proc. Natl. Acad. Sci. U.S.A.* 1998; 95:14681–14686.

233. Nava VE., Rosen A., Veliuona MA., Clem RJ., et al. Sindbis virus induces apoptosis through a caspase-dependent, CrmA-sensitive pathway. *J. Virol.* 1998; 72:452–459.

234. Ng LC., Hapuarachchi HC. Tracing the path of chikungunya virus — evolution and adaptation. *Infect. Genet. Evol.* 2010; 10:876–885.

235. Nimmo R., Ciau-Uitz A., Ruiz-Herguido C., Soneji S., et al. MiR-142-3p controls the specification of definitive hemangioblasts during ontogeny. *Dev. Cell* 2013; 26:237–249.

236. Nishiyama T., Kaneda R., Ono T., Tohyama S., et al. miR-142-3p is essential for hematopoiesis and affects cardiac cell fate in zebrafish. *Biochem. Biophys. Res. Commun.* 2012; 425:755–761.

237. Oaten S., Jagelman S., Webb H. Further studies of macrophages in relationship to avirulent Semliki Forest virus infection. *Br. J. Exp. Path.* 1980; 61:150–155.

238. Oliver KR., Scallan M., Dyson H., Fazakerley JK . Susceptibility to a neurotropic virus and its changing distribution in the developing brain is a function of CNS maturity. *J Neurovirol.* 1997; 3:38–48.

239. Oliver KR., Fazakerley JK. Transneuronal spread of Semliki Forest virus in the developing mouse olfactory system is determined by neuronal maturity. *Neuroscience* 1998; 82:867–877.

240. Ou J., Rice CM., Dalgarno L., Strauss EG., et al. Sequence studies of several alphavirus genomic RNAs in the region containing the start of the subgenomic RNA. *Proc. Natl. Acad. Sci. U.S.A.* 1982; 79:5235–5239.

241. Owen KE., Kuhn RJ. Identification of a region in the Sindbis virus nucleocapsid protein that is involved in specificity of RNA encapsidation. *J. Virol.* 1996; 70:2757–2763.

242. Ozden S., Huerre M., Riviere J-P., Coffey LL., et al. Human muscle satellite cells as targets of chikungunya virus infection. *PLoS One* 2007; 2:e527.

243. Papapetrou EP., Kovalovsky D., Beloeil L., Angelo DS., et al. Harnessing endogenous miR-181a to segregate transgenic antigen receptor expression in developing versus post-thymic T cells in murine hematopoietic chimeras. *J. Clin. Invest.* 2009; 119:157–168.

244. Parashar D., Cherian S. Antiviral perspectives for chikungunya virus. *Biomed Res. Int.* 2014; 2014:631642.

245. Park EK., Jung HS., Yang HI., Yoo MC., et al. Optimized THP-1 differentiation is required for the detection of responses to weak stimuli. *Inflamm. Res.* 2007; 56:45–50.

246. Parola P., de Lamballerie X., Jourdan J., Rovery C., et al. Novel chikungunya virus variant in travelers returning from Indian Ocean islands. *Emerg. Infect. Dis.* 2006; 12:1493–1499.

247. Pastorino BAM., Peyrefitte CN., Almeras L., Grandadam M., et al. Expression and biochemical characterization of nsP2 cysteine protease of chikungunya virus. *Virus Res.* 2008; 131:293–298.

248. Pathak S., Webb HE. Possible mechanisms for the transport of Semliki Forest virus into and within mouse brain: an electron-microscopic study. *J. Neurol. Sci.* 1974; 23:175–184.

249. Pathak S., Webb HE., Oaten SW., Bateman S. An electron-microscopic study of the development of virulent and avirulent strains of Semliki Forest virus in mouse brain. *J. Neurol. Sci.* 1976; 28:289–300.

250. Pathak S., Webb H. An electron-microscopic study of avirulent and virulent Semliki forest virus in the brains of different ages of mice. *J. Neurol. Sci.* 1978; 39:199–211.

251. Pellegrini S., John J., Shearer M., Kerr IM., et al. Use of a selectable marker regulated by alpha interferon to obtain mutations in the signaling pathway. *Mol. Cell. Biol.* 1989; 9:4605–4612.

252. Peränen J., Kääriäinen L. Biogenesis of type I cytopathic vacuoles in Semliki Forest virus-infected BHK cells. *J. Virol.* 1991; 65:1623–1627.

253. Perera R., Owen KE., Tellinghuisen TL., Gorbalenya AE., et al. Alphavirus nucleocapsid protein contains a putative coiled coil α-helix important for core assembly. *J. Virol.* 2001; 75:1–10.

254. Perez JT., Pham AM., Lorini MH., Chua MA., et al. MicroRNA-mediated species-specific attenuation of influenza A virus. *Nat. Biotechnol.* 2009; 27:572–576.

255. Perl A. Mechanisms of viral pathogenesis in rheumatic disease. *Ann. Rheum. Dis.* 1999; 58:454–461.

256. Perri S., Driver DA., Gardner JP., Sherrill S., et al. Replicon vectors derived from Sindbis virus and Semliki Forest virus that establish persistent replication in host cells. *J. Virol.* 2000; 74:9802–9807.

257. Pfeffer M., Kinney RM., Kaaden O-R. The alphavirus 3'-nontranslated region: size heterogeneity and arrangement of repeated sequence elements. *Virology* 1998; 240:100–108.

258. Phalen T., Kielian M. Cholesterol is required for infection by Semliki Forest virus. *J. Cell Biol.* 1991; 112:615–623.

259. Pham AM., Langlois RA., tenOever BR. Replication in cells of hematopoietic origin is necessary for dengue virus dissemination. *PLoS Pathog.* 2012; 8:e1002465.

260. Pialoux G., Gaüzère B-A., Jauréguiberry S., Strobel M. Chikungunya, an epidemic arbovirosis. *Lancet Infect. Dis.* 2007; 7:319–327.

261. Plante K., Wang E., Partidos CD., Weger J., et al. Novel chikungunya vaccine candidate with an IRES-based attenuation and host range alteration mechanism. *PLoS Pathog.* 2011; 7:e1002142.

262. Pohjala L., Utt A., Varjak M., Lulla A., et al. Inhibitors of alphavirus entry and replication identified with a stable chikungunya replicon cell line and virus-based assays. *PLoS One* 2011; 6:e28923.

263. Polo J., Bell B., Driver D., Frolov I., et al. Stable alphavirus packaging cell lines for Sindbis virus- and Semliki Forest virus-derived vectors. *Proc. Natl. Acad. Sci. U.S.A.* 1999; 96:4598–4603.

264. Ponsaerts P., Van den Bosch G., Cools N., Van Driessche A., et al. Messenger RNA electroporation of human monocytes, followed by rapid in vitro differentiation, leads to highly stimulatory antigen-loaded mature dendritic cells. *J. Immunol.* 2002; 169:1669–1675.

265. Powers AM., Brault AC., Shirako Y., Strauss EG., et al. Evolutionary relationships and systematics of the alphaviruses. *J. Virol.* 2001; 75:10118–10131.

266. Powers AM., Logue CH. Changing patterns of chikungunya virus: re-emergence of a zoonotic arbovirus. *J. Gen. Virol.* 2007; 88:2363–2377.

267. Powers AM. Chikungunya virus outbreak expansion and microevolutionary events affecting epidemiology and epidemic potential. *Res. Rep. Trop. Med.* 2015; 6:11–19.

268. Prestwood TR., May MM., Plummer EM., Morar MM., et al. Trafficking and replication patterns reveal splenic macrophages as major targets of dengue virus in mice. *J. Virol.* 2012; 86:12138–12147.

269. Pugachev K., Mason P., Shope R., Frey T. Double-subgenomic Sindbis virus recombinants expressing immunogenic proteins of Japanese encephalitis virus induce significant protection in mice against lethal JEV infection. *Virology* 1995; 212:587–594.

270. Pushko P., Parker M., Ludwig GV., Davis NL., et al. Replicon-helper systems from attenuated Venezuelan equine encephalitis virus: expression of heterologous genes in vitro and immunization against heterologous pathogens in vivo. *Virology* 1997; 239:389–401.

271. Pusztai R., Gould E., Smith H. Infection pattern in mice of an avirulent and virulent strain of Semliki Forest virus. *Br J Exp Pathol.* 1971; 52:669–677.

272. Rajapakse S., Rodrigo C., Rajapakse A. Atypical manifestations of chikungunya infection. *Trans. R. Soc. Trop. Med. Hyg.* 2010; 104:89–96.

273. Ramkissoon S., Mainwaring L., Ogasawara Y., Keyvanfar K., et al. Hematopoietic- specific microRNA expression in human cells. *Leuk Res.* 2006; 30:643–647.

274. Ratnik K., Viru L., Merits A. Control of the rescue and replication of Semliki Forest virus recombinants by the insertion of miRNA target sequences. *PLoS One* 2013; 8:e75802.

275. Reddy AM., Zheng Y., Jagadeeswaran G., Macmil SL., et al. Cloning, characterization and expression analysis of porcine microRNAs. *BMC Genomics* 2009; 10:65.

276. Reed D., Lind C., Lackemeyer M., Sullivan L., et al. Genetically engineered, live attenuated vaccines protect nonhuman primates against aerosol challenge with a virulent IE strain of Venezuelan equine encephalitis virus. *Vaccine* 2005; 23:3139–3147.

277. Rezza G., Nicoletti L., Angelini R., Romi R., et al. Infection with chikungunya virus in Italy: an outbreak in a temperate region. *Lancet* 2007; 370:1840–1846.

278. Rice CM., Levis R., Strauss JH., Huang HV. Production of infectious RNA transcripts from Sindbis virus cDNA clones: mapping of lethal mutations, rescue of a temperature-sensitive marker, and in vitro mutagenesis to generate defined mutants. *J. Virol. Methods* 1987; 61:3809–3819.

279. Rikkonen M., Peränen J., Kääriäinen L. ATPase and GTPase activities associated with Semliki Forest virus nonstructural protein nsP2. *J. Virol.* 1994; 68:5804–5810.

280. Robin Y., Bourdin P., Le Gonidec G., Heme G. Virus de la foret de Semliki et encephalomyelites equines au Senegal. *Ann Microbiol (Inst Pasteur)* 1974; 125:235–241.

281. Rose PP., Hanna SL., Spiridigliozzi A., Wannissorn N., et al. Natural resistance-associated macrophage protein is a cellular receptor for Sindbis virus in both insect and mammalian hosts. *Cell Host Microbe* 2011; 10:97–104.

282. Rosen A., Casciola-Rosen L., Ahearn J. Novel packages of viral and self-antigens are generated during apoptosis. *J. Exp. Med.* 1995; 181:1557–1561.

283. Ross, B. The Newala Epidemic. *J. Hyg. (Lond).* 1956; 54:177–191.

284. Roussel A., Lescar J., Vaney M-C., Wengler G., et al. Structure and interactions at the viral surface of the envelope protein E1 of Semliki Forest virus. *Structure* 2006; 14:75–86.

285. Roy CJ., Adams AP., Wang E., Plante K., et al. Chikungunya vaccine candidate is highly attenuated and protects nonhuman primates against telemetrically monitored disease following a single dose. *J. Infect. Dis.* 2014; 209:1891–1899.

286. Rubach JK., Wasik BR., Rupp JC., Kuhn RJ., et al. Characterization of purified Sindbis virus nsP4 RNA-dependent RNA polymerase activity in vitro. *Virology* 2009; 384:201–208.

287. Rulli NE., Suhrbier A., Hueston L., Heise MT., et al. Ross River virus: molecular and cellular aspects of disease pathogenesis. *Pharmacol. Ther.* 2005; 107:329–342.

288. Rulli NE., Rolph MS., Srikiatkhachorn A., Anantapreecha S., et al. Protection from arthritis and myositis in a mouse model of acute chikungunya virus disease by bindarit, an inhibitor of monocyte chemotactic protein-1 synthesis. *J. Infect. Dis.* 2011; 204:1026–1030.

289. Ryman KD., Klimstra WB., Johnston RE. Attenuation of Sindbis virus variants incorporating uncleaved PE2 glycoprotein is correlated with attachment to cell-surface heparan sulfate. *Virology* 2004; 322:1–12.

290. Ryman KD., Gardner CL., Burke CW., Meier KC., et al. Heparan sulfate binding can contribute to the neurovirulence of neuroadapted and nonneuroadapted Sindbis viruses. *J. Virol.* 2007; 81:3563–3573.

291. Salonen A., Vasiljeva L., Merits A., Magden J., et al. Properly folded nonstructural polyprotein directs the Semliki Forest virus replication complex to the endosomal compartment. *J. Virol.* 2003; 77:1691–1702.

292. Salonen A., Ahola T., Kääriäinen L. Viral RNA replication in association with cellular membranes. *Curr. Top. Microbiol. Immunol.* 2005; 285:139–173.

293. Salvador B., Zhou Y., Michault A., Muench MO., et al. Characterization of chikungunya pseudotyped viruses: identification of refractory cell lines and demonstration of cellular tropism differences mediated by mutations in E1 glycoprotein. *Virology* 2009; 393:33–41.

294. Sam I-C., Kümmerer BM., Chan Y-F., Roques P., et al. Updates on chikungunya epidemiology, clinical disease, and diagnostics. *Vector Borne Zoonotic Dis.* 2015; 15:223–230.

295. Sánchez-San Martín C., Liu CY., Kielian M. Dealing with low pH: entry and exit of alphaviruses and flaviviruses. *Trends Microbiol.* 2009; 17:514–521.

296. Sanger F., Nicklen S., Coulson A. DNA sequencing with chain-terminating. *Proc. Natl. Acad. Sci. U. S. A.* 1977; 74:5463–5467.

297. Sawicki DL., Sawicki SG., Keränen S., Kääriäinen L. Specific Sindbis virus-coded function for minus-strand RNA synthesis. *J. Virol.* 1981; 39:348–358.

298. Scallan MF., Allsopp TE., Fazakerley JK. Bcl-2 acts early to restrict Semliki Forest virus replication and delays virus-induced programmed cell death. *J. Virol.* 1997; 71:1583–1590.

299. Schuffenecker I., Iteman I., Michault A., Murri S., et al. Genome microevolution of chikungunya viruses causing the Indian Ocean outbreak. *PLoS Med.* 2006; 3:e263.

300. Schwartz O., Albert ML. Biology and pathogenesis of chikungunya virus. *Nat. Rev. Microbiol.* 2010; 8:491–500.

301. Seamer J., Randles WJ., Fitzgeorge R. The course of Semliki Forest virus infection in mice. *Br. J. Exp. Path.* 1967; 48:395–402.

302. Senkel S., Waldner C., Ryffel GU., Thomas H. Improved conditional expression systems resulting in physiological level of HNF4alpha expression confirm HNF4alpha induced apoptosis in the pancreatic beta-cell line INS-1. *BMC Res. Notes* 2009; 2:210.

303. Shen X., Sun W., Shi Y., Xing Z., et al. Altered viral replication and cell responses by inserting microRNA recognition element into PB1 in pandemic influenza A virus (H1N1) 2009. *Mediators Inflamm.* 2015; 2015:976575.

304. Shimizu S., Narita M., Tsujimoto Y. Bcl-2 family proteins regulate the release of apoptogenic cytochrome c by the mitochondrial channel VDAC. *Nature* 1999; 399:483–487.

305. Shimoni Z., Niven M., Pitlick S., Bulvik S. Treatment of West Nile virus encephalitis with intravenous immunoglobulin. *Emerg. Infect. Dis.* 2001; 7:759.

306. Shirako Y., Strauss JH. Regulation of Sindbis virus RNA replication: uncleaved P123 and nsP4 function in minus-strand RNA synthesis, whereas cleaved products from P123 are required for efficient plus-strand RNA synthesis. *J. Virol.* 1994; 68:1874–1885.

307. Shirako Y., Strauss JH. Requirement for an aromatic amino acid or histidine at the N terminus of Sindbis virus RNA polymerase. *J. Virol.* 1998; 72:2310–2315.

308. Shirako Y., Strauss EG., Strauss JH. Suppressor mutations that allow Sindbis virus RNA polymerase to function with nonaromatic amino acids at the N-terminus: evidence for interaction between nsP1 and nsP4 in minus-strand RNA synthesis. *Virology* 2000; 276:148–160.

309. Silva LA., Khomandiak S., Ashbrook AW., Weller R., et al. A single-amino-acid polymorphism in chikungunya virus E2 glycoprotein influences glycosaminoglycan utilization. *J. Virol.* 2014; 88:2385–2397.

310. Simizu B., Yamamoto K., Hashimoto K., Ogata T. Structural proteins of chikungunya virus. *J. Virol.* 1984; 51:254–258.

311. Simon F., Javelle E., Oliver M., Leparc-Goffart I., et al. Chikungunya virus infection. *Curr. Infect. Dis. Rep.* 2011; 13:218–228.

312. Simpson DA., Davis NL., Lin S., Russell D., et al. Complete nucleotide sequence and full-length cDNA clone of S.A. AR86, a South African alphavirus related to Sindbis. *Virology* 1996; 222:464–469.

313. Singh SK., Unni SK. Chikungunya virus: host pathogen interaction. *Rev. Med. Virol.* 2011; 21:78–88.

314. Sissoko D., Malvy D., Ezzedine K., Renault P., et al. Post-epidemic chikungunya disease on Reunion Island: course of rheumatic manifestations and associated factors over a 15-month period. *PLoS Negl Trop Dis* 2009; 3:e389.

315. Smale ST. Transfection by electroporation of RAW 264.7 macrophages. *Cold Spring Harb. Protoc.* 2010; 5:1–3.

316. Smerdou C., Liljestro P. Two-helper RNA system for production of recombinant Semliki Forest virus particles. *J. Virol.* 1999; 73:1092–1098.

317. Smit JM., Waarts B., Kimata K., Klimstra WB., et al. Adaptation of alphaviruses to heparan sulfate: interaction of Sindbis and Semliki Forest viruses with liposomes containing lipid-conjugated heparin. *J. Virol.* 2002; 76:10128–10137.

318. Smithburn KC., Haddow AJ. Semliki Forest virus: I. Isolation and pathogenic properties. *J. Immunol.* 1944; 49:141–157.

319. Solignat M., Gay B., Higgs S., Briant L., et al. Replication cycle of chikungunya: a re-emerging arbovirus. *Virology* 2009; 393:183–197.

320. Soumahoro M-K., Gérardin P., Boëlle P-Y., Perrau J., et al. Impact of chikungunya virus infection on health status and quality of life: a retrospective cohort study. *PLoS One* 2009; 4:e7800.

321. Sourisseau M., Schilte C., Casartelli N., Trouillet C., et al. Characterization of reemerging chikungunya virus. *PLoS Pathog.* 2007; 3:e89.

322. Sprick MR., Rieser E., Stahl H., Grosse-Wilde A., et al. Caspase-10 is recruited to and activated at the native TRAIL and CD95 death-inducing signalling complexes in a FADD-dependent manner but can not functionally substitute caspase-8. *EMBO J.* 2002; 21:4520–4530.

323. Spuul P., Salonen A., Merits A., Jokitalo E., et al. Role of the amphipathic peptide of Semliki forest virus replicase protein nsP1 in membrane association and virus replication. *J. Virol.* 2007; 81:872–883.

324. Spuul P., Balistreri G., Kääriäinen L., Ahola T. Phosphatidylinositol 3-kinase-, actin-, and microtubule-dependent transport of Semliki Forest virus replication complexes from the plasma membrane to modified lysosomes. *J. Virol.* 2010; 84:7543–7557.

325. Srinivasula SM., Ahmad M., Fernandes-Alnemri T., Alnemri ES. Autoactivation of procaspase-9 by Apaf-1-mediated oligomerization. *Mol. Cell* 1998; 1:949–957.

326. Staikowsky F., Talarmin F., Grivard P., Souab A., et al. Prospective study of chikungunya virus acute infection in the Island of La Réunion during the 2005-2006 outbreak. *PLoS One* 2009; 4:e7603.

327. Staples JE., Breiman RF., Powers AM. Chikungunya fever: an epidemiological review of a re-emerging infectious disease. *Clin. Infect. Dis.* 2009; 49:942–948.

328. Strauss EG., Rice CM., Strauss JH. Sequence coding for the alphavirus nonstructural proteins is interrupted by an opal termination codon. *Proc. Natl. Acad. Sci. U.S.A.* 1983; 80:5271–5275.

329. Strauss EG., Levinson R., Rice CM., Dalrymple J., et al. Nonstructural proteins nsP3 and nsP4 of Ross River and O'nyong-nyong viruses: sequence and comparison with those of other alphaviruses. *Virology* 1988; 164:265–274.

330. Strauss EG., de Groot RJ., Levinson R., Strauss JH. Identification of the active site residues in the nsP2 proteinase of Sindbis virus. *Virology* 1992; 191:932–940.

331. Strauss JH., Strauss EG. The alphaviruses: gene expression, replication, and evolution. *Microbiol. Rev.* 1994; 58:491–562.

332. Sudeep AB., Parashar D. Chikungunya: an overview. *J. Biosci.* 2008; 33:443–449.

333. Suhrbier A., Mahalingam S. The immunobiology of viral arthritides. *Pharmacol. Ther.* 2009; 124:301–308.

334. Sun W., Shen W., Yang S., Hu F., et al. miR-223 and miR-142 attenuate hematopoietic cell proliferation, and miR-223 positively regulates miR-142 through LMO2 isoforms and CEBP-β. *Cell Res.* 2010; 20:1158–1169.

335. Sun Y., Varambally S., Maher CA., Cao Q., et al. Targeting of microRNA-142-3p in dendritic cells regulates endotoxin-induced mortality. *Blood* 2011; 117:6172–6184.

336. Sun Y., Sun J., Tomomi T., Nieves E., et al. PU.1-dependent transcriptional regulation of miR-142 contributes to its hematopoietic cell-specific expression and modulation of IL-6. *J. Immunol.* 2013; 190:4005–4013.

337. Sun C., Gardner CL., Watson AM., Ryman KD., et al. Stable, high-level expression of reporter proteins from improved alphavirus expression vectors to track replication and dissemination during encephalitic and arthritogenic disease. *J. Virol.* 2014; 88:2035–2046.

338. Sun Y., Varambally S., Maher CA., Cao Q., et al. Targeting of microRNA-142-3p in dendritic cells regulates endotoxin-induced mortality. *Immunobiology* 2015; 117:6172–6184.

339. Suomalainen M., Liljeström P., Garoff H. Spike protein-nucleocapsid interactions drive the budding of alphaviruses. *J. Virol.* 1992; 66:4737–4747.

340. Swaminathan G., Martin-Garcia J., Navas-Martin S. RNA viruses and microRNAs: challenging discoveries for the 21st century. *Physiol. Genomics* 2013; 45:1035–1048.

341. Takada A., Kawaoka Y. Antibody-dependent enhancement of viral infection: molecular mechanisms and in vivo implications. *Rev. Med. Virol.* 2003; 13:387–398.

342. Takkinen K. Complete nucleotide sequence of the nonstructural protein genes of Semliki Forest virus. *Nucleic Acids Res.* 1986; 14:5667–5682.

343. Takkinen K., Peränen J., Keränen S., Söderlund H., et al. The Semliki Forest virus-specific nonstructural protein nsP4 is an autoproteinase. *Eur J Biochem* 1990; 189:33–38.

344. Takkinen K., Peränen J., Kääriäinen L. Proteolytic processing of Semliki Forest virus-specific non-structural polyprotein. *J. Gen. Virol.* 1991; 72:1627–1633.

345. Tamberg N., Lulla V., Fragkoudis R., Lulla A., et al. Insertion of EGFP into the replicase gene of Semliki Forest virus results in a novel, genetically stable marker virus. *J. Gen. Virol.* 2007; 88:1225–1230.

346. Tamm K., Merits A., Sarand I. Mutations in the nuclear localization signal of nsP2 influencing RNA synthesis, protein expression and cytotoxicity of Semliki Forest virus. *J. Gen. Virol.* 2008; 89:676–686.

347. Tang BL. The cell biology of chikungunya virus infection. *Cell. Microbiol.* 2012; 14:1354–1363.

348. Tani H., Mizutani R., Salam K., Tano K., et al. Genome-wide determination of RNA stability reveals hundreds of short-lived noncoding transcripts in mammals. *Genome Res* 2012; 22:947–956.

349. Teng T., Foo S-S., Simamarta D., Lum F., et al. Viperin restricts chikungunya virus replication and pathology. *J. Clin. Invest.* 2012; 122:4447–4460.

350. tenOever BR. RNA viruses and the host microRNA machinery. *Nat. Rev. Microbiol.* 2013; 11:169–180.

351. Teo T-H., Lum F-M., Lee WWL., Ng LFP. Mouse models for chikungunya virus: deciphering immune mechanisms responsible for disease and pathology. *Immunol. Res.* 2012; 53:136–147.

352. Teodoro JG., Branton PE. Regulation of apoptosis by viral gene products. *J. Virol.* 1997; 71:1739–1746.

353. Thiboutot MM., Kannan S., Kawalekar OU., Shedlock DJ., et al. Chikungunya: a potentially emerging epidemic? *PLoS Negl. Trop. Dis.* 2010; 4:e623.

354. Thomas JM., Klimstra WB., Ryman KD., Heidner HW. Sindbis virus vectors designed to express a foreign protein as a cleavable component of the viral structural polyprotein. *J. Virol.* 2003; 77:5598–5606.

355. Thomas M., Liu X., Whangbo J., McCrossan G., et al. Apoptosis triggers specific, rapid, and global mRNA decay with 3’ uridylated intermediates degraded by DIS3L2. *Cell Rep.* 2015; 11:1079–1089.

356. Thon-Hon VG., Denizot M., Li-Pat-Yuen G., Giry C., et al. Deciphering the differential response of two human fibroblast cell lines following chikungunya virus infection. *Virol. J.* 2012; 9:213.

357. Thorburn A. Death receptor-induced cell killing. *Cell. Signal.* 2004; 16:139–144.

358. Thornberry N., Lazebnik Y. Caspases: enemies within. *Scienc* 1998; 281:1312–1316.

359. Tirado S., Yoon K. Antibody-dependent enhancement of virus infection and disease. *Viral Immunol.* 2003; 16:69–86.

360. Tomar S., Hardy RW., Smith JL., Kuhn RJ. Catalytic core of alphavirus nonstructural protein nsP4 possesses terminal adenylyltransferase activity. *J. Virol.* 2006; 80:9962–9969.

361. Townson H., Nathan MB. Resurgence of chikungunya. *Trans. R. Soc. Trop. Med. Hyg.* 2008; 102:308–309.

362. Trobaugh DW., Gardner CL., Sun C., Haddow AD., et al. RNA viruses can hijack vertebrate microRNAs to suppress innate immunity. *Nature* 2014; 506:245–248.

363. Tsetsarkin KA., Higgs S., McGee CE., de Lamballerie X., et al. Infectious clones of chikungunya virus (La Réunion isolate) for vector competence studies. *Vector-Borne Zoonotic Dis.* 2006; 6:325–337.

364. Tsetsarkin KA., Vanlandingham DL., McGee CE., Higgs S. A single mutation in chikungunya virus affects vector specificity and epidemic potential. *PLoS Pathog.* 2007; 3:e201.

365. Tsetsarkin KA., McGee CE., Higgs S. Chikungunya virus adaptation to Aedes albopictus mosquitoes does not correlate with acquisition of cholesterol dependence or decreased pH threshold for fusion reaction. *Virol. J.* 2011; 8:376.

366. Tsetsarkin KA., Liu G., Kenney H., Bustos-Arriaga J., et al. Dual miRNA targeting restricts host range and attenuates neurovirulence of flaviviruses. *PLoS Pathog.* 2015; 11:e1004852.

367. Tsetsarkin KA., Higgs S., McGee CE., Lamballerie X De., et al. Infectious clones of chikungunya virus (La Réunion Isolate) for vector competence studies. *Vector-Borne Zoonotic Dis.* 2006; 6:325–337.

368. Ubol S., Tucker PC., Griffin DE., Hardwick JM. Neurovirulent strains of alphavirus induce apoptosis in bcl-2-expressing cells: role of a single amino acid change in the E2 glycoprotein. *Proc. Natl. Acad. Sci. U.S.A.* 1994; 91:5202–5206.

369. Urban C., Rhême C., Maerz S., Berg B., et al. Apoptosis induced by Semliki Forest virus is RNA replication dependent and mediated via Bak. *Cell Death Differ.* 2008; 15:1396–1407.

370. Vanlandingham DL., Tsetsarkin KA., Hong C., Klingler K., et al. Development and characterization of a double subgenomic chikungunya virus infectious clone to express heterologous genes in Aedes aegypti mosquitoes. *Insect Biochem. Mol. Biol.* 2005; 35:1162–1170.

371. Varjak M., Zusinaite E., Merits A. Novel functions of the alphavirus nonstructural protein nsP3 C-terminal region. *J. Virol.* 2010; 84:2352–2364.

372. Vashishtha M., Phalen T., Marquardt MT., Ryu JS., et al. A single point mutation controls the cholesterol dependence of Semliki Forest virus entry and exit. *J. Cell Biol.* 1998; 140:91–99.

373. Vasiljeva L., Merits A., Auvinen P., Kääriäinen L. Identification of a novel function of the alphavirus capping apparatus: RNA 5'-triphosphatase activity of Nsp2. *J. Biol. Chem.* 2000; 275:17281–17287.

374. Vasiljeva L., Merits A., Golubtsov A., Sizemskaja V., et al. Regulation of the sequential processing of Semliki Forest virus replicase polyprotein. *J. Biol. Chem.* 2003; 278:41636–41645.

375. Vaux DL., Korsmeyer SJ. Cell death in development. *Cell* 1999; 96:245–254.

376. Vierboom M., Jonker M., Tak P., Hart B. Preclinical models of arthritic disease in non-human primates. *Drug Discov. Today* 2007; 12:327–335.

377. Voss JE., Vaney M-C., Duquerroy S., Vonrhein C., et al. Glycoprotein organization of chikungunya virus particles revealed by X-ray crystallography. *Nature* 2010; 468:709–712.

378. Wallace B., Shaffer J., Murphy R., Bonner J., et al. Hybridization of synthetic oligodeoxyribonucleotides to phi chi 174 DNA: the effect of single base pair mismatch. *Nucleic Acids Res.* 1979; 6:3543–3557.

379. Walsh G., Tan E., dela Cruz E., Abalosa R., et al. The Philippine cynomolgus monkey (Macaca fasicularis) provides a new nonhuman primate model of tuberculosis that resembles human disease. *Nat. Med.* 1996; 2:430–436.

380. Wang Y-F., Sawicki SG., Sawicki DL. Sindbis virus nsP1 functions in negative-strand RNA synthesis. *J. Virol.* 1991; 65:985–988.

381. Wang K-S., Kuhn RJ., Strauss EG., Ou S., et al. High-affinity laminin receptor is a receptor for Sindbis virus in mammalian cells. *J. Virol.* 1992; 66:4992–5001.

382. Wang X-S., Gong J-N., Yu J., Wang F., et al. MicroRNA-29a and microRNA-142-3p are regulators of myeloid differentiation and acute myeloid leukemia. *Blood* 2012; 119:4992–5004.

383. Wauquier N., Becquart P., Nkoghe D., Padilla C., et al. The acute phase of chikungunya virus infection in humans is associated with strong innate immunity and T CD8 cell activation. *J. Infect. Dis.* 2011; 204:115–123.

384. Way SJR., Lidbury BA., Banyer JL. Persistent Ross River virus infection of murine macrophages: an in vitro model for the study of viral relapse and immune modulation during long-term infection. *Virology* 2002; 301:281–292.

385. Weaver SC., Brault AC., Kang W., Holland JJ. Genetic and fitness changes accompanying adaptation of an arbovirus to vertebrate and invertebrate cells. *J. Virol.* 1999; 73:4316–4326.

386. Weger-Lucarelli J., Chu H., Aliota MT., Partidos CD., et al. A novel MVA vectored chikungunya virus vaccine elicits protective immunity in mice. *PLoS Negl. Trop. Dis.* 2014; 8:e2970.

387. Weiss B., Nitschko H., Ghattas I., Wright R., et al. Evidence for specificity in the encapsidation of Sindbis virus RNAs. *J. Virol.* 1989; 63:5310–5318.

388. Wellink J., van Kammen A. Proteases involved in the processing of viral polyproteins. *Arch. Virol.* 1988; 98:1–26.

389. Westaway EG., Brinton MA., Gaidamovich SY., Horzinek MC., et al. Togaviridae. *Intervirology* 1985; 24:125–139.

390. White E. Mechanisms of apoptosis regulation by viral oncogenes in infection and tumorigenesis. *Cell Death Differ.* 2006; 13:1371–1377.

391. Willems WR., Kaluza G., Boschek CB., Bauer H., et al. Semliki Forest virus: cause of a fatal case of human encephalitis. *Science* 1979; 203:1127–1129.

392. Willis SN., Adams JM. Life in the balance: how BH3- only proteins induce apoptosis. *Curr. Opin. Cell Biol.* 2005; 17:617–622.

393. Wilson NS., Dixit V., Ashkenazi A. Death receptor signal transducers: nodes of coordination in immune signaling networks. *Nat. Immunol.* 2009; 10:348–355.

394. Win MK., Chow A., Dimatatac F., Go CJ., et al. Chikungunya fever in Singapore: acute clinical and laboratory features, and factors associated with persistent arthralgia. *J. Clin. Virol.* 2010; 49:111–114.

395. Wintachai P., Wikan N., Kuadkitkan A., Jaimipuk T., et al. Identification of prohibitin as a chikungunya virus receptor protein. *J. Med. Virol.* 2012; 84:1757–1770.

396. Wu L., Cai C., Wang X., Liu M., et al. MicroRNA-142-3p, a new regulator of RAC1, suppresses the migration and invasion of hepatocellular carcinoma cells. *FEBS Lett.* 2011; 585:1322–1330.

397. Yen L-C., Lin Y-L., Sung H-H., Liao J-T., et al. Neurovirulent flavivirus can be attenuated in mice by incorporation of neuron-specific microRNA recognition elements into viral genome. *Vaccine* 2011; 31:5915–4922.

398. Yi R., Qin Y., Macara I., Cullen BR. Exportin‐5 mediates the nuclear export of pre-microRNAs and short hairpin RNAs. *Genes Dev* 2003; 17:3011–3016.

399. Ylösmäki E., Martikainen M., Hinkkanen A., Saksela K. Attenuation of Semliki Forest virus neurovirulence by microRNA-mediated detargeting. *J. Virol.* 2013; 87:335–344.

400. Yoshida H., Kong YY., Yoshida R., Elia AJ., et al. Apaf1 is required for mitochondrial pathways of apoptosis and brain development. *Cell* 1998; 94:739–750.

401. Yuan W., Sun W., Yang S., Du J., et al. Downregulation of microRNA-142 by proto-oncogene LMO2 and its co-factors. *Leukemia* 2008; 22:1067–1071.

402. Zhang X., Fugère M., Day R., Kielian M. Furin processing and proteolytic activation of Semliki Forest virus. *J. Virol.* 2003; 77:2981–2989.

403. Zhang Y., Si B-Y., Kang X-P., Hu Y., et al. The confirmation of three repeated sequence elements in the 3' untranslated region of chikungunya virus. *Virus Genes* 2013; 46:165–166.

404. Zou H., Li Y., Liu X., Wang X. An APAf-1-cytochrome C multimeric complex is a functional apoptosome that activates procaspase-9. *J. Biol. Chem.* 1999; 274:11549–11556.

ANNEX 1: Cell culture flask and multidishes

Type	Details	Manufacturer	Catalogue number
TC Flask, 175 cm^2	• Nunclon™ Delta surface • Cap filtered and angled	Thermo Scientific™ Nunc™	178883
TC Flask, 80 cm^2	• Nunclon™ Delta surface • Cap filtered and angled	Thermo Scientific™ Nunc™	178905
TC Flask, 25 cm^2	• Nunclon™ Delta surface • Cap filtered and angled	Thermo Scientific™ Nunc™	136196
Multidish, 96-wells	• Nunclon delta surface	Thermo Scientific™ Nunc™	167008
Multidish, 24-wells	• Nunclon delta surface	Thermo Scientific™ Nunc™	142475
Multidish, 6-wells	• Nunclon delta surface	Thermo Scientific™ Nunc™	140675
100 mm cell culture dish	• Round • 100 mm x 20 mm • TC Treated	Corning	430167
100 mm petri dish	• Sterile • Square (100 mm x 100 mm)	Thermo Scientific™ Sterilin™	109
LUMITRAC™200 96-well plates, white	• Sterile • Suitable for measurement of luminescence	Greiner Bio-One	655075

ANNEX 2: Plasticware

Name	Details	Manufacturer	Catalogue number
Syringe 60 ml	• Luer Lock Tip • Sterile	Terumo Medical Products	SS-60L
Syringe 20 ml	• Luer Lock Tip • Sterile	BD Plastipak™	300629
Syringe 2 ml	• Luer Lock Tip • Sterile	Terumo	SS*02LZ1
1.8 ml CryoTube™	• Internal thread • Suitable for LN_2	Thermo Scientific™ Nunc™	V7634-500EA
1.5mL Screw Cap Microtube	• Sterile • DNase-, RNase-free	Sarstedt	72.692.005
1.7ml MaxyClear microtubes	• Sterile • DNase-, RNase-free	Axygen	MCT-175-C
PCR Tubes	• 0.2ml Thin Wall • Flat Cap	Axygen	PCR-02-C
50 ml centrifuge tube	• Conical base • Sterile • DNase-, RNase-free • Non-pyrogenic, non-cytotoxic	Greiner Bio-One	227261
50 ml centrifuge tube	• Skirted base • Sterile • DNase-, RNase-free • Non-pyrogenic, non-cytotoxic	Greiner Bio-One	210261
Ultra-Clear™ ultracentrifugation tube	• Thinwall • 38.5 ml • 25 x 89 mm	Beckman	344058
Bijoux bottle	• 7 ml • Sterile	Thermo Scientific™ Sterilin™	129A
Universal bottle	• 30 ml • Sterile	Thermo Scientific™ Sterilin™	128A
Bio-Pure™ pipetting reservoir	• 50 ml	Sigma-Aldrich®	Z679968-100EA
Syringe filter 0.20 µm	• Hydrophilic	Sartorious	16534
Syringe filter 0.45 µm	• Hydrophilic	Sartorious	16555
Stericup-GP Filter Unit	• 0.22 µm Millipore Express PLUS (PES) membrane • 250 ml capacity	Millipore	SCGPU02RE

5 ml Serological Pipettes	• Sterile and certified non-pyrogenic • Individually wrapped	Thermo Scientific™ Nunc™	170355
10 ml Serological Pipettes	• Sterile and certified non-pyrogenic • Individually wrapped	Thermo Scientific™ Nunc™	170356
25 ml Serological Pipettes	• Sterile and certified non-pyrogenic • Individually wrapped	Thermo Scientific™ Nunc™	170357
TipOne Filter Pipette Tip, XL, 10µl	• Sterile, RNase-, DNase, DNA- and pyrogene-free • Filtered	Starlab	S1120-3810
TipOne Filter Pipette Tip, 20µl	• Sterile, RNase-, DNase, DNA- and pyrogene-free • Filtered	Starlab	S1120-1810
TipOne Filter Pipette Tip, 200µl	• Sterile, RNase-, DNase, DNA- and pyrogene-free • Filtered	Starlab	S1120-8810
TipOne Filter Pipette Tip, XL, 1000µl	• Sterile, RNase-, DNase, DNA- and pyrogene-free • Filtered	Starlab	S1122-1830
Petri dish	• 90 mm • Triple vent	Thermo Scientific™ Sterilin™	101VR20
Bacteria Spreader	• L-form with curved end	Gosselin	ETAR-01
Disposable forceps	• Sterile • Single packed	Servoprax (Mediware)	H7301
Scienceware® Cloning cylinders	• 4.7 x 8 mm • Polystyrene	Sigma-Aldrich®	C7983-50 EA
Mr. Frosty™	• 1.0 to 2.0 ml tubes	Thermo Scientific™	5100-0001
Gene Pulser®/Micropulser™ Electroporation Cuvettes	• 0.4 cm gap	Bio-Rad	165-2088
Parafilm	• 2" Wide • 250 Ft/Roll	Benis Flexible Packaging	PM992
MicroAmp® Optical Adhesive Film	• Suitable for qPCR.	Life Technologies Applied Biosystems®	4360954
Peel-A-Way Disposable Embedding Molds	• 20 x 20 x 22 mm	Thermo Scientific™ Shandon™	2219
Half Area 96 well UV microplate	• Non-sterile • DNase- and RNase-free	Corning	3679
Aluminium film for PCR plates	• For molecular biology	Dominique Dutscher	016925
Reservoir, quarter	• 40 ml • Sterile	Beckman Coulter	372790

ANNEX 3: Sharps

Name	Details	Manufacturer	Catalogue number
Needle 25 G	• 25 G x 1 ½”	Terumo	NN-2538R
Needle 21 G	• 21 G x 1 ½”	Terumo	NN-2138R
Needle 19 G	• 19 G x 1 ½”	Terumo	NN-1938R
Disposable scalpels	• Surgical steel blades • Sterile	Swann-Morton	0510

ANNEX 4: Cell culture media components and supplementary reagents

Name	Details	Manufacturer	Catalogue number
Dulbecco's Modified Eagle Medium (DMEM)	• 4mM L-glutamine • 4.5 g/L glucose • Phenol red	Invitrogen™ Life Technologies (GIBCO®)	41965-039
Glasgow Minimum Essential Medium (GMEM)	• 2mM L-glutamine • Phenol red	Invitrogen™ Life Technologies (GIBCO®)	21710-025
Roswell Park Memorial Institute 1640 (RPMI 1640)	• No Phenol red	Invitrogen™ Life Technologies (GIBCO®)	32404
Opti-MEM® Reduced Serum Media	• HEPES • 2.4 g/L sodium bicarbonate • L-glutamine	Invitrogen™ Life Technologies (GIBCO®)	31985
Foetal bovine serum (FBS)	• South American origin • EU-approved	Invitrogen™ Life Technologies (GIBCO®)	10270-106
Newborn calf serum (NBCS)	• UK origin	SeraLab	S-101-F
4-(2-Hydroxyethyl)piperazine-1-ethanesulfonic acid (HEPES)	• 1 M in H_2O (238 g/L HEPES in H_2O) • 50 x concentrated	Sigma-Aldrich®	83264
GlutaMAX™	• 100 x concentrated	Invitrogen™ Life Technologies (GIBCO®)	35050
Tryptose Phosphate Broth (TPB)	• 29.5 g/L in deionized water	Invitrogen™ Life Technologies (GIBCO®)	18050-039
Penicillin-Streptomycin solution (P/S)	• 100 x concentrated • 5000 U/ml penicillin • 5000 µg/ml of streptomycin	Invitrogen™ Life Technologies (GIBCO®)	15070
Trypsin-EDTA	• 0.05% trypsin-EDTA	Invitrogen™ Life Technologies (GIBCO®)	25300
Phosphate Buffered Saline (PBS)	• pH 7.4 • No Ca^{2+} and Mg^{2+}	Invitrogen™ Life Technologies (GIBCO®)	10010-015
Phosphate Buffered Saline (PBS)	• pH 7.1-7.5 • With Ca^{2+} and Mg^{2+}	Sigma-Aldrich®	D8662-1L
Phorbol 12-myristate 13-acetate (PMA)	• ≥99% (TLC)	Sigma-Aldrich®	P8139-5MG

Recombinant human colony stimulating factor 1 (rhCSF-1)	• Storage stock • 1 x 10^8 U/mL	Received from Prof David Hume, The Roslin Institute	N/A
Albumin, from bovine serum (BSA)	• ≥98% (agarose gel electrophoresis) • lyophilized powder	Sigma-Aldrich®	A7030-100G
Collagenase, Type I	• From *Clostridium hytoliticum*	Sigma-Aldrich®	C0130-500MG
Dimethyl sulfoxide (DMSO)	• ≥99.9%	Sigma-Aldrich®	D8418
Hygromycin B	• From *Streptomyces sp.* • Sterile-Filtered Solution in 25 mM HEPES	Calbiochem	400053
Doxycycline hyclate	• ≥98% (TLC)	Sigma-Aldrich®	D9891-5G
Histopaque®-1077	• 1.077 g/ml	Sigma-Aldrich®	10771-500ML
UltraPure™ EDTA	• pH 8.0 • 0.5 M in H_2O • Sterile, molecular biology grade	Invitrogen™ Life Technologies	15575-020

ANNEX 5: Chemicals

Name	Details	Manufacturer	Catalogue number
Citrate-dextrose solution (ACD)	• Sterile	Sigma-Aldrich®	029K8712
Carboxymethylcellulose sodium salt (CMC)	• High viscosity	Sigma-Aldrich®	C5013-500G
EDTA powder	• ACS reagent • 99.4-100%	Sigma-Aldrich®	E9884-1KG
Sucrose	• Molecular biology grade, ≥99.5%	Sigma-Aldrich®	S0389-5KG
Tris(hydroxymethyl)aminomethane (TRIS)	• ACS reagent • ≥99.8%	Sigma-Aldrich®	252859-500G
TRIS-HCl	• pH=7.0	Sigma-Aldrich®	T2413
Tris-Acetate-EDTA (TAE) buffer, 50 x	• 50 x • 0.22 μm filtered	Life Technologies	B49
Sodium chloride (NaCl)	• ACS reagent • ≥99.5%	Sigma-Aldrich®	S9888-5KG
Sodium hydroxide (NaOH) solution	• 1.0 M • Sterile	Sigma-Aldrich® Fluka®	72082-100ML
Hydrochloric acid (HCl) solution	• 0.1 M • Sterile	Sigma-Aldrich® Fluka®	84428-100ML
10% Neutral Buffered Formalin	• 10% v/v formalin • For histology	Leica Microsystems	3800600E
Toluidine Blue	N/A	Sigma-Aldrich®	T3260
Ethanol	• Molecular biology grade, 200 proof	Sigma-Aldrich®	E7023-500ML
Propan-2-ol	• Molecular Biology Grade, >99.5%	Sigma-Aldrich®	I9516-500ML
2-Methylbutane (Isopentane)	• Anhydrous • ≥99 %	Sigma-Aldrich®	277258-1L
Chloroform	• Anhydrous • ≥99%	Sigma-Aldrich®	288306-100ML
Imalgène® 1000 (ketamine chlorhydrate)	N/A	Rhône Mérieux	N/A
Sodium pentothal	• 500 mg • Powder	Abbott Laboratories	N/A
Silicone Vacuum Grease	N/A	Beckman Coulter	335148
Ammonium chloride, NH_4Cl	• Powder	Sigma-Aldrich®	254134-100G
Potassium bicarbonate, $KHCO_3$	• ACS reagent • 99.7%	Sigma-Aldrich®	237205-500G

ANNEX 6: Molecular biology kits and reagents

Name	Details	Manufacturer	Catalogue number
Dual-Glo® Luciferase Assay System	• No lysis required • RLuc and FLuc	Promega	E2940
Dual-Luciferase® Reporter Assay System	• Lysis required • RLuc, GLuc, FLuc	Promega	E1960
CellTiter-Glo® Luminescent Cell Viability Assay	• 10 × 10ml • Based on quantitation of the ATP present	Promega	G7571
Nuclease-free water (H_2O)	• Miolecular biology grade • RNase-, DNasae-free	Sigma-Aldrich®	W4502
TRIzol® Reagent	• 100 ml	Life Technologies Ambion™	15596-026
RNAlater® Solutions	• 100 ml	Life Technologies Ambion™	AM7020
Lipofectamine® 2000 Transfection Reagent	• 1.5 ml	Invitrogen™ Life Technologies	11668
FuGENE® 6 Transfection Reagent	• 0.5 ml	Promega	E2693
50 bp DNA ladder	• For 100 lanes	New England Biolabs	N3236S
100bp DNA Ladder	• For 50 lanes	Promega	G2101
1kb DNA Ladder	• For 100 lanes	Promega	G5711
6 x Blue/Orange Loading Dye	• 6 x loading dye • 3 x 1 ml	Promega	G1881
Ultrapure™ Agarose	• For DNA gel electrophoresis	Invitrogen™ Life Technologies	16500-500
SYBR® Safe DNA Gel Stain	• 400 µL	Life Technologies	S33102
GoTaq® DNA Polymerase	• 500 Units	Promega	M3005
KOD Hot Start DNA Polymerase	• 1000 Units	Merck Millipore Novagene	71086-4
Pfu DNA Polymerase	• 500 Units	Promega	M774B
Vent® DNA Polymerase	• 1000 Units	New England Biolabs	M0254L
dNTPs	• 25mM each • 2 x 500 µl	Bioline	BIO-39029
MEGAscript® SP6 Kit	• For 40 reactions	Life Technologies Ambion™	AM1330

m7G(5')ppp(5')G Cap Analog	• 40 mM • 100 Units	Life Technologies Ambion™	AM8052
RNasin® Plus RNase Inhibitor	• 10,000 Units	Promega	N2615
SuperScript™ III Reverse Transcriptase	• 10,000 Units • 200 Units/µl • 50 reactions	Invitrogen™ Life Technologies	18080-044
SuperScript™ III Platinum One Step Quantitative RT-PCR System	• 100 reactions	Invitrogen™ Life Technologies	11732-020
RNase H	• 30 Units	Invitrogen™ Life Technologies	18021-014
High Capacity cDNA Reverse Transcription Kit	• 200 reactions	Life Technologies Applied Biosystems®	4368814
FastStart SYBR® Green Master Mix	• 50 reactions	Roche	04673484001
TaqMan® Universal PCR Master Mix	• 1 x 5 ml	Life Technologies Applied Biosystems®	4304437
TaqMan® miR-142-3P Assay	• Assay ID: 000464 • 50 assays	Life Technologies Applied Biosystems®	4427975
TaqMan® miR16 Assay	• Assay ID: 000391 • 50 assays	Life Technologies Applied Biosystems®	4427975
Thermosensitive Alkaline Phosphatase (TSAP)	• 100 Units	Promega	M9910
T4 DNA Ligase	• 20,000 Units • 400 Units/µl	New England Biolabs	M0202S
Bovine Serum Albumin (BSA), Acetylated	• Enzyme stabiliser • 10 mg/ml	Promega	R3961
SpeI	• 500 Units • 10 Units/µl	New England Bioloabs	R0133S
NotI	• 200 Units • 10 Units/µl	Roche	11014714001
AvrII	• 100 Units • 5 Units/µl	New England Bioloabs	R0174S
PmeI	• 500 Units • 10 Units/µl	New England Bioloabs	R0560S
ApaI	• 5,000 Units • 10 Units/µl	Promega	R6361
BamHI	• 2,500 Units • 10 Units/µl	Promega	R6021
SacI	• 2,000 Units • 20 Units/µl	New England Bioloabs	R0156S

SbfI	• 500 Units • 10 Units/µl	New England Bioloabs	R0642S
XhoI	• 3,000 Units • 10 Units/µl	Promega	R6161
EcorV	• 2,000 Units • 10 Units/µl	Promega	R6351
BglII	• 500 Units • 10 Units/µl	Promega	R6081
MluI	• 1,000 Units • 10 Units/µl	Promega	R6381
XbaI	• 2,000 Units • 10 Units/µl	Promega	R6181
NdeI	• 4,000 Units • 20 Units/µl	New England Biolabs	R0111S
FseI	• 100 Units • 2 Units/µl	New England Biolabs	R0588S
BglII	• 2,500 Units • 10 Units/µl	Promega	R6085
EcorV	• 2,000 Units • 10 Units/µl	Promega	R6351

ANNEX 7: Competent bacteria and supplementary reagents

Name	Details	Manufacturer	Catalogue number
Subcloning Efficiency™ DH5α™ Competent Cells	• 4 x 500 µl	Invitrogen™ Life Technologies	18265-017
SURE® 2 Supercompetent Cells	• 10 x 100 µl	Stratagene	200152
SOC medium	• 5 ml aliquots • 0.2 µm filtered	Sigma-Aldrich®	S1797-10x5ML
Bacto™ Agar	-	BD	214010
Tryptone Soya Broth	• 30g in 1L of H_2O	Thermo Scientific™ Oxoid™	CM0129
Ampicillin powder	• 100 mg/ml (1000x concentration)	Sigma-Aldrich®	A0166-25G
Kanamycin powder	• 50 mg/ml (1000x concentration)	Sigma-Aldrich®	K1876-5G
LB Broth	• Miller (Luria-Bertani) formulation • 25 g in H_2O, 1000 ml total volume	BD Difco™	244610
LB Agar	• Miller (Luria-Bertani) formulation • 40 g in H_2O, 1000 ml total volume	BD Difco™	244510

ANNEX 8: Nucleic acid extraction and purification kits

Name	Details	Manufacturer	Catalogue number
DNeasy® Blood & Tissue Kit	• For 50 samples	Qiagen	69504
RNeasy® Mini Kit	• For 50 samples	Qiagen	74104
RNase-Free DNase Set	• For 50 samples • DNase treatment with Qiagen RNA purification kits • On-column treatment	Qiagen	79254
QIAamp Viral RNA Mini Kit	• For 50 samples	Qiagen	52904
NucleoSpin® Gel and PCR Clean-up	• For 50 samples • Binding capacity 25 µg • Optimal recovery of fragments <15 µg and between 100 and500 bp in length	Macherey-Nagel	740609.50
Illustra™ GFX™ PCR DNA and Gel Band Purification Kit	• For 100 samples	GE Healthcare	45-001-489
ISOLATE Plasmid Mini Kit	• For 50 samples • Binding capacity 13 µg	Bioline	BIO-52026
EndoFree® Plasmid Purification Maxi Kit	• For 10 samples Maxi-Prep Kit • Endotoxin-free • Binding capacity 500 µg	Qiagen	12362
NucleoSpin® 96 Virus	• 96-well plates format • < 150 µL cell-free biological fluids (serum, plasma)	Macherey-Nagel	740691.4

ANNEX 9: Immunobiology reagents

Name	Details	Manufacturer	Catalogue number
CD14 MicroBeads	• Against human CD14	Millenyi Biotec	130-050-201
MACS MS Separation columns	• 25 columns	Millenyi Biotec	130-042-201
Microscope slides	• 76 x 26 mm	Knittle Glass	-
Cover glass	• 13 mm diameter • Thickness No. 1 • Boroslilicate glass	VWR	631-0149
VECTASHIELD® Mounting Medium with DAPI	• Ready to use	Vector Laboratories	H-1200
VECTASHIELD® HardSet Antifade Mounting Medium	• Ready to use	Vector Laboratories	H-1400
4',6-Diamidino-2-Phenylindole, (DAPI)	• Dihydrochloride • 10 mg	Life Technologies	D1306
CAS BLOCK™	• Ready to use	ZYMED laboratories	00-8120
PE Rat anti-mouse F4/80 antibody	• 1:100 dilution for flow cytometry	Biolegend	122616
PE Rat IgG2b	• 1:100 dilution for flow cytometry • κ Isotype control	Biolegend	400608
OCT Cryoembedding Matrix	• 125 ml	Thermo Scientific™ Raymond Lamb	12678646
Triton™ X-100	• Laboratory grade	Sigma-Aldrich ®	X100-500ML
Rabbit anti-SFV nsP3 primary antibody	• Polyclonal	Dr Tero Ahola, University of Helsinki	N/A
Donkey anti-Rabbit secondary Antibody, Alexa Fluor® 488 conjugate	• Polyclonal, IgG • Conjugated to Alexa Fluor® 488	Life Technologies	R37118
Goat anti-Rat IgG (H+L) secondary antibody, Alexa Fluor® 594 conjugate	• Polyclonal, IgG (H+L) • Conjugated to Alexa Fluor® 594	Life Technologies	A-11007
Rat anti-Mouse MARCO primary antibody	• Monoclonal • Clone ED31 • IgG1	AbD Serotec®	MCA1849T
Rat anti-Mouse CD169 primary antibody, Alexa Fluor® 647 conjugate	• Monoclonal • Clone MOMA-1 • IgG2a	AbD Serotec®	MCA947A647

ANNEX 10: Equipment

Name	Details	Manufacturer
Zeiss Observer.D1	• Inverted microscope • Hal 100 halogen illuminator • Colibri LED illumination system • AxioCam MRc camera	Carl Zeiss
Zeiss Axioskop 2	• Upright microscope • HBO 100 illuminator - 100-watt high-pressure mercury plasma arc-discharge lamp • HAL 100 halogen illuminator • Supply unit Ebq 100 ISOLATED for 100 W high-pressure mercury burner • AxioCam MRc camera	Carl Zeiss
Venti 96-well Thermal Cycler	• Innovative VeriFlex™ Blocks allow for precise PCR optimization and enable you to run up to 6 independent assays • Sample Ramp Rate - ± 3.35 °C⁄se • Block Temperature Range - 4.0-99.9 °C • Temperature Accuracy - ±0.25°C (35°C to 99.9°C) • Temperature Uniformity - <0.5°C	Life Technologies Applied Biosystems®
MultiImage Light Cabinet FluorChem HD2	• 4.19 Megapixel camera with 16-bit A/D, cooled to -25ºC absolute and regulated • Manual 28-70 mm F2.8 zoom lens • Orange Filter —for gels stained with ethidium bromide, coomassie blue, or SYPRO® Orange. 590/55 nm. • Green Filter —for gels or plates with GFP, SYBR® Safe, SYBR® Gold, Fluorescein, SYBR® Green. 537/35 nm • Red Filter —used for gels stained with SYPRO® Red, SYPRO® Ruby, Texas Red, or Rhodamine. 620/40 nm	Alpha Innotech
L8-70M Ultracentrifuge	• Max Speed – 70,000 RPM • SW28.1 Swing Bucket Rotor (6 x 38.5 ml)	Beckman Coulter
Optima™ L-100K Ultracentrifuge	• Max Speed – 100,000 RPM • SW32 Ti Swing Bucket Rotor (6 x 38.5 ml)	Beckman Coulter
3 S-R Bench Top Centrifuge	• Refrigerated • Swing-out rotor for 4 buckets (20 x 50 ml tubes or 48 x 15 ml tubes) • Max RCF – 3,800 x g • Max Speed – 4,300 RPM	Thermo Scientific™ Heraeus™
5810 R Centrifuge	• Refrigerated • Rectangular swing-out rotor for 4 buckets (20 x 50 ml tubes or 64 x 15 ml tubes) • Max RCF - 3,100 x g • Max Speed – 4,000 RPM	Eppendorf

Sigma 3-16K Centrifuge	• Refrigerate • Fixed-angle rotor for 30 microfuge tubes, 1.5/2.0 ml • Swing-out rotor for 4 buckets (12 x 50 ml tubes or 28 x 15 ml tubes) • Max RCF (fixed-angle rotor) – 21,930 x g • Max RCF (swing-out rotor) – 3,960 x g • Max Speed (fixed angle rotor) – 14,000 RPM • Max Speed (swing-out rotor) – 4,500 RPM	Sigma
Pico™ 17 Microcentrifuge	• Non-refrigerated • 24 x 1.5/2.0 ml Fixed-Angle Rotor • Max RCF - 17,000 x g • Max Speed – 13,300 RPM	Thermo Scientific™ Heraeus™
Microcentrifuge 5415R	• Refrigerated • Fixed-angle rotor for 24 microfuge tubes, 1.5/2.0 ml tubes • Max RCF - 16,100 x g • Max Speed – 13,200 RPM	Eppendorf
PicoFuge™ (HF-120)	• Microcentrifuge • 200 µl-tube strips or 200 µl tubes • Maximum RCF - 2,810 x g • Maximum Speed - 6,300 RPM	Stratagene
Sprout™ Mini-Centrifuge	• Microcentrifuge • 8-tube 200 µl-tube strips or 1.5/2.0 ml tubes • Maximum RCF – 2,000 x g	Heathrow Scientific LLC
Incubator MCO-5AC-PE	• Humidified • CO_2 • Temp control range and fluctuation - ambient temp +5 to +50, ±0.1 °C • Temperature uniformity - ±0.25°C • CO_2 control range - 0-20%	Panasonic
Rotor-Gene 3000 Real-Time PCR Machine	• Centrifugal rotary format • Uniformity – ± 0.01°C • 72 x 0.1ml strip tubes	Corbett Life Science, Qiagen
ICycler IQ™ Real Time PCR	• My IQ™ Real Time Module • 96-well plate format	Bio-Rad
PowerPac™ Basic Power Supply	• Power supply for gel electrophoresis.	Bio-Rad
Wide Mini-Sub® Cell GT Cell	• Electrophoresis gel tank • 15 x 10 cm gel trays	Bio-Rad
Mini-Sub® Cell GT Cell	• Electrophoresis gel tank • 7 x 10 cm gel trays	Bio-Rad
Sub-Cell® GT Cell	• Electrophoresis gel tank • 15 x 25 cm gel trays	Bio-Rad
Mini-Gel Caster 1704422	• For use with Mini-Sub and wide Mini-Sub cell GT systems	Bio-Rad

QBT2 Digital Block Heater	• Temperature range Ambient + 5 °C to 150 °C • Setting range 15 °C to 150 °C • Stability at 37 °C ± 0.1 °C	Grant
Hotplate Stirrer CB302	• Plate size - 30x30cm • Max. plate temperature - 300°C • Stirrer speed – 100-1,500 RPM	Stuart
Thermomixer® Dry Block Heating Shakers	• Thermoblock for 24 x 1.5 ml tubes • Temperature control range - 4°C above room temperature to 99°C • Mixing frequency - 300-1,400 RPM • Incubating accuracy - ±1°C from values set between 20 and 45°C	Eppendorf
PIPETMAN Classic™	• 0.2-2.0 µl • 1.0-10.0 µl • 2.0-20 µl • 20-200 µl • 100-1000 µl	Gilson
BioPette™ Plus Multichannel	• 8-channel • 20-200 µl	Labnet International
Transferpette® S Multichannel	• 8-channel • 20-200 µl	BrandTech
Pipette Aid™ Express™	• Cordless • Fitted with a 0.2 µm filter	Thermo Scientific™ Falcon™
Vortex/Shaker SA8	• Speed range – 200-2,500 RPM	Stuart
WhirliMixer™ vortex	• Speed range – 200-1,400 RPM	Fisher Scientific
InnOva™ 4300 Incubator Shaker	• Speed range - 25-500 RPM • Temperature range - 5°C above ambient to 60°C	New Brunswick
NanoDrop™	• Full spectrum spectrophotometer (220nm-750nm) • Nucleic acid concentration and purity of samples up to 3700 ng/µl (dsDNA) without dilution	Thermo Scientific™
SSM4 Sea-saw rocker	• Speed range - 5 to 70 RPM • Angle of tilt - 7°	Stuart
DR89 Dark Reader blue transilluminator	• Multiple high intensity blue LEDs • Visible light – no DNA damage • Suitable for visualising SYBR® Green, GelStar, GelGreen, SYPRO® Ruby, ProQ Diamond, fluorescein and GFP	Clare Chemical Research
VACUSAFE™ Laboratory Aspirator	• Vacuum range from -300 to -600 mbar • Pump flow rate - 8 l/min (air) • Aspiration rate of liquids - 17 ml/s (aspiration pipette)	Integra Biosciences

GloMax® Microplate Reader	• Luminescence, fluorescence, absorbance • Dual injectors • Detector - head-on photomultiplier tube (PMT) for photon-counting • Detection Limit - 3 x 10-21 moles of Luciferase or 1 x 10-18moles of AT • Linear Dynamic Range - > 8 logs • Spectral Range - 350 - 650 nm	Promega
S20 SevenEasy™ pH Meter	• Automatic temperature compensation (ATC)	Mettler Toledo
Milli-Q® Water Purification System and Q-POD Water Delivery Unit	• High quality, ultrapure water, free of particulates, bacteria, pyrogens, RNAse, DNase, proteases, VOCs, endocrine disruptors and organics for LC	Merck Millipore
Gene Pulser Xcell™ Eukaryotic Electroporation System	• Main unit, CE module and a ShockPod™ cuvette chamber	Bio-Rad
Microwave (NN-E442W)	N/A	Panasonic
BD FACSCalibur™ Flow Cytometer	• Dual-laser design (air-cooled argon laser and red diode laser) – high sensitivity, minimal need for compensation and flexibility • Multicolour analysis capabilities	BD
COULTER® HmX Hematology Analyzer	• 75 samples-per-hour throughput • Continuous auto-loading for complete walkaway operation • Closed vial sampling for improved operator safety	Beckman Coulter
ICycler IQ™ Real Time PCR	• My IQ™ Real Time Module • 96-well format	Bio-Rad

ANNEX 11: Buffers and solutions

1. **MACS Buffer (2mM EDTA and 1% w/v FBS in PBS)**
    - 448 ml of Mg^{2+}- and Ca^{2+}-free PBS (Sigma-Aldrich®, Annex 4)
    - 2 ml of 0.5 M EDTA (Life Technologies, Annex4)
    - 5 ml of FBS (Invitrogen™ Life Technologies, Annex 4)

2. **10 x TNE buffer (0.5 M Tris-HCl, 1.0 M NaCl, 1.0 mM EDTA, pH=7.4)**
    - 500 ml of 1.0 M Tris-HCl (Sigma-Aldrich®, Annex 5)
    - 58.5g of NaCl (Sigma-Aldrich®, Annex 5)
    - 100 ml of 1.86g in EDTA solution in 500 ml of H_2O (Sigma-Aldrich®, Annex 5)
    - Milli-Q H_2O up to 1000 ml total volume (Merck Millipore, Annex 10)
    - NaOH or HCl to adjust pH to 7.4 (Sigma-Aldrich®, Annex 5)
    - Autoclave at 121ºC for 15 minutes

3. **1 x TNE buffer (50 mM Tris-HCl, 100 mM NaCl, 0.1 mM EDTA, pH=7.4)**
    - 100 ml of 10 x TNE buffer
    - Milli-Q H_2O up to 1000 ml total volume (Merck Millipore, Annex 10)
    - NaOH or HCl to adjust pH to 7.4 (Sigma-Aldrich®, Annex 5)
    - Autoclave at 121ºC for 15 minutes

4. **20% w/v sucrose in TNE buffer**
    - 100 ml of 10 x TNE buffer
    - 200 g of sucrose (Sigma-Aldrich®, Annex 5)
    - Milli-Q H_2O up to 1000 ml total volume (Merck Millipore, Annex 10)
    - Autoclave as per sugar cycle

5. **5% w/v sucrose in H_2O**
    - 50 g of sucrose (Sigma-Aldrich®, Annex 5)
    - Milli-Q H_2O up to 1000 ml total volume (Merck Millipore, Annex 10)
    - Autoclave as per sugar cycle

6. **10% w/v sucrose in H_2O**
    - 100 g of sucrose (Sigma-Aldrich®, Annex 5)
    - Milli-Q H_2O up to 1000 ml total volume (Merck Millipore, Annex 10)
    - Autoclave as per sugar cycle

7. **20% w/v sucrose in H_2O**
    - 200 g of sucrose (Sigma-Aldrich®, Annex 5)
    - Milli-Q H_2O up to 1000 ml total volume (Merck Millipore, Annex 10)
    - Autoclave as per sugar cycle

8. **Tryptone Soya Broth**
    - 30 g of Tryptone Soya Broth (Thermo Scientific™ Oxoid™, Annex 7)
    - Milli-Q H_2O up to 1000 ml total volume (Merck Millipore, Annex 10)
    - Autoclave at 121ºC for 15 minutes

9. **LB Broth**
    - 25 g of LB Broth (BD, Annex 7)
    - Milli-Q H_2O up to 1000 ml total volume (Merck Millipore, Annex 10)
    - Autoclave at 121ºC for 15 minutes

10. **LB Agar**
    - 40 g of LB Broth (BD, Annex 7)
    - Milli-Q H_2O up to 1000 ml total volume (Merck Millipore, Annex 10)
    - Autoclave at 121ºC for 15 minutes

11. **2% w/v CMC in PBS**
    - 10 g of CMC (Sigma-Aldrich®, Annex 5)
    - PBS with Mg^{2+} and Ca^{2+} up to 500 ml total volume (Sigma-Aldrich®, Annex 4)
    - Allowed to soak up overnight, autoclaved at 121ºC for 15 minutes

12. 0.75% w/v PBSA

- 7.5 g BSA (Sigma-Aldrich®, Annex 4)
- PBS with Mg^{2+} and Ca^{2+} up to 1000 ml total volume(Sigma-Aldrich®, Annex 4)
- Filtered through 0.22µl membrane (Millipore, Annex 2)

13. 4% w/v Agar

- 4 g of Bacto™ Agar (BD, Annex 7)
- PBS with Mg^{2+} and Ca^{2+} up to 100 ml total volume (Sigma-Aldrich®, Annex 4)
- Autoclave at 121ºC for 15 minutes

14. 1 x TAE

- 20 ml of 50 x TAE buffer (Life Technologies, Annex 5)
- Milli-Q H_2O up to 1000 ml total volume (Merck Millipore, Annex 10)

15. 0.3% v/v Triton™ X-100 in PBS

- 1.5 ml Triton™ X-100 (Sigma-Aldrich®, Annex 9)
- 498.5 ml PBS with Mg^{2+} and Ca^{2+} (Sigma-Aldrich®, Annex 4)

16. RBC lysis buffer

- 8.29 g of NH_4Cl (Sigma-Aldrich®, Annex 5)
- 1 g of $KHCO_3$ (Sigma-Aldrich®, Annex 5)
- 32.7 mg EDTA (Sigma-Aldrich®, Annex 5)
- Milli-Q H_2O up to 1000 ml total volume (Merck Millipore, Annex 10)

17. FACS buffer

- 99 ml of Mg^{2+}- and Ca^{2+}-free PBS (Sigma-Aldrich, Annex 4)
- 1 ml of FBS (Invitrogen™ Life Technologies GIBCO®, Annex 4)

ANNEX 12: PCR primers and cycling parameters

1. CHIKV E1 Control (Go-Taq®)

CHIKV E1 For (22 bases; 54.5% GC; Tm=56.7 ºC):
AAGCTCCGCGTCCTTTACCAAG

CHIKV E1 Rev (21 bases; 47.6% GC; Tm=52.4 ºC):
CCAAATTGTCCTGGTCTTCCT

Fragment size – 209 bp

Denaturation	–	95 ºC	– 2 min	**x 1**
Denaturation **Annealing** **Elongation**	– – –	95 ºC 60 ºC 72 ºC	– 30 sec – 30 sec – 30 sec	**x 35**
Elongation	–	72 ºC	– 5 min	**x 1**
4 ºC				∞

2. CHIKV nsp4-E1 Recombination Control (Go-Taq®)

CHIK nsp4 For (19 bases; 52.6% GC; Tm=51.1 ºC):
GCTCCAGATCCAACTTCGA

CHIK E1 Rev (19 bases, 52.6% GC; Tm=51.1 ºC):
GCAGCTGAGAATTCCCTTC

Fragment size – 3,614 bp

Denaturation	–	95 ºC	– 2 min	**x 1**
Denaturation **Annealing** **Elongation**	– – –	95 ºC 55 ºC 72 ºC	– 30 sec – 30 sec – 4 min	**x 35**
Elongation	–	72 ºC	– 5 min	**x 1**
4 ºC				∞

3. CHIKV nsp4-E3 Recombination Control (Go-Taq®)

CHIK nsp4 For (19 bases; 52.6% GC; Tm=51.1 ºC):
GCTCCAGATCCAACTTCGA

CHIK E3 Rev (19 bases, 52.6% GC; Tm=51.1 ºC):
CATGACGTTGTCCTCAAGC

Fragment size – 1,052 bp

Denaturation	–	95 ºC	– 2 min	**x 1**
Denaturation **Annealing** **Elongation**	– – –	95 ºC 55 ºC 72 ºC	– 30 sec – 30 sec – 1 min	**x 35**
Elongation	–	72 ºC	– 5 min	**x 1**
4 ºC				∞

4. ICRES1 2SG Cloning Control (Go-Taq®)

ICRES1 2SG Control For (22 bases; 54.5% GC; Tm=56.7 ºC):
GCTGACGAAGTGATCAGATGGC

ICRES1 2SG Control Rev (22 bases, 54.5 % GC; Tm=56.7 ºC):
CGAGGCTGGTACCTCCTATTGT

Fragment size
– 601 bp (miR-142-3P RE)
– 598 bp (miRNA RE Control)

Denaturation	–	95 ºC	– 2 min	**x 1**
Denaturation **Annealing** **Elongation**	– – –	95 ºC 55 ºC 72 ºC	– 30 sec – 30 sec – 45 sec	**x 35**
Elongation	–	72 ºC	– 5 min	**x 1**
4 ºC				∞

5. ICRES1 and ChikRepl nsP3 Cloning Control (Go-Taq®)

ICRES1 nsP3 For (22 bases; 54.5% GC; Tm=56.7 ºC):
CTGCACAGGAGGCGAGTACAAT

ICRES1 nsP3 Rev (22 bases, 54.5 % GC; Tm=56.7 ºC):
TCACAGTCAGGTTTCTCCCTCG

Fragment size
- 399 bp (miR-142-3P RE)
- 396 bp (miRNA RE Control)

Denaturation	–	95 ºC	– 2 min	**x 1**
Denaturation **Annealing** **Elongation**	– – –	95 ºC 58 ºC 72 ºC	– 30 sec – 30 sec – 30 sec	**x 35**
Elongation	–	72 ºC	– 5 min	**x 1**
4 ºC				∞

6. ChikRepl 3' UTR Cloning Control (Go-Taq®)

ICRES1 2SG Control For (22 bases; 54.5% GC; Tm=56.7 ºC):
GCTGACGAAGTGATCAGATGGC

ChikRepl SG Control Rev (22 bases, 54.5 % GC; Tm=56.7 ºC):
TATTCAGGGGTTGCGTAGCCCT

Fragment size
- 503 bp (miR-142-3P RE)
- 500 bp (miRNA RE Control)

Denaturation	–	95 ºC	– 2 min	**x 1**
Denaturation **Annealing** **Elongation**	– – –	95 ºC 58 ºC 72 ºC	– 30 sec – 30 sec – 30 sec	**x 35**
Elongation	–	72 ºC	– 5 min	**x 1**
4 ºC				∞

7. SFV4 SbfI Site Cloning Control (Go-Taq®)

SFV4 SbfI Control For (19 bases; 57.9 % GC; Tm=53.2 ºC):
CATTGAGAATGCCGTCCGG

SFV4 SbfI Control Rev (19 bases; 57.9 % GC; Tm=53.2 ºC):
GTTTCCGGTTCCACAGGTG

Fragment size – 367 bp

Denaturation	–	95 ºC	– 2 min	**x 1**
Denaturation **Annealing** **Elongation**	– – –	95 ºC 51 ºC 72 ºC	– 30 sec – 30 sec – 30 sec	**x 35**
Elongation	–	72 ºC	– 5 min	**x 1**
4 ºC				∞

8. SFV4 SacI Site Cloning Control (Go-Taq®)

SFV4 SacI Control For (19 bases; 57.9 % GC; Tm=53.2 ºC):
GAGTATCACGCAGGTGCAG

SFV4 SacI Control For (19 bases; 57.9 % GC; Tm=53.2 ºC):
CGGCGTCAGTTCTTTCAGC

Fragment size – 409 bp

Denaturation	–	95 ºC	– 2 min	**x 1**
Denaturation **Annealing** **Elongation**	– – –	95 ºC 51 ºC 72 ºC	– 30 sec – 30 sec – 30 sec	**x 35**
Elongation	–	72 ºC	– 5 min	**x 1**
4 ºC				∞

9. SFV4 3’ UTR Cloning Control (Go-Taq®)

SFV4 3’ UTR For (22 bases; 54.5 % GC; Tm=56.7 ºC):
TGTTTCCAGACATGTCGGGCAC

SFV4 3’ UTR Rev (22 bases; 54.5 % GC; Tm=56.7 ºC):
AATTGCGCAGGTCTTGTTGCGC

Fragment size
- 400 bp (miR-142-3P RE)
- 397 bp (miR-142-3P Antisense RE)
- 397 bp (miRNA RE Control)
- 888 bp (GLuc)
- 1,043 bp (GLuc-miR-142-3P RE)
- 1,040 bp (GLuc-miR-142-3P Antisense RE)
- 1,040 bp (GLuc-miRNA RE Control)

Denaturation	–	95 ºC	– 2 min	**x 1**
Denaturation **Annealing** **Elongation**	– – –	95 ºC 55 ºC 72 ºC	– 30 sec – 30 sec – 60 sec	**x 35**
Elongation	–	72 ºC	– 5 min	**x 1**
4 ºC				∞

10. SFV4 nsP3 Cloning Control (Go-Taq®)

SFV4 nsP3 For (22 bases; 59.1 % GC; Tm=58.6 ºC):
ACGGCTGACGTACACCCTGAAC

SFV4 nsP3 Rev (22 bases; 59.1 % GC; Tm=58.6 ºC):
AACGCATCGACCTCGTGCTCGT

Fragment size
– 401 bp (miR-142-3P RE)
– 398 bp (miR-142-3P Antisense RE)
– 398 bp (miRNA RE Control)

Denaturation	–	95 ºC	– 2 min	**x 1**
Denaturation **Annealing** **Elongation**	– – –	95 ºC 58 ºC 72 ºC	– 30 sec – 30 sec – 30 sec	**x 35**
Elongation	–	72 ºC	– 5 min	**x 1**
4 ºC				∞

11. pMK NotI-PmeI Cloning Control (Go-Taq®)

---

pMK NotI-PmeI Control For (19 bases; 57.9 % GC; Tm=53.2 ºC):
GACCTGCTCAAGAAGTGGC

pMK NotI-PmeI Control Rev (19 bases; 57.9 % GC; Tm=53.2 ºC):
GAAAGGAAGGCCCATGAGG

Fragment size
– 292 bp (GLuc-miR-142-3P RE)
– 289 bp (GLuc-miR-142-3P Antisense RE)
– 289 bp (GLuc-miRNA RE Control)

Denaturation	–	95 ºC	– 2 min	**x 1**
Denaturation **Annealing** **Elongation**	– – –	95 ºC 51 ºC 72 ºC	– 30 sec – 30 sec – 30 sec	**x 35**
Elongation	–	72 ºC	– 5 min	**x 1**
4 ºC				∞

12. pcDNA™3.1+ and pcDNA™5/FRT/TO Cloning Control (Go-Taq®)

---

pcDNA Control For (18 bases; 61.1 % GC; Tm=52.6 ºC):
AAATGGGCGGTAGGCGTG

pcDNA Control Rev (18 bases; 61.1 % GC; Tm=52.6 ºC):
AGAAGGCACAGTCGAGGC

Fragment size
- 610 bp (miR-142 'Core')
- 1,105 bp (miR-142 'Short')
- 1,201 bp (miR-142 'Long-3')
- 1,249 bp (miR-142 'Long-5')
- 961 bp (mCherry)

Denaturation	95 ºC	– 2 min	**x 1**
Denaturation **Annealing** **Elongation**	95 ºC 51 ºC 72 ºC	– 30 sec – 30 sec – 1 min 30 sec	**x 35**
Elongation	72 ºC	– 5 min	**x 1**
4 ºC			∞

13. miRNA RE 5'AvrII and 3'PmeI (Vent® or Go-Taq®)

miRNA RE AvrII For (26 bases; 57.7 % GC; Tm=62.7 ºC):
ATCCCTAGGTCCGGACCAGGTTCGAA

miRNA RE PmeI Rev (28 bases; 50.0 % GC; Tm=61.4 ºC):
CGCGTTTAAACCAATTGAGCTCCTGAGG

Fragment size
– 161 bp (miR-142-3P RE)
– 158 bp (miRNA RE Control)

Denaturation	–	95 ºC	– 2 min	**x 1**
Denaturation **Annealing** **Elongation**	– – –	95 ºC 44 ºC 72 ºC	– 30 sec – 30 sec – 30 sec	**x 1**
Denaturation **Annealing** **Elongation**	– – –	95 ºC 58 ºC 72 ºC	– 30 sec – 30 sec – 30 sec	**x 35**
Elongation	–	72 ºC	– 5 min	**x 1**
4 ºC				∞

14. miRNA RE 5’ SpeI and 3’ SpeI (Go-Taq ®)

miRNA RE SpeI For (26 bases; 57.7 % GC; Tm=62.7 ºC):
CGCACTAGTTCCGGACCAGGTTCGAA

miRNA RE SpeI Rev (26 bases; 53.8 % GC; Tm=61.1 ºC):
CGCACTAGTCAATTGAGCTCCTGAGG

Fragment size
– 159 bp (miR-142-3P RE)
– 156 bp (miRNA RE Control)

Denaturation	–	95 ºC	– 2 min	**x 1**
Denaturation **Annealing** **Elongation**	– – –	95 ºC 44 ºC 72 ºC	– 30 sec – 30 sec – 30 sec	**x 1**
Denaturation **Annealing** **Elongation**	– – –	95 ºC 58 ºC 72 ºC	– 30 sec – 30 sec – 30 sec	**x 35**
Elongation	–	72 ºC	– 5 min	**x 1**
4 ºC				∞

15. miRNA RE 5’ ApaI and 3’ BamHI (Pfu or Go-Taq®)

---

miRNA RE ApaI For (26 bases; 61.5 % GC; Tm=64.3 ºC):
ATAGGGCCCTCCGGACCAGGTTCGAA

miRNA RE BamHI Rev (26 bases; 57.7 % GC; Tm=62.7 ºC):
CGTGGATCCCAATTGAGCTCCTGAGG

Fragment size
– 159 bp (miR-142-3P RE)
– 156 bp (miR-142-3P Antisense RE)
– 156 bp (miRNA RE Control)

Denaturation	–	95 ºC	– 2 min	**x 1**
Denaturation **Annealing** **Elongation**	– – –	95 ºC 44 ºC 72 ºC	– 30 sec – 30 sec – 30 sec	**x 1**
Denaturation **Annealing** **Elongation**	– – –	95 ºC 58 ºC 72 ºC	– 30 sec – 30 sec – 30 sec	**x 35**
Elongation	–	72 ºC	– 5 min	**x 1**
4 ºC				∞

16. miRNA RE 5’ XhoI and 3’ XhoI (Go-Taq®)

miRNA RE XhoI For (26 bases; 57.7 % GC; Tm=62.7 ºC):
ATCCTCGAGTCCGGACCAGGTTCGAA

miRNA RE XhoI Rev (26 bases; 57.7 % GC; Tm=62.7 ºC):
CTCCTCGAGCAATTGAGCTCCTGAGG

Fragment size
– 159 bp (miR-142-3P RE)
– 156 bp (miR-142-3P Antisense RE)
– 156 bp (miRNA RE Control)

Denaturation	–	95 ºC	– 2 min	**x 1**
Denaturation **Annealing** **Elongation**	– – –	95 ºC 44 ºC 72 ºC	– 30 sec – 30 sec – 30 sec	**x 1**
Denaturation **Annealing** **Elongation**	– – –	95 ºC 58 ºC 72 ºC	– 30 sec – 30 sec – 30 sec	**x 35**
Elongation	–	72 ºC	– 5 min	**x 1**
4 ºC				∞

17. miRNA RE 5'NotI and 3' PmeI (Pfu or Go-Taq®)

---

miRNA RE NotI For (26 bases; 69.2 % GC; Tm=67.4 ºC):
AGCGGCCGCTCCGGACCAGGTTCGAA

miRNA RE PmeI Rev (28 bases; 50.0 % GC; Tm=61.4 ºC):
CGCGTTTAAACCAATTGAGCTCCTGAGG

Fragment size
- 161 bp (miR-142-3P RE)
- 158 bp (miR-142-3P Antisense RE)
- 158 bp (miRNA RE Control)

Denaturation	–	95 ºC	– 2 min	**x 1**
Denaturation **Annealing** **Elongation**	– – –	95 ºC 44 ºC 72 ºC	– 30 sec – 30 sec – 30 sec	**x 1**
Denaturation **Annealing** **Elongation**	– – –	95 ºC 58 ºC 72 ºC	– 30 sec – 30 sec – 30 sec	**x 35**
Elongation	–	72 ºC	– 5 min	**x 1**
4 ºC				∞

18. miR-142 'Core' 5' EcorV and 3' XhoI (Pfu or Go-Taq®)

miR-142 Core EcorV For (28 bases; 57.1 % GC; Tm=64.3 ºC):
CTCGATATCGGGTTGGGGGGATCTTAGG

miR-142 Core XhoI Rev (28 bases; 57.1 % GC; Tm=64.3 ºC):
ATACTCGAGTAGGGAGGGGCCGTAAGGT

Fragment size – 311 bp

Denaturation	–	95 ºC	– 2 min	**x 1**
Denaturation	–	95 ºC	– 30 sec	
Annealing	–	66 ºC (Pfu) / 60 ºC (Go-Taq®)	– 30 sec	**x 35**
Elongation	–	72 ºC	– 60 sec	
Elongation	–	72 ºC	– 5 min	**x 1**
4 ºC				∞

19. miR-142 'Short' 5' EcorV and 3' XhoI (Pfu or Go-Taq®)

miR-142 Short EcorV For (27 bases; 59.3 % GC; Tm=64.3 ºC):
CTCGATATCGCCAGCCAGGGGTTCACA

miR-142 XhoI Rev (27 bases; 59.3 % GC; Tm=64.3 ºC):
ATACTCGAGTCCCCACCCCAGCAACAG

Fragment size – 806 bp

Denaturation	–	95 ºC	– 2 min	**x 1**
Denaturation	–	95 ºC	– 30 sec	
Annealing	–	66 ºC (Pfu) / 60 ºC (Go-Taq®)	– 30 sec	**x 35**
Elongation	–	72 ºC	– 1 min 30 sec	
Elongation	–	72 ºC	– 5 min	**x 1**
4 ºC				∞

20. miR-142 'Long-1' 5' EcorV and 3' XhoI (Pfu or Go-Taq®)

---

miR-142 Long-1 EcorV For (27 bases; 59.3 % GC; Tm=64.3 ºC):
CTCGATATCCACGGTTGGGGTGGACTG

miR-142 XhoI Rev (27 bases; 59.3 % GC; Tm=64.3 ºC):
ATACTCGAGTCCCCACCCCAGCAACAG

Fragment size – 899 bp

Denaturation	–	95 ºC – 2 min		**x 1**
Denaturation	–	95 ºC	– 30 sec	
Annealing	–	66 ºC (Pfu) / 60 ºC (Go-Taq®)	– 30 sec	**x 35**
Elongation	–	72 ºC	– 1 min 30 sec	
Elongation	–	72 ºC – 5 min		**x 1**
4 ºC				∞

21. miR-142 'Long-2' 5' EcorV and 3' XhoI (Pfu or Go-Taq®)

---

miR-142 Long-2 EcorV For (27 bases; 59.3 % GC; Tm=64.3 ºC):
CTCGATATCCCTCACGGTTGGGGTGGA

miR-142 XhoI Rev (27 bases; 59.3 % GC; Tm=64.3 ºC):
ATACTCGAGTCCCCACCCCAGCAACAG

Fragment size – 902 bp

Denaturation	–	95 ºC – 2 min		**x 1**
Denaturation	–	95 ºC	– 30 sec	
Annealing	–	66 ºC (Pfu) / 60 ºC (Go-Taq®)	– 30 sec	**x 35**
Elongation	–	72 ºC	– 1 min 30 sec	
Elongation	–	72 ºC – 5 min		**x 1**
4 ºC				∞

22. miR-142 'Long-3' 5' EcorV and 3' XhoI (Pfu or Go-Taq®)

---

miR-142 Long-3 EcorV For (27 bases; 59.3 % GC; Tm=64.3 ºC):
CTCGATATCGGTTGGGGTGGACTGGAG

miR-142 XhoI Rev (27 bases; 59.3 % GC; Tm=64.3 ºC):
ATACTCGAGTCCCCACCCCAGCAACAG

Fragment size – 902 bp

Denaturation	–	95 ºC – 2 min		**x 1**
Denaturation	–	95 ºC	– 30 sec	
Annealing	–	66 ºC (Pfu) / 60 ºC (Go-Taq®)	– 30 sec	**x 35**
Elongation	–	72 ºC	– 1 min 30 sec	
Elongation	–	72 ºC – 5 min		**x 1**
4 ºC				∞

23. miR-142 'Long-4' 5' EcorV and 3' XhoI (Pfu or Go-Taq®)

---

miR-142 Long-4 EcorV For (27 bases; 59.3 % GC; Tm=64.3 ºC):
CTCGATATCGGACCTCACGGTTGGGGT

miR-142 XhoI Rev (27 bases; 59.3 % GC; Tm=64.3 ºC):
ATACTCGAGTCCCCACCCCAGCAACAG

Fragment size – 905 bp

Denaturation	–	95 ºC – 2 min		**x 1**
Denaturation	–	95 ºC	– 30 sec	
Annealing	–	66 ºC (Pfu) / 60 ºC (Go-Taq®)	– 30 sec	**x 35**
Elongation	–	72 ºC	– 1 min 30 sec	
Elongation	–	72 ºC – 5 min		**x 1**
4 ºC				∞

24. miR-142 ‘Long-5’ 5’ EcorV and 3’ XhoI (Pfu or Go-Taq®)

miR-142 Long-5 EcorV For (27 bases; 59.3 % GC; Tm=64.3 ºC):
CTCGATATCCTGGTGGGGAGGCTGAAG

miR-142 XhoI Rev (27 bases; 59.3 % GC; Tm=64.3 ºC):
ATACTCGAGTCCCCACCCCAGCAACAG

Fragment size – 950 bp

Denaturation	–	95 ºC – 2 min		**x 1**
Denaturation	–	95 ºC	– 30 sec	
Annealing	–	66 ºC (Pfu) / 60 ºC (Go-Taq®)	– 30 sec	**x 35**
Elongation	–	72 ºC	– 1 min 30 sec	
Elongation	–	72 ºC – 5 min		**x 1**
4 ºC				∞

25. mCherry 5’ EcorV and 3’ XhoI (Pfu or Go-Taq®)

mCherry EcorV For (26 bases; 53.8 % GC; Tm=61.1 ºC):
GACGATATCATGGTGAGCAAGGGCGA

mCherry XhoI Rev (26 bases; 53.8 % GC; Tm=61.1 ºC):
CGCCTCGAGTTACTTGTACAGCTCGT

Fragment size – 729 bp

Denaturation	–	95 ºC – 2 min		**x 1**
Denaturation	–	95 ºC	– 30 sec	
Annealing	–	60 ºC (Pfu) / 58 ºC (Go-Taq®)	– 30 sec	**x 35**
Elongation	–	72 ºC	– 1 min 30 sec	
Elongation	–	72 ºC – 5 min		**x 1**
4 ºC				∞

26. pcDNA™ ORF 5' MluI and 3' MluI (Pfu or Go-Taq®)

pcDNA ORF For (26 bases; 53.8 % GC; Tm=61.1 ºC):
CGGGCCAGATATACGCGTTGACATTG

pcDNA ORF MluI Rev (26 bases; 53.8 % GC; Tm=61.1 ºC):
ATAACGCGTAAGCCATAGAGCCCACC

Fragment size – 1,325 bp (miR-142 'Core')
– 1,820 bp (miR-142 'Short')

Denaturation	– 95 ºC	– 2 min		**x 1**
Denaturation **Annealing** **Elongation**	– 95 ºC – 60 ºC (Pfu) / 58 ºC (Go-Taq®) – 72 ºC		– 30 sec – 30 sec – 30 sec	**x 35**
Elongation	– 72 ºC	– 5 min		**x 1**
4 ºC				∞

ANNEX 13: SFV4 sequence

ATGGCGGATGTGTGACATACACGACGCCAAAAGATTTTGTTCCAGCTCCTGCCACCTCGGCTACGCGA
GAGATTAACCACCCACGATGGCCGCCAAAGTGCATGTTGATATTGAGGCTGACAGCCCATTCATCAAG
TCTTTGCAGAAGGCATTTCCGTCGTTCGAGGTGGAGTCATTGCAGGTCACACCAAATGACCATGCAAA
TGCCAGAGCATTTTCGCACCTGGCTACCAAATTGATCGAGCAGGAGACTGACAAAGACACACTCATCT
TGGATATCGGCAGTGCGCCTTCCAGGAGAATGATGTCTACGCACAAATACCACTGCGTATGCCCTATG
CGCAGCGCAGAAGACCCCGAAAGGCTCGTATGCTACGCAAAGAAACTGGCAGCGGCCTCCGGGAAGGT
GCTGGATAGAGAGATCGCAGGAAAAATCACCGACCTGCAGACCGTCATGGCTACGCCAGACGCTGAAT
CTCCTACCTTTTGCCTGCATACAGACGTCACGTGTCGTACGGCAGCCGAAGTGGCCGTATACCAGGAC
GTGTATGCTGTACATGCACCAACATCGCTGTACCATCAGGCGATGAAAGGTGTCAGAACGGCGTATTG
GATTGGGTTTGACACCACCCCGTTTATGTTTGACGCGCTAGCAGGCGCGTATCCAACCTACGCCACAA
ACTGGGCCGACGAGCAGGTGTTACAGGCCAGGAACATAGGACTGTGTGCAGCATCCTTGACTGAGGGA
AGACTCGGCAAACTGTCCATTCTCCGCAAGAAGCAATTGAAACCTTGCGACACAGTCATGTTCTCGGT
AGGATCTACATTGTACACTGAGAGCAGAAAGCTACTGAGGAGCTGGCACTTACCCTCCGTATTCCACC
TGAAAGGTAAACAATCCTTTACCTGTAGGTGCGATACCATCGTATCATGTGAAGGGTACGTAGTTAAG
AAAATCACTATGTGCCCCGGCCTGTACGGTAAAACGGTAGGGTACGCCGTGACGTATCACGCGGAGGG
ATTCCTAGTGTGCAAGACCACAGACACTGTCAAAGGAGAAAGAGTCTCATTCCCTGTATGCACCTACG
TCCCCTCAACCATCTGTGATCAAATGACTGGCATACTAGCGACCGACGTCACACCGGAGGACGCACAG
AAGTTGTTAGTGGGATTGAATCAGAGGATAGTTGTGAACGGAAGAACACAGCGAAACACTAACACGAT
GAAGAACTATCTGCTTCCGATTGTGGCCGTCGCATTTAGCAAGTGGGCGAGGGAATACAAGGCAGACC
TTGATGATGAAAAACCTCTGGGTGTCCGAGAGAGGTCACTTACTTGCTGCTGCTTGTGGGCATTTAAA
ACGAGGAAGATGCACACCATGTACAAGAAACCAGACACCCAGACAATAGTGAAGGTGCCTTCAGAGTT
TAACTCGTTCGTCATCCCGAGCCTATGGTCTACAGGCCTCGCAATCCCAGTCAGATCACGCATTAAGA
TGCTTTTGGCCAAGAAGACCAAGCGAGAGTTAATACCTGTTCTCGACGCGTCGTCAGCCAGGGATGCT
GAACAAGAGGAGAAGGAGAGGTTGGAGGCCGAGCTGACTAGAGAAGCCTTACCACCCCTCGTTCCCAT
CGCGCCGGCGGAGACGGGAGTCGTCGACGTCGACGTTGAAGAACTAGAGTATCACGCAGGTGCAGGGG
TCGTGGAAACACCTCGCAGCGCGTTGAAAGTCACCGCACAGCCGAACGACGTACTACTAGGAAATTAC
GTAGTTCTGTCCCCGCAGACCGTGCTCAAGAGCTCCAAGTTGGCCCCCGTGCACCCTCTAGCAGAGCA
GGTGAAAATAATAACACATAACGGGAGGGCCGGCCGTTACCAGGTCGACGGATATGACGGCAGGGTCC
TACTACCATGTGGATCGGCCATTCCGGTCCCTGAGTTTCAAGCTTTGAGCGAGAGCGCCACTATGGTG
TACAACGAAAGGGAGTTCGTCAACAGGAAACTATACCATATTGCCGTTCACGGACCGTCGCTGAACAC
CGACGAGGAGAACTACGAGAAAGTCAGAGCTGAAAGAACTGACGCCGAGTACGTGTTCGACGTAGATA
AAAAATGCTGCGTCAAGAGAGAGGAAGCGTCGGGTTTGGTGTTGGTGGGAGAGCTAACCAACCCCCCG
TTCCATGAATTCGCCTACGAAGGGCTGAAGATCAGGCCGTCGGCACCATATAAGACTACAGTAGTAGG
AGTCTTTGGGGTTCCGGGATCAGGCAAGTCTGCTATTATTAAGAGCCTCGTGACCAAACACGATCTGG
TCACCAGCGGCAAGAAGGAGAACTGCCAGGAAATAGTCAACGACGTGAAGAAGCACCGCGGACTGGAC
ATCCAGGCAAAAACAGTGGACTCCATCCTGCTAAACGGGTGTCGTCGTGCCGTGGACATCCTATATGT
GGACGAGGCTTTCGCTTGCCATTCCGGTACTCTGCTAGCCCTAATTGCTCTTGTTAAACCTCGGAGCA
AAGTGGTGTTATGCGGAGACCCCAAGCAATGCGGATTCTTCAATATGATGCAGCTTAAGGTGAACTTC
AACCACAACATCTGCACTGAAGTATGTCATAAAAGTATATCCAGACGTTGCACGCGTCCAGTCACGGC
CATCGTGTCTACGTTGCACTACGGAGGCAAGATGCGCACGACCAACCCGTGCAACAAACCCATAATCA
TAGACACCACAGGACAGACCAAGCCCAAGCCAGGAGACATCGTGTTAACATGCTTCCGAGGCTGGGTA
AAGCAGCTGCAGTTGGACTACCGTGGACACGAAGTCATGACAGCAGCAGCATCTCAGGGCCTCACCCG
CAAAGGGGTATACGCCGTAAGGCAGAAGGTGAATGAAAATCCCTTGTATGCCCCTGCGTCGGAGCACG
TGAATGTACTGCTGACGCGCACTGAGGATAGGCTGGTGTGGAAAACGCTGGCCGGCGATCCCTGGATT
AAGGTCCTATCAAACATTCCACAGGGTAACTTTACGGCCACATTGGAAGAATGGCAAGAAGAACACGA
CAAAATAATGAAGGTGATTGAAGGACCGGCTGCGCCTGTGGACGCGTTCCAGAACAAAGCGAACGTGT
GTTGGGCGAAAAGCCTGGTGCCTGTCCTGGACACTGCCGGAATCAGATTGACAGCAGAGGAGTGGAGC
ACCATAATTACAGCATTTAAGGAGGACAGAGCTTACTCTCCAGTGGTGGCCTTGAATGAAATTTGCAC
CAAGTACTATGGAGTTGACCTGGACAGTGGCCTGTTTTCTGCCCCGAAGGTGTCCCTGTATTACGAGA
ACAACCACTGGGATAACAGACCTGGTGGAAGGATGTATGGATTCAATGCCGCAACAGCTGCCAGGCTG
GAAGCTAGACATACCTTCCTGAAGGGGCAGTGGCATACGGGCAAGCAGGCAGTTATCGCAGAAAGAAA
AATCCAACCGCTTTCTGTGCTGGACAATGTAATTCCTATCAACCGCAGGCTGCCGCACGCCCTGGTGG
CTGAGTACAAGACGGTTAAAGGCAGTAGGGTTGAGTGGCTGGTCAATAAAGTAAGAGGGTACCACGTC
CTGCTGGTGAGTGAGTACAACCTGGCTTTGCCTCGACGCAGGGTCACTTGGTTGTCACCGCTGAATGT

CACAGGCGCCGATAGGTGCTACGACCTAAGTTTAGGACTGCCGGCTGACGCCGGCAGGTTCGACTTGG
TCTTTGTGAACATTCACACGGAATTCAGAATCCACCACTACCAGCAGTGTGTCGACCACGCCATGAAG
CTGCAGATGCTTGGGGGAGATGCGCTACGACTGCTAAAACCCGGCGGCAGCCTCTTGATGAGAGCTTA
CGGATACGCCGATAAAATCAGCGAAGCCGTTGTTTCCTCCTTAAGCAGAAAGTTCTCGTCTGCAAGAG
TGTTGCGCCCGGATTGTGTCACCAGCAATACAGAAGTGTTCTTGCTGTTCTCCAACTTTGACAACGGA
AAGAGACCCTCTACGCTACACCAGATGAATACCAAGCTGAGTGCCGTGTATGCCGGAGAAGCCATGCA
CACGGCCGGGTGTGCACCATCCTACAGAGTTAAGAGAGCAGACATAGCCACGTGCACAGAAGCGGCTG
TGGTTAACGCAGCTAACGCCCGTGGAACTGTAGGGGATGGCGTATGCAGGGCCGTGGCGAAGAAATGG
CCGTCAGCCTTTAAGGGAGAAGCAACACCAGTGGGCACAATTAAAACAGTCATGTGCGGCTCGTACCC
CGTCATCCACGCTGTAGCGCCTAATTTCTCTGCCACGACTGAAGCGGAAGGGGACCGCGAATTGGCCG
CTGTCTACCGGGCAGTGGCCGCCGAAGTAAACAGACTGTCACTGAGCAGCGTAGCCATCCCGCTGCTG
TCCACAGGAGTGTTCAGCGGCGGAAGAGATAGGCTGCAGCAATCCCTCAACCATCTATTCACAGCAAT
GGACGCCACGGACGCTGACGTGACCATCTACTGCAGAGACAAAAGTTGGGAGAAGAAAATCCAGGAAG
CCATAGACATGAGGACGGCTGTGGAGTTGCTCAATGATGACGTGGAGCTGACCACAGACTTGGTGAGA
GTGCACCCGGACAGCAGCCTGGTGGGTCGTAAGGGCTACAGTACCACTGACGGGTCGCTGTACTCGTA
CTTTGAAGGTACGAAATTCAACCAGGCTGCTATTGATATGGCAGAGATACTGACGTTGTGGCCCAGAC
TGCAAGAGGCAAACGAACAGATATGCCTATACGCGCTGGGCGAAACAATGGACAACATCAGATCCAAA
TGTCCGGTGAACGATTCCGATTCATCAACACCTCCCAGGACAGTGCCCTGCCTGTGCCGCTACGCAAT
GACAGCAGAACGGATCGCCCGCCTTAGGTCACACCAAGTTAAAAGCATGGTGGTTTGCTCATCTTTTC
CCCTCCCGAAATACCATGTAGATGGGGTGCAGAAGGTAAAGTGCGAGAAGGTTCTCCTGTTCGACCCG
ACGGTACCTTCAGTGGTTAGTCCGCGGAAGTATGCCGCATCTACGACGGACCACTCAGATCGGTCGTT
ACGAGGGTTTGACTTGGACTGGACCACCGACTCGTCTTCCACTGCCAGCGATACCATGTCGCTACCCA
GTTTGCAGTCGTGTGACATCGACTCGATCTACGAGCCAATGGCTCCCATAGTAGTGACGGCTGACGTA
CACCCTGAACCCGCAGGCATCGCGGACCTGGCGGCAGATGTGCATCCTGAACCCGCAGACCATGTGGA
CCTCGAGAACCCGATTCCTCCACCGCGCCCGAAGAGAGCTGCATACCTTGCCTCCCGCGCGGCGGAGC
GACCGGTGCCGGCGCCGAGAAAGCCGACGCCTGCCCCAAGGACTGCGTTTAGGAACAAGCTGCCTTTG
ACGTTCGGCGACTTTGACGAGCACGAGGTCGATGCGTTGGCCTCCGGGATTACTTTCGGAGACTTCGA
CGACGTCCTGCGACTAGGCCGCGCGGGTGCATATATTTTCTCCTCGGACACTGGCAGCGGACATTTAC
AACAAAAATCCGTTAGGCAGCACAATCTCCAGTGCGCACAACTGGATGCGGTCGAGGAGGAGAAAATG
TACCCGCCAAAATTGGATACTGAGAGGGAGAAGCTGTTGCTGCTGAAAATGCAGATGCACCCATCGGA
GGCTAATAAGAGTCGATACCAGTCTCGCAAAGTGGAGAACATGAAAGCCACGGTGGTGGACAGGCTCA
CATCGGGGGCCAGATTGTACACGGGAGCGGACGTAGGCCGCATACCAACATACGCGGTTCGGTACCCC
CGCCCCGTGTACTCCCCTACCGTGATCGAAAGATTCTCAAGCCCCGATGTAGCAATCGCAGCGTGCAA
CGAATACCTATCCAGAAATTACCCAACAGTGGCGTCGTACCAGATAACAGATGAATACGACGCATACT
TGGACATGGTTGACGGGTCGGATAGTTGCTTGGACAGAGCGACATTCTGCCCGGCGAAGCTCCGGTGC
TACCCGAAACATCATGCGTACCACCAGCCGACTGTACGCAGTGCCGTCCCGTCACCCTTTCAGAACAC
ACTACAGAACGTGCTAGCGGCCGCCACCAAGAGAAACTGCAACGTCACGCAAATGCGAGAACTACCCA
CCATGGACTCGGCAGTGTTCAACGTGGAGTGCTTCAAGCGCTATGCCTGCTCCGGAGAATATTGGGAA
GAATATGCTAAACAACCTATCCGGATAACCACTGAGAACATCACTACCTATGTGACCAAATTGAAAGG
CCCGAAAGCTGCTGCCTTGTTCGCTAAGACCCACAACTTGGTTCCGCTGCAGGAGGTTCCCATGGACA
GATTCACGGTCGACATGAAACGAGATGTCAAAGTCACTCCAGGGACGAAACACACAGAGGAAAGACCC
AAAGTCCAGGTAATTCAAGCAGCGGAGCCATTGGCGACCGCTTACCTGTGCGGCATCCACAGGGAATT
AGTAAGGAGACTAAATGCTGTGTTACGCCCTAACGTGCACACATTGTTTGATATGTCGGCCGAAGACT
TTGACGCGATCATCGCCTCTCACTTCCACCCAGGAGACCCGGTTCTAGAGACGGACATTGCATCATTC
GACAAAAGCCAGGACGACTCCTTGGCTCTTACAGGTTTAATGATCCTCGAAGATCTAGGGGTGGATCA
GTACCTGCTGGACTTGATCGAGGCAGCCTTTGGGGAAATATCCAGCTGTCACCTACCAACTGGCACGC
GCTTCAAGTTCGGAGCTATGATGAAATCGGGCATGTTTCTGACTTTGTTTATTAACACTGTTTTGAAC
ATCACCATAGCAAGCAGGGTACTGGAGCAGAGACTCACTGACTCCGCCTGTGCGGCCTTCATCGGCGA
CGACAACATCGTTCACGGAGTGATCTCCGACAAGCTGATGGCGGAGAGGTGCGCGTCGTGGGTCAACA
TGGAGGTGAAGATCATTGACGCTGTCATGGGCGAAAAACCCCCATATTTTTGTGGGGGATTCATAGTT
TTTGACAGCGTCACACAGACCGCCTGCCGTGTTTCAGACCCACTTAAGCGCCTGTTCAAGTTGGGTAA
GCCGCTAACAGCTGAAGACAAGCAGGACGAAGACAGGCGACGAGCACTGAGTGACGAGGTTAGCAAGT
GGTTCCGGACAGGCTTGGGGGCCGAACTGGAGGTGGCACTAACATCTAGGTATGAGGTAGAGGGCTGC
AAAAGTATCCTCATAGCCATGGCCACCTTGGCGAGGGACATTAAGGCGTTTAAGAAATTGAGAGGACC
TGTTATACACCTCTACGGCGGTCCTAGATTGGTGCGTTAATACACAGAATTCTGATTATAGCGCACTA
TTATAGCACCATGAATTACATCCCTACGCAAACGTTTTACGGCCGCCGGTGGCGCCCGCGCCCGGCGG
CCCGTCCTTGGCCGTTGCAGGCCACTCCGGTGGCTCCCGTCGTCCCCGACTTCCAGGCCCAGCAGATG
CAGCAACTCATCAGCGCCGTAAATGCGCTGACAATGAGACAGAACGCAATTGCTCCTGCTAGGCCTCC
CAAACCAAAGAAGAAGAAGACAACCAAACCAAAGCCGAAAACGCAGCCCAAGAAGATCAACGGAAAAA

CGCAGCAGCAAAAGAAGAAAGACAAGCAAGCCGACAAGAAGAAGAAGAAACCCGGAAAAAGAGAAAGA
ATGTGCATGAAGATTGAAAATGACTGTATCTTCGAAGTCAAACACGAAGGAAAGGTCACTGGGTACGC
CTGCCTGGTGGGCGACAAAGTCATGAAACCTGCCCACGTGAAAGGAGTCATCGACAACGCGGACCTGG
CAAAGCTAGCTTTCAAGAAATCGAGCAAGTATGACCTTGAGTGTGCCCAGATACCAGTTCACATGAGG
TCGGATGCCTCAAAGTACACGCATGAGAAGCCCGAGGGACACTATAACTGGCACCACGGGGCTGTTCA
GTACAGCGGAGGTAGGTTCACTATACCGACAGGAGCGGGCAAACCGGGAGACAGTGGCCGGCCCATCT
TTGACAACAAGGGGAGGGTAGTCGCTATCGTCCTGGGCGGGGCCAACGAGGGCTCACGCACAGCACTG
TCGGTGGTCACCTGGAACAAAGATATGGTGACTAGAGTGACCCCCGAGGGGTCCGAAGAGTGGTCCGC
CCCGCTGATTACTGCCATGTGTGTCCTTGCCAATGCTACCTTCCCGTGCTTCCAGCCCCCGTGTGTAC
CTTGCTGCTATGAAAACAACGCAGAGGCCACACTACGGATGCTCGAGGATAACGTGGATAGGCCAGGG
TACTACGACCTCCTTCAGGCAGCCTTGACGTGCCGAAACGGAACAAGACACCGGCGCAGCGTGTCGCA
ACACTTCAACGTGTATAAGGCTACACGCCCTTACATCGCGTACTGCGCCGACTGCGGAGCAGGGCACT
CGTGTCATAGCCCCGTAGCAATTGAAGCGGTCAGGTCCGAAGCTACCGACGGGATGCTGAAGATTCAG
TTCTCGGCACAAATTGGCATAGATAAGAGTGACAATCATGACTACACGAAGATAAGGTACGCAGACGG
GCACGCCATTGAGAATGCCGTCCGGTCATCTTTGAAGGTAGCCACCTCCGGAGACTGTTTCGTCCATG
GCACAATGGGACATTTCATACTGGCAAAGTGCCCACCGGGTGAATTCCTGCAGGTCTCGATCCAGGAC
ACCAGAAACGCGGTCCGTGCCTGCAGAATACAATATCATCATGACCCTCAACCGGTGGGTAGAGAAAA
ATTTACAATTAGACCACACTATGGAAAAGAGATCCCTTGCACCACTTATCAACAGACCACAGCGAAGA
CCGTGGAGGAAATCGACATGCATATGCCGCCAGATACGCCGGACAGGACGTTGCTATCACAGCAATCT
GGCAATGTAAAGATCACAGTCGGAGGAAAGAAGGTGAAATACAACTGCACCTGTGGAACCGGAAACGT
TGGCACTACTAATTCGGACATGACGATCAACACGTGTCTAATAGAGCAGTGCCACGTCTCAGTGACGG
ACCATAAGAAATGGCAGTTCAACTCACCTTTCGTCCCGAGAGCCGACGAACCGGCTAGAAAAGGCAAA
GTCCATATCCCATTCCCGTTGGACAACATCACATGCAGAGTTCCAATGGCGCGCGAACCAACCGTCAT
CCACGGCAAAAGAGAAGTGACACTGCACCTTCACCCAGATCATCCCACGCTCTTTTCCTACCGCACAC
TGGGTGAGGACCCGCAGTATCACGAGGAATGGGTGACAGCGGCGGTGGAACGGACCATACCCGTACCA
GTGGACGGGATGGAGTACCACTGGGGAAACAACGACCCAGTGAGGCTTTGGTCTCAACTCACCACTGA
AGGGAAACCGCACGGCTGGCCGCATCAGATCGTACAGTACTACTATGGGCTTTACCCGGCCGCTACAG
TATCCGCGGTCGTCGGGATGAGCTTACTGGCGTTGATATCGATCTTCGCGTCGTGCTACATGCTGGTT
GCGGCCCGCAGTAAGTGCTTGACCCCTTATGCTTTAACACCAGGAGCTGCAGTTCCGTGGACGCTGGG
GATACTCTGCTGCGCCCCGCGGGCGCACGCAGCTAGTGTGGCAGAGACTATGGCCTACTTGTGGGACC
AAAACCAAGCGTTGTTCTGGTTGGAGTTTGCGGCCCCTGTTGCCTGCATCCTCATCATCACGTATTGC
CTCAGAAACGTGCTGTGTTGCTGTAAGAGCCTTTCTTTTTTAGTGCTACTGAGCCTCGGGGCAACCGC
CAGAGCTTACGAACATTCGACAGTAATGCCGAACGTGGTGGGGTTCCCGTATAAGGCTCACATTGAAA
GGCCAGGATATAGCCCCCTCACTTTGCAGATGCAGGTTGTTGAAACCAGCCTCGAACCAACCCTTAAT
TTGGAATACATAACCTGTGAGTACAAGACGGTCGTCCCGTCGCCGTACGTGAAGTGCTGCGGCGCCTC
AGAGTGCTCCACTAAAGAGAAGCCTGACTACCAATGCAAGGTTTACACAGGCGTGTACCCGTTCATGT
GGGGAGGGGCATATTGCTTCTGCGACTCAGAAAACACGCAACTCAGCGAGGCGTACGTCGATCGATCG
GACGTATGCAGGCATGATCACGCATCTGCTTACAAAGCCCATACAGCATCGCTGAAGGCCAAAGTGAG
GGTTATGTACGGCAACGTAAACCAGACTGTGGATGTTTACGTGAACGGAGACCATGCCGTCACGATAG
GGGGTACTCAGTTCATATTCGGGCCGCTGTCATCGGCCTGGACCCCGTTCGACAACAAGATAGTCGTG
TACAAAGACGAAGTGTTCAATCAGGACTTCCCGCCGTACGGATCTGGGCAACCAGGGCGCTTCGGCGA
CATCCAAAGCAGAACAGTGGAGAGTAACGACCTGTACGCGAACACGGCACTGAAGCTGGCACGCCCTT
CACCCGGCATGGTCCATGTACCGTACACACAGACACCTTCAGGGTTCAAATATTGGCTAAAGGAAAAA
GGGACAGCCCTAAATACGAAGGCTCCTTTTGGCTGCCAAATCAAAACGAACCCTGTCAGGGCCATGAA
CTGCGCCGTGGGAAACATCCCTGTCTCCATGAATTTGCCTGACAGCGCCTTTACCCGCATTGTCGAGG
CGCCGACCATCATTGACCTGACTTGCACAGTGGCTACCTGTACGCACTCCTCGGATTTCGGCGGCGTC
TTGACACTGACGTACAAGACCAACAAGAACGGGGACTGCTCTGTACACTCGCACTCTAACGTAGCTAC
TCTACAGGAGGCCACAGCAAAAGTGAAGACAGCAGGTAAGGTGACCTTACACTTCTCCACGGCAAGCG
CATCACCTTCTTTTGTGGTGTCGCTATGCAGTGCTAGGGCCACCTGTTCAGCGTCGTGTGAGCCCCCG
AAAGACCACATAGTCCCATATGCGGCTAGCCACAGTAACGTAGTGTTTCCAGACATGTCGGGCACCGC
ACTATCATGGGTGCAGAAAATCTCGGGTGGTCTGGGGGCCTTCGCAATCGGCGCTATCCTGGTGCTGG
TTGTGGTCACTTGCATTGGGCTCCGCAGATAAGTTAGGGTAGGCAATGGCATTGATATAGCAAGAAAA
TTGAAAACAGAAAAAGTTAGGGTAAGCAATGGCATATAACCATAACTGTATAACTTGTAACAAAGCGC
AACAAGACCTGCGCAATTGGCCCCGTGGTCCGCCTCACGGAAACTCGGGGCAACTCATATTGACACAT
TAATTGGCAATAATTGGAAGCTTACATAAGCTTAATTCGACGAATAATTGGATTTTTATTTTATTTTG
CAATTGGTTTTTAATATTTCCAAAAAAAAAAAAAAAAAAAAAAAAAAAAAAAAAAAAAAAAAAAAAA
AAAAAAAAAAAAAAAAAAAAA

ANNEX 14: ICRES1 sequence

ATGGCTGCGTGAGACACACGTAGCCTACCAGTTTCTTACTGCTCTACTCTGCAAAGCAAGAGATTAAT
AACCCATCATGGATCCTGTGTACGTGGACATAGACGCTGACAGCGCCTTTTTGAAGGCCCTGCAACGT
GCGTACCCCATGTTTGAGGTGGAACCAAGGCAGGTCACACCGAATGACCATGCTAATGCTAGAGCGTT
CTCGCATCTAGCTATAAAACTAATAGAGCAGGAAATTGACCCCGACTCAACCATCCTGGATATCGGCA
GTGCGCCAGCAAGGAGGATGATGTCGGACAGGAAGTACCACTGCGTCTGCCCGATGCGCAGTGCGGAA
GATCCCGAGAGACTCGCCAATTATGCGAGAAAGCTAGCATCTGCCGCAGGAAAAGTCCTGGACAGAAA
CATCTCTGGAAAGATCGGGGACTTACAAGCAGTAATGGCCGTGCCAGACACGGAGACGCCAACATTCT
GCTTACACACAGACGTCTCATGTAGACAGAGAGCAGACGTCGCTATATACCAAGACGTCTATGCTGTA
CACGCACCCACGTCGCTATACCACCAGGCGATTAAAGGGGTCCGAGTGGCGTACTGGGTTGGGTTCGA
CACAACCCCGTTCATGTACAATGCCATGGCGGGTGCCTACCCCTCATACTCGACAAACTGGGCAGATG
AGCAGGTACTGAAGGCTAAGAACATAGGATTATGTTCAACAGACCTGACGGAAGGTAGACGAGGCAAG
TTGTCTATTATGAGAGGGAAAAAGCTAAAACCGTGCGACCGTGTGCTGTTCTCAGTAGGGTCAACGCT
CTACCCGGAAAGCCGCAAGCTACTTAAGAGCTGGCACCTGCCATCGGTGTTCCATTTAAAGGGCAAAC
TCAGCTTCACATGCCGCTGTGATACAGTGGTTTCGTGTGAGGGCTACGTCGTTAAGAGAATAACGATG
AGCCCAGGCCTTTATGGAAAAACCACAGGGTATGCGGTAACCCACCACGCAGACGGATTCCTGATGTG
CAAGACTACCGACACGGTTGACGGCGAAAGAATGTCATTCTCGGTGTGCACATACGTGCCGGCGACCA
TTTGTGATCAAATGACCGGCATCCTTGCTACAGAAGTCACGCCGGAGGATGCACAGAAGCTGTTGGTG
GGGCTGAACCAGAGAATAGTGGTTAACGGCAGAACGCAACGGAATACGAACACCATGAAAAATTATCT
GCTTCCCGTGGTCGCCCAAGCCTTCAGTAAGTGGGCAAAGGAGTGCCGGAAAGACATGGAAGATGAAA
AACTCCTGGGGGTCAGAGAAAGAACACTGACCTGCTGCTGTCTATGGGCATTCAAGAAGCAGAAAACA
CACACGGTCTACAAGAGGCCTGATACCCAGTCAATTCAGAAGGTTCAGGCCGAGTTTGACAGCTTTGT
GGTACCGAGTCTGTGGTCGTCCGGGTTGTCAATCCCTTTGAGGACTAGAATCAAATGGTTGTTAAGCA
AGGTGCCAAAAACCGACCTGATCCCATACAGCGGAGACGCCCGAGAAGCCCGGGACGCAGAAAAAGAA
GCAGAGGAAGAACGAGAAGCAGAACTGACTCGCGAAGCCCTACCACCTCTACAGGCAGCACAGGAAGA
TGTTCAGGTCGAAATCGACGTGGAACAGCTTGAGGACAGAGCGGGCGCAGGAATAATAGAGACTCCGA
GAGGAGCTATCAAAGTTACTGCCCAACCAACAGACCACGTCGTGGGAGAGTACCTGGTACTCTCCCCG
CAGACCGTACTACGTAGCCAGAAGCTCAGTCTGATTCACGCTTTGGCGGAGCAAGTGAAGACGTGCAC
GCACAACGGACGAGCAGGGAGGTATGCGGTCGAAGCGTACGACGGCCGAGTCCTAGTGCCCTCAGGCT
ATGCAATCTCGCCTGAAGACTTCCAGAGTCTAAGCGAAAGCGCAACGATGGTGTATAACGAAAGAGAG
TTCGTAAACAGAAAGCTACACCATATTGCGATGCACGGACCAGCCCTGAACACCGACGAAGAGTCGTA
TGAGCTGGTGAGGGCAGAGAGGACAGAACACGAGTACGTCTACGACGTGGATCAGAGAAGATGCTGTA
AGAAGGAAGAAGCCGCAGGACTGGTACTGGTGGGCGACTTGACTAATCCGCCCTACCACGAATTCGCA
TATGAAGGGCTAAAAATCCGCCCTGCCTGCCCATACAAAATTGCAGTCATAGGAGTCTTCGGAGTACC
GGGATCTGGCAAGTCAGCTATTATCAAGAACCTAGTTACCAGGCAGGACCTGGTGACTAGCGGAAAGA
AAGAAAACTGCCAAGAAATCACCACCGACGTGATGAGACAGAGAGGTCTAGAGATATCTGCACGTACG
GTTGACTCGCTGCTCTTGAATGGATGCAACAGACCAGTCGACGTGTTGTACGTAGACGAGGCGTTTGC
GTGCCACTCTGGAACGCTACTTGCTTTGATCGCCTTGGTGAGACCAAGGCAGAAAGTTGTACTTTGTG
GTGACCCGAAGCAGTGCGGCTTCTTCAATATGATGCAGATGAAAGTCAACTATAATCACAACATCTGC
ACCCAAGTGTACCACAAAAGTATCTCCAGGCGGTGTACACTGCCTGTGACCGCCATTGTGTCATCGTT
GCATTACGAAGGCAAAATGCGCACTACGAATGAGTACAACAAGCCGATTGTAGTGGACACTACAGGCT
CAACAAAACCTGACCCTGGAGACCTCGTGTTAACGTGCTTCAGAGGGTGGGTTAAACAACTGCAAATT
GACTATCGTGGATACGAGGTCATGACAGCAGCCGCATCCCAAGGGTTAACCAGAAAAGGAGTTTACGC
AGTTAGACAAAAAGTTAATGAAAACCCGCTCTATGCATCAACGTCAGAGCACGTCAACGTACTCCTAA
CGCGTACGGAAGGTAAACTGGTATGGAAGACACTTTCCGGCGACCCGTGGATAAAGACGCTGCAGAAC
CCACCGAAAGGAAACTTCAAAGCAACTATTAAGGAGTGGGAGGTGGAGCATGCATCAATAATGGCGGG
CATCTGCAGTCACCAAATGACCTTCGATACATTCCAAAATAAAGCCAACGTTTGTTGGGCTAAGAGCT
TGGTCCCTATCCTCGAAACAGCGGGGATAAAACTAAATGATAGGCAGTGGTCTCAGATAATTCAAGCC
TTCAAAGAAGACAAAGCATACTCACCTGAAGTAGCCCTGAATGAAATATGTACGCGCATGTATGGGGT
GGATCTAGACAGCGGGCTATTTTCTAAACCGTTGGTGTCTGTGTATTACGCGGATAACCACTGGGATA
ATAGGCCTGGAGGGAAAATGTTCGGATTTAACCCCGAGGCAGCATCCATTCTAGAAAGAAAGTATCCA
TTCACAAAAGGGAAGTGGAACATCAACAAGCAGATCTGCGTGACTACCAGGAGGATAGAAGACTTTAA
CCCTACCACCAACATCATACCGGCCAACAGGAGACTACCACACTCATTAGTGGCCGAACACCGCCCAG
TAAAAGGGGAAAGAATGGAATGGCTGGTTAACAAGATAAACGGCCACCACGTGCTCCTGGTCAGTGGC
TATAACCTTGCACTGCCTACTAAGAGAGTCACTTGGGTAGCGCCGTTAGGTGTCCGCGGAGCGGACTA

CACATACAACCTAGAGTTGGGTCTGCCAGCAACGCTTGGTAGGTATGACCTAGTGGTCATAAACATCC
ACACACCTTTTCGCATACACCATTACCAACAGTGCGTCGACCACGCAATGAAACTGCAAATGCTCGGG
GGTGACTCATTGAGACTGCTCAAACCGGGCGGCTCTCTATTGATCAGAGCATATGGTTACGCAGATAG
AACCAGTGAACGAGTCATCTGCGTATTGGGACGCAAGTTTAGATCGTCTAGAGCGTTGAAACCACCAT
GTGTCACCAGCAACACTGAGATGTTTTTCCTATTCAGCAACTTTGACAATGGCAGAAGGAATTTCACA
ACTCATGTCATGAACAATCAACTGAATGCAGCCTTCGTAGGACAGGTCACCCGAGCAGGATGTGCACC
GTCGTACCGGGTAAAACGCATGGACATCGCGAAGAACGATGAAGAGTGCGTAGTCAACGCCGCTAACC
CTCGCGGGTTACCGGGTGGCGGTGTTTGCAAGGCAGTATACAAAAAATGGCCGGAGTCCTTTAAGAAC
AGTGCAACACCAGTGGGAACCGCAAAAACAGTTATGTGCGGTACGTATCCAGTAATCCACGCTGTTGG
ACCAAACTTCTCTAATTATTCGGAGTCTGAAGGGGACCGGGAATTGGCAGCTGCCTATCGAGAAGTCG
CAAAGGAAGTAACTAGGCTGGGAGTAAATAGTGTAGCTATACCTCTCCTCTCCACAGGTGTATACTCA
GGAGGGAAAGACAGGCTGACCCAGTCACTGAACCACCTCTTTACAGCCATGGACTCGACGGATGCAGA
CGTGGTCATCTACTGCCGCGACAAAGAATGGGAGAAGAAAATATCTGAGGCCATACAGATGCGGACCC
AAGTAGAGCTGCTGGATGAGCACATCTCCATAGACTGCGATATTGTTCGCGTGCACCCTGACAGCAGC
TTGGCAGGCAGAAAAGGATACAGCACCACGGAAGGCGCACTGTACTCATATCTAGAAGGGACCCGTTT
TCATCAGACGGCTGTGGATATGGCGGAGATACATACTATGTGGCCAAAGCAAACAGAGGCCAATGAGC
AAGTCTGCCTATATGCCCTGGGGGAAAGTATTGAATCGATCAGGCAGAAATGCCCGGTGGATGATGCA
GACGCATCATCTCCCCCCAAAACTGTCCCGTGCCTTTGCCGTTACGCTATGACTCCAGAACGCGTCAC
CCGGCTTCGCATGAACCACGTCACAAGCATAATTGTGTGTTCTTCGTTTCCCCTCCCAAAGTACAAAA
TAGAAGGAGTGCAAAAAGTCAAATGCTCTAAGGTAATGCTATTTGACCACAACGTGCCATCGCGCGTA
AGTCCAAGGGAATATAGATCTTCCCAGGAGTCTGCACAGGAGGCGAGTACAATCACGTCACTGACGCA
TAGTCAATTCGACCTAAGCGTTGATGGCGAGATACTGCCCGTCCCGTCAGACCTGGATGCTGACGCCC
CAGCCCTAGAACCAGCACTAGACGACGGGGCGACACACACGCTGCCATCCACAACCGGAAACCTTGCG
GCCGTGTCTGATTGGGTAATGAGCACCGTACCTGTCGCGCCGCCCAGAAGAAGGCGAGGGAGAAACCT
GACTGTGACATGTGACGAGAGAGAAGGGAATATAACACCCATGGCTAGCGTCCGATTCTTTAGGGCAG
AGCTGTGTCCGGTCGTACAAGAAACAGCGGAGACGCGTGACACAGCAATGTCTCTTCAGGCACCACCG
AGTACCGCCACGGAACCGAATCATCCGCCGATCTCCTTCGGAGCATCAAGCGAGACGTTCCCCATTAC
ATTTGGGGACTTCAACGAAGGAGAAATCGAAAGCTTGTCTTCTGAGCTACTAACTTTCGGAGACTTCT
TACCAGGAGAAGTGGATGACTTGACAGACAGCGACTGGTCCACGTGCTCAGACACGGACGACGAGTTA
AGACTAGACAGGGCAGGTGGGTATATATTCTCGTCGGACACCGGTCCAGGTCATTTACAACAGAAGTC
AGTACGCCAGTCAGTGCTGCCGGTGAACACCCTGGAGGAAGTCCACGAGGAGAAGTGTTACCCACCTA
AGCTGGATGAAGCAAAGGAGCAACTATTACTTAAGAAACTCCAGGAGAGTGCATCCATGGCCAACAGA
AGCAGGTATCAGTCGCGCAAAGTAGAAAACATGAAAGCAGCAATCATCCAGAGACTAAAGAGAGGCTG
TAGACTATACTTAATGTCAGAGACCCCAAAAGTCCCTACTTACCGGACTACATATCCGGCGCCTGTGT
ACTCGCCTCCGATCAACGTCCGATTGTCCAATCCCGAGTCCGCAGTGGCAGCATGCAATGAGTTCTTA
GCTAGAAACTATCCAACTGTCTCATCATACCAAATTACCGACGAGTATGATGCATATCTAGACATGGT
GGACGGGTCGGAGAGTTGCCTGGACCGAGCGACATTCAATCCGTCAAAACTCAGGAGCTACCCGAAAC
AGCACGCTTACCACGCGCCCTCCATCAGAAGCGCTGTACCGTCCCCATTCCAGAACACACTACAGAAT
GTACTGGCAGCAGCCACGAAAAGAAACTGCAACGTCACACAGATGAGGGAATTACCCACTTTGGACTC
AGCAGTATTCAACGTGGAGTGTTTCAAAAAATTCGCATGCAACCAAGAATACTGGGAAGAATTTGCTG
CCAGCCCTATTAGGATAACAACTGAGAATTTAGCAACCTATGTTACTAAACTAAAAGGGCCAAAAGCA
GCAGCGCTATTCGCAAAAACCCATAATCTACTGCCACTACAGGAAGTACCAATGGATAGGTTCACAGT
AGATATGAAAAGGGACGTAAAGGTGACTCCTGGTACAAAGCATACAGAGGAAAGACCTAAGGTGCAGG
TTATACAGGCGGCTGAACCCTTGGCGACAGCATACCTATGTGGGATTCACAGAGAGCTGGTTAGGAGG
CTGAACGCCGTCCTCCTACCCAATGTACATACACTATTTGACATGTCTGCCGAGGATTTCGATGCCAT
CATAGCCGCACACTTTAAGCCAGGAGACACTGTTTTGGAAACGGACATAGCCTCCTTTGATAAGAGCC
AAGATGATTCACTTGCGCTTACTGCTTTGATGCTGTTAGAGGATTTAGGGGTGGATCACTCCCTGCTG
GACTTGATAGAGGCTGCTTTCGGAGAGATTTCCAGCTGTCACCTACCGACAGGTACGCGCTTCAAGTT
CGGCGCCATGATGAAATCAGGTATGTTCCTAACTCTGTTCGTCAACACATTGTTAAACATCACCATCG
CCAGCCGAGTGCTGGAAGATCGTCTGACAAAATCCGCGTGCGCGGCCTTCATCGGCGACGACAACATA
ATACATGGAGTCGTCTCCGATGAATTGATGGCAGCCAGATGTGCCACTTGGATGAACATGGAAGTGAA
GATCATAGATGCAGTTGTATCCTTGAAAGCCCCTTACTTTTGTGGAGGGTTTATACTGCACGATACTG
TGACAGGAACAGCTTGCAGAGTGGCAGACCCGCTAAAAAGGCTTTTTAAACTGGGCAAACCGCTAGCG
GCAGGTGACGAACAAGATGAAGATAGAAGACGAGCGCTGGCTGACGAAGTGATCAGATGGCAACGAAC
AGGGCTAATTGATGAGCTGGAGAAAGCGGTATACTCTAGGTACGAAGTGCAGGGTATATCAGTTGTGG
TAATGTCCATGGCCACCTTTGCAAGCTCCAGATCCAACTTCGAGAAGCTCAGAGGACCCGTCATAACT
TTGTACGGCGGTCCTAAATAGGTACGCACTACAGCTACCTATTTTGCAGAAGCCGACAGCAAGTATCT
AAACACTAATCAGCTACAATGGAGTTCATCCCAACCCAAACTTTTTACAATAGGAGGTACCAGCCTCG
ACCCTGGACTCCGCGCCCTACTATCCAAGTCATCAGGCCCAGACCGCGCCCTCAGAGGCAAGCTGGGC

AACTTGCCCAGCTGATCTCAGCAGTTAATAAACTGACAATGCGCGCGGTACCACAACAGAAGCCACGC
AGGAATCGGAAGAATAAGAAGCAAAAGCAAAAACAACAGGCGCCACAAAACAACACAAATCAAAAGAA
GCAGCCACCTAAAAAGAAACCGGCTCAAAAGAAAAAGAAGCCGGGCCGCAGAGAGAGGATGTGCATGA
AAATCGAAAATGATTGTATTTTCGAAGTCAAGCACGAAGGTAAGGTAACAGGTTACGCGTGCCTGGTG
GGGGACAAAGTAATGAAACCAGCACACGTAAAGGGGACCATCGATAACGCGGACCTGGCCAAACTGGC
CTTTAAGCGGTCATCTAAGTATGACCTTGAATGCGCGCAGATACCCGTGCACATGAAGTCCGACGCTT
CGAAGTTCACCCATGAGAAACCGGAGGGGTACTACAACTGGCACCACGGAGCAGTACAGTACTCAGGA
GGCCGGTTCACCATCCCTACAGGTGCTGGCAAACCAGGGGACAGCGGCAGACCGATCTTCGACAACAA
GGGACGCGTGGTGGCCATAGTCTTAGGAGGAGCTAATGAAGGAGCCCGTACAGCCCTCTCGGTGGTGA
CCTGGAATAAAGACATTGTCACTAAAATCACCCCCGAGGGGGCCGAAGAGTGGAGTCTTGCCATCCCA
GTTATGTGCCTGTTGGCAAACACCACGTTCCCCTGCTCCCAGCCCCCTTGCACGCCCTGCTGCTACGA
AAAGGAACCGGAGGAAACCCTACGCATGCTTGAGGACAACGTCATGAGACCTGGGTACTATCAGCTGC
TACAAGCATCCTTAACATGTTCTCCCCACCGCCAGCGACGCAGCACCAAGGACAACTTCAATGTCTAT
AAAGCCACAAGACCATACTTAGCTCACTGTCCCGACTGTGGAGAAGGGCACTCGTGCCATAGTCCCGT
AGCACTAGAACGCATCAGAAATGAAGCGACAGACGGGACGCTGAAAATCCAGGTCTCCTTGCAAATCG
GAATAAAGACGGATGACAGCCACGATTGGACCAAGCTGCGTTATATGGACAACCACATGCCAGCAGAC
GCAGAGAGGGCGGGGCTATTTGTAAGAACATCAGCACCGTGTACGATTACTGGAACAATGGGACACTT
CATCCTGGCCCGATGTCCAAAAGGGGAAACTCTGACGGTGGGATTCACTGACAGTAGGAAGATTAGTC
ACTCATGTACGCACCCATTTCACCACGACCCTCCTGTGATAGGTCGGGAAAAATTCCATTCCCGACCG
CAGCACGGTAAAGAGCTACCTTGCAGCACGTACGTGCAGAGCACCGCCGCAACTACCGAGGAGATAGA
GGTACACATGCCCCCAGACACCCCTGATCGCACATTAATGTCACAACAGTCCGGCAACGTAAAGATCA
CAGTCAATGGCCAGACGGTGCGGTACAAGTGTAATTGCGGTGGCTCAAATGAAGGACTAACAACTACA
GACAAAGTGATTAATAACTGCAAGGTTGATCAATGTCATGCCGCGGTCACCAATCACAAAAAGTGGCA
GTATAACTCCCCTCTGGTCCCGCGTAATGCTGAACTTGGGGACCGAAAAGGAAAAATTCACATCCCGT
TTCCGCTGGCAAATGTAACATGCAGGGTGCCTAAAGCAAGGAACCCCACCGTGACGTACGGGAAAAAC
CAAGTCATCATGCTACTGTATCCTGACCACCCAACACTCCTGTCCTACCGGAATATGGGAGAAGAACC
AAACTATCAAGAAGAGTGGGTGATGCATAAGAAGGAAGTCGTGCTAACCGTGCCGACTGAAGGGCTCG
AGGTCACGTGGGGCAACAACGAGCCGTATAAGTATTGGCCGCAGTTATCTACAAACGGTACAGCCCAT
GGCCACCCGCATGAGATAATTCTGTATTATTATGAGCTGTACCCCACTATGACTGTAGTAGTTGTGTC
AGTGGCCACGTTCATACTCCTGTCGATGGTGGGTATGGCAGCGGGGATGTGCATGTGTGCACGACGCA
GATGCATCACACCGTATGAACTGACACCAGGAGCTACCGTCCCTTTCCTGCTTAGCCTAATATGCTGC
ATCAGAACAGCTAAAGCGGCCACATACCAAGAGGCTGCGATATACCTGTGGAACGAGCAGCAACCTTT
GTTTTGGCTACAAGCCCTTATTCCGCTGGCAGCCCTGATTGTTCTATGCAACTGTCTGAGACTCTTAC
CATGCTGCTGTAAAACGTTGGCTTTTTTAGCCGTAATGAGCGTCGGTGCCCACACTGTGAGCGCGTAC
GAACACGTAACAGTGATCCCGAACACGGTGGGAGTACCGTATAAGACTCTAGTCAATAGACCTGGCTA
CAGCCCCATGGTATTGGAGATGGAACTACTGTCAGTCACTTTGGAGCCAACACTATCGCTTGATTACA
TCACGTGCGAGTACAAAACCGTCATCCCGTCTCCGTACGTGAAGTGCTGCGGTACAGCAGAGTGCAAG
GACAAAAACCTACCTGACTACAGCTGTAAGGTCTTCACCGGCGTCTACCCATTTATGTGGGGCGGCGC
CTACTGCTTCTGCGACGCTGAAAACACGCAGTTGAGCGAAGCACACGTGGAGAAGTCCGAATCATGCA
AAACAGAATTTGCATCAGCATACAGGGCTCATACCGCATCTGCATCAGCTAAGCTCCGCGTCCTTTAC
CAAGGAAATAACATCACTGTAACTGCCTATGCAAACGGCGACCATGCCGTCACAGTTAAGGACGCCAA
ATTCATTGTGGGGCCAATGTCTTCAGCCTGGACACCTTTCGACAACAAAATTGTGGTGTACAAAGGTG
ACGTCTATAACATGGACTACCCGCCCTTTGGCGCAGGAAGACCAGGACAATTTGGCGATATCCAAAGT
CGCACACCTGAGAGTAAAGACGTCTATGCTAATACACAACTGGTACTGCAGAGACCGGCTGTGGGTAC
GGTACACGTGCCATACTCTCAGGCACCATCTGGCTTTAAGTATTGGCTAAAAGAACGCGGGGCGTCGC
TGCAGCACACAGCACCATTTGGCTGCCAAATAGCAACAAACCCGGTAAGAGCGGTGAACTGCGCCGTA
GGGAACATGCCCATCTCCATCGACATACCGGAAGCGGCCTTCACTAGGGTCGTCGACGCGCCCTCTTT
AACGGACATGTCGTGCGAGGTACCAGCCTGCACCCATTCCTCAGACTTTGGGGGCGTCGCCATTATTA
AATATGCAGCCAGCAAGAAAGGCAAGTGTGCGGTGCATTCGATGACTAACGCCGTCACTATTCGGGAA
GCTGAGATAGAAGTTGAAGGGAATTCTCAGCTGCAAATCTCTTTCTCGACGGCCTTAGCCAGCGCCGA
ATTCCGCGTACAAGTCTGTTCTACACAAGTACACTGTGCAGCCGAGTGCCACCCCCCGAAGGACCACA
TAGTCAACTACCCGGCGTCACATACCACCCTCGGGGTCCAGGACATCTCCGCTACGGCGATGTCATGG
GTGCAGAAGATCACGGGAGGTGTGGGACTGGTTGTTGCTGTTGCCGCACTGATTCTAATCGTGGTGCT
ATGCGTGTCGTTCAGCAGGCACTAACTTGACAATTAAGTATGAAGGTATATGTGTCCCCTAAGAGACA
CACTGTACATAGCAAATAATCTATAGATCAAAGGGCTACGCAACCCCTGAATAGTAACAAAATACAAA
ATCACTAAAAATTATAAAAACAGAAAAATACATAAATAGGTATACGTGTCCCCTAAGAGACACATTGT
ATGTAGGTGATAAGTATAGATCAAAGGGCCGAATAACCCCTGAATAGTAACAAAATATGAAAATCAAT
AAAAATCATAAAATAGAAAAACCATAAACAGAAGTAGTTCAAAGGGCTATAAAACCCCTGAATAGTAA
CAAAACATAAAATTAATAAAAATCAAATGAATACCATAATTGGCAAACGGAAGAGATGTAGGTACTTA

AGCTTCCTAAAAGCAGCCGAACTCACTTTGAGAAGTAGGCATAGCATACCGAACTCTTCCACGATTCT
CCGAACCCACAGGGACGTAGGAGATGTTATTTTGTTTTTAATATTTCAAAAAAAAAAAAAAAAAAAA
AAA

ANNEX 15: miRNA RE sequences

1. miR-142-3P RE (141 bases)

TCCGGACCAGGTTCGAATCTCCATAAAGTAGGAAACACTACAGTCATCCATAAAGTAGGAAACACTAC
AGATCTCCATAAAGTAGGAAACACTACAATCGTCCATAAAGTAGGAAACACTACAACCTCAGGAGCTC
AATTG

2. miR-142-3P Antisense RE (138 bases)

TCCGGACCAGGTTCGAATGTAGTGTTTCCTACTTTATGGAGTGATGTAGTGTTTCCTACTTTATGGAG
ATCTGTAGTGTTTCCTACTTTATGGAATCGTGTAGTGTTTCCTACTTTATGGACCTCAGGAGCTCAAT
TG

3. miRNA RE Control (138 bases)

TCCGGACCAGGTTCGAAAGGTATTTCATCCTTTGTGATGTGTGAAGGTATTTCATCCTTTGTGATGTC
TAGAGGTATTTCATCCTTTGTGATGTATCGAGGTATTTCATCCTTTGTGATGTCCTCAGGAGCTCAAT
TG

ANNEX 16: Hek 293 miR-142 sequences

1. miR-142 'Core' (293 bases)

GGGTTGGGGGGATCTTAGGAAGCCACAAGGAGGGCTGGGGGGCTCTTGGAGCAGGAGTCAGGAGGCCT
GGGCAGCCTGAAGAGTACACGCCGACGGACAGACAGACAGTGCAGTCACCCATAAAGTAGAAAGCACT
ACTAACAGCACTGGAGGGTGTAGTGTTTCCTACTTTATGGATGAGTGTACTGTGGGCTTCGGAGATCA
CGCCACTGCTGCCGCCCGCTGCCCGCCACCATCTTCCTCGGCGCTCGGGGACCTCGTGTGACAGGTGA
GCACCTTACGGCCCCTCCCTA

2. miR-142 'Short' (788 bases)

GCCAGCCAGGGGTTCACAGAACTGAAGGTGAGGCCTCCAGAGGCCCTAGTCTCTACCTGAGTGTCTCT
GAAACTGGGGGGATGGGGTGGAGCCTTTAGGGGGAAGGGAAGAGGGAACTGAAGAGGAAGTGGGGGAG
GGAGGTAGAGGAGGCAAGTCTGGCGCCATGCTGAGTCACCGCCCACAAGGCCCAGGGCGGGCCCTCGG
GGGGCCCTGGCAGGGTTGGGGGGATCTTAGGAAGCCACAAGGAGGGCTGGGGGGCTCTTGGAGCAGGA
GTCAGGAGGCCTGGGCAGCCTGAAGAGTACACGCCGACGGACAGACAGACAGTGCAGTCACCCATAAA
GTAGAAAGCACTACTAACAGCACTGGAGGGTGTAGTGTTTCCTACTTTATGGATGAGTGTACTGTGGG
CTTCGGAGATCACGCCACTGCTGCCGCCCGCTGCCCGCCACCATCTTCCTCGGCGCTCGGGGACCTCG
TGTGACAGGTGAGCACCTTACGGCCCCTCCCTACCCTGCCCAGATGCCTGAAAGGCCTCCATGGCTTT
CCTGCCCTTCCTGGTTCCGGACAGCTGGGGAAAGGCCACAGCAGCTCCTCTGCTGCCCTGCAGTCTTT
GGGGGCGGGGAGGGCTGGACATGTGGAACCCTGATGCAGCCGCAGCGTCAAGGACGAGGAAGGGGTGG
GAAGGGATGGTACGTGGAGGGGAATGGGTGGTGGGACCAGGGACCCAATGCTAATAAAGACTGGACTG
TGCTTCTCTTTTGTCTGAGACTCTGTTGCTGGGGTGGGGA

3. miR-142 'Long-3' (878 bases)

GGTTGGGGTGGACTGGAGACCAAGACCTTGGCAGGGGAGCTGTGGCTGCCTCATTTGGACGCTGGAGG
GTGGCTAGCGTGGCTGGAAGCGGCCAGCCAGGGGTTCACAGAACTGAAGGTGAGGCCTCCAGAGGCCC
TAGTCTCTACCTGAGTGTCTCTGAAACTGGGGGGATGGGGTGGAGCCTTTAGGGGGAAGGGAAGAGGG
AACTGAAGAGGAAGTGGGGGAGGGAGGTAGAGGAGGCAAGTCTGGCGCCATGCTGAGTCACCGCCCAC
AAGGCCCAGGGCGGGCCCTCGGGGGGCCCTGGCAGGGTTGGGGGGATCTTAGGAAGCCACAAGGAGGG
CTGGGGGGCTCTTGGAGCAGGAGTCAGGAGGCCTGGGCAGCCTGAAGAGTACACGCCGACGGACAGAC
AGACAGTGCAGTCACCCATAAAGTAGAAAGCACTACTAACAGCACTGGAGGGTGTAGTGTTTCCTACT
TTATGGATGAGTGTACTGTGGGCTTCGGAGATCACGCCACTGCTGCCGCCCGCTGCCCGCCACCATCT
TCCTCGGCGCTCGGGGACCTCGTGTGACAGGTGAGCACCTTACGGCCCCTCCCTACCCTGCCCAGATG
CCTGAAAGGCCTCCATGGCTTTCCTGCCCTTCCTGGTTCCGGACAGCTGGGGAAAGGCCACAGCAGCT
CCTCTGCTGCCCTGCAGTCTTTGGGGGCGGGGAGGGCTGGACATGTGGAACCCTGATGCAGCCGCAGC
GTCAAGGACGAGGAAGGGGTGGGAAGGGATGGTACGTGGAGGGGAATGGGTGGTGGGACCAGGGACCC
AATGCTAATAAAGACTGGACTGTGCTTCTCTTTTGTCTGAGACTCTGTTGCTGGGGTGGGGA

4. miR-142 'Long-5' (932 bases)

CTGGTGGGGAGGCTGAAGGGTGGGGACTGAGGCTCTGGGCAGTCAGGACCTCACGGTTGGGGTGGACT
GGAGACCAAGACCTTGGCAGGGGAGCTGTGGCTGCCTCATTTGGACGCTGGAGGGTGGCTAGCGTGGC
TGGAAGCGGCCAGCCAGGGGTTCACAGAACTGAAGGTGAGGCCTCCAGAGGCCCTAGTCTCTACCTGA
GTGTCTCTGAAACTGGGGGGATGGGGTGGAGCCTTTAGGGGGAAGGGAAGAGGGAACTGAAGAGGAAG
TGGGGGAGGGAGGTAGAGGAGGCAAGTCTGGCGCCATGCTGAGTCACCGCCCACAAGGCCCAGGGCGG
GCCCTCGGGGGGCCCTGGCAGGGTTGGGGGGATCTTAGGAAGCCACAAGGAGGGCTGGGGGGCTCTTG
GAGCAGGAGTCAGGAGGCCTGGGCAGCCTGAAGAGTACACGCCGACGGACAGACAGACAGTGCAGTCA
CCCATAAAGTAGAAAGCACTACTAACAGCACTGGAGGGTGTAGTGTTTCCTACTTTATGGATGAGTGT
ACTGTGGGCTTCGGAGATCACGCCACTGCTGCCGCCCGCTGCCCGCCACCATCTTCCTCGGCGCTCGG
GGACCTCGTGTGACAGGTGAGCACCTTACGGCCCCTCCCTACCCTGCCCAGATGCCTGAAAGGCCTCC
ATGGCTTTCCTGCCCTTCCTGGTTCCGGACAGCTGGGGAAAGGCCACAGCAGCTCCTCTGCTGCCCTG

CAGTCTTTGGGGGCGGGGAGGGCTGGACATGTGGAACCCTGATGCAGCCGCAGCGTCAAGGACGAGGA
AGGGGTGGGAAGGGATGGTACGTGGAGGGGAATGGGTGGTGGGACCAGGGACCCAATGCTAATAAAGA
CTGGACTGTGCTTCTCTTTTGTCTGAGACTCTGTTGCTGGGGTGGGGA

ANNEX 17: Cloning of SFV4-3H-zsGreen-2SG-miRNA RE

First, all three miRNA REs were amplified by PCR using Pfu DNA polymerase from 1 µl of annealed and extended oligonucleotides (see 4.3). The protocol described in 2.11.3 was followed. The cycling parameters and primers used are described in Annex 12 (protocol 15). The primers added ApaI and BamHI restriction sites to 5' and 3' ends of the miRNA REs, respectively. The PCR products were run on a 1% agarose gel as described in 2.14 and then purified as described in 2.15.6. SFV4-3H-zsGreen-2SG-GLuc icDNA and all three amplified miRNA REs were digested with ApaI and BamHI as described in 2.16. The digest products were run on a 1% agarose gel as described in 2.14 and then were purified as described in 2.15.6. Finally, the miRNA REs were ligated to the linearized SFV4-3H-zsGreen icDNA following the protocol in 2.18. At the end of the ligation, 5 µl of the reaction mixture was used to transform DH5α *E. coli* as described in 2.19.3. Transformed bacteria were plated on a selective LB agar plate with 50 µg/ml kanamycin and incubated overnight at 37 ºC. Colonies from each ligation were tested by colony PCR as described in 2.11.5. The cycling parameters and primers used are described in Annex 12 (protocol 9). The primers had been designed to anneal within the genome of SFV, approximately 100-150 bases upstream and downstream of the cloning site.

PCR-positive colonies were cultured for 16 hours at 37 ºC in 5 ml of LB broth with 50 µg/ml kanamycin. Plasmids were purified from bacteria cultures as described in 2.15.8 (Mini-Prep). Purified plasmids were sequenced using SFV4 3' UTR For primer (TGTTTCCAGACATGTCGGGCAC) (Annex 10, protocol 9) at GATC Biotech. One icDNA with the correct sequence (Supplementary Data, Appendix 8) was chosen for each construct. It was subsequently amplified as described in 2.15.9 (Maxi-Prep). This final icDNA stock was re-sequenced as described above.

ANNEX 18: Generating SFV4-3F-zsGreen-miRNA RE and SFV4-3F-zsGreen-2SG-GLuc-miRNA RE constructs

First, pCMV-SFV4-3F-zsGreen-2SG-GLuc icDNA was generated as outlined in Annex Figure 1. In brief, pSP6-SFV4-3F-zsGreen and pCMV-SFV4-2SG-GLuc were digested with SacI and SbfI as described in 2.16 and run on a 1% agarose gel as described in 2.14. The 7,653 bp fragment fromSFV4-3F-zsGreen (icDNA nucleotides 1,803 to 9,456) and the 8,699 bp fragment from SFV4-2SG-GLuc (icDNA nucleotides 10,181 to 1,802) were purified as described in 2.15.6. The two fragments were ligated to each other following 2.18. At the end of the ligation, 5 µl of the reaction mixture was used to transform DH5α *E. coli* as described in 2.19.3. Transformed bacteria were plated on a selective LB agar plate with 50 µg/ml kanamycin and incubated overnight at 37 ºC. The following day only a single colony was present. It was cultured for 16 hours at 37 ºC in 5 ml of LB broth with 50 µg/ml kanamycin. Finally, the plasmid was purified from the bacteria culture as described in 2.15.8 (Mini-Prep).

The correct ligation was confirmed by PCR. Two protocols were used, each of them designed to amplify a region of SFV around one of the two the ligation sites. The cycling parameters and primers used are described in Annex 12 (protocols 7 and 8). The purified plasmid was sequenced at GATC Biotech using SFV4 SbfI Control Rev (GTTTCCGGTTCCACAGGTG) and SFV4 SacI Control Rev (CGGCGTCAGTTCTTTCAGC) primers (details in Annex 10, protocols 7 and 8). Sequencing data confirmed that the plasmid was correctly ligated (Supplementary Data, Appendix 8). Finally, the plasmid was amplified as described in 2.15.9 (Maxi-Prep). This final icDNA stock was re-sequenced as described above.

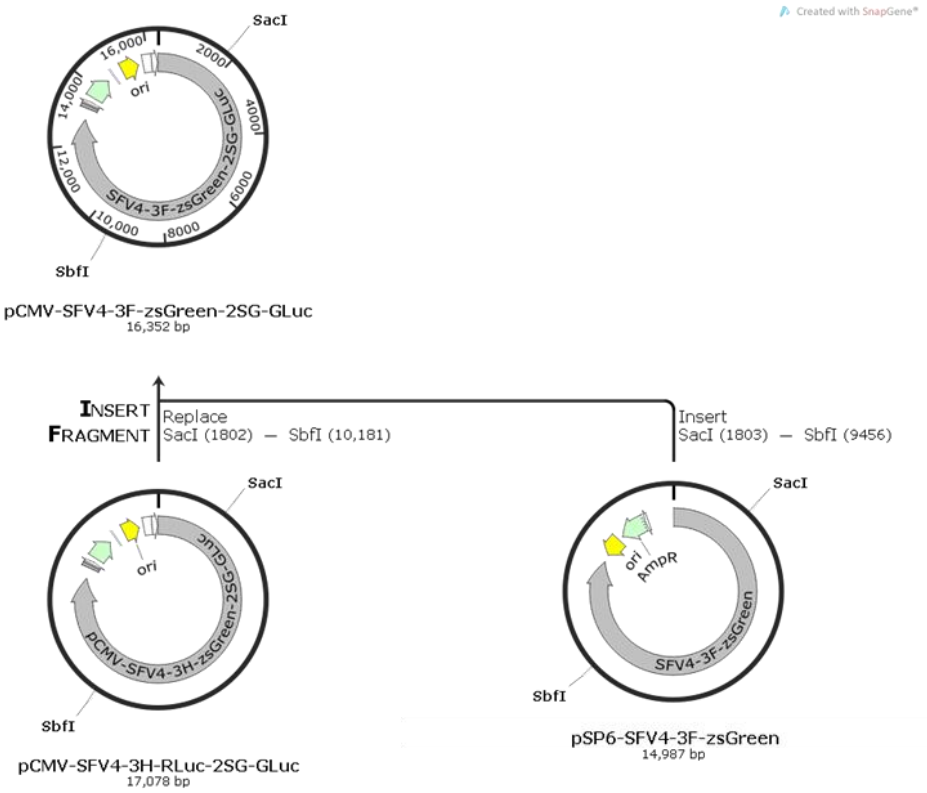

Figure 1. SFV4-3F-zsGreen-2SG-GLuc cloning summary. pSP6-SFV4-3F-zsGreena and pCMV-SFV4-2SG-GLuc plasmids were cut with SbfI and SacI. The 1,803 to 9,456 fragment from SFV4-3F-zsGreen icDNA and the 10,181 to 1,802 fragment from SFV4-2SG-GLuc icDNA were ligated to each other. Figure generated with SnapGene, GSL Biotech LLC.

MiR-142-3P RE and miRNA RE Control, were cloned into pCMV-SFV-3F-zsGreen virus following the protocol outlined in 4.4. The resulting constructs were called SFV4-3F-zsGreen-miR-142-3P RE and SFV4-3F-zsGreen-miRNA RE Control. Altogether, these viruses were named SFV4-3F-zsGreen-miRNA RE. Their sequences are provided in Supplementary Data, Appendix 1.

The cloning of the miRNA REs downstream of GLuc in SFV4-3F-zsGreen-2SG-GLuc was a two-step process. The three REs were first cloned into an intermediate vector pMK-SFV4-2SG-GLuc that was kindly donated by Stacey Human, The Roslin Institute and the Pirbright Institute. In brief, pMK-SFV4-2SG-GLuc encoded a cassette that contained a duplicated SFV subgenomic promoter, a Koazak

sequence, GLuc, and a 140 bp insert between NotI and PmeI restriction sites. This entire cassette was inserted into the vector between ApaI and BamHI restriction sites.

First, all three miRNA REs were amplified by PCR using Pfu DNA polymerase from SFV4-3H-zsGreen-miRNA RE constructs generated in 4.4. The protocol described in 2.11.3 was followed. The cycling parameters and primers used are described in Annex 12 (protocol 17). The primers added NotI and PmeI restriction sites to 5' and 3' ends of the miRNA REs, respectively. The PCR products were run on a 1% agarose gel as described in 2.14 and then purified as described in 2.15.6. Next, pMK-SFV4-3SG-GLuc vector and all three amplified miRNA REs were digested with NotI and PmeI as described in 2.16. The digest products were run on a 1% agarose gel as described in 2.14 and then purified as described in 2.15.6. Finally, the miRNA REs were ligated to the linearized pMK-SFV4-2SG-GLuc following the protocol in 2.18. At the end of the ligation, 1 µl of the reaction mixture was used to transform DH5α *E. coli* as described in 2.19.3. Transformed bacteria were plated on a selective LB agar plate with 50 µg/ml kanamycin and incubated overnight at 37 ºC.

Colonies from each ligation were tested by colony PCR as described in 2.11.5. The cycling parameters and primers used are described in Annex 12 (protocol 11). The primers had been designed to anneal approximately 100-150 bases upstream and downstream of the cloning site. PCR-positive colonies were cultured for 16 hours at 37 ºC in 5 ml of LB broth with 50 µg/ml kanamycin. Plasmids were purified from bacteria cultures as described in 2.15.8 (Mini-Prep). Purified plasmids were sequenced using pMK NotI-PmeI Control For primer (GACCTGCTCAAGAAGTGGC) (Annex 10, protocol 11) at GATC Biotech. One icDNA with the correct sequence (Supplementary Data, Appendix 13) was chosen for each construct. The above cloning is summarised in Annex Figure 2.

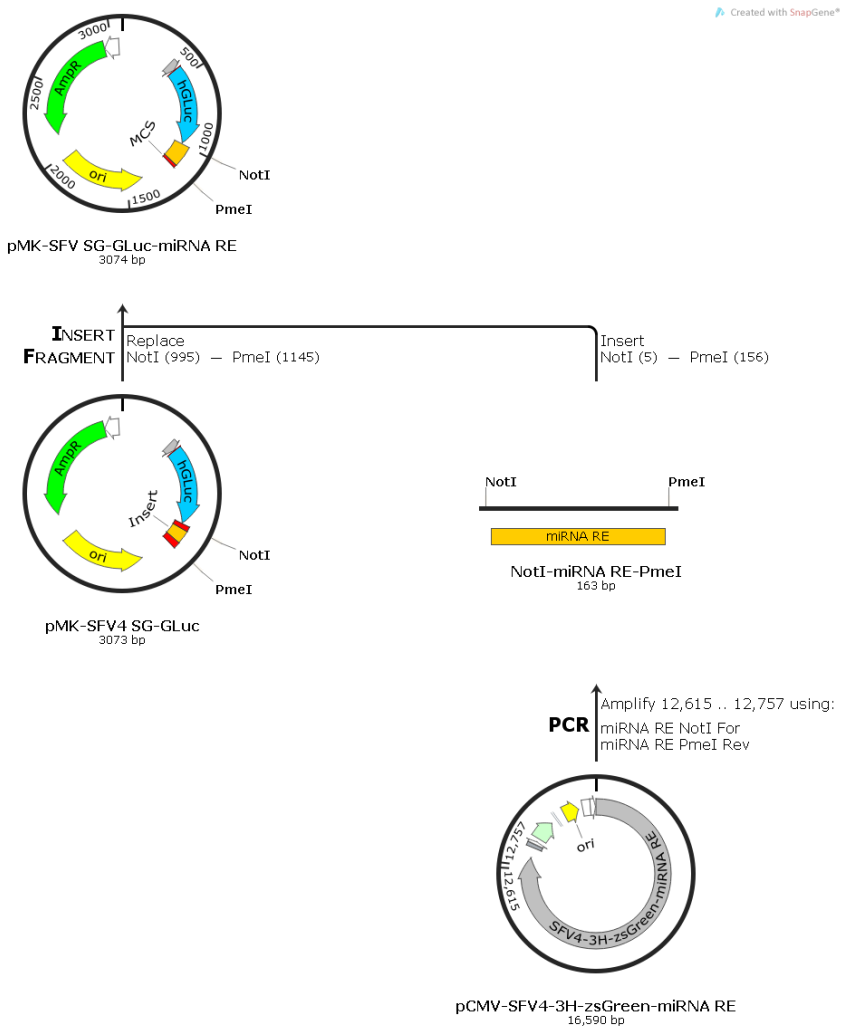

Figure 2. pMK-SFV4-2SG-GLuc-miRNA RE cloning summary. Three REs were amplified by PCR from the viruses generated in 4.4. The PCR primers added NotI and PmeI restriction sites. pMK-SFV4-2SG-GLuc plasmid and the three RE were digested with NotI and PmeI, purified, and then ligated together. Figure generated with SnapGene, GSL Biotech LLC.

Next, pCMV-SFV4-3F-zsGreen-2SG-GLuc and pMK-SFV4-2SG-GLuc-miRNA RE plasmids were digested with ApaI and BamHI as described in 2.16. The digested products were run on a 1% agarose gel as described in 2.14 and purified as described in 2.15.6. The GLuc-miRNA RE cassettes from pMK vectors were ligated to the linearized SFV4 vector following 2.18. At the end of the ligation, 1 µl of the reaction mixture was used to transform DH5α *E. coli* as described in 2.19.3. Transformed

bacteria were plated on a selective LB agar plate with 50 µg/ml kanamycin and incubated overnight at 37 ºC. The cloning was completed according to the protocol outlined in 4.4. The cloning described above is summarised in Annex Figure 3.

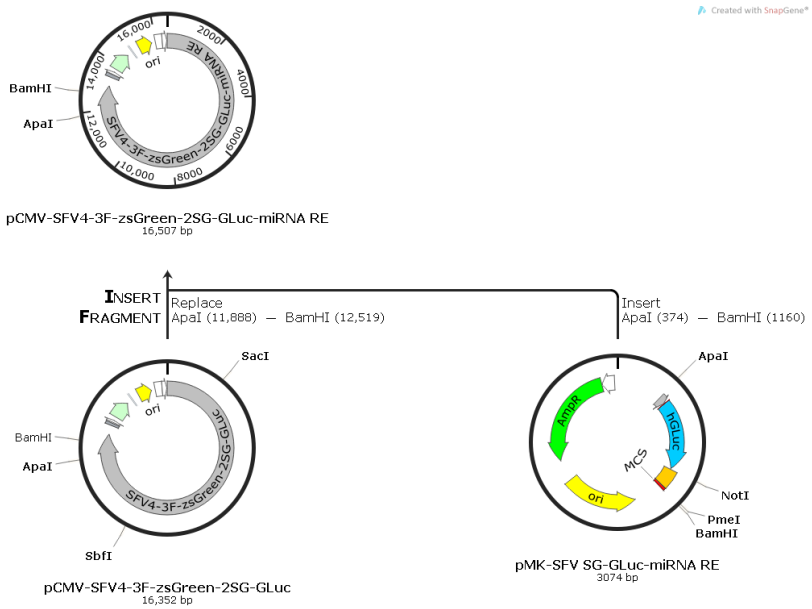

Figure 3. pCMV-SFV4-3F-zsGreen-2SG-GLuc-miRNA RE cloning summary pCMV-SFV4-3F-zsGreen-2SG-GLuc and pMK-SFV4-2SG-GLuc plasmids were digested with ApaI and BamHI, purified, and then ligated together. Figure generated with SnapGene, GSL Biotech LLC.

ANNEX 19: Generating Hek 293 miR-142 and Hek 293 Control cells

First, genomic DNA was extracted from 1 x 10^6 of Thp-1 cells as described in 2.15.2. Next, miR-142 'Core', 'Short', 'Long-3' and 'Long-5' were amplified from 200 ng of the extracted DNA using Pfu DNA Polymerase. The protocol described in 2.11.3 was followed. The primers added EcorV and XhoI restriction sites to 5' and 3' ends of the PCR products, respectively. The cycling parameters and primers used are described in Annex 12 (protocols 18, 19, 22 and 24, respectively). The PCR products were run on a 1% agarose gel and then purified as described in 2.15.6. Next, pcDNA^{TM}5/FRT/TO vector and all four miR-142 constructs were digested with EcorV and XhoI as described in 2.16. The digest products were run on a 1% agarose gel and then purified as described in 2.15.6. Finally, the miR-142 constructs were ligated to the linearized pcDNA^{TM}5/FRT/TO vector following 2.18. At the end of the ligation, 1 µl of the reaction mixture was used to transform DH5α *E. coli* as described in 2.19.3. Transformed bacteria were plated on a selective LB agar plate with 100 µg/ml ampicillin and incubated overnight at 37 ºC.

Colonies from each ligation were tested by colony PCR as described in 2.11.5. The cycling parameters and primers used are described in Annex 12 (protocol 12). The primers had been designed to anneal approximately 100-200 bases upstream and downstream of the cloning site. PCR-positive colonies were cultured for 16 hours at 37 ºC in 5 ml of LB broth with 100 µg/ml ampicillin. Plasmids were purified from bacteria cultures as described in 2.15.8 (Mini-Prep). Purified plasmids were sequenced using pcDNA Control For primer (AAATGGGCGGTAGGCGTG) (Annex 10, protocol 12) at GATC Biotech. One icDNA with the correct sequence (Supplementary Data, Appendix 12) was chosen for each construct. Sequences of all pcDNA5/FRT/TO are provided in Supplementary Data, Appendix 6.

Next, cells were cloned as described in 2.2.11 using pcDNA^{TM}5/FRT/TO plasmids encoding miR-142 'Core', 'Short', 'Long-3', 'Long-5', and an unmodified pcDNA^{TM}5/FRT/TO plasmid. The resulting cell lines were called Hek 293 miR-142

‘Core’, Hek 293 miR-142 ‘Short’, Hek 293 miR-142 ‘Long-3’, Hek 293 miR-142 ‘Long-5’ and Hek 293 Control. Six clones of each cell line were sub-cultured.

ANNEX 20: Generating pcDNA^{TM}3.1+ plasmids that co-express miR-142-3P and mCherry

First, mCherry was cloned into pcDNA3.1+ vector. In brief, mCherry was amplified by PCR using Pfu DNA polymerase from 100 ng of pSP6-ICRES1-3F-mCherry. The protocol described in 2.11.3 was followed. The cycling parameters and primers used are described in Annex 12 (protocol 25). The primers added EcorV and XhoI restriction sites to 5' and 3' ends of the mCherry, respectively. The cloning was completed as described in 4.11. The resulting construct was called pcDNA3.1+ mCherry. Its sequence is provided in Supplementary Data, Appendix 5.

Next, the entire expression cassette from pcDNA3.1+ miR-142 'Core' and pcDNA3.1+ miR-142 'Short' (from CMV enhancer/promoter to bGH poly(A) site) was cloned into the pcDNA3.1+ mCherry (Figure 4). In brief, miR-142 'Core' and miR-142 'Short' expression cassettes were amplified by PCR using Pfu DNA polymerase from 100 ng of pcDNA3.1+ miR-142 'Core' and pcDNA3.1+ miR-142 'Short'. The protocol described in 2.11.3 was followed. The cycling parameters and primers used are described in Annex 12 (protocol 26). The primers added MluI restriction site to both 5' and 3' ends of the product. The PCR products were run on a 1% agarose gel as described in 2.14 and then purified as described in 2.15.6. Next, pcDNA3.1+ mCherry and both PCR products were digested with MluI as described in 2.16. The digest products were run on a 1% agarose gel as described in 2.14 and then purified as described in 2.15.6. The linearized pcDNA3.1+ mCherry was dephosphorylated using TSAP as described in 2.17. Finally, the miR-142 expression cassettes were ligated to the linearized pcDNA3.1+ mCherry vector following 2.18. At the end of the ligation, 1 µl of the reaction mixture was used to transform DH5α *E. coli* as described in 2.19.3. Transformed bacteria were plated on a selective LB agar plate with 100 µg/ml ampicillin and incubated overnight at 37 ºC

Resulting colonies were tested by a control digest using XbaI as described in 2.16. This digest gave a distinct band pattern in clones that were ligated in the correct orientation (data not shown). Control digest-positive colonies were cultured for 16

hours at 37 ºC in 5 ml of LB broth with 100 µg/ml ampicillin. Plasmids were purified from bacteria cultures as described in 2.15.8 (Mini-Prep). Purified plasmids were sequenced at Source Bioscience using the following primers:

1. pcDNA MluI Site Sequencing For (CTGCTTGTGTGTTGGAGGTCG).
2. pcDNA miR-142 Sequencing Rev (GCCCACAGTACACTCATCC).
3. pcDNA miR-142 Sequencing For (GGAGCAGGAGTCAGGAGG).

One icDNA with the correct sequence (Supplementary Data, Appendix 11) was chosen for each construct and subsequently amplified as described in 2.15.9 (Maxi-Prep). This final icDNA stock was re-sequenced as described above.

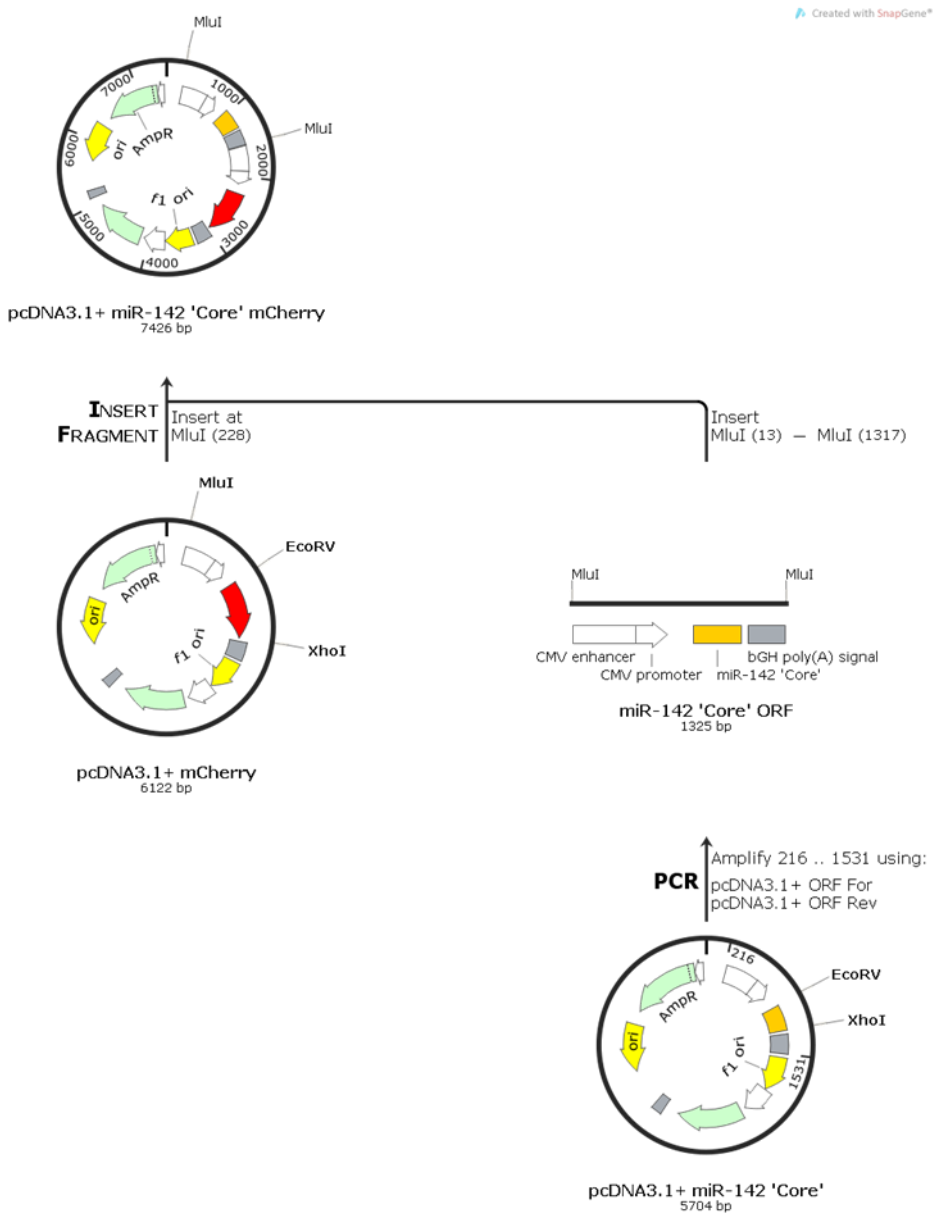

Figure 4. pcDNA3.1+ miRNA RE mCherry cloning summary. The miR-142 expression cassette was amplified by PCR and then ligated into pcDNA3.1+ mCherry plasmid via MluI site.

ANNEX 21: Incorporating miRNA REs into chikungunya replicon ChikRepl-3F-zsGreen-2SG-mCherry

First, the two miRNA REs were amplified by PCR using Vent® DNA polymerase from 1 µl of annealed and extended oligonucleotides (see 4.3). The protocol described in 2.11.2 was followed. The cycling parameters and primers used are described in Annex 12 (protocol 13). The primers added AvrII and PmeI restriction sites to 5' and 3' ends of the miRNA REs, respectively. The PCR products were run on a 1% agarose gel as described in 2.14 and then purified as described in 2.15.6. PSP6-ChikRepl-3F-zsGreen-2SG-mCherry and the two amplified miRNA REs were digested with AvrII and PmeI as described in 2.16. The digest products were run on a 1% agarose gel as described in 2.14 and then were purified as described in 2.15.6. Finally, the miRNA REs were ligated to the linearized pSP6-ChikRepl-3F-zsGreen-2SG-mCherry following the protocol in 2.18. At the end of the ligation, 1 µl of the reaction mixture was used to transform SURE2® *E. coli* as described in 2.19.2. Transformed bacteria were plated on a selective LB agar plate with 100 µg/ml ampicillin and incubated overnight at 37 ºC.

Colonies from each ligation were tested by colony PCR as described in 2.11.5. The cycling parameters and primers used are described in Annex 12 (protocol 6). The primers had been designed to anneal approximately 150-200 bases upstream and downstream of the cloning site.

PCR-positive colonies were cultured for 16 hours at 37 ºC in 5 ml of LB broth with 100 µg/ml ampicillin. Plasmids were purified from bacteria cultures as described in 2.15.8 (Mini-Prep). Purified plasmids were sequenced using ICRES1 2SG Control For primer (GCTGACGAAGTGATCAGATGGC) (Annex 10, protocol 6) at MRC PPU DNA Sequencing and Services. One icDNA with the correct sequence (Supplementary Data, Appendix 10) was chosen for each construct. It was subsequently amplified as described in 2.15.9 (Maxi-Prep). This final icDNA stock was re-sequenced as described above.